LLNL-TR-402227-DRAFT

LAWRANCE
LIVERMORE
NATIONAL
LABORATORY

Spatial Variability of Reactive Mineral and Radionuclide K_d Distributions in the Tuff Confining Unit: Yucca Flat, Nevada Test Site

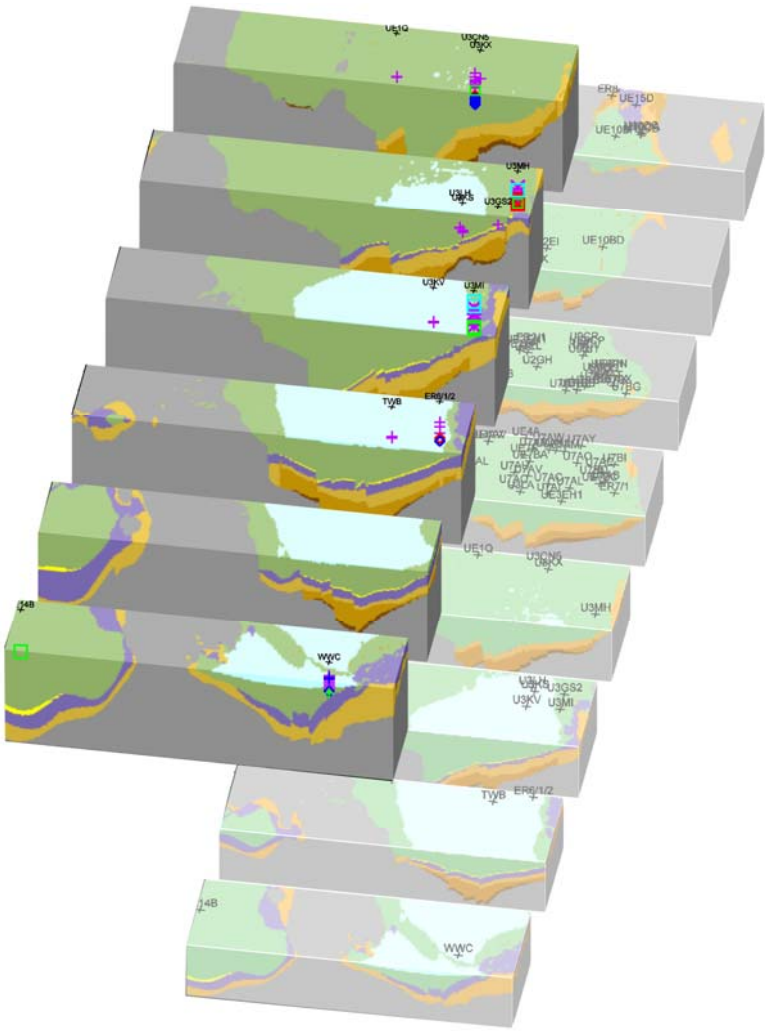

Steven F. Carle,
Mavrik Zavarin, and
Gayle A. Pawloski

February 2008

DISLAIMER

This work performed under the auspices of the U.S. Department of Energy by Lawrence Livermore National Laboratory under Contract DE-AC52-07NA27344.

Spatial Variability of Reactive Mineral and Radionuclide K_d Distributions in the Tuff Confining Unit: Yucca Flat, Nevada Test Site

Steven F. Carle,
Mavrik Zavarin, and
Gayle A. Pawloski

February 2008

Lawrence Livermore National Laboratory
Livermore, California 94551

Contents

List of Figures

List of Tables

1. Introduction

1.1 Background

Yucca Flat is a north-south elongated basin within the Nevada Test Site, Nevada, formed in the past 11 million years by basin-and-range extension. Alluvial deposits of thickness to 900 m overly Miocene volcanic rocks of generally rhyolitic composition erupted from caldera sources west and northwest of the basin. The Miocene volcanic rocks originated as nonwelded to densely welded ash-flow tuffs, ash-fall deposits, and reworked tuffs. With basin subsidence, the volcanic rocks came in contact with groundwater, causing zeolitization and/or argillization. The volcanic rocks unconformably overly Paleozoic sedimentary rocks including a regional carbonate aquifer extending beneath and beyond Yucca Flat.

Between 1951 and 1992, 659 underground nuclear tests (747 detonations) were conducted in Yucca Flat (U.S. Department of Energy, 2000), including 325 within the Miocene volcanic rocks. Residual radionuclide contaminants from underground nuclear tests include fission products, device components, and activation products. Approximately one-third of underground nuclear tests in Yucca Flat were conducted below or within 100 m of the water table. The U.S. Department of Energy is conducting remedial activities at the Nevada Test Site.

The Underground Test Area (UGTA) project addresses groundwater contamination resulting from historical underground nuclear testing conducted by the U.S. Department of Energy on the Nevada Test Site. As part of the UGTA project, groundwater flow and transport models are being developed at multiple scales including the Corrective Action Unit (CAU) scale designed to encompass groundwater flow and contaminant transport processes associated with different testing areas at the Nevada Test Site. One CAU-scale model will address groundwater flow and contaminant transport in the Yucca Flat and Climax Stock testing areas as outlined in red in Figure 1-1. The UGTA project will also use smaller scale flow and transport models in the Yucca Flat and Climax Stock areas to examine complex test-related procsses such as (1) test-induced effective stresses and pressurization of pore fluids, (2) infiltration of rainfall and captured runoff into test-induced craters and collapse chimneys, and (3) thermal groundwater flow and radionuclide transport extended from previous studies at Frenchman Flat and Pahute Mesa CAUs (Tompson et al., 1998; Pawloski et al., 2001; Wolfsberg et al., 2001; Carle et al., 2007).

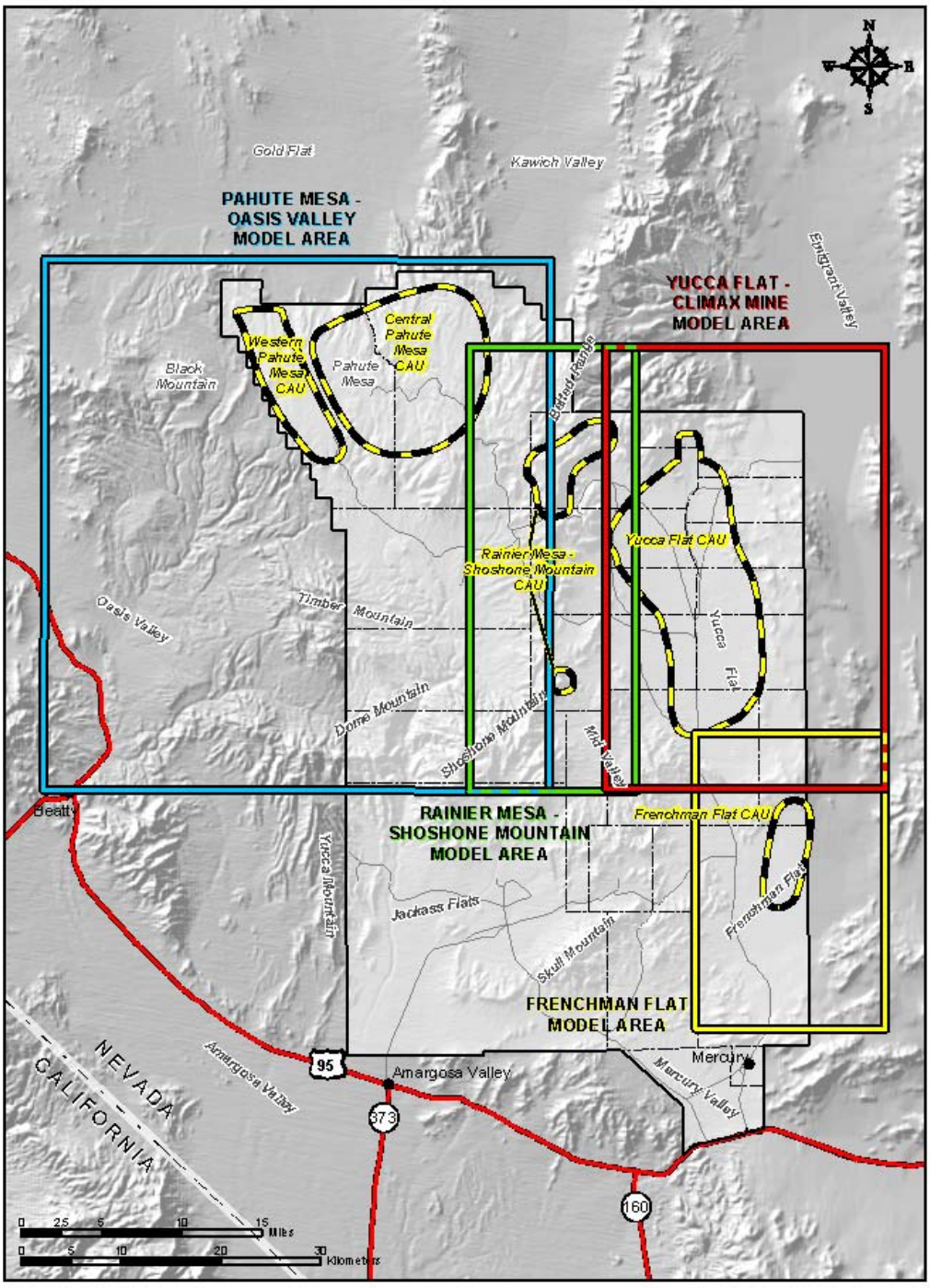

Figure 1-1. Map of Nevada Test Site showing outlines of CAU-scale groundwater flow and contaminant transport model boundaries (from Bechtel Nevada, 2006).

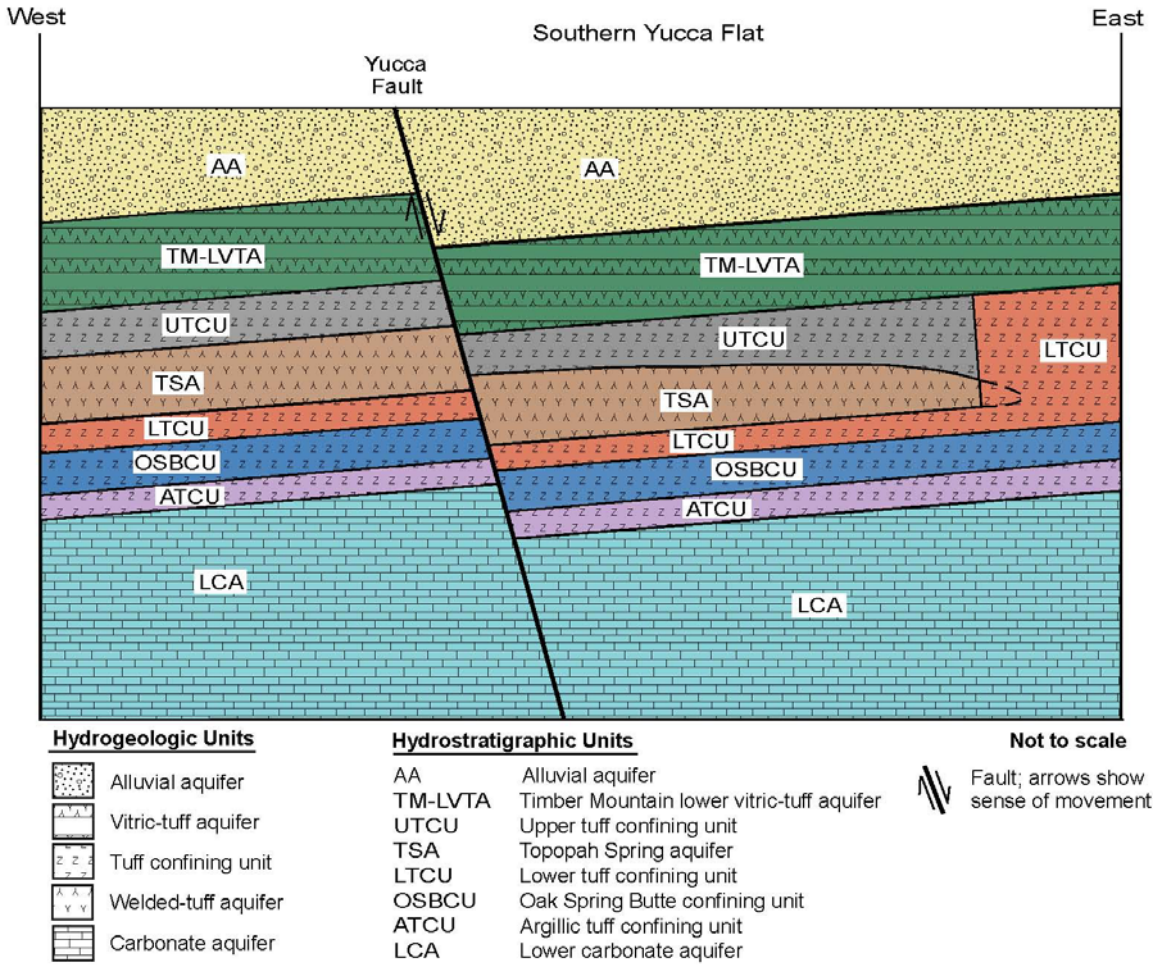

Figure 1-2. Schematic cross section of hydrogeologic and hydrostratigraphic units in southern Yucca Flat (from Bechtel Nevada, 2006).

As part of the hydrogeologic and flow and transport model development efforts for the UGTA project, rocks beneath Yucca Flat have been categorized into hydrogeologic units (HGUs) and hydrostratigraphic units (HSUs) to provide a geometric framework for development of CAU and sub-CAU scale flow and transport models (Bechtel Nevada, 2006). Figure 1-2shows a schematic cross section of HGUs and HSUs in southern Yucca Flat. Volcanic rocks within Yucca Flat are separated into aquifers and confining units. The Tuff Confining Unit (TCU) is a hydrogeologic unit that contains four confining HSUs – the Upper Tuff confining unit (UTCU), Lower Tuff confining unit (LTCU), Oak Springs Butte confining unit (OSBCU), and Argillic Tuff confining unit (ATCU). Much of the volcanic rocks within TCU confining units consist of zeolitized and argillized bedded tuffs with relatively low permeabilility. Volcanic aquifer HSUs are located either above the TCU, such as the Timber Mountain lower vitric-tuff aquifer (TM-LVTA) or interlayered within TCU HSUs, such as the Topapah Spring aquifer (TSA). The aquifer HSUs of the Miocene volcanics largely consist of unalterred or fractured welded tuffs.

Most underground nuclear tests conducted in Yucca Flat were located within or above the TCU. The hydraulic and mineralogic properties of the TCU suggest that the TCU will retard both groundwater flow and radionuclide transport.

As part of UGTA project, mineral percentages using X-ray diffraction (XRD) methods were compiled for 4,135 rock samples from the southwestern Nevada volcanic field (Warren, 2007). These mineral percentage data derive from a variety of sources including containment program perspecti and newly acquired data, which leads to variability in detection limits and data quality. 1,172 of these rock samples are located within HSUs of the TCU.

In this report and elsewhere (Zavarin et al., 2004; Stoller-Navarro, 2007), "reactive minerals" are defined as calcite, zeolite, smectite, hematite, and mica while all other minerals are defined as "non-reactive minerals". The reactive minerals are known to effectively sorb radionuclides of interest. At the NTS, the zeolite category is dominated by clinoptilolite but includes mordenite and analcime. The hematite category includes all iron oxides. However, due to its crystalline nature, hematite is more easily identified by XRD than goethite or hydrous ferric oxide. The mica category includes both illite and biotite/muscovite. The categories of reactive minerals are based on their similar sorptive properties. The non-reactive minerals may, in fact, contribute to the retardation of certain radionuclides but their contribution will be limited. One exception is the role of manganese oxides. While manganese oxides may provide a significant radionuclide sink, information regarding their abundance and sorptive behavior is limitied and cannot be addressed at this time. Manganese oxides minerals, when present, are typically identified as fracture lining minerals. The role of fracture lining minerals is not addressed in this report.

Observed variability of reactive mineral percentages within the TCU indicates that radionuclide sorption properties will vary spatially within the TCU. Accordingly, HSUs have been further subdivided into reactive mineral categories (RMCs) and reactive mineral units (RMUs) to address spatial variability of radionuclide sorption properties in radionuclide transport models (Stoller-Navarro, 2007). RMCs are categorized by ranges of reactive mineral percentages (Chapter 4), while RMUs are mapped as equivalent to or subunits of HSUs based on reactive mineralogic characteristics and lithology (Chapter 5).

Analysis of spatial variability of reactive mineral percentages in the TCU is needed to develop accurate and realistic approaches to populating radionuclide transport models with radionuclide sorption properties. Many UGTA transport models assume linear exchange processes between solutes in pore fluid and minerals in porous media solids through use of K_d coefficents known to depend on reactive mineral percentages (Viswanathan, 2003; Zavarin et al., 2004). Since the percentages of reactive minerals are

known to vary spatially in the TCU, K_d coefficients for different radionuclides are expected to vary spatially in the TCU.

This study uses the TCU XRD data to analyze and simulate frequency distributions and spatial variability of reactive minerals and radionuclide K_d coefficients in the TCU. An important objective of this study is to integrate HGU, HSU, RMC, and RMU frameworks of UGTA flow and transport modeling efforts with theoretically sound geostatistical analysis of spatial variability and stochastic simulation of reactive mineral distributions and K_d.

1.2 Document Organization

Chapter 2 states objectives and summarizes key technical elements of this report, including relationship to UGTA work, approach to characterization of spatial variability of reactive mineral distributions and *Kd*, and subsequent geostatistical analyses.

Chapter 3 evaluates the TCU XRD data with consideration of factors affecting subsequent geostatistical analyses:

- Location and spacing of data,
- Effects of different XRD methods,
- Properties of compositional data,
- Transformation of data (e.g. logarithmic, additive log ratio),
- Characteristics of reactive mineral frequency distributions in the composite XRD data set.

Chapters 4 and 5 evaluate reactive mineral distributions with respect to RMC and RMU frameworks developed for the UGTA project, with consideration of feasibility to apply geostatistical methods to characterization of reactive mineral distributions and K_d within RMCs and RMUs.

Chapter 6 describes use of the additive log ratio (ALR) and other relationships between reactive and non-reactive mineral abundances to define criteria for distinction of five reactive mineral facies (RMFs). RMFs are closely related to individual or grouped RMUs having similar lithologic and reactive mineral distribution characteristics.

Chapter 7 evaluates reactive mineral distributions in RMFs, including XRD method-specific corrections. Justification of the ALR transformation is demonstrated by Gaussian distributions obtained for the ubiquitous reactive reactive minerals mica, smectite, and

zeolite in RMFs. The spatial distribution of RMFs is intepreted in relation to RMCs, RMUs, and hydrostratigraphic units (HSUs) in the TCU.

Chapter 8 applies the component additivity methodology of Zavarin et al. (2004) to convert distributions of reactive minerals into distributions of $\log\{K_d\}$ for ten radionuclide classes. Chapter 9 applies variogram analysis to investigate spatial variability of $\log\{K_d\}$ within RMFs.

Chapter 10 addresses geostatistical simulation of spatial variability of K_d and $\log\{K_d\}$ and reactive mineral distributions, including issues related to data limitations, effects of spatial correlation and scale, properties of compositional data, and uncertainties in component additivity methodology parameters for estimating K_d. Simulation approaches are proposed involving direct simulation of $\log\{K_d\}$ and simulation of ALR transformed variables with subsequent backtransformation to mineral fractions and K_d.

Chapter 11 provides conclusions and recommendations.

1.3 Previous Work

Using a subset of mineralogic data examined in this study, Prothro (2005) identified three "mineralogic zones" based on relative abundances of primary and secondary minerals within the TCU. These three zones closely correlate to the three most voluminous reactive mineral facies (RMFs) – **L-UTCU Zeolitic**, **OSBCU Zeolitic**, and **Argillic** – that will be defined in this report. Relative to Prothro (2005), this study interprets more XRD data over a wider extent of Yucca Flat with focus on reactive minerals that impact the spatial variability of radionuclide K_d.

Ware et al. (2005) conducted laboratory experiments on sorption and desorption processes to estimate K_d for ^{137}Cs, ^{237}Np, ^{239}Pu, ^{90}Sr, ^{233}U transport in TCU and Lower Carbonate Aquifer (LCA) rocks. Zavarin et al. (2007) provide ranges of retardation factors for ^{14}C, ^{137}Cs, ^{237}Np, ^{239}Pu, Sm, ^{90}Sr, ^{233}U transport in TCU and LCA rocks derived from laboratory and numerical experiments. However, these studies do not provide sufficient number and resolution of K_d estimates to characterize spatial variability of K_d throughout the TCU. Additionally, sorption characteristics for Am, ^{41}Ca, and Eu are not evaluated.

Shaw Environmental Inc. (2003) compiled K_d estimates for central and western Pahute Mesa derived from modeling studies, laboratory experiments and qualitative evaluation. Papelis and Um (2003) conducted laboratory studies to estimate K_d for Cs, Sr, and Pb in Frenchman Flat. Conca (2000) compiled K_d ranges for radionuclides in volcanic rocks at Yucca Mountain. Some of these K_d may be obtained from similar lithologies or

stratigraphic units as in the TCU. However, K_d data from Pahute Mesa, Frenchman Flat, or Yucca Mountain may not be relevant to Yucca Flat because of different mineralogic distributions relating to lithology, proximity to eruptive sources, and diagnenitic history.

Stoller-Navarro (2007) provides preliminary estimates of K_d distributions in vitric, devitrified, and zeolitic tuff categories (grouped from RMCs) based on Yucca Flat/Climax mine mineralogy and water chemistry data. These estimates compare K_d distributions derived from laboratory experiments and the mechanistic model using the component additivity approach (Section 8.1). Stoller-Navarro (2007) also examines K_d distributions derived from laboratory measurements on similar volcanic rocks for the Yucca Mountain Project.

2. Objectives and Key Technical Elements

The overall objective of this report is to characterize spatial variability of reactive minerals and K_d affecting prediction of radionuclide transport behavior within the Tuff Confining Unit (TCU) in Yucca Flat. Characterization of spatial variability of reactive minerals and K_d includes these objectives:

- Definition and identification of reactive mineral facies (RMFs) as zones within the TCU having distinctive distributions of reactive minerals.
- Evaluation of spatial variability of reactive mineral distributions and Kd within RMFs using geostatistical techniques.
- Integration of RMF and geostatistical interpretations with other UGTA frameworks for interpreting spatial distributions reactive minerals and Kd, particularly reactive mineral category (RMC) and reactive mineral unit (RMU) approaches by (Stoller-Navarro, 2007) and mineral zonation interpretation (Prothro, 2005).

Key technical elements used to address the objectives of this report are summarized below.

2.1 Links to UGTA CAU Modeling and Stratigraphic Frameworks

The Tuff Confining Unit (TCU) hydrogeologic unit in Yucca Flat (Bechtel Nevada, 2006) largely consists of low permeability volcanic rocks with relatively high percentages of reactive minerals including calcite, hematite, mica, smectite, and zeolite. The TCU is conceptualized as barrier to both groundwater flow and contaminant transport in Yucca Flat. Corrective Action Unit (CAU) and sub-CAU scale contaminant transport models for the Yucca Flat and Climax Mine will assume linear sorption isotherms to account for effects of reactive chemistry. The linear isotherm employs distribution coefficients, K_d (mL/g units), to simulate a ratio between moles of contaminant sorbed per mass of the porous medium relative to the moles of contaminant per solution volume.

The component additivity approach (Zavarin et al., 2004) links reactive mineral percentages to estimates of K_d. Details of the component additivity approach are given Section 8.1. X-ray diffraction (XRD) analyses provide estimates of mineral percentages for 4,135 splits of samples collected within the southwestern Nevada volcanic field (Warren, 2007). Chapter 3 provides further details on the XRD data set. 1,172 of these

XRD data are attributed to hydrostratigraphic units (HSUs) located within the TCU – the upper tuff confining unit (UTCU), lower tuff confining unit (LTCU), Oak Springs Butte confining unit (OSBCU), and the argillic tuff confining unit (ATCU) (Bechtel Nevada, 2006). The HSUs will be used in CAU flow and transport models to distinguish differences in hydraulic properties within the TCU. HSUs may be further subdivided into reactive mineral units (RMUs) based on lithology, stratigraphic relationships, and mineral distributions to distinguish variations in transport properties, particularly K_d, within the TCU (Stoller-Navarro, 2007). The reactive mineral category (RMC) approach also addresses spatial variation in reactive mineral heterogeneity, but through categorization based on mineral percentage ranges and ratios independent of stratigraphic relationships.

2.2 Consideration of XRD Methods

An essential step in utilization of the TCU XRD data is recognition of strengths and limitations of the four XRD methods used – external standard ("E"), full spectrum ("F"), internal standard ("I"), and semi-quantitiative ("S"). These methods vary in ability to resolve mineral percentages as detailed in Section 3.3 and disussed throughout this report. Importantly, the ability to resolve low percentages of reactive, silicate, and glass minerals is critical to distinguishing uniquely mineralized zones (e.g. RMUs or RMFs) in the TCU. The most accurate "F" data provide a measurement standard to guide interpretation of mineral percentage data from other XRD methods. The most numerous "S" data have large uncertainty caused by mineral percentage estimates derived from ranges. This report incorporates consideration of differences in accuracy and resolution of XRD methods throughout all interpretation of spatial variability of reactive mineral percentage and K_d (Chapters 4-10).

2.3 Approaches to Characterization of Spatial Variability of Reactive Mineral Distributions

The objective of this report is to characterize spatial variability of reactive minerals and K_d affecting prediction of radionuclide transport behavior within the Tuff Confining Unit (TCU) below Yucca Flat. An essential step in utilization of the TCU XRD data is recognition of strengths and limitations of the four XRD methods used – external standard ("E"), full spectrum ("F"), internal standard ("I"), and semi-quantitiative ("S"). These methods vary in ability to resolve mineral percentages as detailed throughout this report. Importantly, the ability to resolve low percentages of reactive, silicate, and glass minerals is critical to distinguishing uniquely mineralized zones (e.g. RMUs or RMFs) in the TCU. The most accurate "F" data provide a measurement standard to guide interpretation of mineral percentage data from other XRD methods. The most numerous "S" data have large uncertainty caused by mineral percentage estimates derived from

ranges. This report incorporates consideration of differences in accuracy and resolution of XRD methods throughout all interpretation of spatial variability of reactive mineral percentage and K_d (Chapters 4-10).

Chapters 4 and 5 evaluate reactive mineral frequency distributions in the RMC and RMU frameworks using linear and logarithmic scaling of reactive mineral percentages. In the interest of consolidating limited data and simplifying characterization of spatial variation of reactive minerals and K_d, this report defines criteria for identifying reactive mineral facies (RMFs) corresponding to individual or groups of RMUs or RMCs having distinctive distributions of reactive minerals (Chapter 6). RMFs are also distinguished by ratios between smectite and zeolite compared to silicate or glass minerals.

Five RMFs are distinguished as given in bold type throughout this report:

- **L-UTCU Zeolitic** composed primarily of zeolitic bedded tuffs within the LTCU and UTCU HSUs.
- **OSBCU Zeolitic** composed primarily of zeolitic bedded tuffs within the OSBCU HSU.
- **Argillic** composed of argillized bedded tuffs primarily located within the ATCU HSU and secondarily located within the OSBCU and LTCU HSUs.
- **Devitrified** composed primarily of RMUs distinguished by partially welded to welded ash flow tuffs having devitrified mineralogy indicated by high ratios of silicate minerals compared to smectite and zeolite.
- **Vitric** composed of glassy tuffs, primarily distinguished by vitric RMCs and high ratios of glass compared to smectite and zeolite.

At typical vertical sequence within the TCU includes the three most voluminous RMFs, **L-UTCU Zeolitic**, **OSBCU Zeolitic**, and **Argillic,** which closely relate to the three mineralization zones in the TCU described by Prothro (2005). This sequence exhibits trends of increasing smectite and decreasing zeolite with depth. **Devitrified** and **Vitric** RMFs are sporadically located mostly within the OSBCU and LTCU HSUs.

2.4 Implementation of Additive Log Ratio Transformation

Mineral percentage data represent a vector with components summing to 100%. Compositional data present theoretical challenges to implementation of geostatistical techniques. Parametric geostatistical techniques are more feasibly applied to populations of data characterized by Gaussian distributions.

Difficulties arise in implementation of geostatistical methods to raw percentage or logarithm of mineral percentage values because of non-Gaussian characteristics including finite limits (e.g. 0% to 100%, or Log{100}=2). Additionally, spurious correlations and singular covariance matrices are induced by the summing constraint of mineral percentages adding up to 100% (Aitchison, 1986; Pawlosky-Glahn and Olea, 2004).

To address the difficulties of applying geostatistical techniques to mineral percentage data, Chapter 7 implements the additive log ratio (ALR) transformation to XRD data as the logarithm of the ratio between a reactive mineral percentage divided by the sum of non-reactive mineral percentages. The ALR transformation produces Gaussian distributions within RMFs for the more ubiquitous reactive minerals mica, smectite, and zeolite.

2.5 Estimation of K_d Distributions in RMFs

XRD data in the TCU are less numerous for calcite and particularly hematite compared to mica, smectite, and zeolite. Nonetheless, the XRD data indicate calcite and hematite are usually absent throughout the TCU. Where present, calcite and hematite percentages are typically a few percent. Because mica, smectite, and zeolite are generally ubiquitous with few exceptions in the TCU, mica, smectite, and zeolite dominate K_d distributions estimated by the component additivity method (Chapter 8). Importantly, K_d for seven of ten radionuclide classes – Am, Eu, Ni, Np, Pu, Sm, U – is dominated by smectite distribution because sorption of these radionuclides to mica and zeolite is not included in the component additivity approach. Due to the low surface area of mica and zeolite and the weak ion exchange properties of these radionuclides under ambient groundwater conditions, Zavarin et al. (2004) suggested that sorption of these radionuclides to mica and zeolite will be insignificant when compared to smectite. K_d for ^{41}Ca and Sr is dominated by zeolite and secondarily by smectite, and K_d for Cs is dominated by mica and secondarily by zeolite and smectite.

Using XRD method-specific corrections to zero-valued data, final estimations of $\log\{K_d\}$ distributions assume ubiquitous (all non-zero percentage) smectite in all RMFs, ubiquitous zeolite in the **L-UTCU Zeolitic** and **OSBCU Zeolitic** RMFs, and ubiquitous mica in all RMFs except the **L-UTCU Zeolitic,** because thin peralkaline tuff beds occurring in the LTCU HSU have zero mica. The zero-value corrections tighten $\log\{K_d\}$ distribution estimates and, consequently, should reduce uncertainty in CAU contaminant transport modeling predictions. The seven radionuclide classes with K_d dominated by smectite - Am, Eu, Ni, Np, Pu, Sm, U – show similar trends between RMFs characterized by increasing $\log\{K_d\}$ with depth and similar $\log\{K_d\}$ between **OSBCU Zeolitic**, **Devitrified** , and **Vitric** RMFs. For the seven radionuclides that sorb to smectite (and zeolite or mica), reactive mineral and $\log\{K_d\}$ distributions for different RMFs (or

RMUs) could be consolidated in the OSBCU HSU. Estimates of $\log\{K_d\}$ distributions for Cs are similar for all RMFs in the TCU because mica distributions are similar throughout the TCU. While Cs also sorbs to zeolite and smectite, overall zeolite and smectite distribution depth trends in the TCU counteract effects on K_d for Cs. Estimates of $\log\{K_d\}$ distributions for ^{41}Ca and Sr reflect differences in zeolite for different RMFs. Distinction of **Devitrified** and **Vitric** RMFs is most important for ^{41}Ca and Sr because large contrasts in zeolite abundance would produce large contrasts in K_d, particularly within the OSBCU HSU.

2.6 Geostatistical Analysis of Spatial Variability and Stochastic Simulation

The reactive mineral facies (RMF) and additive log ratio (ALR) approaches used in this study were largely chosen with implementation of geostatistical analysis in mind (Chapters 9 and 10). Two important considerations for implementation of geostatistical analysis are:

- Sufficient numbers of data are needed to perform analysis of spatial variability using variograms and cross-covariance matrices. Accuracy of variogram analysis improves as the number of data pairs is increased. Hence, grouping of categories (e.g. RMUs) with similar statistical properties into RMFs is advantageous to geostatistical analysis.

- Frequency distributions are preferably Gaussian and, thus, amenable to characterization by bivariate statistics (e.g., mean, variance, covariance, variogram, etc.). The ALR transformation – the logarithm of the ratio between reactive mineral and sum of non-reactive minerals - consistently produced Gaussian distributions for ubiquitous reactive minerals in RMFs.

Variogram analysis was performed on radionuclide $\log\{K_d\}$ distributions estimated in each RMF by the component additivity methodology (Chapter 9). Vertical and lateral direction $\log\{K_d\}$ variogram analysis was performed separately for “F” and “S” method data recognizing differences in number and quality of data. Numbers of “E” and “I” method data were not sufficient for variogram analysis, as detailed in Sections 3.3 and 3.4. No vertical or lateral spatial continuity was detected by “F” method $\log\{K_d\}$ variogram analysis, suggesting correlation scales of reactive mineral spatial variability are less than the minimum measurement spacing (6 m in the vertical). Variograms generated by “S” data impart an erroneous impression of spatial correlation caused by semi-quantitative estimates derived from reactive mineral percentage range. “S” data

composing most of the TCU XRD data set are not useful for analysis of spatial variability.

For radionuclide $\log\{K_d\}$ distributions dominated by smectite (Am, Eu, Ni, Np, Pu, Sm, and U), variograms with similar differences between smectite and calcite component additivity coefficients will produce similar variogram structures. Although calcite is of relatively low abundance, a small percentage of calcite can produce a large degree of variability in K_d because of high component additivity coefficients for calcite. Variograms of $\log\{K_d\}$ for zeolite-sorbing radionuclides (^{41}Ca and Sr) have similar structure, while Cs, a strong sorber to mica, has a unique variogram structure.

Stochastic simulation involves generating "realizations" of a regionalized variable (e.g., $\log\{K_d\}$) or vector of variables (e.g., reactive mineral percentages or ALR) that honor a model of spatial correlation. If spatial correlation of $\log\{K_d\}$ could be detected (e.g. by closely-spaced full spectrum XRD data), stochastic simulation techniques are available to generate realizations of $\log\{K_d\}$ with spatial correlation structure honoring variogram models. However since no spatial correlation of $\log\{K_d\}$ was detected, no stochastic simulations of $\log\{K_d\}$ were generated in this study (Section 9.3.2).

An alternative approach to stochastic simulation is to generate realizations of reactive mineral distributions rather than $\log\{K_d\}$, then apply the component additivity methodology to the simulated reactive mineral distributions to generate $\log\{K_d\}$ realizations (Chapter 10). Smectite, mica, and zeolite, which are generally ubiquitous in the TCU and also dominate K_d, are amenable to geostatistical characterization by spatial cross-covariance matrices of the ALR. Spatial cross-covariances of ALR in the **L-UTCU Zeolitic** and **OSBCU Zeolitic** could be measured from full spectrum XRD data, although with uncertainty caused by limited number of data. The ALR cross-covariances indicated no spatial correlation except, possibly, for smectite in the **OSBCU Zeolitic** RMF. A stochastic simulation algorithm was applied to the zero-lag ALR cross-covariance matrix (Section 10.2). Subsequent ALR backtransformation applied to simulated ALR distributions produced nonsymmetric mineral percentage distributions consistent with XRD data distributions including bounding between 0 and 100%. If spatial correlation of ALRs could be detected (e.g., if closely spaced full spectrum XRD data were obtained), this cross-correlated simulation method could be expanded to consider spatial cross-correlations (Section 10.3). Some advantages of the ALR cross-correlated simulation approach are:

- The stochastic simulations could be conditioned to XRD data.

- The reactive mineral realizations would apply to all radionuclide classes instead of separately as in the direct $\log\{K_d\}$ simulation approach.

- Assessment of uncertainties in the component additivity methodology parameters could be implemented independent of the reactive mineral realizations (Section 10.4).

Comparisons of $\log\{K_d\}$ generated from ALR mineral percentage simulation and direct $\log\{K_d\}$ simulation indicate similar distributions and mean and standard deviation statistics, although the ALR mineral percentage approach can address finite maxima and asymmetry in K_d distribution (Section 10.5).

3. TCU X-Ray Diffraction Data Set

The data analyzed in this report consist of a subset of a compilation of x-ray diffraction (XRD) analyses for 4,135 splits of samples collected within the southwestern Nevada volcanic field described by Warren (2007), resulting in nearly 51,000 records of mineral abundance. These data were compiled into Excel spreadsheet format by Stoller Navarro Corporation (Stoller-Navarro, 2007) to consolidate and cross-reference other information, including location, lithology, stratigraphic unit, hydrogeologic unit, hydrostratigraphic unit (HSU), geologic formation, reactive mineral unit (RMU), reactive mineral category (RMC), XRD method, and comments, into one line per sample. The data subset examined in this study consists of only XRD data within the HSUs of Upper Tuff Confining Unit (UTCU), Lower Tuff Confining Unit (LTCU), Oak Springs Butte Confining Unit (OSBCU), Argillic Tuff Confining Unit (ATCU), which are located predominantly in the hydrogeologic unit named as the Tuff Confining Unit (TCU). This results in a subset of 1,172 samples.

Information considered for each sample used in this study includes location (easting, northing, elevation), RMC, RMU, XRD method, mineral percentages of the reactive minerals calcite, hematite, mica, smectite, and zeolite, and mineral percentages of the non-reactive minerals glass, quartz, cristobalite, and tridymite. For most samples, the data do not include estimates of all of the above-mentioned mineral percentages, particularly hematite and tridymite. For a mineral percentage datum having no estimate, the datum is treated as a "null observation," not a zero value. It is essential to distinguish between either zero, low quantity (below detection limit), or null observation. Occurrence of null observations largely depends on the XRD method, analyst, and original objective for collecting the XRD data.

Reactive mineral percentage data in conjunction with the component additivity methodogy (Zavarin et al., 2004) are used to formulate K_d factors models of radionuclide transport. Non-reactive mineral percentage data are useful, where present, in distinguishing vitric or devitrified tuffs from zeolitic or argillic tuffs. As will be described in Chapter 5 through 7, the RMUs will form a primary basis for categorizing XRD data into reactive mineral facies (RMFs) for subsequent characterization of spatial variation of reactive mineral percentages and K_d distributions within the TCU as detailed in Chapters 8 through 10.

3.1 Location of HSUs and Wells with XRD Data

Figure 3-1 shows locations of drill holes having XRD data in the TCU in Yucca Flat superposed on cutaway block views of the TCU HSUs – UTCU, LTCU, OSBCU, and ATCU. The HSU grid was obtained from the Yucca Flat HSU model developed by

Bechtel Nevada (2006). The cutaway views reveal how the HSUs within the TCU are vertically displaced to varying elevations by faulting and deformation within Yucca Flat. Some of the vertical relief with the TCU HSUs is attributable to the morphology of tuff deposition, such as topography at time of deposition, proximity to source, and direction of depositional processes. The green colored areas represent HSUs above the TCU. Notably, the UTCU is usually separated vertically above the main portion of the TCU by HSUs distinguished as aquifer units not in the TCU – Topapah Spring Aquifer (TSA) and Lower-Vitric Tuff Aquifer (LVTA). The beginning of Section 5 and Figure 5-1 describe further details on TCU hydrostratigraphy.

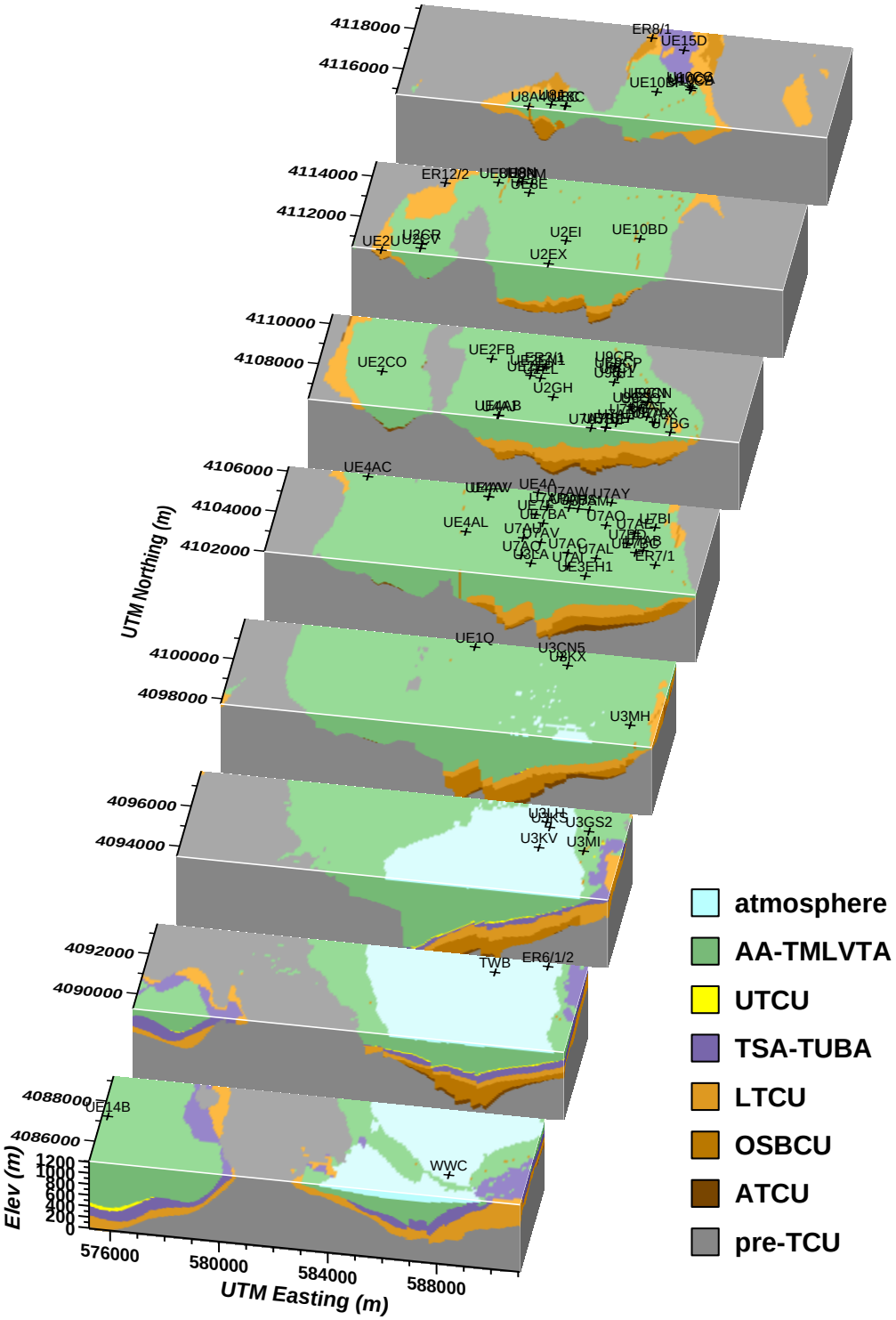

Figure 3-1. Location of drill holes with XRD data within TCU in Yucca Flat and vicinity.

3.2 Spatial Distribution of XRD Data

Figure 3-2 through Figure 3-11 plot XRD data for each reactive mineral on a cutaway block views for northern and southern portions of Yucca Flat. For this report, separation of views of Yucca Flat into northern and southern halves provides better resolution of data location compared to Figure 3-1. In these views, vertical exaggeration is raised from 2:1 to 4:1 compared to Figure 3-1 to improve visualization of vertical spatial variation of mineral percentages. Generally, the reactive mineral percentage data indicate more variability along the elevation axis compared to lateral directions. Two drill holes, UE-14b and ER-12-2, include data within HSUs of the TCU but are not located within Yucca Flat: (1) UE-14B is located in Mid Valley, and (2) ER-12-2 is located on Rainier Mesa.

3.2.1 Zonation

Prothro (2005) maps vertical mineral zonation in the TCU as consisting of three zones: (1) an upper zone characterized by abundance of the zeolite mineral clinoptilolite, (2) a middle zone with felsic minerals dominant over clinoptilolite and clay minerals, and (3) a basal argillic zone. This zonation results in an overall decrease in zeolite abundance and increase in smectite abundance with depth as evident in Figure 3-8 to Figure 3-11 . However, it is difficult to identify zonal boundaries from vertical profiles of the mineralogic percentage data alone because of large variations in mineral percentages of smectite and zeolite within the zones.

Identification of zonation associated with calcite, hematite, and mica is not obvious compared to smectite and zeolite. Figure 3-2 and Figure 3-3 show calcite percentage data. Most data indicate zero calcite. The majority of non-zero calcite data occur toward greater depth near central Yucca Flat typically at percentages of 3% or less. Hematite data show a similar pattern to calcite, with a majority of the data indicating zero hematite. Non-zero hematite data appears more abundant at greater depths in central Yucca Flat, typical at percentages of 3% or less. Figure 3-6 and Figure 3-7 indicate mica is generally ubiquitous throughout the TCU, with highest values ranging to 10%. Most of the high mica percentage data originate from the “E” method data, which is constitutes only 17% of the data. From visualization alone, it is difficult to determine whether the data indicate any zonation of mica abundance beyond variations that could be attributable to XRD method.

3.2.2 Data Clustering

Data clustering is an important consideration for statistical and geostatistical analysis. Figure 3-2 through Figure 3-11 indicate that many of the data are clustered in small volumes, particularly near east-central and northern Yucca Flat. Because of variation of well depths, the data can be preferentially sampled in shallow zones. Vertical data

spacing varies for different methods. Weighting of data values should be considered in statistical analysis to equalize effects of intensive sampling using certain methods or preferential locations. Figure 3-2 through Figure 3-11 indicate the "S" method data are relatively numerous and closely spaced and, thus, "S" data statistics could be affected by clustering.

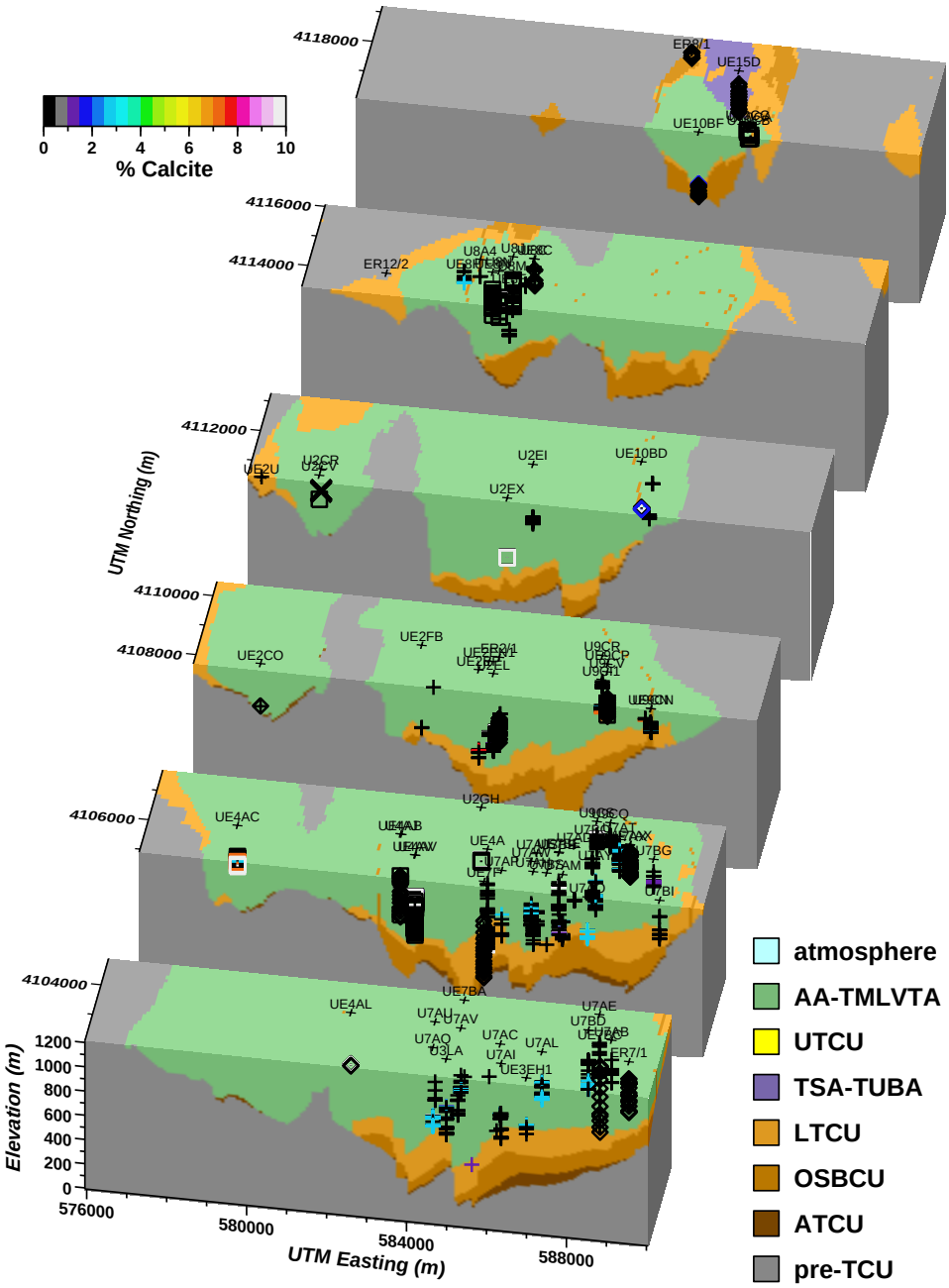

Figure 3-2. Locations and values of calcite percentage for XRD data within reactive mineral units of TCU in northern Yucca Flat. Percentages scaled by color. □, ◊, ×, and + symbols indicate data analyzed by E, F, I, and S methods, respectively.

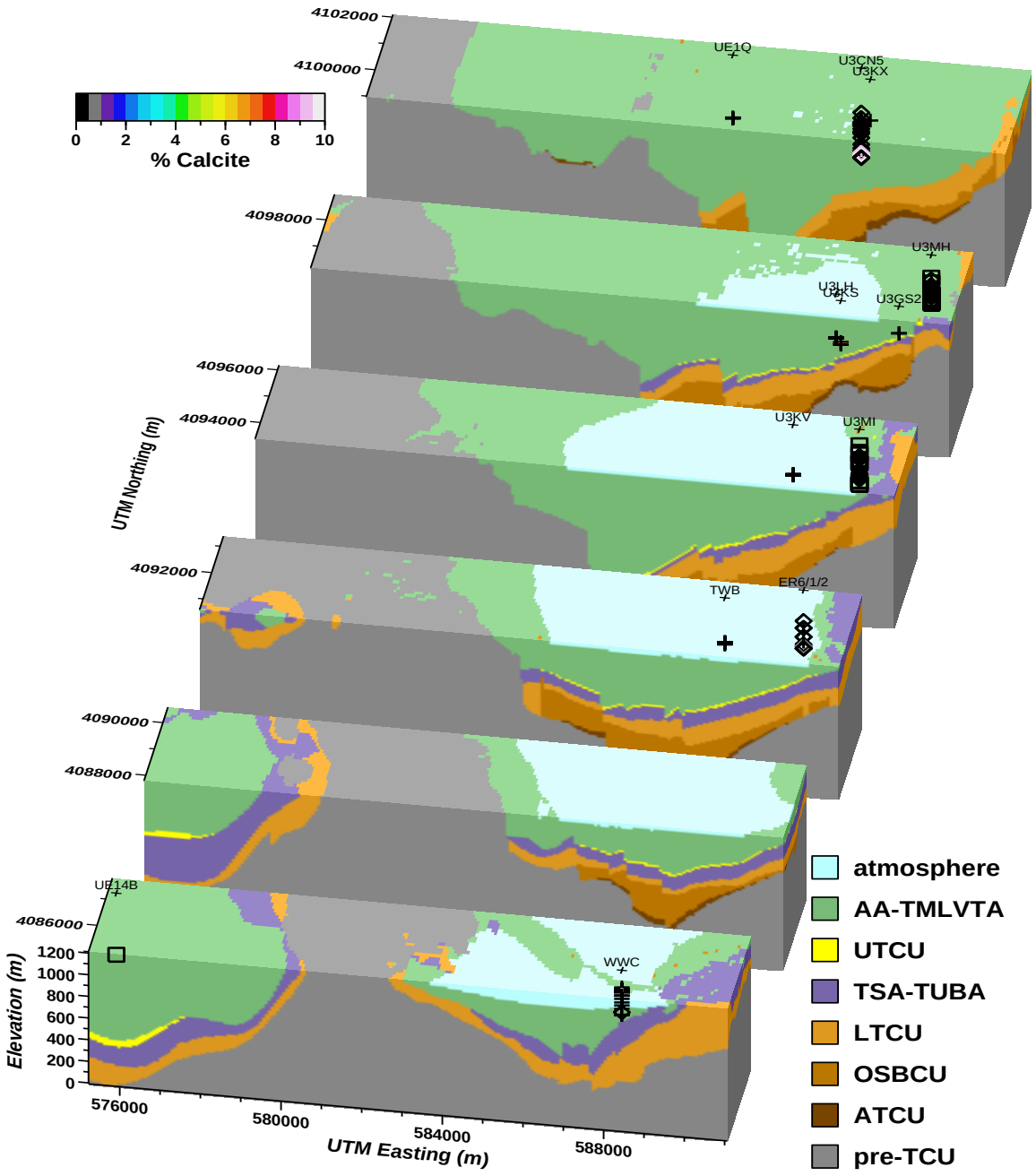

Figure 3-3. Location and values of calcite percentage for XRD data within reactive mineral units of TCU in southern Yucca Flat. Percentages scaled by color. □, ◊, ×, and + symbols indicate data analyzed by E, F, I, and S methods, respectively.

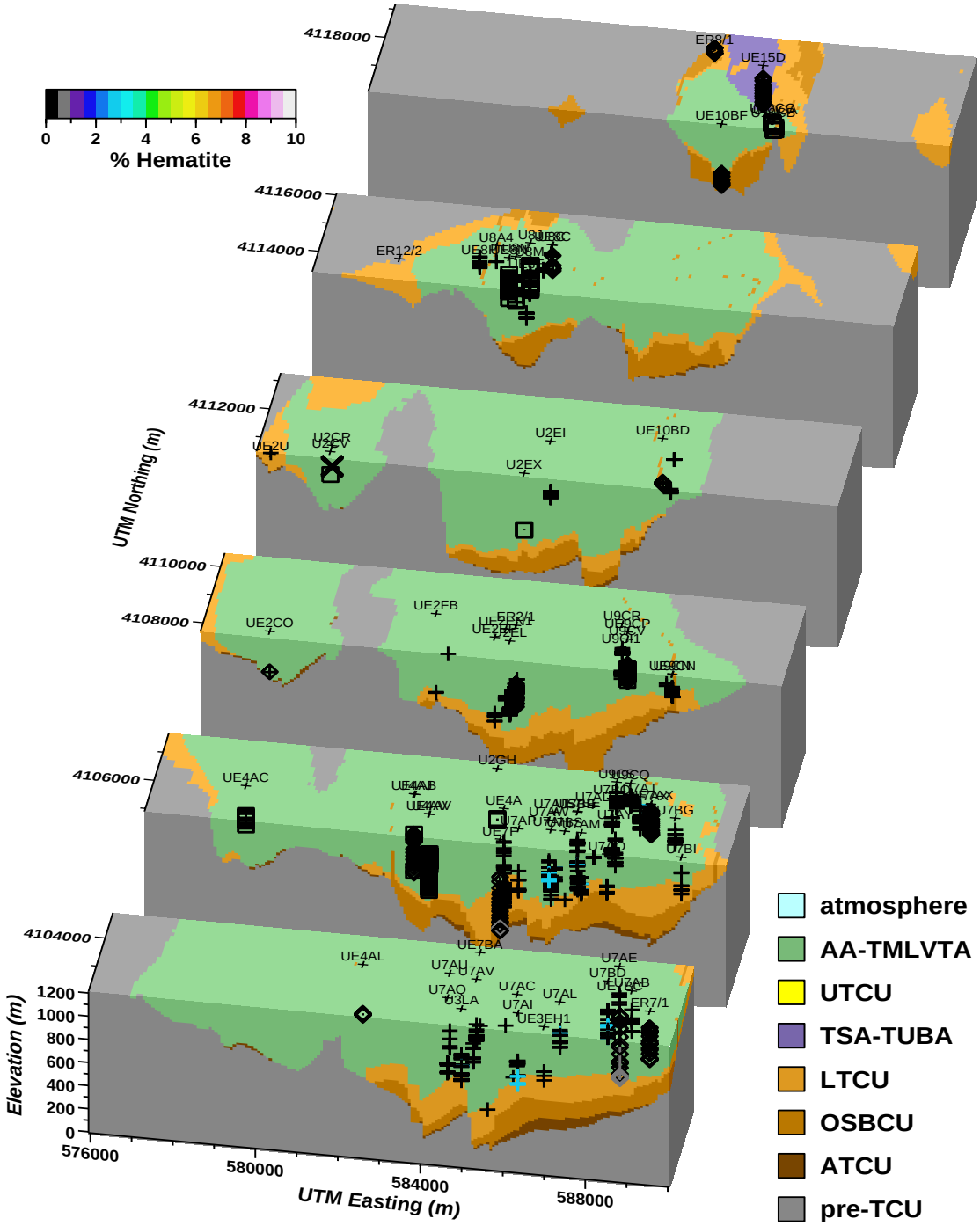

Figure 3-4. Location and values of hematite percentage for XRD data within reactive mineral units of TCU in northern Yucca Flat. Percentages scaled by color. □, ◊, ×, and + symbols indicate data analyzed by E, F, I, and S methods, respectively.

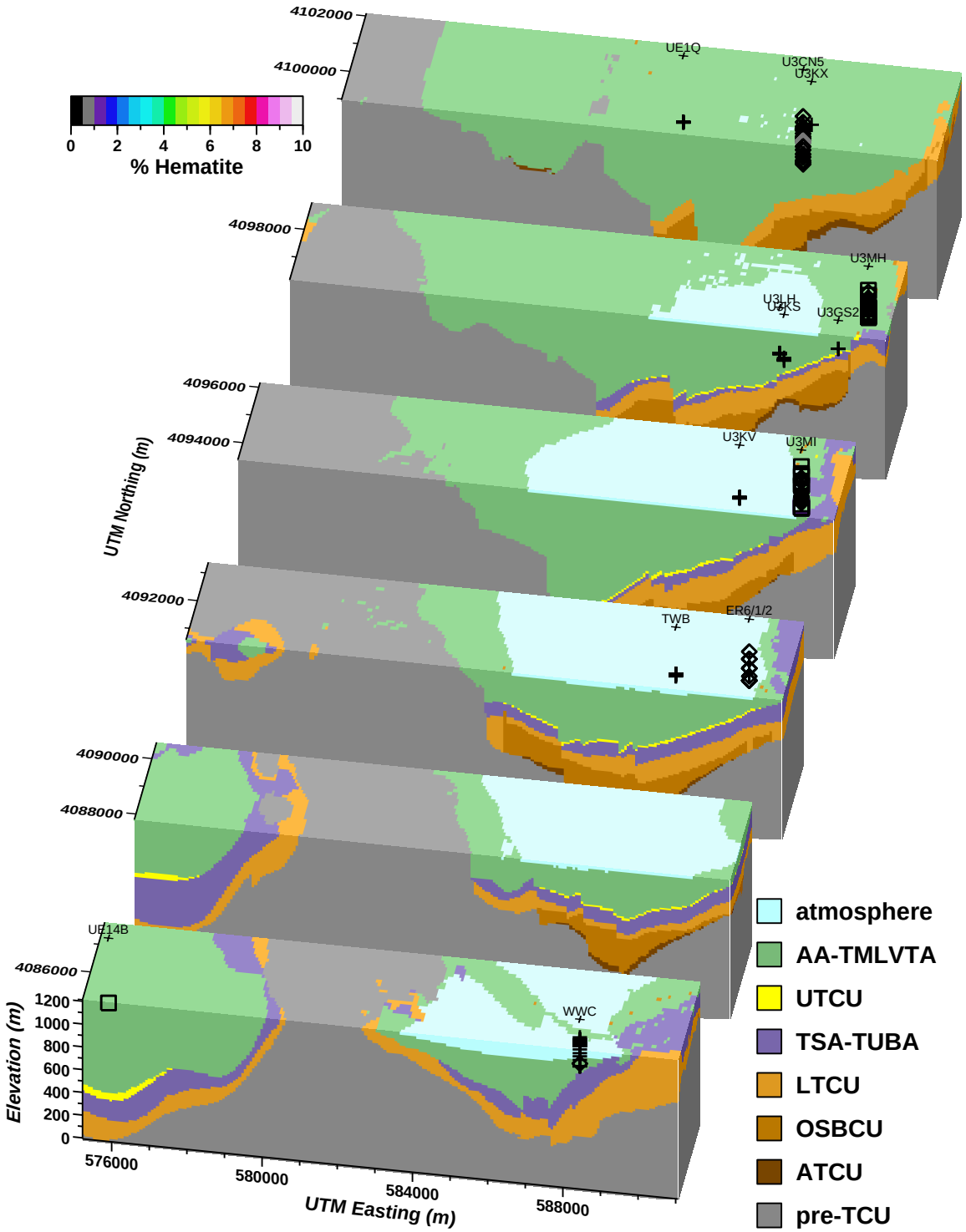

Figure 3-5. Location and values of hematite percentage for XRD data within reactive mineral units of TCU in southern Yucca Flat. Percentages scaled by color. □, ◊, ×, and + symbols indicate data analyzed by E, F, I, and S methods, respectively

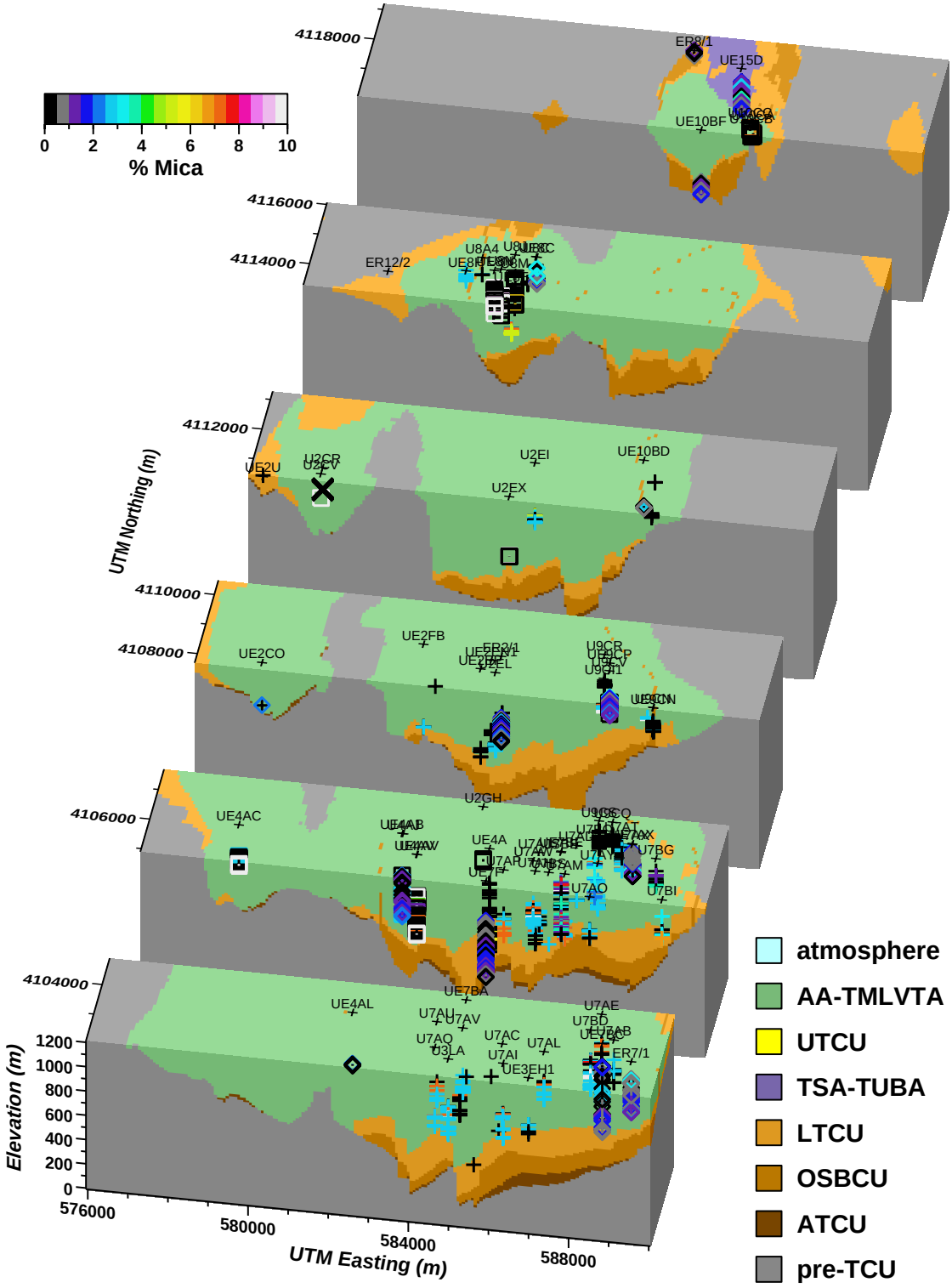

Figure 3-6. Location and values of mica percentage for XRD data within reactive mineral units of TCU in northern Yucca Flat. Percentages scaled by color. □, ◊, ×, and + symbols indicate data analyzed by E, F, I, and S methods, respectively.

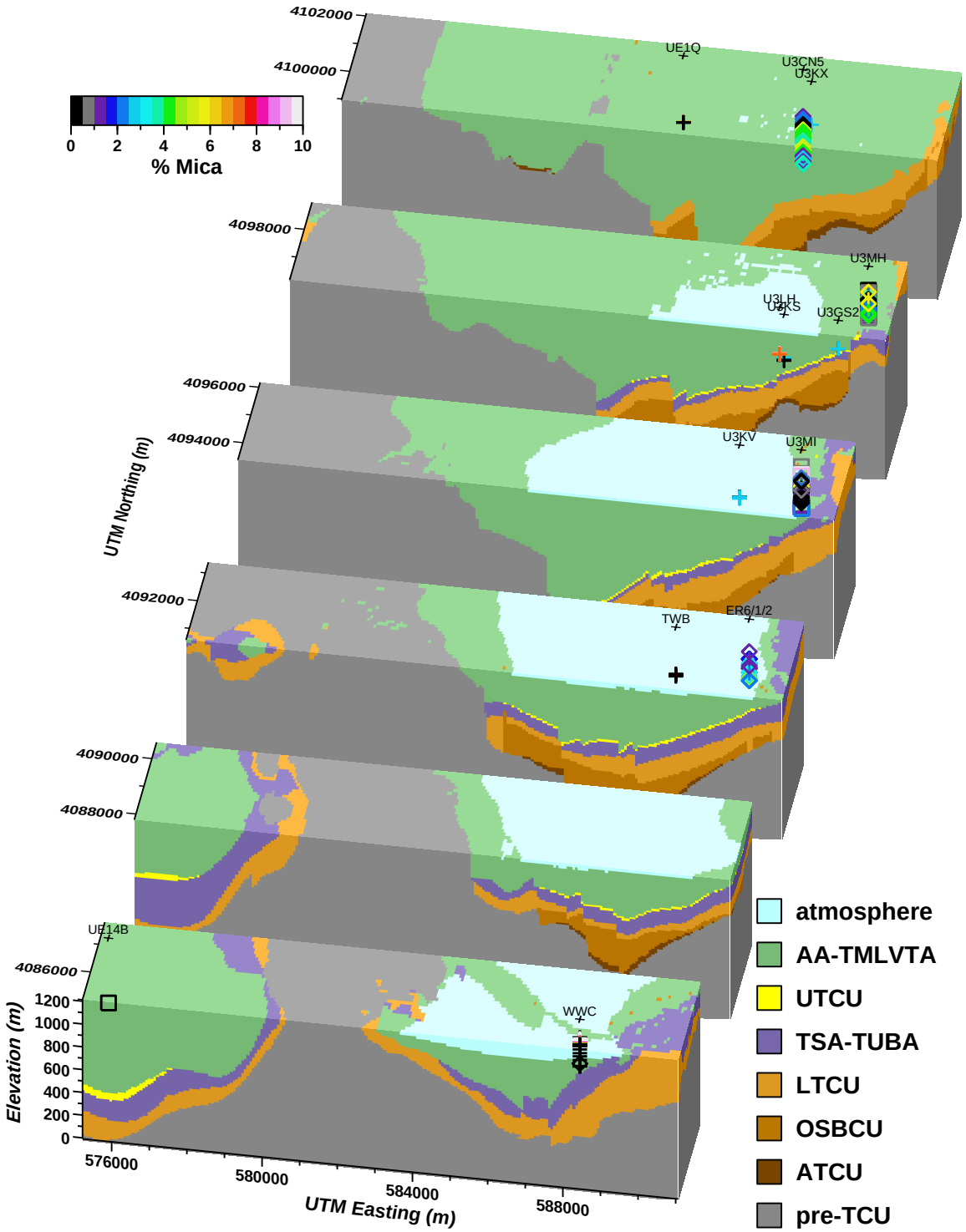

Figure 3-7. Location and values of mica percentage for XRD data within reactive mineral units of TCU in southern Yucca Flat. Percentages scaled by color. □, ◊, ×, and + symbols indicate data analyzed by E, F, I, and S methods, respectively.

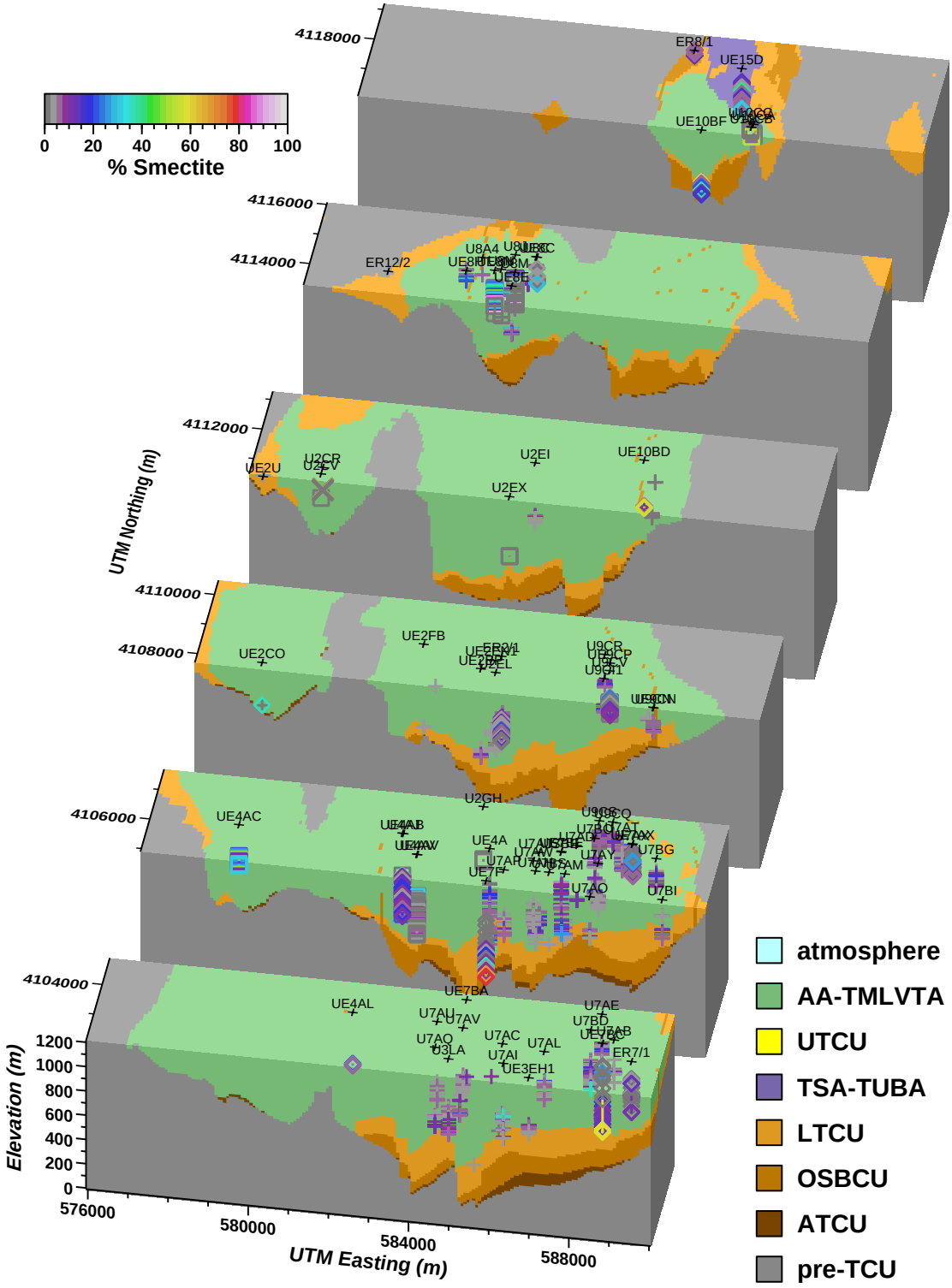

Figure 3-8. Location and values of smectite percentage for XRD data within reactive mineral units of TCU in northern Yucca Flat. Percentages scaled by color. □, ◊, ×, and + symbols indicate data analyzed by E, F, I, and S methods, respectively.

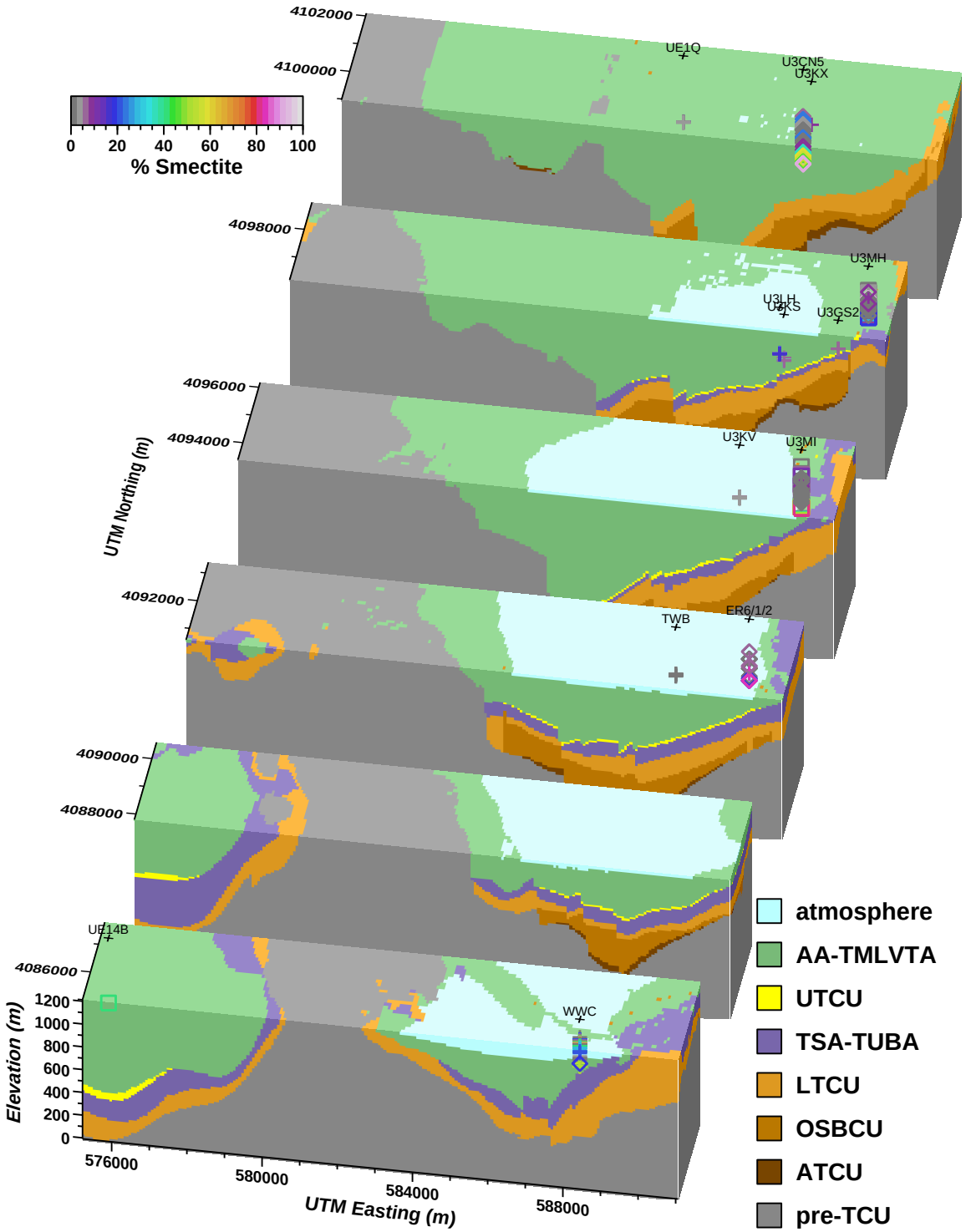

Figure 3-9. Location and values of smectite percentage for XRD data within reactive mineral units of TCU in southern Yucca Flat. □, ◊, ×, and + symbols indicate data analyzed by E, F, I, and S methods, respectively.

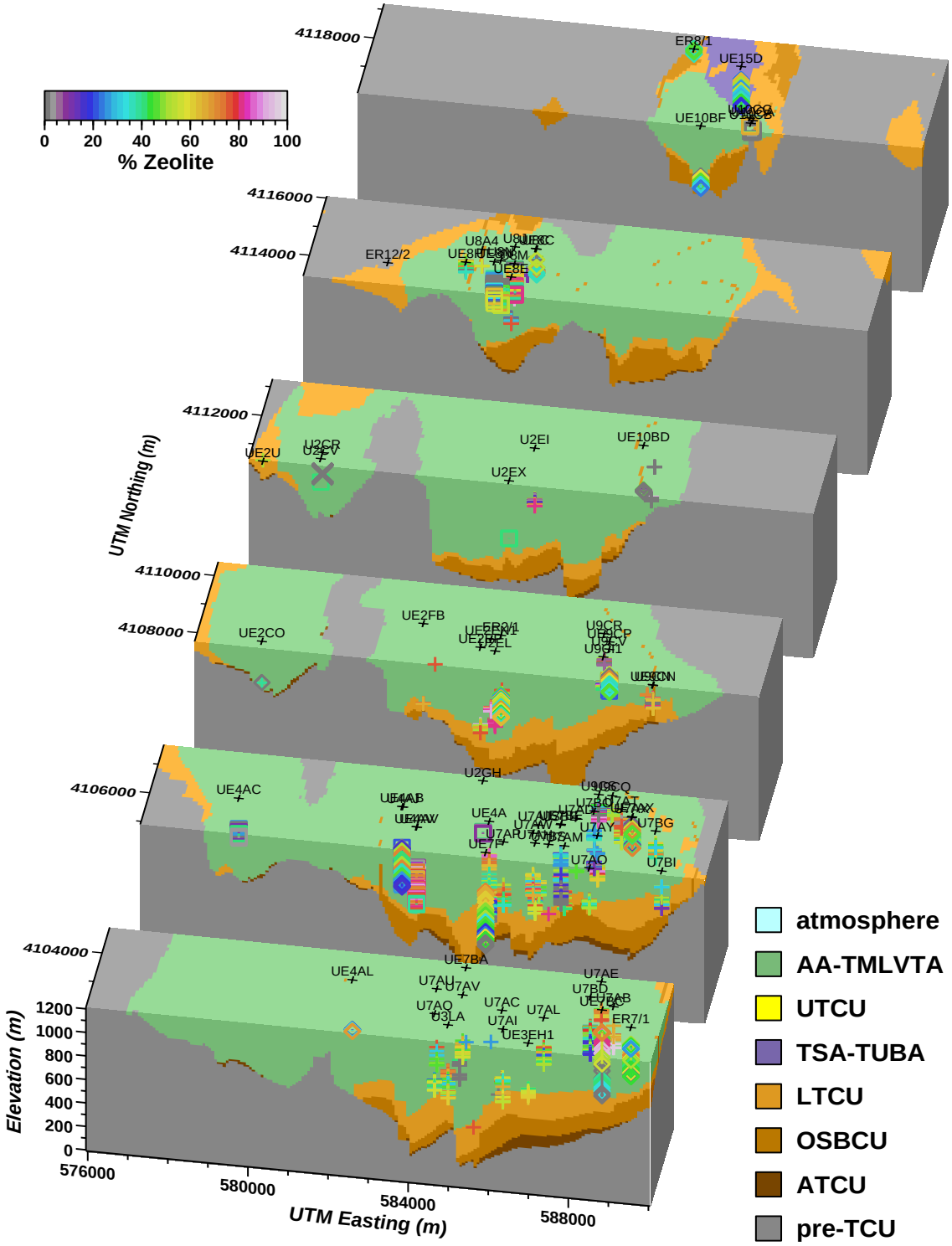

Figure 3-10. Location and values of zeolite percentage for XRD data within reactive mineral units of TCU in northern Yucca Flat. □, ◊, ×, and + symbols indicate data analyzed by E, F, I, and S methods, respectively.

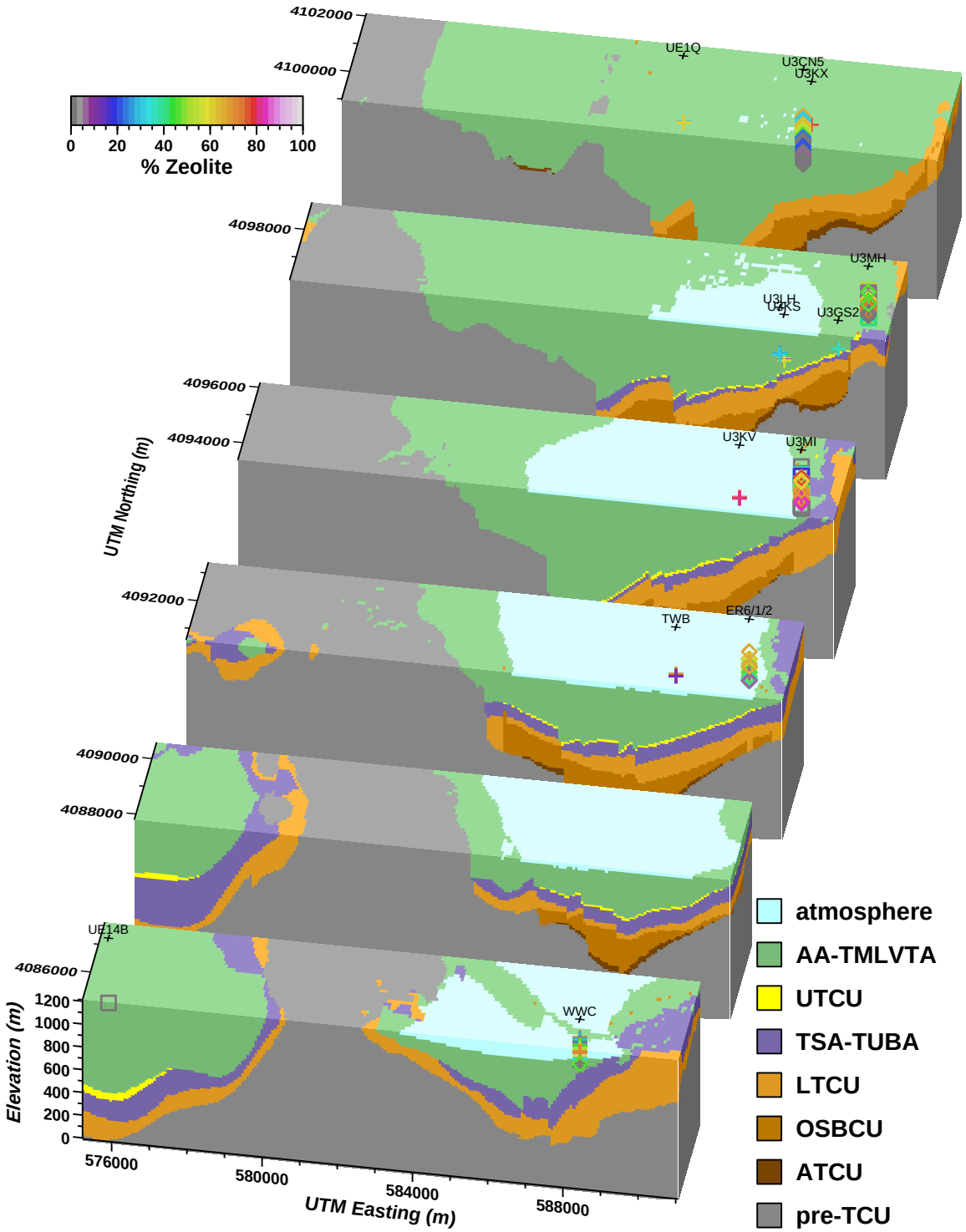

Figure 3-11. Location and values of zeolite percentage for XRD data within reactive mineral units of TCU in southern Yucca Flat. □, ◊, ×, and + symbols indicate data analyzed by E, F, I, and S methods, respectively.

3.3 XRD Methods and Considerations

As discussed above, the mineral percentage values in the XRD data subset analyzed in the study were generated by four different methods: "E" for external standard (Pawloski, 1983), "F", for full spectrum (Chipera and Bish, 2002), "I" for internal standard (Bish and Chipera, 1989), and "S" for subjective. Most "S" method data were generated by various analysts in the 1960s and 1970s. "S" data are quantified by ranges of mineralogic percentage and, thus, differ from "E", "F", and "I" data, which provide numerical estimates of the mineral percentage and, in some cases, a quantification of uncertainty (e.g., Pawloski, 1983). Warren (2007) assigned numerical estimates and uncertainties to "S" data based on the mode (mean of extreme values) of estimation ranges. Uncertainty in the XRD mineral percentage estimates has been reduced over time by technological advances in methodology, with the "F" data having least uncertainty (general within 1 to 2%) followed by "I" and "E" data. Further details on the methods and resulting effects on estimation uncertainty are discussed by Warren (2007).

Variation in data quality between the different methods presents several considerations to be addressed in performing geostatistical analyses:

- **Resolution.** "Resolution" in this report refers to the smallest mineral percentage that is resolved by the method. Each method has limited resolution, which further varies by analyst and technology. Furthermore, resolution is limited by the objectives of the original data analysis, such as whether or not certain minerals were carefully targeted for analysis. Resolution reflects the precision of the measurements, in particular the magnitude of variations in mineral percentage that can actually be detected. Importantly, resolution pertains also directly to the meaning of a "zero" value. The difference between the true mineral percentage and "zero" can span from a fraction of a percent to several percent depending on method resolution. This is particularly problematic for minerals that tend to occur in small non-zero percentages either ubiquitously, such as mica or smectite, or locally, such as calcite and hematite in the TCU. Furthermore, detection of small percentages is needed to define the low-valued portion of mineral frequency distributions. Small fractions of these minerals may actually exist, but remain undetected to various degrees because of variable resolution of the different methods.

- **Uncertainty.** All of the mineral percentage estimates are uncertain, and this uncertainty varies between methods and analysts. Uncertainty in the data will propagate to uncertainty in geostatistical analysis. In particular, the magnitude of a variogram measurement includes variation associated with both actual spatial variability and local uncertainty including data error.

- **Inconsistency.** The different XRD methods have different resolution and uncertainty, which limits feasibility of combining data from different methods to identify distinctive zones of mineralogic characteristics (e.g. Prothro, 2005). Inconsistency between data from different XRD methods limits feasibility of applying geostatistical methods to the pooled data set.

Limitations of data resolution are particularly problematic because characterizing the spatial distribution of low reactive mineral percentages is crucial to prediction of the more mobile regions of reactive transport. Analogously, characterization of the spatial distribution of high-permeability is crucial to prediction of flow behavior. For example, the TCU data set indicates that devitrified and vitric rocks associated with moderately welded to welded ash flow tuffs tend to have the lowest reactive mineral percentages. If ash flow tuffs are permeable, ash-flow tuffs could provide preferential transport pathways for sorbing radionuclide classes. Limitations in XRD data quantity, resolution, and uncertainty (which all vary by method) hamper prediction of the actual distributions of mineral percentages in localized zones, particularly those with the lowest reactive mineral percentages (e.g. devitrified or vitric tuffs).

The “F” and “S” method data provide the bulk of the most useful data on reactive mineral percentage distributions in the TCU. “S” data are the most numerous. However, given “S” data are based on estimates of percentage range, the “S” data have limited resolution and, thus, relatively lower accuracy and higher uncertainty at lower percentages compared to “F” data. “S” data are relatively accurate for high mineral percentages because the range of uncertainty is smaller relative to the magnitude. “E” data, while generally accurate at high percentage, suffer from poor resolution of low smectite percentages. This is problematic for estimation of K_d s for the 7of 10 radionuclide classes which have large dependence on smectite percentage. The “E” data have difficulty resolving the lower portion of the smectite frequency distribution in zeolitic, vitric, and devitrified tuffs. Only five “I” data are present in the TCU, and these are all within the ATCU.

In use and analysis of the TCU XRD data set, it is important to consider strengths and limitations of the different methods. For example it will be shown that after consideration of resolution limitations, the semi-quantitative “S” data provide similar reactive mineral frequency distributions in comparison to the most accurate “F” data. This is fortunate because the “S” data are far more abundant than the “F,” “I”, and “E” data. However, in conducting geostatistical analysis of spatial variability, the “S” data suffer from two main drawbacks: (1) larger uncertainty at small percentages and (2) systematic errors originating from assignment of constant values through vertical intervals or zones. The “S” data are useful defining distinguishing zones with similar mineral percentage characteristics, particularly zones characterized by high zeolite or smectite percentages.

However, the "S" data have limited value for interpreting spatial variability of K_d because data values estimated as the mode of a range impart false indications of spatial continuity.

3.4 Data Processing

Data processing relates to selection and handling of data used in the geostatistical analysis. Data spacing and quality affect geostatistical analysis. If data spacings are preferential to certain locations, the frequency distributions will be biased to the data values characteristic of locations with intensive sampling. For example, much of the "E" data were targeted in zones with low electrical resistivity with the objective of identifying clayey intervals. Data quality derives from the resolution and uncertainty of the data, which relates to sample quality and method and individual analyst as discussed above in Section 3.3.

3.4.1 Consideration of XRD Method

Plots of mineral percentage data with elevation for each drill hole indicate that data analyzed by the "S" method tend to produce continuous segments of identical percentage values, often with very close data spacing. In contrast, data analyzed by the "F" method, considered the most accurate, indicate that mineral percentage is variable over short distances. "E" data indicate mineral percentage is variable over short distances. However, "E" data lack resolution of smectite at low percentage.

For example, Figure 3-12 plots mineral percentage data for smectite, zeolite, and total felsic minerals in boreholes U9Cl1, U9CN, U9CQ, U9CR, U9CS, and U9CV of Area 9, Yucca Flat. These data fall within the Lower and Upper Tuff Confining Units (L-UTCU) and the Oak Springs Confining Unit (OSBCU), which are predominately zeolitized bedded tuffs. The "S" method was used for all data except for U9CV, where the "E" method was used. "S" method data produce continuous bands closely-spaced and like-valued data for smectite and zeolite percentage. Zero values for smectite and zeolite are plotted for reference at 0.12, and null observations are plotted at 0.11. Felsic mineral totals of {quartz + cristobalite + tridymite + feldspar}, indicators of devitrified tuffs, are plotted at 0.12 unless non-zero. Data for U9CV (triangle symbols), however, show wide variation of zeolite percentage and either zero values or wide variation of smectite percentage within vertical distances of a few meters. "E" data contain non-zero felsic totals, whereas "S" data are predominately zero values. Both "S" and "E" data show similar zeolite distributions. Limitations on resolution of low smectite percentage are apparent for both methods. Smectite percentages for "S" data lie at fixed values of 0, 3, 5, 8, 10, and up, indicating that "S" data resolve smectite percentage to about 2 to 3% at best. Smectite percentages for "E" data are usually zero or greater than 10%, indicating the "E" method detection limit for smectite is typically above 10%. The "S" data indicate

smectite percentage in the L-UTCU HSU is typically less than 10%. The “E” method does not appear to resolve the majority of the true non-zero portion of the smectite frequency distribution in the L-UTCU. The “E” data contain key silicate mineral percentages, particularly quartz, cristobalite, tridymite, and fedspar, useful for distinguishing devitrified tuffs from zeolitic, argillic, or vitric tuffs. The “S” data typically lacks silicate mineral percentages, making it less useful for distinction of devitrified tuffs.

Data processing decisions in this study were made in light of the variable quality of the data, including how data quality will affect distinction of zones with consistent statistical properties of reactive mineral and K_d spatial variability, namely “reactive mineral facies” or “RMFs” as will be detailed in Chapter 6. The main factors in distinguishing RMFs are prior classification of samples by “reactive mineral unit” or “RMU” as described by Stoller-Navarro (2007) combined with measures of vitric, devitrified, and argillic characteristics detailed in Chapter 6. The vitric, devitrified, and argillic characteristics used to distinguish RMFs are different than the “reactive mineral category” (RMC) categories described by Stoller-Navarro (2007). However, since prior classification of RMC’s is defined by abundances of reactive minerals related to mafic, vitric, and devitrified characteristics, RMC criteria partially overlap with RMFs. In particular, estimates of glass percentage are useful in distinguishing vitric from non-vitric facies, and estimates of silicate mineral percentages are useful in distinguishing devitrified facies from non-devitrified facies.

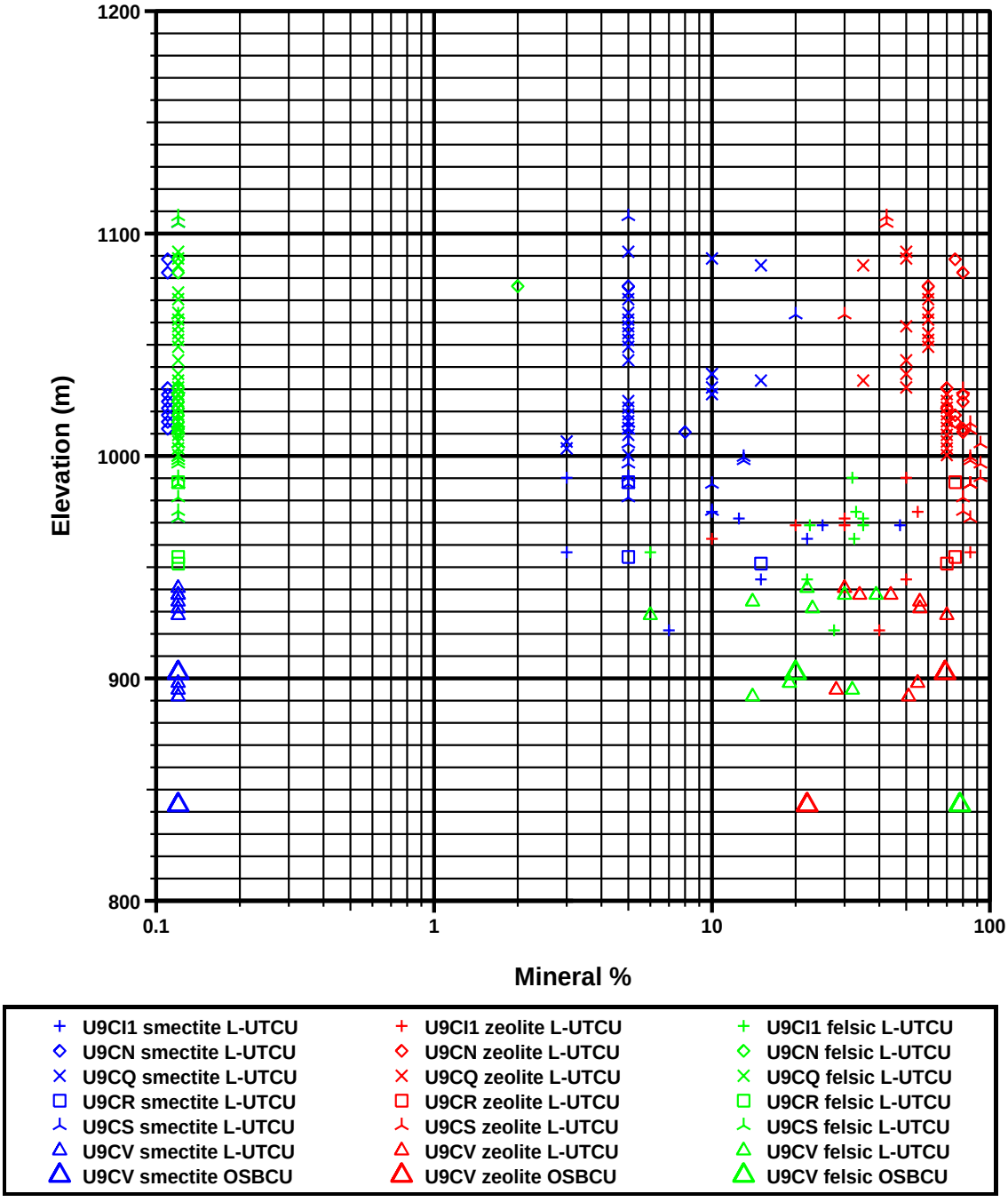

Figure 3-12. XRD mineral percentages for smectite, zeolite, and total felsic minerals (quartz, cristobalite, tridymite, and feldspar) for selected Area 9 drill holes in Yucca Flat. Zero values are plotted at a value of 0.12 and null observations are plotted at a value of 0.11.

3.4.2 Total Mineral Percentage

Fundamentally, we assume that the "F" data (the most accurate data) have sufficient resolution of reactive mineral percentages to establish spatial variability of K_d, whereas the variable quality and quantity of "E", "I", and "S" data may limit characterization of spatial variability of K_d. One indication of data quality is the total of the reactive mineral percentages, which ideally would sum to 100%. However, importance of total percentage can be deceiving for any XRD data where some mineral percentages were not analyzed for (null observations). Using only total percentage as a means to filter out data of poor quality can lead to bias toward data with higher percentages of the few minerals analyzed for, such as zeolite and smectite. Ultimately, this bias would lead toward overestimation of K_d and insufficient attention to characterization of zones with low K_d and, hence, greater radionuclide mobility. Concern for bias is particularly pertinent to "S" data, which is commonly limited to analysis of selected minerals. To avoid bias, this study utilizes all "S" data regardless of total percentage except where zero, and minerals not analyzed for are treated as null observations, not zero values.

In data processing for computation of additive log ratio (Sections 3.4.4 and 6.1) and K_d, the total percentage of minerals is factored into consideration as follows:

- Resolution of the total is assumed to be 2% for F data and 5% for S data.
- If the total of reactive mineral percentages is less than or equal to [100% - resolution], the exact value of the data is used in all further data processing.
- If the total of reactive mineral percentages is greater than or equal to [100% - resolution], the reactive mineral percentages are renormalized by multiplication by a factor of 100%/[100% - resolution].

The above procedure ensures that reactive mineral totals remained less than 100%, which is necessary for implementation of additive log ratio methods (Sections 3.4.4 and 6.1). Furthermore, given limited resolution of the methods, it is realistic to assume that the true percentage of non-reactive minerals is at least a small non-zero percentage.

3.4.3 Compositional Data

The term "compositional data" refers to vector data with components that sum to a constant value, usually unity or 100%. Mineral percentage data, therefore, are compositional data with mineral percentages as components of the vector, where the total of the components is, ideally, 100%.

Application of geostatistical methods to compositional data is not straightforward. The summing constraint inherent to compositional data causes singularity in cokriging equations formulated by cross-covariance matrices of compositional data. The summing

constraint also produces spurious cross-correlations not indicative of a legitimate statistical cross-correlation. Frequency distributions for compositional data are bounded (e.g., between 0 and 100%) and are typically skewed (on either linear or logarithmic scales) and, thus, do not fit the classical geostatistical assumption of a Gaussian distribution.

3.4.4 Additive Log Ratio

Criteria for distinction of reactive mineral facies (RMFs) will substantially rely on use of the "additive log ratio" (ALR) transformation. As described in detail in Section 6.1, the ALR transformation is recommended in geostatistical analysis of compositional data (Aitchison 1986; Pawlosky-Glahn and Olea, 2004; Aitchison, 2007).

In practice, the ALR is defined as the logarithm of the ratio between fractions (or percentages) of a component and the complement of the sum of component fractions analyzed. The ALR is applied to a finite number of components open to interpretation. Any base of logarithm, such as natural or base 10, can be used in the ALR. Base 10 scalability is more readily interpretable and will be used exclusively in this study. In ALR analysis of reactive mineral distributions, the components analyzed may be logically limited to the reactive minerals such that the complement (or non-reactive percentage) will be [100% – sum of reactive mineral percentages] as follows:

$$ALR(\text{reactive mineral } i) = \log_{10}\left[\frac{\%\text{reactive mineral } i}{100\% - \sum_{j}^{n} \%\text{reactive mineral } j}\right],$$

where "*n*" is the number of reactive minerals. Compositional data analysis for reactive mineral distributions using the ALR could, conceivably, extend to other key minerals, such as glass or felsic minerals, that are instrumental to distinguishing RMFs.

3.5 Basic Statistics and Frequency Distributions

In this section, basic statistics and frequency distributions for the entire TCU XRD data set are examined irrespective of data location, bias, method, or lithology. Further analysis in Chapters 4 through 7 consider data location, bias, method, and lithology in grouping data by reactive mineral categories (RMCs), reactive mineral units (RMUs), and reactive mineral facies (RMFs). The purpose of this section is to obtain a preliminary understanding of the characteristics of reactive mineral frequency distributions for the entire TCU data set.

The frequency distributions of reactive minerals will be evaluated in three scales: linear, logarithmic (base 10), and logarithmic of reactive/non-reactive ratio or "additive log ratio" (ALR). Each scale offers certain advantages and disadvantages. Ultimately, this geostatistical study needs a scale of measurement that is amenable to geostatistical analysis of discrete populations of data. For example, if the data are to be analyzed as a continuous random variable, a Gaussian frequency distribution for the random variable is preferable. Non-parametric geostatistical approaches can be applied to non-Gaussian frequency distributions, however, non-parametric approaches require more complicated model development. Moreover, separation of the data into discrete populations is a key step for identification of mineralization zones with distinctive radionuclide transport properties.

3.5.1 Linear Scaling

Table 3-1 gives basic statistics of reactive mineral percentage for the reactive minerals - calcite, hematite, mica, smectite, and zeolite. The "skewness" statistic indicates degree of asymmetry or tailing in the distribution, with positive skewness indicating tailing toward high data values, negative skewness indicating tailing toward low data values, and zero skewness indicating a symmetric distribution. Figure 3-13 shows TCU XRD data frequency distributions of reactive mineral percentages plotted on a linear scale. Data entries without numerical values are treated as "null observations" assuming the corresponding minerals were not analyzed for in the sample record. Typically for "S" method data, not all reactive minerals were analyzed for, particularly calcite and hematite. Notably, 1,151 of 1,172 XRD data contain analyses for zeolite, while only 228 of 1,172 XRD contain analyses for hematite. Generally, the linear scale frequency distributions indicate relative abundance of reactive minerals in the TCU:

- Calcite percentages are usually (84%) zero. Where non-zero, calcite abundance is usually only a few percent.
- Like calcite, hematite percentages are usually (84%) zero and, where non-zero, hematite abundance is usually only a few percent. Hematite is usually not analyzed for, with only about 19% of the data containing hematite percentage estimates.
- Mica percentages are usually (64%) non-zero and typically limited to a few percent.
- Smectite percentages are usually (88%) non-zero and vary from a few percent to a few tens of percent. The overall smectite frequency distribution is clearly skewed right on a linear scale.

- Zeolite percentages are usually (92%) non-zero and on the order of few tens of percent. The zeolite data frequency distribution has the most Gaussian-like distribution on a linear scale compared to other reactive minerals. The zeolite frequency distribution has obvious peaks and valleys, much of which is related to "S" method resolution (see Section 3.3)

On the linear scale, it is difficult to determine whether the frequency distributions are multi-modal (composed of different populations or zones), particularly in relation to the low mineral percentages.

Table 3-1. Basic statistics for reactive mineral percentages in TCU XRD data set.

Mineral	Calcite	Hematite	Mica	Smectite	Zeolite
#Data	836	228	1,024	1,145	1,151
Mean	0.82	0.29	2.24	9.63	44.46
Abs. Dev.	1.39	0.48	1.91	8.45	22.70
Std. Dev.	3.65	0.84	3.29	13.66	26.93
Skewness	9.56	3.83	4.23	3.19	-0.26

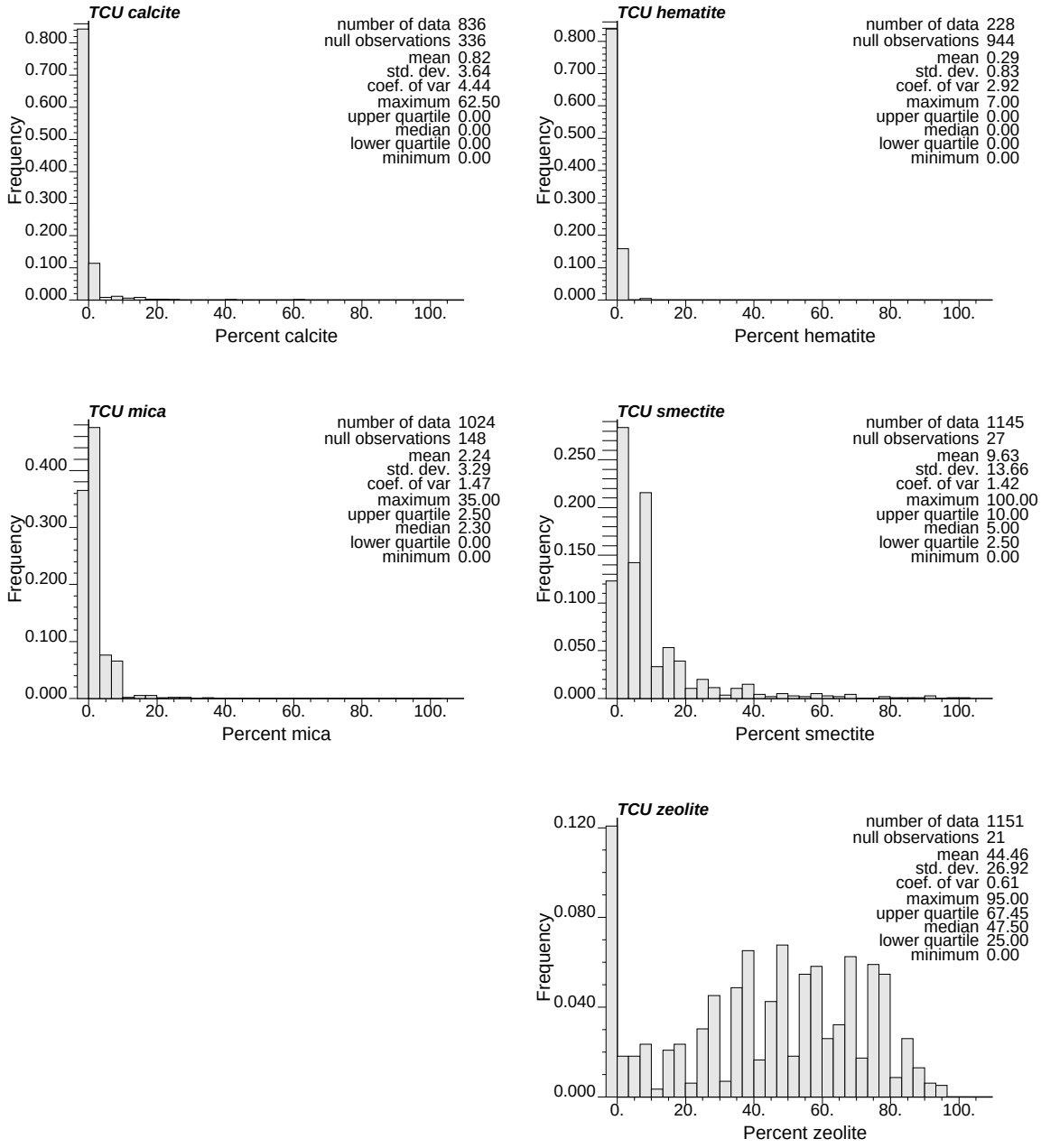

Figure 3-13. Linear-scale frequency distributions of reactive mineral percentage for all TCU data including E, F, I, and S methods.

3.5.2 Logarithmic Scaling

Table 3-2 gives basic statistics of reactive mineral percentage for the reactive minerals - calcite, hematite, mica, smectite, and zeolite. Figure 3-14 shows the TCU XRD data frequency distributions plotted on a logarithmic scale. Zero values are plotted as below 0.1 to enable inclusion in the logarithmic frequency plots. Other than zero values, no

XRD data actually have values less than or equal to 0.1. The logarithmic-scaled plots improve visualization of the frequency distributions for data with low percentages, particularly calcite, hematite, and mica. Mica and smectite logarithmic-scaled frequency distributions show potential to be characterized by Gaussian distribution(s). The zeolite frequency distribution, however, appears tailed strongly left (negatively skewed) on the logarithmic scale.

Because mica generally occurs in low percentage, a large proportion of the "zero" values are likely non-zero quantities below the detection limits of the various methods. Similarly, many "zero" data for smectite could be non-zero quantities. Strong negative skewness, including low and zero zeolite percentages, in the zeolite frequency distribution is indicative of a bi-modal distribution between zeolitic and non-zeolitic (e.g. devitrified, argillic, or vitric) populations.

While logarithmic scaling is often used to apply statistical techniques to compositional data, questions arise in examining logarithmic-scaled bulk reactive mineral percentage distributions in the TCU:

- How should zero-valued data be treated?
- How can skewed distributions, particularly for zeolite, be addressed?
- How can finite (<100%) distributions be addressed?

Use of the additive log ratio (ALR) transformation provides a first step toward addressing skewed and finite distributions (Section 3.5.3). As previously discussed in Section 3.3, addressing zero-valued data will require careful consideration of the XRD methods and understanding of the relationship of reactive mineral distributions to rock characteristics. Previous interpretations of XRD data by Stoller Navarro (2007) using reactive mineral categories (RMCs) and reactive mineral facies (RMFs) must be examined to gain insight on characterization of reactive mineral distributions in the TCU (Chapters 4 and 5).

Table 3-2. Basic statistics for $\log_{10}$ {reactive mineral percentage} of non-zero data in TCU XRD data set.

Mineral	Calcite	Hematite	Mica	Smectite	Zeolite
#Data	131	37	650	1,004	1,012
Mean	0.46	0.08	0.43	0.81	1.62
Abs. Dev.	0.32	0.37	0.20	0.35	0.23
Std. Dev.	0.47	0.45	0.31	0.45	0.34
Skewness	0.01	-0.89	-0.18	0.05	-2.52

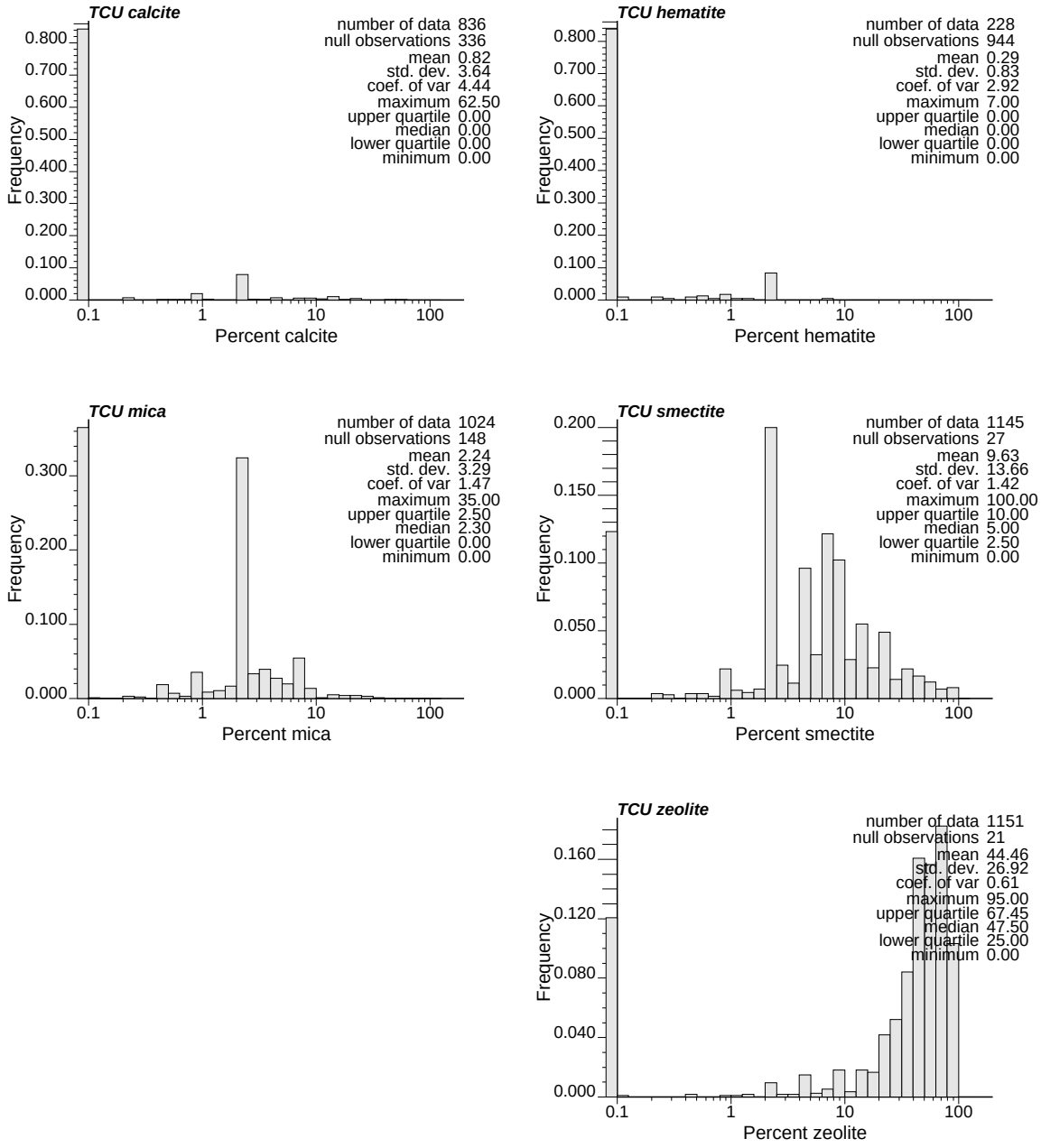

Figure 3-14. Logarithmic-scale frequency distributions of reactive mineral percentage for all TCU data including E, F, I, and S methods.

3.5.3 ALR Scaling

Table 3-3 gives basic statistics of the additive log ratio (ALR) for the reactive minerals - calcite, hematite, mica, smectite, and zeolite. Figure 3-15 shows the TCU XRD data plotted as the logarithm (base 10) of the reactive/non-reactive mineral ratio. This approach utilizes the additive log ratio (ALR) approach advocated by Aitchison(1986)

and Pawlosky-Glahn and Olea(2004) for geostatistical analysis of compositional data (see Sections 3.4.4 and 6.1). The ALR approach produces frequency distributions with Gaussian or multi-Gaussian-like characteristics for all three of the reactive minerals with relatively ubiquitous characteristics - mica, smectite, and zeolite. The ALR approach potentially offers a single framework for characterizing frequency distributions of reactive minerals in the TCU (as opposed to characterizing some mineral distribution in a linear scale and others in a logarithmic scale).

Table 3-3. Basic statistics for additive log ratio (ALR) in TCU XRD data set for non-zero values.

Mineral	Calcite	Hematite	Mica	Smectite	Zeolite
#Data	131	37	650	1,004	1,012
Mean	-1.15	-1.58	-1.17	-0.75	0.09
Abs. Dev.	0.38	0.41	0.28	0.38	0.40
Std. Dev.	0.53	0.50	0.38	0.50	0.55
Skewness	0.03	-0.81	0.09	0.49	-0.89

In Figure 3-15, the zero valued reactive mineral percentages are assigned values of -3.0, considering that no measured ALRs reached as low as -3.0. Left tails of ALR frequency distributions diminish rapidly below about -1.0 to -1.5, indicating the lower limits of the XRD methods detect reactive/non-reactive mineral ratios down to about 1:10 to 1:30. ALR values as low as -2.0 are rare and can be explained, for example, by a very low non-zero reactive mineral percentage (e.g. 1.0 or less) percent combined with other reactive mineral percentages equaling zero.

ALR frequency distributions associated with non-zero data are generally bell-shaped for mica, smectite, and zeolite. The ALR transformation permits infinite tails on *both* sides of the frequency distribution, unlike the linear and logarithmic scales. Frequency distributions for calcite and hematite remain difficult to characterize because of predominately zero-value data with typically low calcite and hematite percentages where non-zero. Mica data show near-zero skewness, smectite data show slight right skewness, while non-zero zeolite data show prominent negative skew. Right skewness for smectite frequency distribution could relate, in part, to the lack of resolution for low smectite percentages. The large negative ALR skewness for zeolite appears related to bi-modal characteristics in the frequency distribution. Even if the ALR frequency distributions appear Gaussian, multiple sub-populations or zones with Gaussian frequency distributions may

exist.

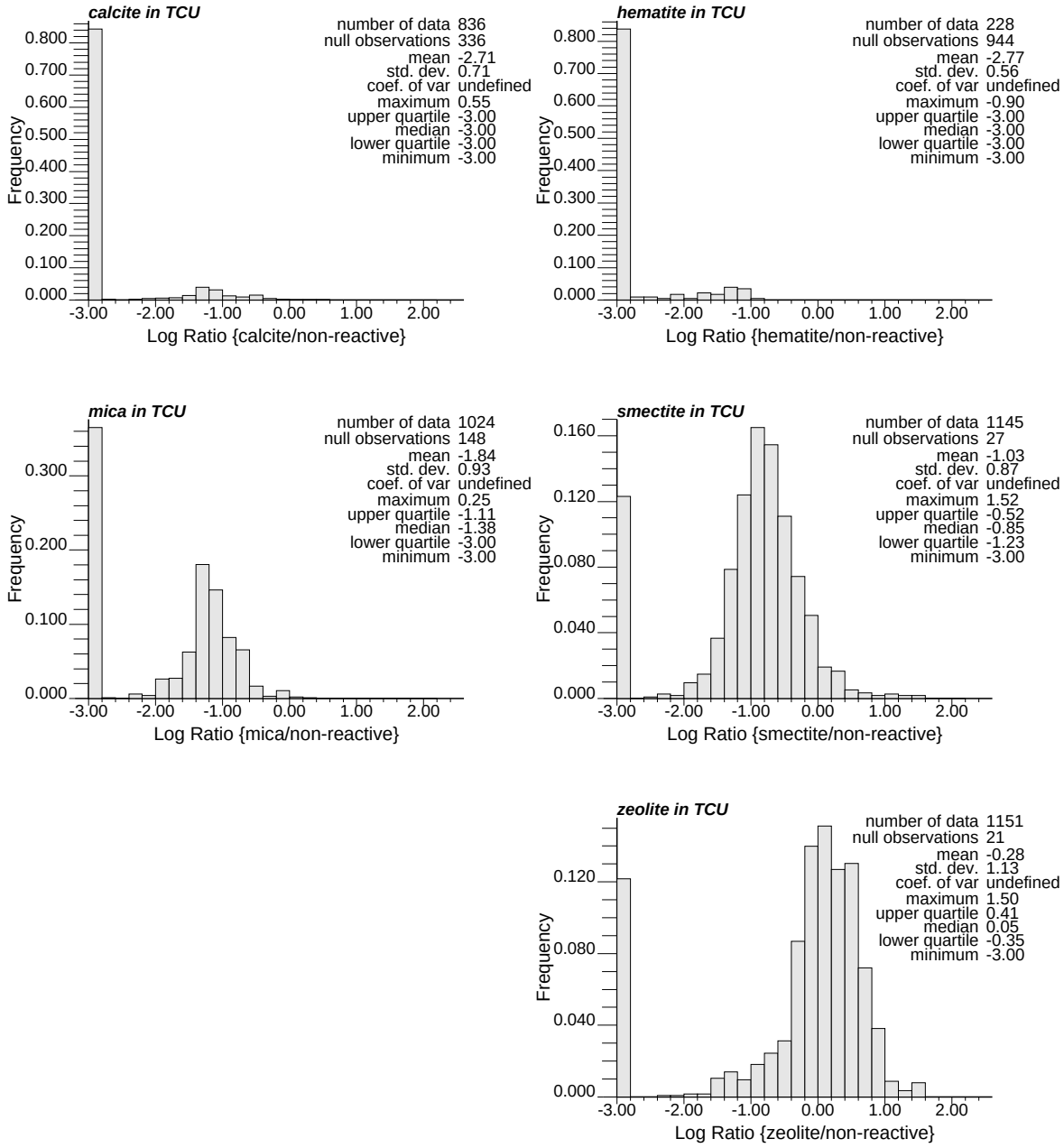

Figure 3-15. Frequency distributions of log ratio reactive/non-reactive mineral percentage for all TCU data including E, F, I, and S methods.

Similar to the logarithmic approach, the topic of "how to treat zero values" in the data is a very important consideration in applying the ALR approach. This topic will be examined in greater detail in Section 7.2. Preliminarily, Figure 3-16 examines the simplified assumption of fitting a Gaussian distribution to ALR values for non-zero data, by treating zero-valued data as "null observations". A Gaussian distribution appears to provide a

reasonable fit to all non-zero ALR transformed data. A naïve statistical approach might examine only these non-zero data, given that a Gaussian assumption could be justified, without consideration of geological and data quality aspects. Consideration of geology and data quality raises important issues open to interpretation:

- The calcite and hematite ALR frequency distributions remain difficult to interpret because typical calcite and hematite percentages in the TCU are at or below XRD detection limits.

- A significant proportion of mica, smectite, and zeolite data have zero values, but it is plausible that a large proportion of the zero-valued data represent non-zero percentages below the detection limit. This issue is particularly important to characterization of mica distributions because mica is typically present in low percentages near or below the detection limit. Much of the zero-valued mica data could represent non-zero mica percentage below the detection limit.

- The smectite ALR frequency distribution appears to fit a Gaussian distribution very closely for all TCU data. However, this fit could be very deceiving. An argillic zone having high smectite percentage is known to occur at the base of the TCU. Since the argillic zone is deepest, it tends to have the lowest density of sampling within the TCU (relatively fewer deep drill holes and samples chosen for XRD analysis). Thus, many of the high ALR values for smectite may be underrepresented by the composite TCU data set.

- The zeolite ALR frequency distribution shows a pronounced left skew. This skewness and other deviations from a Gaussian distribution for all reactive mineral frequency distributions could be caused by combinations of different populations of data representing different zones within the TCU (Prothro, 2005). For example, the abundant bedded tuffs within middle to upper portions of the TCU are predominantly zeolitic. However, there are patterns of zeolite abundance related to lithologic and diagenetic processes. Zeolite abundance tends to increase upward within the TCU except for welded or vitric ash-flow tuffs, which tend to contain higher felsic or glass proportions and lower zeolite proportions.

To address geologic and data quality issues, Chapters 4, 5, and 7 re-evaluate reactive mineral frequency distributions in relation to sub-populations or zones defined by RMCs, RMUs, and RMFs, respectively.

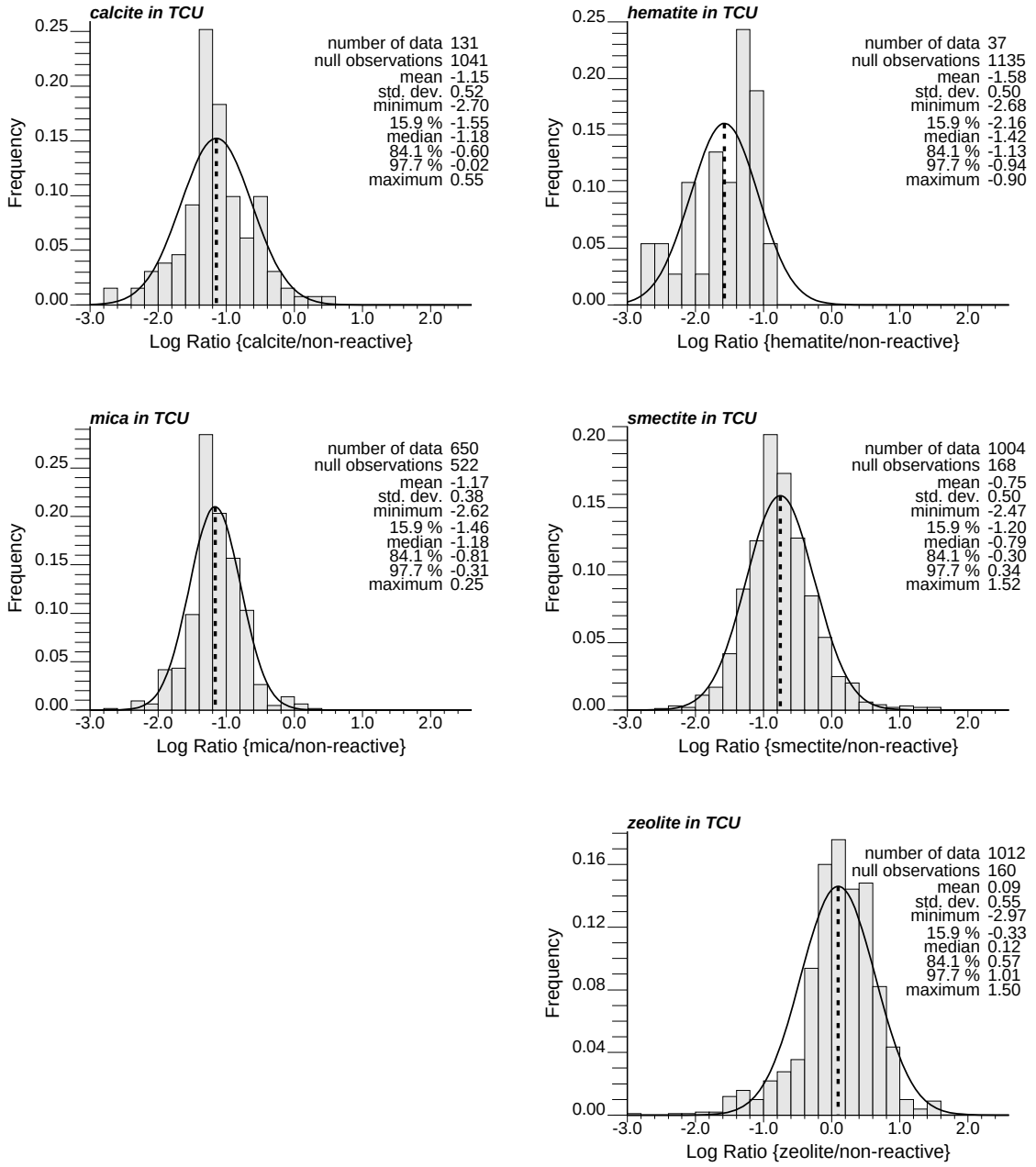

Figure 3-16. Frequency distributions of log ratio reactive/non-reactive mineral percentage for all TCU non-zero reactive mineral percentage data including E, F, I, and S methods, with Gaussian distribution fit to mean and variance.

4. Reactive Minerals in RMCs

Reactive mineral categories (RMCs) have been defined by Stoller-Navarro (2007) to categorize discrete populations of data for assignment of K_d properties in transport models based largely on reactive and non-reactive mineral percentage cutoffs. Table 4-1 summarizes the criteria for definition of the six major RMCs present in the TCU – argillic (ARG), zeolitic (ZEOL), devitrified mafic poor (DMP), devitrified mafic rich (DMR), vitric mafic poor (VMP), and vitric mafic rich (VMR). One RMC atypical to the TCU, carbonate (CC), represents only one sample in the TCU.

Table 4-2 shows the number and fraction of reactive mineral percentage data sorted by RMC. The majority (72.6%) of mineralogic data are categorized into the ZEOL (zeolitic) RMC. Considering 62 data have no RMC categorization because of incomplete mineral percentages as discussed in Section 4.2.1, the proportion of ZEOL RMC data rises to 77.7% for data with an RMC categorization. The preponderance of ZEOL RMC data is explained by two primary factors: (1) the majority of the volume of the TCU consists of zeolitized bedded tuffs, and (2) the zeolitized bedded tuffs occur in the middle to upper formations of the TCU where more data have been obtained relative to lower formations. Of the remaining 27.4% of the mineralogic data, the second largest data fraction of 9.0% is categorized into ARG. Most ARG data are obtained from the lower, argillic portion of the TCU, although some portions of the zeolitized bedded tuffs are categorized into ARG. The remaining data fractions are in order of size are DMR (6.1%), no RMC (5.3%), DMP (4.0%), VMP (1.5%), and VMR (1.2%). The single datum occurrence of the CC (carbonate) RMC, while observed within the TCU, is considered an outlier and will not be evaluated further in this study.

As indicated by Table 4-1, the devitrified RMC's, DMP and DMR, are associated with welded ash flow tuffs. Distinction between "mafic poor" and "mafic rich" largely rests upon a 2.0% RMC cutoff for biotite percentage. "Mica," composed largely of biotite, is relatively ubiquitous in the TCU with a mean percentage of 2.24. Separate DMP and DMR categories are not amenable to characterization by the Gaussian distribution. The 2.0% cutoff used in RMC distinction splits the population of devitrified tuffs into two parts, the sum of which is more likely to be characterized by a Gaussian distribution. As indicated by Table 4-1, the vitric RMCs, VMP and VMR, are associated with non-welded ash flow tuffs and vitrophyric bedded tuffs. Similar to DMP and DMR, the key distinction between VMP and VMR is the 2.0% cutoff for biotite percentage. The VMP and VMR RMCs split the population of non-welded ash flow tuffs and vitrophyric bedded tuffs into two parts, the sum of which is more likely to be characterized by a Gaussian distribution.

Effects of XRD method resolution and uncertainty presents another difficulty in distinguishing between “mafic poor” and “mafic rich” categories. Methods unable to accurately detect mica percentage *above* 2% could result in null observations or data values of “0.0” leading to categorization of the RMC as “mafic poor” even though the true mica percentage is greater than 2%. In particular, for the 5.3% of the data without a RMC category, 44% of mica data values are “0.0” and 52% of mica data values are null observations. All of the data without a RMC category are obtained from “S” (semiquantitative) method data.

RMC categories are not amenable to parametric geostatistical approaches because the mineralogic cutoffs used to categorize RMCs abruptly crop frequency distributions that could otherwise be characterized by a Gaussian distribution (e.g., through use of the additive log ratio transformation in Chapter 6). It would be possible to post-process geostatistical characterizations back into the RMC framework, for example, by applying the RMC definitions to statistical distributions or geostatistical realizations characterized by mean and (co)variance statistics. Also, it would be possible to use non-parametric geostatistical approaches, particularly indicator approaches with cutoff values corresponding to the RMC cutoff values. However, use of indicator approaches would require development of a several indicator variograms at different cutoff values to span the full range of the frequency distribution for each mineralogic zone. Thus, an indicator approach requires much more modeling effort and complication compared to a parametric approach. Secondly, a categorical approach may not be appropriate for the large size of grid blocks used in transport models. For example, if the length scale of mica spatial variability for “mafic poor” and “mafic rich” zones is smaller than the grid block size, designation of “mafic poor” and “mafic rich” grid blocks based on point data will cause the transport model to over predict spatial variability of transport properties attributable to mica spatial variability.

Table 4-1. Definition of reactive mineral categories (RMCs) within TCU in Yucca Flat from Stoller-Navarro (2007). Additional reactive minerals present in quantities significant to prediction of K_d for some or all radionuclide classes, but not included in Stoller-Navarro (2007), are included within square brackets [ ] in column 4.

Reactive Mineral Category (RMC)	Typical Lithology	Major Alteration	Reactive Minerals Present in Significant Quantities	UGTA Criteria
Zeolitic (ZEOL)	Bedded tuffs, Nonwelded tuffs, pumiceous lavas	Primarily zeolitic, may also include argillic	Zeolite [smectite, mica]; if argillic, includes smectite	>30% zeolite; zeolite>clay typically <10% glass
Argillic (ARG)	Bedded tuff	Argillic	Smectite [mica, calcite, zeolite]	>20% clay and clay>zeolite
Vitric, mafic-rich (VMR)	Ash-flow tuffs (nonwelded to Partially welded or vitrophyres), bedded/ash-fall tuffs (unaltered), vitrophyric and pumiceous lava	None (vitric/glassy)	Mica, hematite [smectite, zeolite]	Vitric >30% glass; <30% zeolite; <30% clay mafic-rich >2.0% biotite or >2.5% total Mafic content
Vitric, mafic-poor (VMP)	Ash-flow tuffs (nonwelded to Partially welded or vitrophyres), bedded/ash-fall tuffs (unaltered), vitrophyric and pumiceous lava	None (vitric,glassy)	[mica, smectite, zeolite]	Vitric >30% glass; <30% zeolite; <30% clay mafic-poor <2.0% biotite or <2.5% total Mafic content
Devitrified, mafic-rich (DMR)	Ash-flow tuffs (moderately to densely welded), dense/stony lava	Devitrification, vapor-phase mineralization, quartzo-feldspathic, albitic	Mica, hematite [smectite, zeolite]	Devitrified <30%glass; <30% clay; <30% zeolite; typically >60% quartz and feldspars mafic-rich >2.0% biotite or >2.5% total mafic content
Devitrified, mafic-poor (DMP)	Ash-flow tuffs (moderately to densely welded), dense/stony lava	Devitrification, Vapor-phase Mineralization, Quartzo-feldspathic, albitic	[mica, smectite, zeolite]	Devitrified <30%glass; <30% clay; <30% zeolite; typically >60% quartz and feldspars mafic-poor <2.0% biotite or <2.5% total mafic content

Table 4-2. Number of reactive mineral percentage data in TCU sorted by RMC. Numbers of null observations are given in parentheses.

RMC	Total	Fraction	Calcite	Hematite	Mica	Smectite	Zeolite
ARG	106	9.0%	92 (14)	27 (79)	104 (2)	106 (0)	103 (3)
ZEOL	851	72.6%	565 (286)	168 (683)	742 (109)	834 (17)	851 (0)
DMP	47	4.0%	47 (1)	4 (44)	45 (3)	48 (0)	48(0)
DMR	71	6.1%	61 (10)	12 (59)	71 (0)	71 (0)	70 (1)
VMP	17	1.5%	17 (2)	5 (14)	17 (2)	19 (0)	19 (0)
VMR	14	1.2%	8 (6)	2 (12)	14 (0)	14 (0)	12 (2)
CC	1	0.1%	1 (0)	0 (1)	1 (0)	1 (0)	1 (0)
All RMCs	1110	94.7%	791 (319)	218 (892)	994 (116)	1093 (17)	1104 (6)
No RMC	62	5.3%	45 (17)	10 (52)	30 (32)	52 (10)	47 (15)
All data	1172	100%	836 (336)	228 (944)	1024 (148)	1145 (27)	1151 (21)

4.1 Basic Statistics

Differences in K_d distributions in RMCs depend on differences in reactive mineral distributions between the RMCs. Basic statistics, including mean, absolute deviation, standard deviation, and skewness, give some indication of the characteristics of the reactive mineral distributions. While standard deviation is a common measure of variation, absolute deviation is more robust to outliers. Skewness measures asymmetry in the distribution. Skewness for a Gaussian distribution equals zero. Basic statistics for reactive mineral percentages and $\log_{10}$[reactive mineral percentages] are given below for each RMC. Statistics for non-zero mineral percentages are given in parenthesis. In logarithmic calculations, zero percentage data are assigned a $\log_{10}$ value of -2.

4.1.1 ARG

The principle lithology for the ARG (argillic) RMC is bedded tuff. ARG tuffs are typically argillic, with distinctively high percentages of the clay minerals smectite and kaolinite. The ARG RMC is defined by clay percentage greater than 20% and clay percentage greater than zeolite.

Table 4-3 and Table 4-4 show basic statistics for reactive mineral percentage and $\log_{10}$ percentage in ARG, with statistics for non-zero data given in parenthesis. Smectite percentage in ARG is distinctively high, with a mean value of 43.1%. Considering that all ten radionuclide classes sorb to smectite, the ARG RMC would play a major role in retardation of radionuclide transport within the TCU. Percentages of other reactive minerals are comparable to those in other RMCs except for zeolite in the ZEOL RMC.

Table 4-3. Basic statistics for reactive mineral percentages in ARG RMC. Values in parenthesis are for non-zero data.

Mineral	Calcite	Hematite	Mica	Smectite	Zeolite
#Data	92 (21)	27 (13)	104 (66)	106 (106)	103 (44)
Mean	1.49 (6.53)	0.67 (1.40)	2.85 (4.48)	43.1 (43.1)	6.23 (14.57)
Abs. Dev.	2.43 (4.70)	0.78 (1.03)	2.88 (3.71)	16.5 (16.5)	7.72 (6.78)
Std. Dev.	3.75 (5.41)	1.40 (1.78)	5.53 (6.40)	20.6 (20.6)	8.95 (8.08)
Skewness	2.73 (0.57)	3.43 (2.36)	3.83 (3.17)	0.98 (0.98)	1.05 (-0.18)

Table 4-4. Basic statistics for $\log_{10}$[reactive mineral percentage] in ARG RMC, with zero-valued data assigned $\log_{10}$ value of -2. Values in parenthesis are for non-zero data.

Mineral	Calcite	Hematite	Mica	Smectite	Zeolite
#Data	92 (21)	27 (13)	104 (67)	106 (106)	103 (44)
Mean	-1.40 (0.63)	-1.05 (-0.03)	-0.46 (0.43)	1.59 (1.59)	-0.70 (1.04)
Abs. Dev.	0.93 (0.39)	0.98 (0.26)	1.13 (0.28)	0.16 (0.16)	1.49 (0.31)
Std. Dev.	1.13 (0.45)	1.03 (0.36)	1.22 (0.41)	0.20 (0.20)	1.53 (0.40)
Skewness	1.39 (-0.33)	0.24 (0.84)	-0.33 (0.44)	0.20 (0.20)	0.36 (-1.46)

4.1.2 DMP

The principle lithology for the DMP (devitrified mafic poor) RMC is moderately to densely welded ash flow tuff or dense/stony lava. Devitrification results from vapor-phase mineralization (hot conditions) leading to relative abundance of quartz, feldspar, cristobalite, and tridymite. Devitrified RMC's are defined by less than 30% glass, less than 30% clay, less than 30% zeolite, and, typically, greater than 60% quartz and feldspars. "Mafic-poor" is defined by less than 2.0% biotite or less than 2.5% total mafic content.

Table 4-5 and Table 4-6 show basic statistics for reactive mineral percentage and $\log_{10}$ percentage in DMP, with statistics for non-zero data given in parenthesis. The DMP RMC is distinguished by relatively low percentages of all reactive minerals including mica as categorized by "mafic-poor" compared to the "mafic-rich" DMR RMC. However, distinction of DMP from DMR is relevant only three radionuclide classes that are sorbers to mica - ^{41}Ca, Cs, and Sr. Of these, only Cs sorption can be dominated by mica because ^{41}Ca and Sr also sorb more strongly to zeolite and comparably to smectite relative to mica. Despite being considered neither "argillic" nor "zeolitic," mean smectite and zeolite percentages are still higher than mica in both DMP and DMR RMCs. With typically low percentage, mica usually has a secondary effect on total K_d. Mica

abundance would have the most impact on K_d in devitrified or vitric rocks including DMP, DMR, VMP, and VMR RMCs. Distinction of "mafic poor" and "mafic rich" RMCs (e.g., DMP/DMR and VMP/VMR, see below) will mainly affect Cs transport prediction. Overall, the DMP RMC's relatively low smectite and zeolite percentages will lead to the lowest K_ds in TCU.

Table 4-5. Basic statistics for reactive mineral percentages in DMP RMC. Values in parenthesis are for non-zero data.

Mineral	Calcite	Hematite	Mica	Smectite	Zeolite
#Data	44 (6)	4 (1)	42 (14)	45 (24)	45 (19)
Mean	0.90 (6.62)	0.05 (0.2)	0.45 (1.36)	5.09 (9.55)	6.64 (15.7)
Abs. Dev.	1.56 (6.69)	0.08 (0.0)	0.62 (0.55)	5.03 (3.86)	7.91 (6.07)
Std. Dev.	3.71 (8.53)	0.10 (0.0)	0.74 (0.62)	5.92 (4.75)	9.11 (7.19)
Skewness	4.69 (0.85)	0.75 (0.0)	1.24 (-0.18)	0.76 (0.30)	0.88 (-0.29)

Table 4-6. Basic statistics for $\log_{10}$[reactive mineral percentage] in DMP RMC, with zero-valued data assigned $\log_{10}$ value of -2. Values in parenthesis are for non-zero data.

Mineral	Calcite	Hematite	Mica	Smectite	Zeolite
#Data	44 (6)	4 (1)	42 (14)	45 (24)	45 (19)
Mean	-1.66 (0.48)	-1.67 (-0.70)	-1.31 (0.07)	-0.45 (0.91)	-0.68 (1.13)
Abs. Dev.	0.62 (0.51)	0.49 (0.0)	0.92 (0.20)	1.45 (0.20)	1.53 (0.23)
Std. Dev.	0.92 (0.60)	0.65 (0.0)	1.00 (0.28)	1.48 (0.28)	1.57 (0.30)
Skewness	2.15 (0.30)	0.75 (0.0)	0.75 (0.00)	-0.08 (-1.30)	0.34 (-1.60)

4.1.3 DMR

Like the DMP RMC, the principle lithology for DMR (devitrified mafic rich) is moderately to densely welded ash flow tuff or dense/stony lava. "Mafic-rich" is defined by greater than 2.0% biotite or greater than 2.5% total mafic content. Thus, the difference between DMP and DMR is based on a dividing line near mean biotite or mafic content within the same lithology.

Table 4-7 and Table 4-8 show basic statistics of reactive mineral percentage and $\log_{10}$ percentage in DMR, with statistics for non-zero data given in parentheses. As discussed previously for the DMP RMC, the high mica content in DMR only has significant effect on Cs transport prediction. Smectite and zeolite percentage remain relatively high in DMR compared to mica. Since all radionuclide classes are smectite sorbers, and the mica

sorbers all also zeolite sorbers, distinction of DMP and DMR RMCs has secondary effect on K_d prediction except for Cs.

Table 4-7. Basic statistics for reactive mineral percentages in DMR RMC. Values in parenthesis are for non-zero data.

Mineral	Calcite	Hematite	Mica	Smectite	Zeolite
#Data	61 (8)	12 (4)	71 (68)	71 (66)	70 (53)
Mean	1.02 (7.81)	0.33 (1.00)	4.61 (4.81)	9.42 (10.1)	12.1 (16.0)
Abs. Dev.	1.78 (6.64)	0.47 (0.75)	2.15 (2.08)	5.17 (4.85)	8.76 (6.57)
Std. Dev.	3.69 (7.49)	0.77 (0.87)	2.79 (2.65)	6.83 (6.44)	9.88 (7.40)
Skewness	4.00 (0.54)	2.16 (0.65)	1.29 (1.54)	0.51 (0.58)	0.01 (-0.38)

Table 4-8. Basic statistics for $\log_{10}$[reactive mineral percentage] in DMR RMC, with zero-valued data assigned $\log_{10}$ value of -2. Values in parenthesis are for non-zero data.

Mineral	Calcite	Hematite	Mica	Smectite	Zeolite
#Data	61 (8)	12 (4)	71 (68)	71 (66)	70 (53)
Mean	-1.65 (0.71)	-1.39 (0.17)	0.52 (0.63)	0.71 (0.91)	0.36 (1.12)
Abs. Dev.	0.62 (0.38)	0.81 (0.29)	0.28 (0.18)	0.50 (0.25)	1.15 (0.25)
Std. Dev.	0.93 (0.43)	0.93 (0.45)	0.57 (0.21)	0.81 (0.31)	1.38 (0.32)
Skewness	2.24 (0.44)	0.79 (0.09)	-3.53 (0.57)	-2.55 (-0.63)	-1.05 (-1.14)

4.1.4 VMP

The principle lithology for the VMP (vitric mafic poor) RMC is nonwelded to partially welded ash flow or vitrophyres, unaltered bedded/ash-fall tuffs, or vitrophyric and pumiceous lava. Vitric RMC's are characterized by vitric or glassy mineralization defined as greater than 30% glass, less than 30% clay, less than 30% zeolite, and, typically, greater than 60% quartz and feldspars. As for devitrified tuffs, "mafic-poor" is defined by less than 2.0% biotite or less than 2.5% total mafic content.

Table 4-9 and Table 4-10 show basic statistics for mineral percentage and $\log_{10}$ percentage in VMP, with statistics for non-zero data given in parentheses. Similar to DMP and DMR, distinction of VMP and VMR RMCs will affect Cs transport prediction, with no effect on 7 of the 10 radionuclide classes and little affect on ^{41}Ca and Sr transport. Despite lower smectite percentages relative to ARG and lower zeolite relative to ZEOL, smectite and zeolite will dominate K_d in VMP for 9 of 10 radionuclide classes.

Table 4-9. Basic statistics for reactive mineral percentages in VMP RMC. Values in parenthesis are for non-zero data.

Mineral	Calcite	Hematite	Mica	Smectite	Zeolite
#Data	17 (0)	5 (0)	17 (9)	19 (15)	19 (16)
Mean	0.0 (0.0)	0.0 (0.0)	0.49 (0.93)	5.95 (7.54)	9.76 (11.0)
Abs. Dev.	0.0 (0.0)	0.0 (0.0)	0.47 (0.39)	5.87 (6.37)	8.88 (8.72)
Std. Dev.	0.0 (0.0)	0.0 (0.0)	0.60 (0.50)	7.70 (7.97)	10.2 (10.1)
Skewness	0.0 (0.0)	0.0 (0.0)	0.89 (0.67)	1.35 (1.09)	0.59 (0.37)

Table 4-10. Basic statistics for $\log_{10}$[reactive mineral percentage] in VMP RMC, with zero-valued data assigned $\log_{10}$ value of -2. Values in parenthesis are for non-zero data.

Mineral	Calcite	Hematite	Mica	Smectite	Zeolite
#Data	17 (0)	5 (0)	17 (9)	19 (15)	19 (16)
Mean	-2.00	-2.00	-0.99 (-0.08)	0.09 (0.65)	0.31 (0.74)
Abs. Dev.	0.0	0.0	0.96 (0.19)	0.90 (0.38)	0.90 (0.38)
Std. Dev.	0.0	0.0	1.00 (0.23)	1.18 (0.46)	1.18 (0.46)
Skewness	0.0	0.0	-0.04 (0.24)	-0.92 (0.23)	-0.91 (-0.96)

4.1.5 VMR

As for the VMP RMC, the principle lithology for VMR (vitric mafic rich) is nonwelded to partially welded ash flow or vitrophyres, unaltered bedded/ash-fall tuffs, or vitrophyric and pumiceous lava. As for devitrified tuffs, “mafic-rich” is defined by greater than 2.0% biotite or greater than 2.5% total mafic content.

Table 4-11 and Table 4-12 show basic statistics of reactive mineral percentage and $\log_{10}$ percentage in VMR, with statistics for non-zero data are given in parenthesis. Similar to VMP, smectite and zeolite, despite relatively low percentage compared to ARG and ZEOL RMCs, respectively, will be the dominant sorbers in VMR for 9 of 10 radionuclide classes. Differences in mica content between VMP and VMR would only have a significant effect on K_d for Cs.

Table 4-11. Basic statistics for reactive mineral percentages in VMR RMC. Values in parenthesis are for non-zero data.

Mineral	Calcite	Hematite	Mica	Smectite	Zeolite
#Data	8 (5)	2 (1)	14 (13)	14 (14)	12 (9)
Mean	1.65 (2.64)	1.25 (2.50)	4.91 (5.29)	7.24 (7.24)	6.41 (8.54)
Abs. Dev.	1.47 (0.94)	1.25 (0.0)	4.04 (4.22)	5.54 (5.54)	5.63 (5.60)
Std. Dev.	1.79 (1.53)	1.77 (0.0)	6.06 (6.14)	7.02 (7.02)	7.47 (7.50)
Skewness	0.55 (0.32)	0.00 (0.0)	1.74 (1.67)	1.09 (1.09)	1.23 (1.05)

Table 4-12. Basic statistics for $\log_{10}$[reactive mineral percentage] in VMR RMC, with zero-valued data assigned $\log_{10}$ value of -2. Values in parenthesis are for non-zero data

Mineral	Calcite	Hematite	Mica	Smectite	Zeolite
#Data	8 (5)	2 (1)	14 (13)	14 (14)	12 (9)
Mean	-0.53 (0.35)	-0.80 (0.40)	0.38 (0.57)	0.69 (0.69)	0.09 (0.79)
Abs. Dev.	0.35 (0.20)	1.20 (0.0)	0.34 (0.24)	0.35 (0.35)	1.05 (0.31)
Std. Dev.	1.24 (0.31)	1.70 (0.0)	0.75 (0.33)	0.39 (0.39)	1.30 (0.37)
Skewness	-0.34 (-0.56)	0.00 (0.0)	-2.00 (1.50)	0.52 (0.52)	-0.84 (0.24)

4.1.6 ZEOL

The principle lithologies for the ZEOL (zeolitic) RMC are bedded tuff, nonwelded tuff, and pumiceous lavas. The ZEOL RMC is primarily zeolitic (clinoptilolite with lesser mordenite and analcine) and secondarily argillic (including smectite and kaolinite). The ZEOL RMC is defined by zeolite percentage greater than 30% with zeolite percentage exceeding clay percentage and less than 10% glass. The majority (69%) of the TCU XRD data are categorized into the ZEOL RMC.

Table 4-13 and Table 4-14 show basic statistics for reactive mineral percentage and $\log_{10}$ percentage in ARG, with statistics for non-zero data given in parentheses. Mean zeolite percentage in ZEOL is distinctively high at 57.5%. Smectite is detected in most (733 of 834 or 88%) XRD samples in ZEOL.

The ZEOL RMC would play a major role in retardation of the three radionuclide classes that sorb to zeolite – ^{41}Ca, Cs, and Sr. However, for non-zeolite sorbers – Am, Cs, Eu, Np, Pu, Sm, U – for which smectite is the dominant sorbing mineral, the ZEOL RMC would play a lesser role compared to ARG and would have K_d characteristics similar to devitrified or vitric RMCs.

Table 4-13. Basic statistics for reactive mineral percentages in ZEOL RMC. Values in parenthesis are for non-zero data.

Mineral	Calcite	Hematite	Mica	Smectite	Zeolite
#Data	565 (86)	168 (18)	742 (477)	834 (733)	851 (851)
Mean	0.65 (4.27)	0.24 (2.23)	2.11 (3.28)	6.00 (6.83)	57.5 (57.5)
Abs. Dev.	1.11 (3.43)	0.43 (0.47)	1.73 (1.68)	4.37 (4.25)	14.8 (14.8)
Std. Dev.	2.80 (6.05)	0.74 (0.78)	2.84 (2.95)	6.05 (6.00)	17.2 (17.2)
Skewness	9.09 (3.98)	2.73 (-2.27)	4.01 (4.52)	2.06 (2.17)	0.07 (0.07)

Table 4-14. Basic statistics for $\log_{10}$[reactive mineral percentage] in ZEOL RMC, with zero-valued data assigned $\log_{10}$ value of -2. Values in parenthesis are for non-zero data

Mineral	Calcite	Hematite	Mica	Smectite	Zeolite
#Data	565 (86)	168 (18)	742 (477)	834 (733)	851 (851)
Mean	-1.63 (0.42)	-1.76 (0.24)	-0.45 (0.42)	0.36 (0.69)	1.74 (1.74)
Abs. Dev.	0.62 (0.24)	0.43 (0.28)	1.11 (0.17)	0.63 (0.30)	0.12 (0.12)
Std. Dev.	0.88 (0.41)	0.71 (0.45)	1.18 (0.29)	0.95 (0.38)	0.14 (0.14)
Skewness	2.06 (-0.09)	2.65 (-2.27)	-0.48 (-0.34)	-1.73 (-0.40)	-0.40 (-0.40)

4.2 Frequency Distributions

In this section, reactive mineral frequency distributions are examined within each RMC. The frequency distributions are examined in the context of applicability to geostatistical methods. Some XRD data lacked sufficient information for RMC categorization.

4.2.1 Data with no RMC

In analysis of the TCU data in relation to RMC categories, consideration should be given to a non-trivial portion (5.3%) of the data that are not categorized into a RMC at all. While 5.3% may seem small, the portion represents 19% of data *not* categorized into the ZEOL RMC. Additionally, 5.3% represents a fraction comparable to the ARG, DMP and DMR RMC's and far greater than for VMP and VMR RMC's. Figure 4-1 shows frequency distributions for reactive minerals from the data with no RMC categorization. These data present several difficulties for RMC categorization:

- All "no RMC" data have low percentages or null observations of zeolite and smectite, which precludes categorization into ZEOL or ARG.

- Over half (32 or 62) of the "no RMC" data have "null observations" for mica, which precludes categorization into DMP, DMR, VMP, or VMR categories.
- All of the "no RMC" data were analyzed by the "S" (semi-quantitative) method, which is most uncertain for low mineral percentages.
- Most of the "no RMC" data have no measurements of felsic minerals to help distinguish vitric and devitrified tuffs (see Figure 4-2).

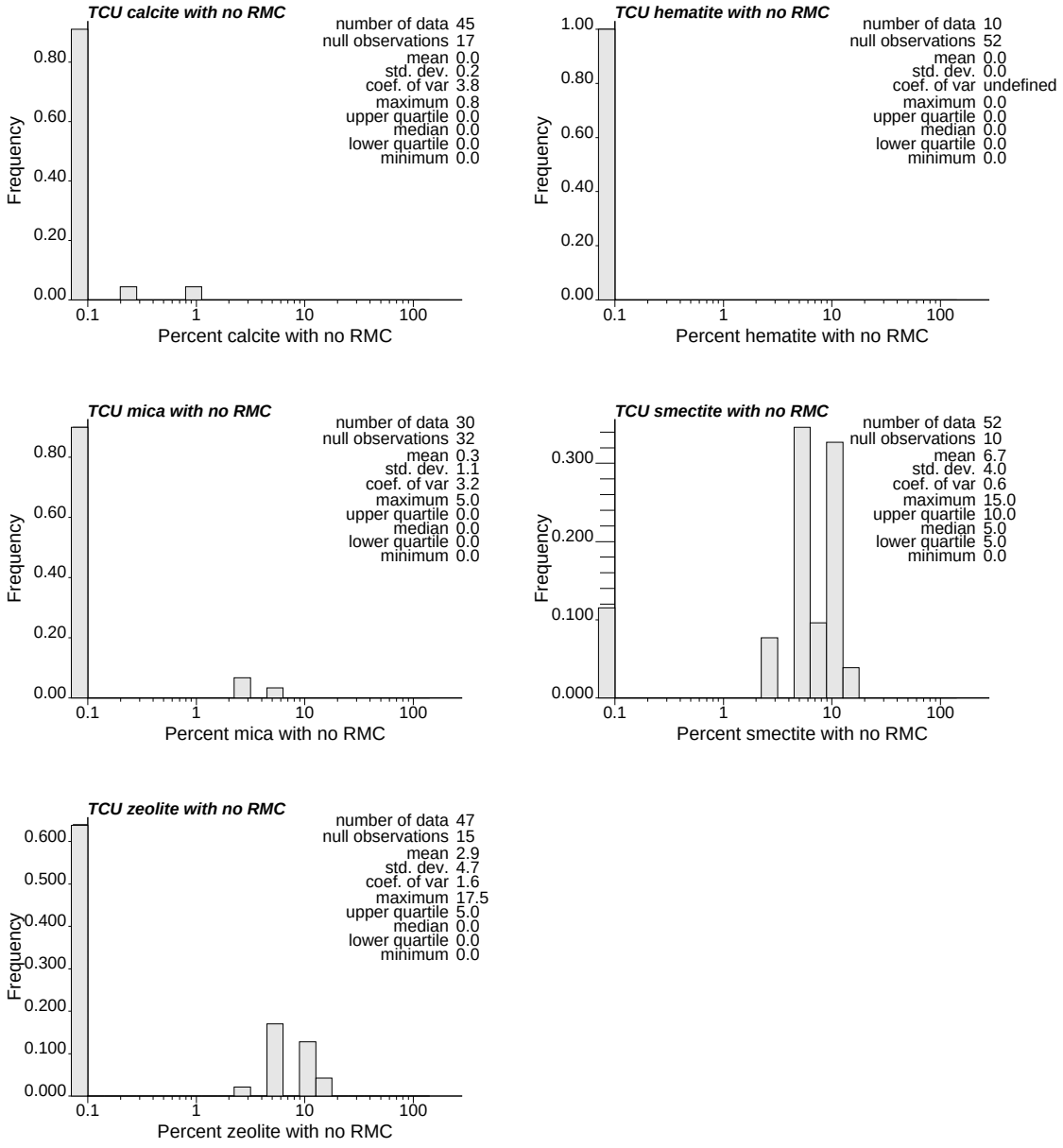

Figure 4-1. Logarithmic scale frequency distributions of reactive mineral percentage for all TCU data with no RMC categorization.

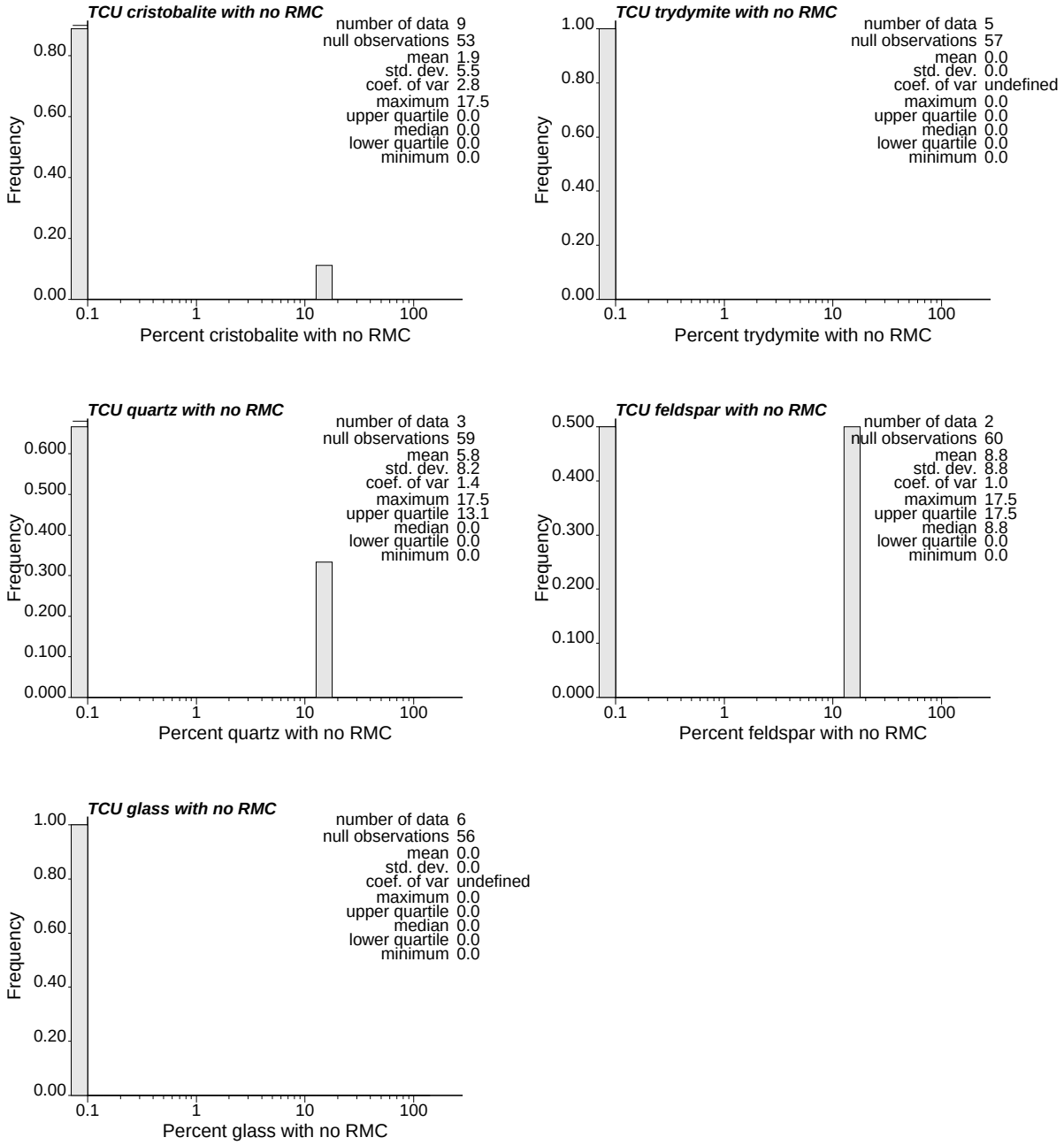

Figure 4-2. Logarithmic scale frequency distributions of felsic mineral percentage for all TCU data with no RMC categorization.

4.2.2 Calcite

Calcite is not used to distinguish RMCs in the TCU except for the CC (carbonate) RMC, of which only 1 datum is present. The CC RMC is treated as an outlier in this study and not included in geostatistical interpretation. Figure 4-3 shows logarithmic-scale frequency distributions for calcite XRD data. Notably, the majority (78-100%) of data in each RMC

indicate zero calcite except for VMR, which has only 8 data. If the VMP and VMR data are combined, the fraction of zero calcite data would be 80%, much like other RMC's. Thus, composite XRD data indicate zero calcite for about 78-88% of samples in the TCU RMCs. Where non-zero, calcite abundance typically ranges from a few percent to less than 20%. There is no obvious preference for calcite to occur in a particular RMC. The XRD data suggest spatial patterns of calcite occurrence might be similar throughout the TCU, except for very rare occurrences of approximately 0.1% probability where carbonate rock occurs within the TCU.

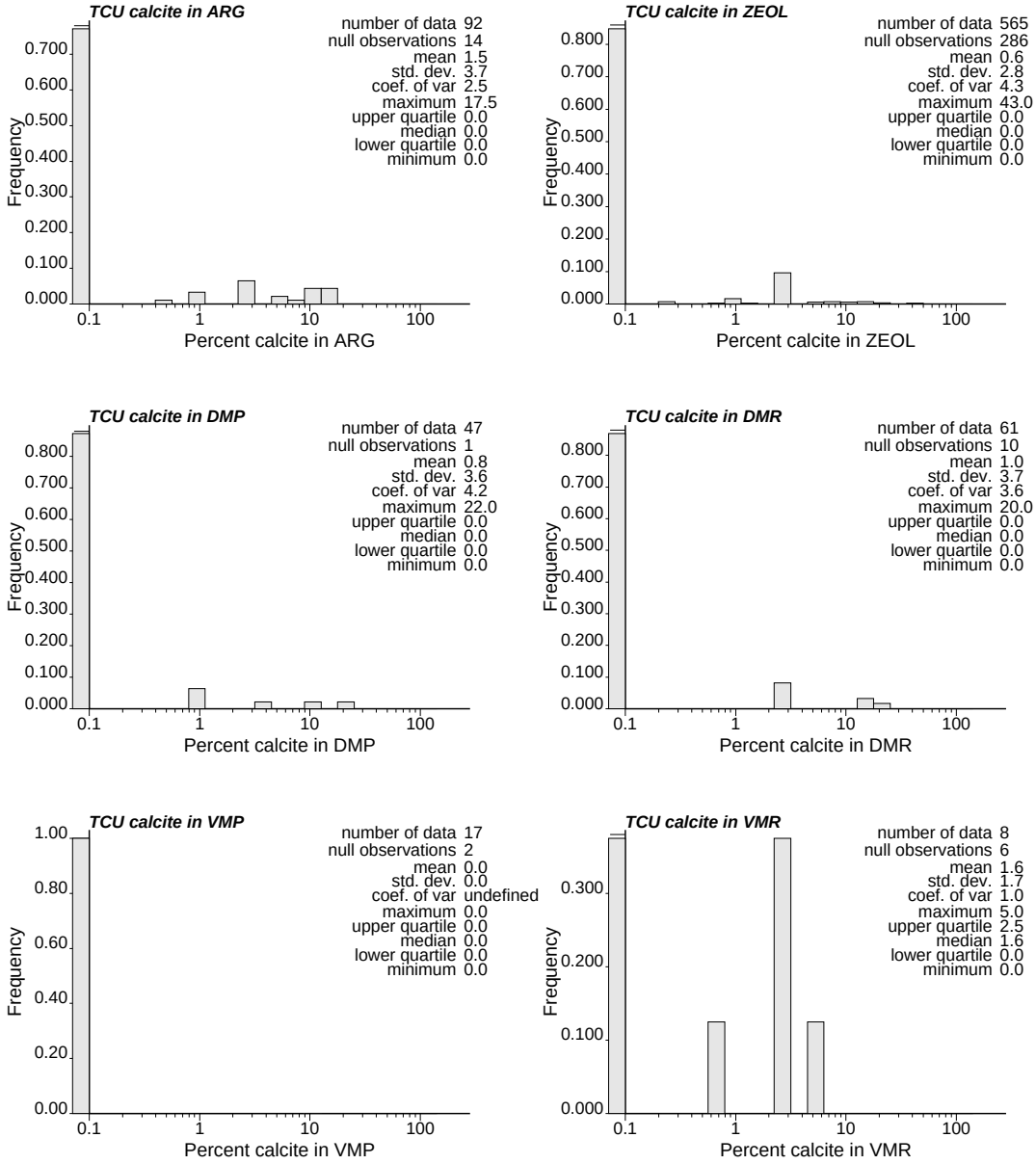

Figure 4-3. Logarithmic scale frequency distributions of calcite percentage within RMCs.

4.2.3 Hematite

Like calcite, hematite is not a factor in distinguishing RMCs in the TCU. Also similar to calcite, most hematite measurements are zero. Figure 4-4 shows logarithmic-scale frequency distributions for hematite XRD data in each RMC. The hematite data differ from calcite, however, in that the large majority of the data are null observations. Hematite measurements in ARG show a smaller proportion (38%) of zero-valued hematite measurements. However, this difference could be related to method used because many of the non-zero measurements are less than 2.5-3%, the typical resolution of "S" method data. Additionally, only 36 hematite data were obtained for the ARG RMC and, thus, XRD sampling of ARG could be biased toward high hematite. Overall, the fraction of hematite percentage of 1% or greater is very similar for each RMC particularly if the VMP and VMR RMCs are combined. Similar to calcite, it is difficult to speculate to what extent zero-valued XRD hematite percentages actually represent finite percentages of hematite. An interpretation similar to calcite – that spatial patterns of hematite occurrence could be similar throughout the TCU – is suggested by the data. However, because hematite data are sparse, there is more uncertainty in interpretation of the hematite data.

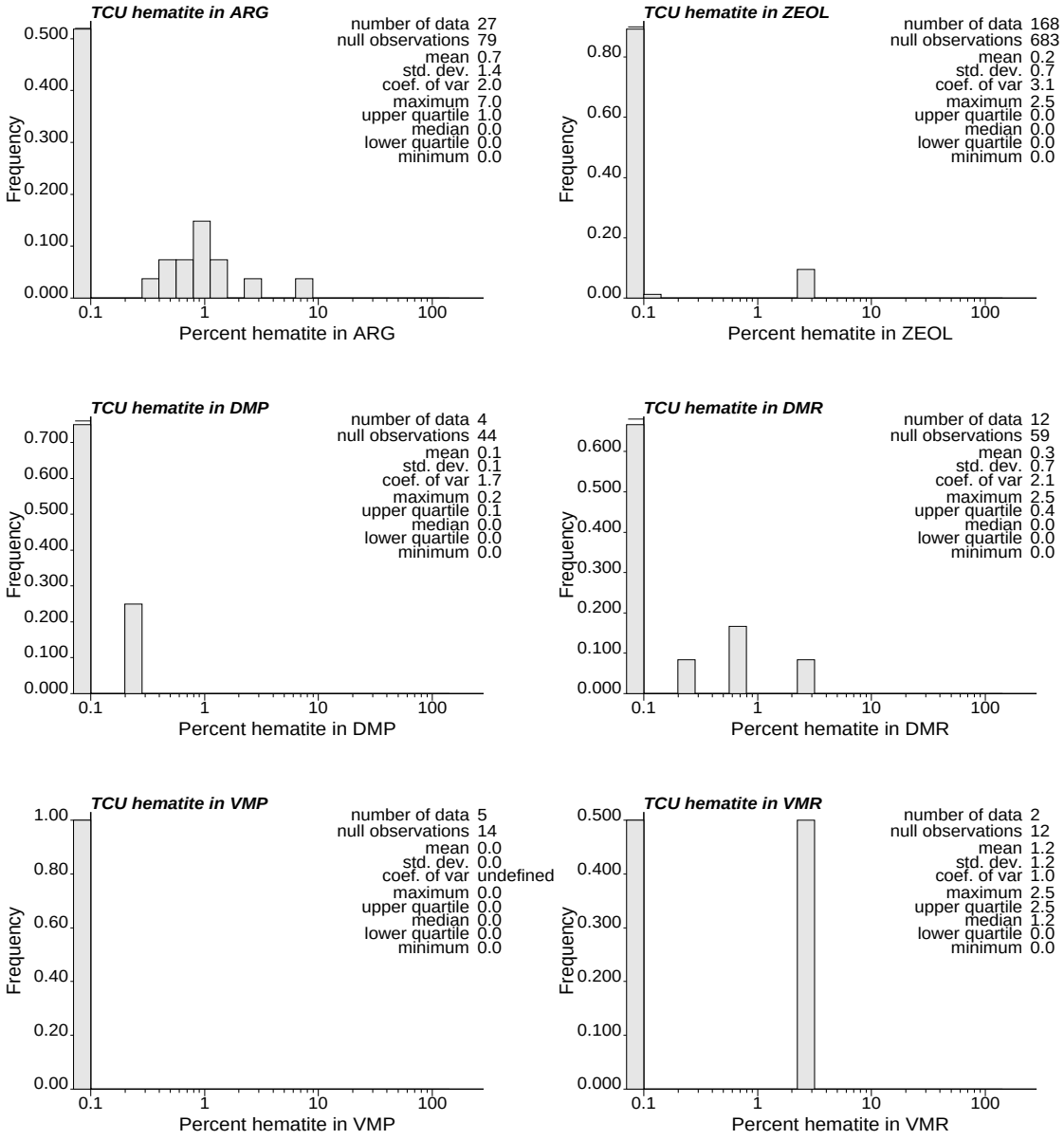

Figure 4-4. Logarithmic scale frequency distributions of hematite percentage within RMCs.

4.2.4 Mica

Compared to calcite and hematite, the XRD data indicate mica is relatively ubiquitous throughout the TCU. Figure 4-5 shows logarithmic-scale frequency distributions for mica XRD data in each RMC. If DMP-DMR and VMP-VMR RMC's are combined as pairs (assuming "devitrified" and "vitric" categories), the mica frequency distributions would look very similar across ARG, ZEOL, and combined DMP-DMR and VMP-VMR RMCs. Comparison of statistics and frequency distributions for mica in different RMCs is complicated by differences in resolution and uncertainty in the different XRD methods

used in the composite XRD dataset. This issue is particularly relevant to mica because a large proportion of the mica percentage frequency distribution is below resolution limits of the XRD methods. Much of the difference in mica percentage statistics relates to the proportions of zero values, which depends on the resolution and accuracy of the methods used. The data suggest slightly lower mica percentage with more zero value mica data in the ZEOL RMC, which could relate to occurrences of peralkaline ash-fall tuffs that are devoid of mica (S. Drellack, personal communication, 2007). Thus, mica appears to be relatively ubiquitous with a frequency distribution that appears to be relatively homogeneous throughout the TCU, with the exception of some peralkaline ash-fall tuffs devoid of mica.

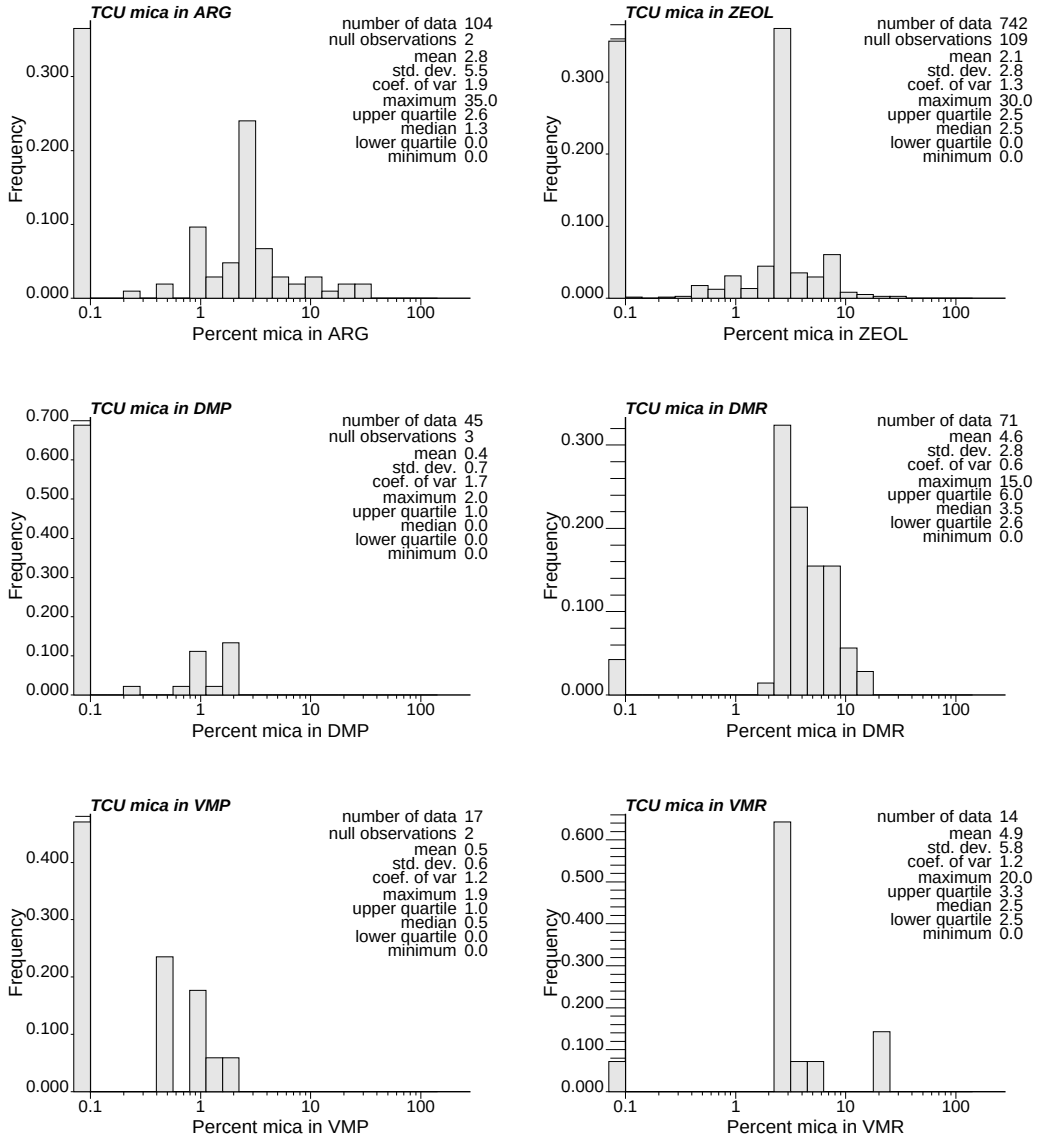

Figure 4-5. Logarithmic scale frequency distributions of mica percentage within RMCs.

4.2.5 Smectite

Figure 4-6 shows logarithmic-scale frequency distributions for smectite XRD data in each RMC. Unlike calcite and hematite, smectite frequency distributions show obvious differences between different RMCs directly attributable to the RMC criteria of definition (Table 4-1). The argillic RMC requires greater than 20% clay, while VMR, VMP, DMR, and DMP require less than 30% clay. The ZEOL RMC requires clay percentage less than zeolite with greater than 30% zeolite. Because smectite is a particular class of clay, the clay percentage cutoffs for RMC definition do not directly translate to discrete cutoffs within RMC smectite frequency distributions. Nonetheless, the ARG RMC contains no less than 15% smectite, whereas other RMCs typically contain less than 15% smectite, including a fraction of zero values. Smectite frequency distributions are similar within the ZEOL, DMP, DMR, VMP, and VMR RMCs. As considered previously, the smaller differences in frequency distributions should not be over-analyzed at this stage because differences in method of XRD analysis affect the frequency distributions. Considering that the ARG RMC is largely derived from the argillic LTARG reactive mineral unit (RMU) at the base of the TCU, the ARG RMC categorization indicates an abundance of smectite similar to what is found in the LTARG RMU.

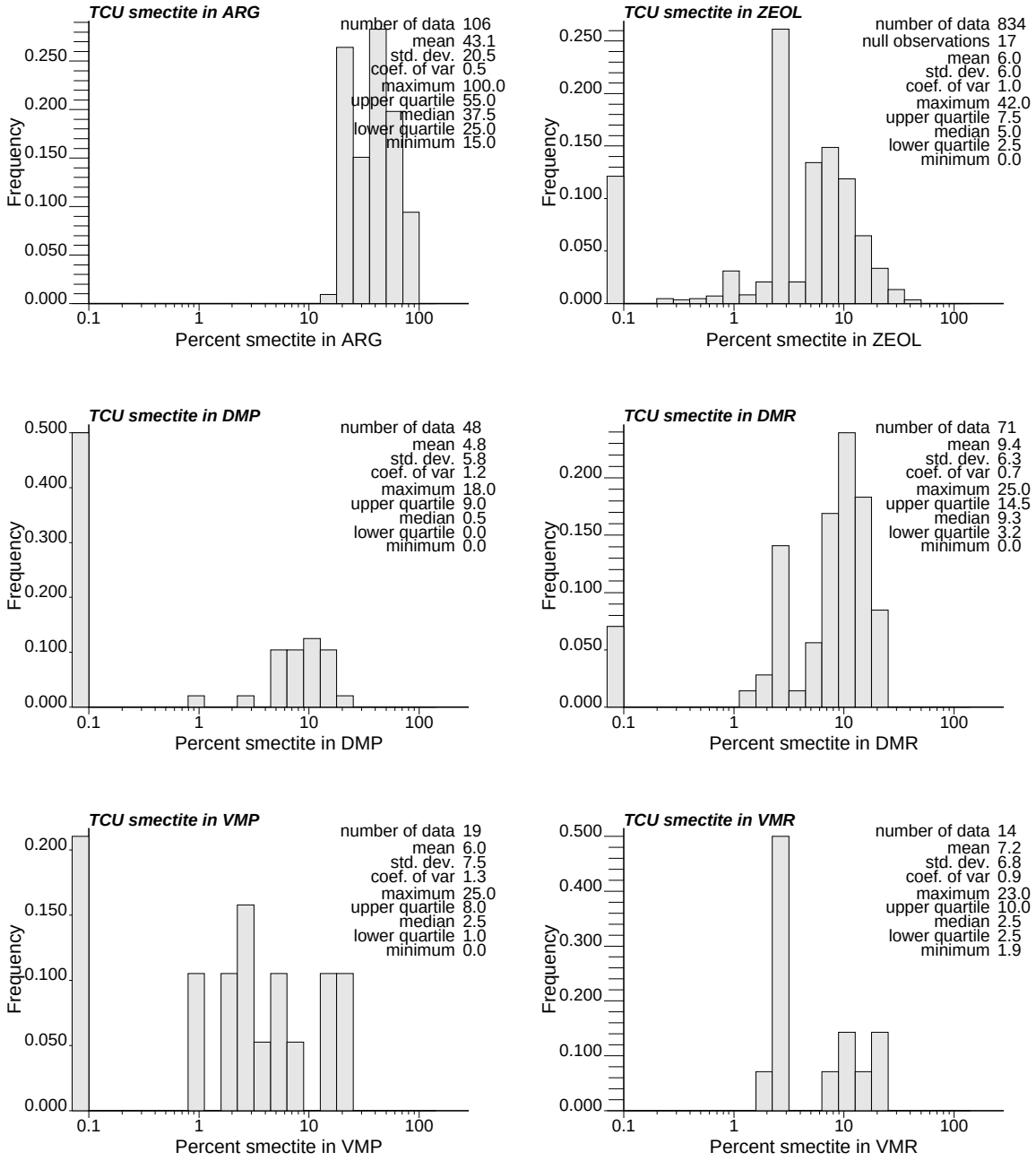

Figure 4-6. Logarithmic scale frequency distributions of smectite percentage within RMCs.

4.2.6 Zeolite

Figure 4-7 shows logarithmic-scale frequency distributions for zeolite XRD data in each RMC. Like smectite, zeolite is considered in the definition of all RMCs. The ZEOL RMC is defined by greater than 30% zeolite and zeolite abundance greater than clay. As such, zeolite percentage is less than 30% in all other RMCs. This 30% zeolite cutoff result in similar zeolite frequency distributions for ARG, DMP, DMR, VMP, and VMR RMCs.

DMR exhibits higher zeolite abundance relative to ARG, DMP, VMP, and VMR, which could be attributed to how ZEOL and DMR are distinguished. The 30% cutoff for distinguishing ZEOL from other RMCs likely oversimplifies actual mineral distributions within typical RMC lithologies. For example, some data categorized as DMP and DMR could represent zeolitic bedded tuffs, rather than ash-flow tuffs, with zeolite percentage below 30%. As for the previously discussed reactive mineral distributions, differences in the frequency distributions of zeolite in ARG, DMP, DMR, VMP, and VMR are also affected by differences in XRD method used. Detailed analysis of differences in composite XRD zeolite frequency distributions for different RMCs should be avoided until effects of XRD method are considered.

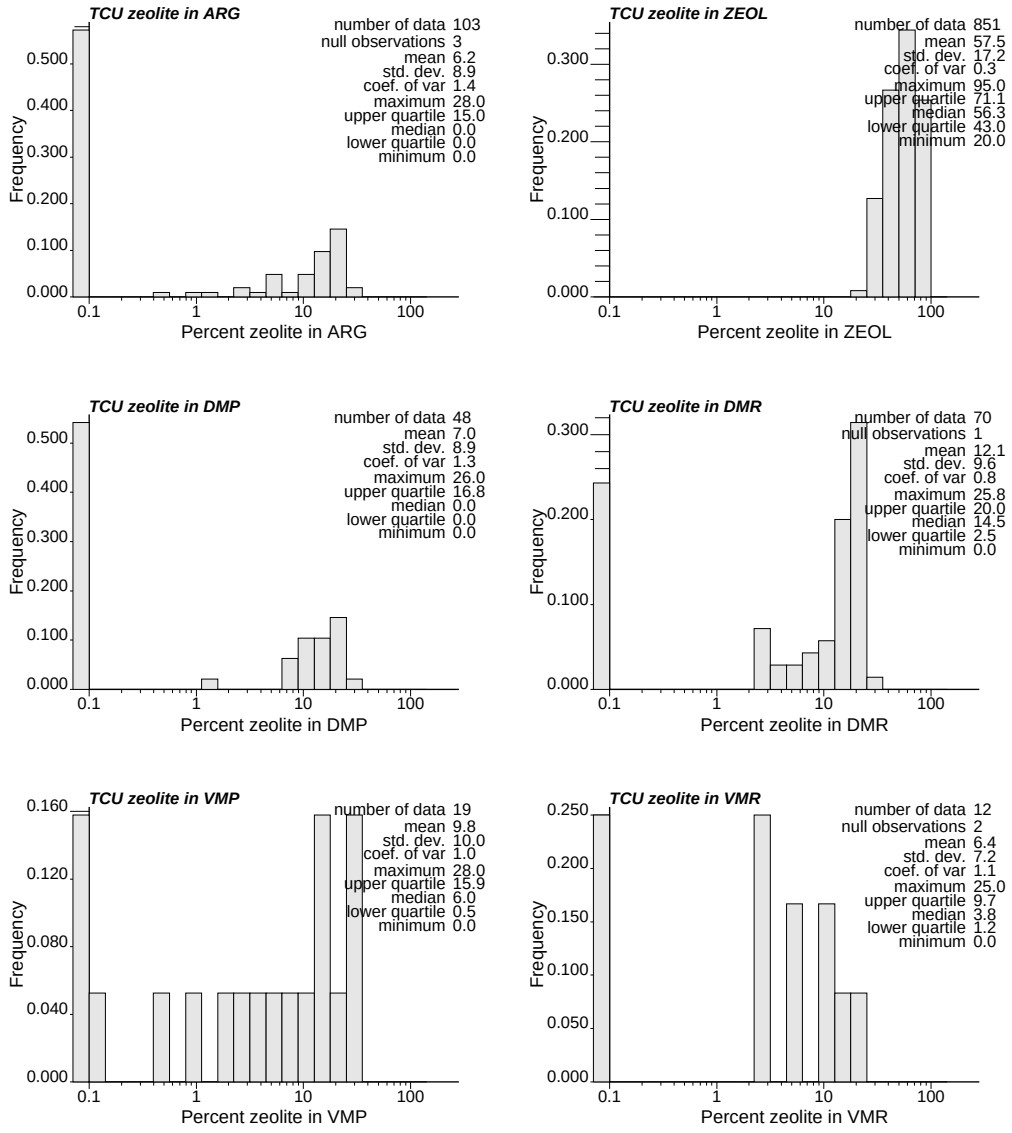

Figure 4-7. Logarithmic scale frequency distributions of zeolite percentage within RMCs.Reactive Mineral Cross Relationships in RMCs

As discussed above, calcite and hematite have practically no impact on RMC definition because calcite and hematite are not used in RMC definitions and occur in similar frequency distributions for all RMCs. Mica has little impact on RMC definition if the mafic-poor and mafic-rich RMCs are combined as DMP-DMR and VMP-VMR into "devitrified" and "vitric" categories. Figure 4-8, a cross-plot of smectite and zeolite $\log_{10}$ percentage, emphasizes how the main differences in RMC population characteristics are attributed to the relative percentages of smectite and zeolite. For the ZEOL RMC, zeolite percentages predominantly lie above 30% zeolite irrespective of smectite percentage. For the ARG RMC, smectite percentages predominantly lie above 20% smectite except where zeolite percentage is greater than 30%. The devitrified RMCs, DMP and DMR, show relatively greater total smectite and zeolite percentage compared to the vitric RMCs, VMP and VMR. Thus, devitrified and vitric rocks could have significant differences K_d.

Figure 4-8 shows the abrupt separation of ARG from non-ARG and ZEOL from non-ZEOL RMCs based primarily on smectite and zeolite percentage cutoffs. Data clusters with relatively high zeolite and smectite percentage suggest a merging of two populations. Many data with high (greater than 20%) total smectite and zeolite would appear to fit into either a high smectite or high zeolite population, but are not categorized as ARG or ZEOL. Instead, the cutoffs lead to categorization of some data with relatively high total amounts of reactive minerals primarily into devitrified (DMP or DMR) RMCs. In turn, the frequency distribution for DMP, DMR, and, to some extent, VMP and VMR, appear bi-modal with one peak consisting of zero or low percentages and another peak centered above a percentages of 10%. It will be problematic to implement a categorical approach to multi-modal reactive mineral percentage frequency distributions unless additional categories are defined.

Mica data are nearly as numerous as smectite and zeolite and, thus, offer potential insights on RMC categorization though cross-plotting with smectite and zeolite. Figure 4-9 and Figure 4-10 show mica-zeolite and smectite-mica cross-plots categorized by RMC. The ubiquity and homogeneity of the mica frequency distributions are evident in both plots, particularly by combining DMP-DMR and VMP-VMR RMCs. The mica-zeolite cross plot mainly shows zonation of ZEOL between non-ZEOL categories. Mica zonation is only evident between mafic-poor and mafic-rich RMCs. If mafic-poor and mafic-rich categories are combined, the mica frequency distributions will be very similar the remaining four categories of ARG, DMP-DMR, VMP-VMR, and ZEOL. This pattern is also evident in the smectite-mica cross plot in Figure 4-10. The main population distinctions relates to smectite percentage between ARG and non-ARG RMCs. Mica distributions strongly overlap and appear nearly identical between all RMC categories where DMP-DMR and VMP-VMR are combined.

Another consideration for reactive mineral categorization is K_d dependency on different reactive minerals for different radionuclides. As discussed in Sections 4.1 and 9.1, only three of ten radionuclide classes – ^{41}Ca, Cs, and Sr – are sorbers to mica. Of these, only Cs has stronger sorption to mica relative to the more abundant smectite and zeolite. Thus, for 9 of 10 radionuclide classes, distinction of high and low mafic zones would have little or no impact on radionuclide transport prediction. Additionally, the XRD data indicate that mica frequency distributions are very similar throughout different lithologies and stratigraphic units in the TCU, with the only exception being a few thin peralkaline tuff beds devoid of mica.

4.3 Geostatistical Analysis in an RMC Framework

The RMC framework defines categories purely on reactive mineral content through mica, smectite, and zeolite cutoffs independent of stratigraphic unit or lithology. This removes the geometric context of mineralogic zonation in the TCU as interpreted by Prothro (2005). Geostatistical indicator methods use cutoff values to define categories and implement a non-parametric approach that avoids dependency on Gaussian assumptions. However, a RMC-based indicator approach would be problematic to implement in the TCU, requiring multiple sets of cutoffs for cross-correlated indicator variables based on mica, smectite, and zeolite content. Traditional geostatistical indicator approaches are designed for one set of cutoffs applied to a single measure of content (e.g., smectite only). Development of multiple indicator variogram and cross-variogram models would be hampered by lack of data in all six RMCs except for ZEOL. Finally, it is doubtful that an indicator approach folding in RMC interpretation would appropriately address the geometric aspects of reactive mineral spatial variation and zonation in the TCU. As described by Prothro (2005) and further discussed in Chapter 5, major zonal variations of reactive mineral distributions in the TCU are related to stratigraphic units and groupings of reactive mineral units. Arguably, characterization of major spatial variations of reactive mineral distributions in the TCU is more defensibly described in the context of geological processes (e.g. depositional, tectonic, erosional, and diagenetic) rather than random processes.

Granted, categories related to stratigraphic units or lithologies will present difficulty from overlapping reactive mineral frequency distributions. Likewise, it is problematic to attribute lithology or stratigraphic units to categories defined solely by mineralogic percentage cutoffs. For example, some bedded tuffs, nonwelded tuffs, or pumiceous lavas would likely contain less than 30% zeolite and, conversely, some non-welded to partially welded ash-flow tuffs could contain greater than 30% zeolite.

Obviously, it is not possible to determine lithology or stratigraphic unit from reactive and felsic mineral percentage data alone. It is important to include consideration of the spatial

context of lithology and stratigraphic unit in geostatistical analysis to address zonal differences in spatial variability within the TCU. Chapter 5 examines reactive mineral distributions in reactive mineral units (RMUs), which have geometric context through definition by hydrostratigraphic units or sub units having characteristic reactive mineral distributions and lithology.

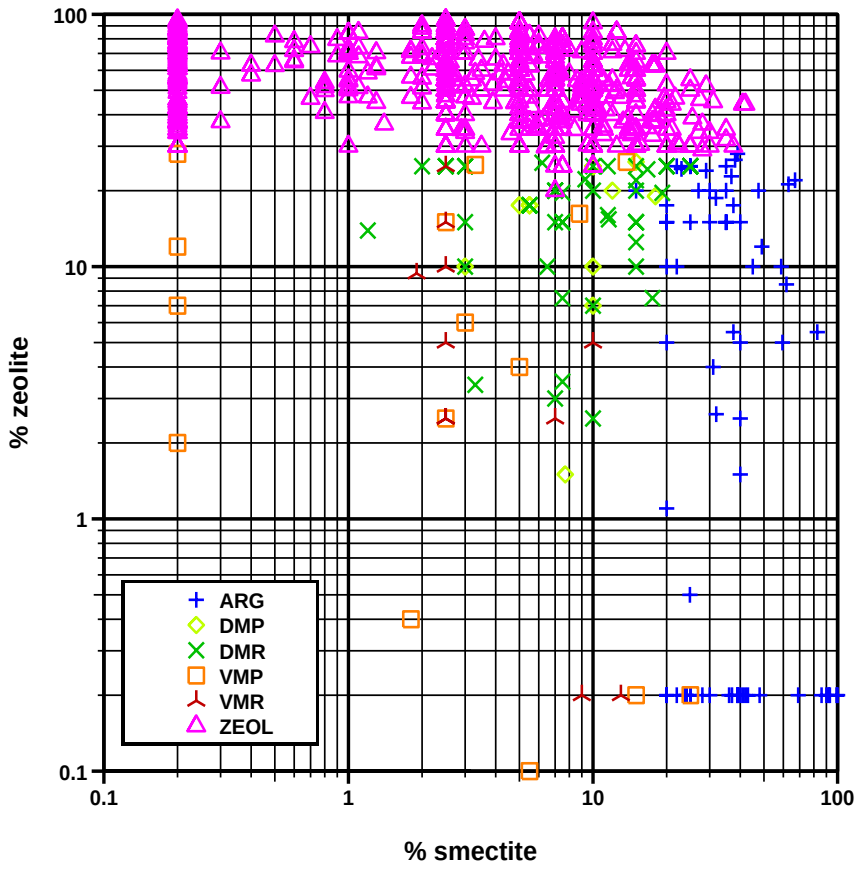

Figure 4-8. Logarithmic cross plot of smectite and zeolite percentage for all XRD data sorted by RMC.

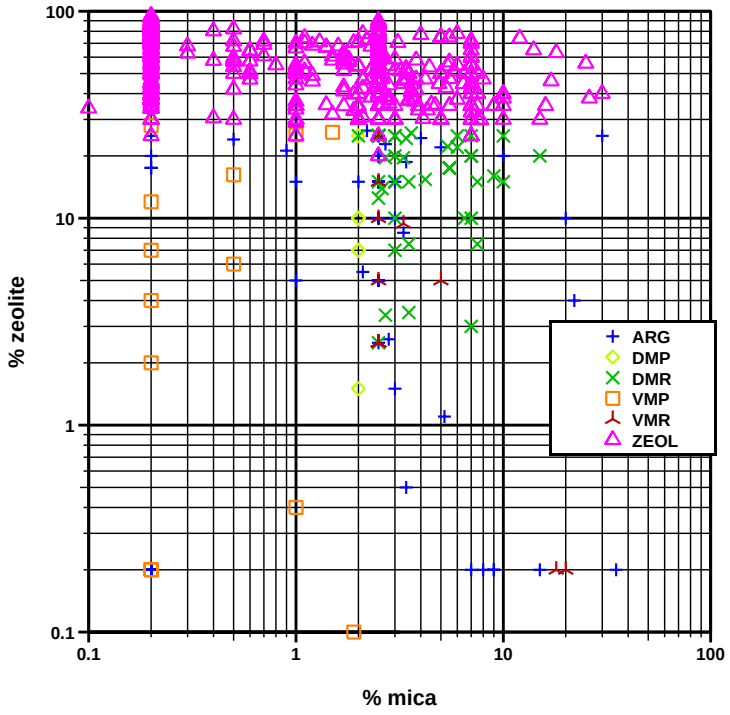

Figure 4-9. Logarithmic cross plot of mica and zeolite percentage for all XRD data sorted by RMC.

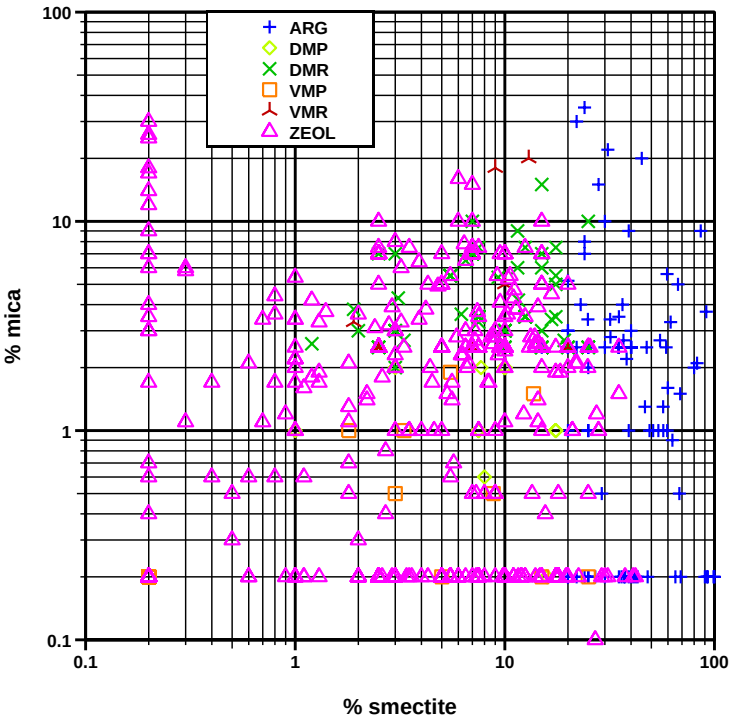

Figure 4-10. Logarithmic cross plot of smectite and mica percentage for all XRD data sorted by RMC.

5. Reactive Minerals in RMUs

Stoller Navarro (2007) identified and named reactive mineral units (RMUs) by grouping contiguous hydrostratigraphic and stratigraphic units with similar distributions of reactive minerals. The RMUs within the TCU are subunits of four hydrostratigraphic units – Upper Tuff Confining Unit (UTCU), Lower Tuff Confining Unit (LTCU), Oak Springs Butte Confining Unit (OSBCU), and Argillic Tuff Confining Unit (ATCU) described by Bechtel-Nevada (2006).

The RMUs differ from RMCs by having a stratigraphic and, therefore, a geometric context. The RMUs are laterally correlative subunits of the TCU. RMUs within the TCU fall into four main categories related to lithology and mineralogy:

- zeolitic -associated with massive zeolitized bedded tuffs,
- devitrified - associated with discontinuous welded ash flow tuffs,
- argillic – associated with argillized bedded tuffs at the base of the TCU, or
- volcaniclastic – associated with zeolitic detrital sediments at the base of the TCU.

Figure 5-1 illustrates the stratigraphic relationships of the RMUs within HSUs of the TCU. RMUs identified as “zeolitic bedded tuffs include “UT ZE” in the UTCU HSU, “TCU UZE” and “TCU LZE” within the LTCU, and “OSB UZE”, “OSB MZE2”, “OSB MZE1”, and “OSB LZE” within the OSBCU. RMUs identified as “devitrified mafic poor” include “BF DMP” within the LTCU and “YF DMR”, “RV DMP”, and “TP DMP” within the OSBCU. Only one RMU, the argillic “LT ARG”, is identified within the ATCU. The volcaniclastic “VC ZE” is part of the OSBCU, however, no mineralogic data are available for the “VC ZE” RMU. Table 5-1 summarizes categorization of RMUs within the TCU with respect to major lithology and mineralogy.

In some cases, data are assigned to another TCU hydrogeologic unit even though the RMU categories are typically in the TCU. For example, one datum with “LTCU” HSU and “TCUUZE” RMU is categorized into the “VTA” hydrogeologic unit. This analysis uses the RMU categorization, whether or not the data are in the TCU, because the mineral distributions within RMUs are found to be consistent whether or not the RMU is entirely located within the TCU. Thus, some non-TCU data can be used to characterize for reactive mineral distributions for RMUs that are mostly located within the TCU.

In this section, reactive mineral frequency distributions are evaluated with respect to RMUs. The RMU-based conceptual model for reactive mineral spatial variability

assumes RMUs are useful to distinguish statistically homogeneous sub-populations or "zones" of reactive mineral distributions in the TCU.

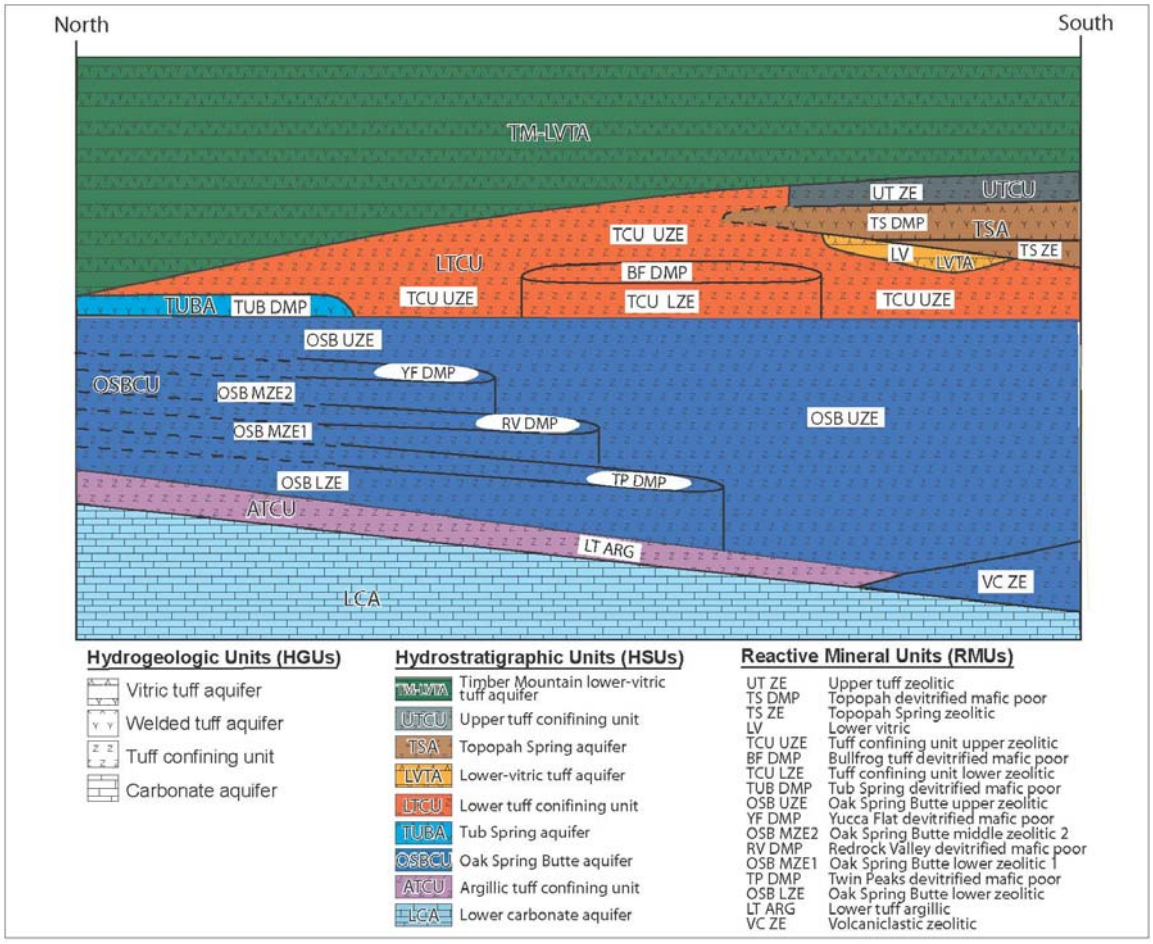

Figure 5-1. Schematic cross section depicting RMU and HSU subdivisions within the TCU and adjacent hydrogeologic units (from Stoller-Navarro, 2007).

The RMU conceptual model has several potential advantages for geostatistical characterization over the mineral percentage cutoff-based RMC approach for geostatistical characterization:

- Mineral percentage frequency distributions can overlap between different categories.
- Frequency distribution for different categories can have tails (e.g., extreme lows or highs).
- The RMUs can relate to geologic structures through coordinated interpretation of lithology, mineralogy, and stratigraphy.

- The RMU framework coordinates mineralogic zonation to vertical successions used in development of hydrostratigraphic framework models for flow and transport within Yucca Flat (Bechtel Nevada, 2006).

Table 5-1. Summary of RMU categorization relative to HSUs, major lithology and mineralogy, and typical stratigraphic unit (summarized from Table 1-3, Stoller-Navarro, 2007) in the TCU. All units are listed in vertical succession with upper most at the top.

HSU[1]	RMU	Major Lithology	Major Mineralogy	Typical Stratigraphic Units[2]
UTCU	UT ZE	bedded tuff	zeolitic	Tmr (lower most) Tmrh, Tp
LTCU	TCU UZE	bedded tuff	zeolitic	Tmrh, Tp, Th, Tw, Tc, Tn, Tub, Ton2, Ton1, To, Tlt
	BF DMP	ash flow tuff	devitrified mafic poor	Tcb
	TCU LZE	bedded tuff	zeolitic	Tc, Tbg, Tn4, Tn3
OSBCU	OSB UZE	bedded tuff	zeolitic	Ton2[3]
	YF DMR	ash flow tuff	devitrified mafic rich	Toy
	OSB MZE[2]	bedded tuff	zeolitic	Ton1[3]
	RV DMP	ash flow tuff	devitrified mafic poor	Tor
	OSB MZE[1]	bedded tuff	zeolitic	To[3]
	TP DMP	ash flow tuff	devitrified mafic poor	Tot
	OSB LZE	bedded tuff	zeolitic	To, Tlt
ATCU	LT ARG	tuff	argillic	To, Tlt
OSBCU	VCZE	volcaniclastic	zeolitic	Tgp, Tgw

[1]See Table 4-4 in Bechtel Nevada (2006) for explanation of HSU nomenclature.

[2]See Tables 4-1 and 4-2 in Bechtel Nevada (2006) for explanation of stratigraphic nomenclature.

[3]Includes older units if the underlying ash-flow tuffs (Toy, Tor, Tot) are not present.

However, there are several possible difficulties to anticipate in using a RMU-based approach to characterize spatial variability of reactive mineral distributions in the TCU:

- By nomenclature, the RMUs appear to map out specific "devitrified mafic poor" or "devitrified mafic rich" units. However, on cross-examination of RMC and RMU categorization, it is not uncommon for "mafic rich" RMCs to be located in a "mafic poor" RMU, and visa versa.

- The RMUs apparently do not distinguish vitric tuffs, which have similar reactive mineral distributions to devitrified tuffs but are formed by different processes.

Consideration of glass content is needed to distinguish vitric tuffs from other tuffs. Many "S" method data do not include glass, preventing distinction of vitric tuffs.

- Data may be too sparse and widely-spaced to characterize spatial variability (or spatial continuity) of mineral percentages or K_d in each RMU.

The reactive mineral facies (RMF) approach described in Chapter 6 takes advantage of the RMU geometric framework for defining zones for geostatistical analysis of reactive mineral distributions with some adjustments to address advantages/disadvantages of the RMC and RMU approaches. Preliminary to describing the RMF approach, reactive mineral frequency distributions in RMUs are evaluated below.

5.1 Calcite

Figure 5-2 shows calcite frequency distributions in RMUs, which show similar patterns of mostly zero calcite and a few non-zero calcite percentages typically below 10% within each RMU. The one exception is the LTARG RMU. Although LTARG data are about 57% zero values, the proportion of non-zero data is notably greater and the values of non-zero calcite percentages are higher in LTARG relative to all other RMUs. Differences in calcite frequency distributions between different RMUs excluding LTARG are not significant. Therefore, calcite data are not generally useful to distinguish RMUs except, possibly, between LTARG and non-LTARG RMUs. The XRD data suggest that the LTARG RMU is not only distinctively argillic but, possibly, relatively calcitic compared to other RMUs in the TCU.

In comparison of calcite frequency distribution to the ARG RMC (Figure 4.3), the LTARG RMU has less data but relatively more non-zero calcite percentages. While argillic zones in bedded tuffs are identified as ARG RMCs, the data indicate calcite is more abundant in argillic zones within LTARG at the base of the TCU. However, sampling location patterns or variations in the XRD methods used may impact interpretability of these subtle differences in calcite distribution within TCU. If calcite is indeed more abundant within LTARG, it may be useful for transport prediction to distinguish the LTARG from other argillic zones and other RMUs because several radionuclide classes – Sm, Eu, Am, Np, and Pu – are relatively strong sorbers to calcite compared to other reactive minerals.

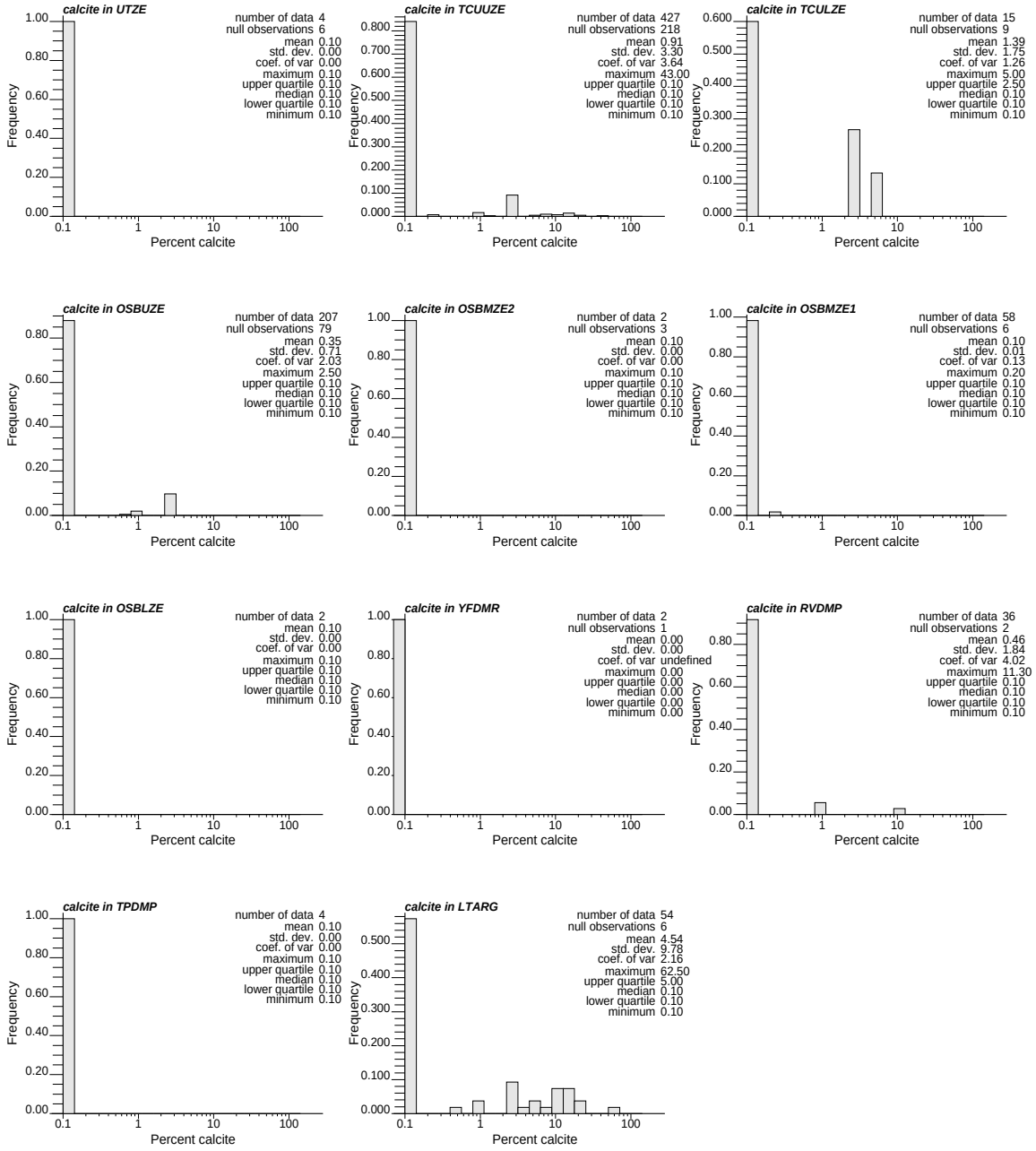

Figure 5-2. Logarithmic scale frequency distributions of calcite percentage within RMUs.

5.2 Hematite

Figure 5-3 shows hematite frequency distributions in RMUs. As discussed in Section 4.2.3 hematite data are far less numerous than for the other reactive minerals, so interpretability of the hematite data is limited. Hematite frequency distributions in RMUs show a similar pattern to calcite, with mostly zero hematite and a few non-zero hematite

percentages, typically below 3%. Like calcite, the LTARG RMU is a possible exception to the overall pattern of hematite occurrence in the TCU. The proportion of non-zero data hematite may be greater in LTARG relative to all other RMUs. Differences in hematite frequency distributions between different RMUs excluding LTARG are not significant. Hematite frequency distributions for LTARG and non-LTARG RMUs appear to be distinct.

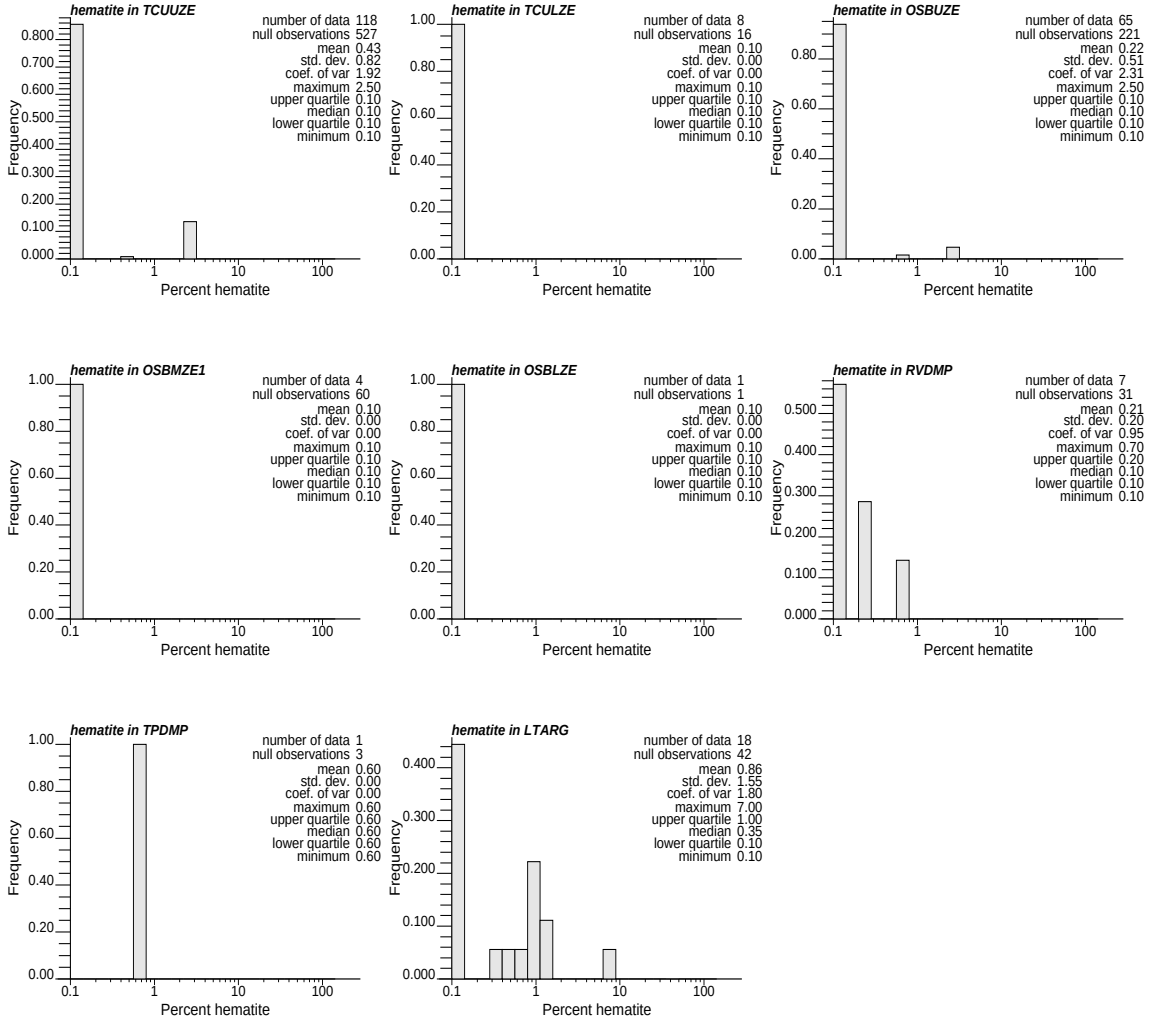

Figure 5-3. Logarithmic scale frequency distributions of hematite percentage within RMUs.

In comparison to hematite in the ARG RMC (Figure 4-4), the LTARG RMU has less data but similar hematite frequency distributions. The data indicate hematite is similar in abundance in argillic zones within and outside the LTARG RMU - different than for calcite, which appears relatively more abundant within the LTARG RMU. As for calcite, variations in the XRD methods used and sampling locations may impact interpretability of these subtle differences in hematite distributions between different RMUs or RMCs of

the TCU. If hematite is indeed more abundant within the LTARG RMU or ARG RMC, it may be useful in transport prediction to distinguish hematite abundance in argillic zones because several radionuclide classes – Np, Pu, and U – are relatively strong sorbers to hematite compared to other reactive minerals.

5.3 Mica

Figure 5-4 shows mica frequency distributions in RMUs, which are generally similar throughout the TCU. Data are most abundant for the TCUUZE (546) and OSBUZE (268) RMUs. The frequency distributions for TCUUZE and OSBUZE are similar for both zero and non-zero data. The most noticeable differences in mica distributions between different RMUs relate to proportions of zero values (e.g. TCULZE) and shape of non-zero frequency distribution (e.g. RVDMP). The mica frequency distributions show a spike of data values between 2.5 to 3.0%, suggesting impacts from method detection limit and accuracy. Many "S" method data resolve mica percentage to 2.5% with an uncertainty of 2.5% (Warren, 2007). Because mica percentages are generally only a few percent, XRD method detection limit directly affects relative proportions of zero and non-zero data and, thus, resolution of the lower tail of the frequency distribution. The combined effects of XRD method detection limits, typically low mica percentage, and uncertainty make it difficult to distinguish truly significant differences in mica frequency distributions between different RMUs.

For most RMUs, it is plausible that mica is ubiquitously non-zero. The shapes of the frequency distributions suggest that many mica data "zero" values could actually represent non-zero percentages. Mica percentage is expected to be zero in some thin, peralkaline, ash fall tuffs of the "Tub" hydrostratigraphic unit within the TCUUZE RMU and the "Tbg" and "Tn4" hydrostratigraphic units within the TCULZE RMU (written communication, Drellack, 2007). As shown in Figure 5-4, over 35% of the 546 mica data in TCUUZE are zero values, but none of the 23 mica data in TCULZE are zero values. Therefore, mica percentage data obtained from peralkaline ash-fall tuffs must originate from the TCUUZE.

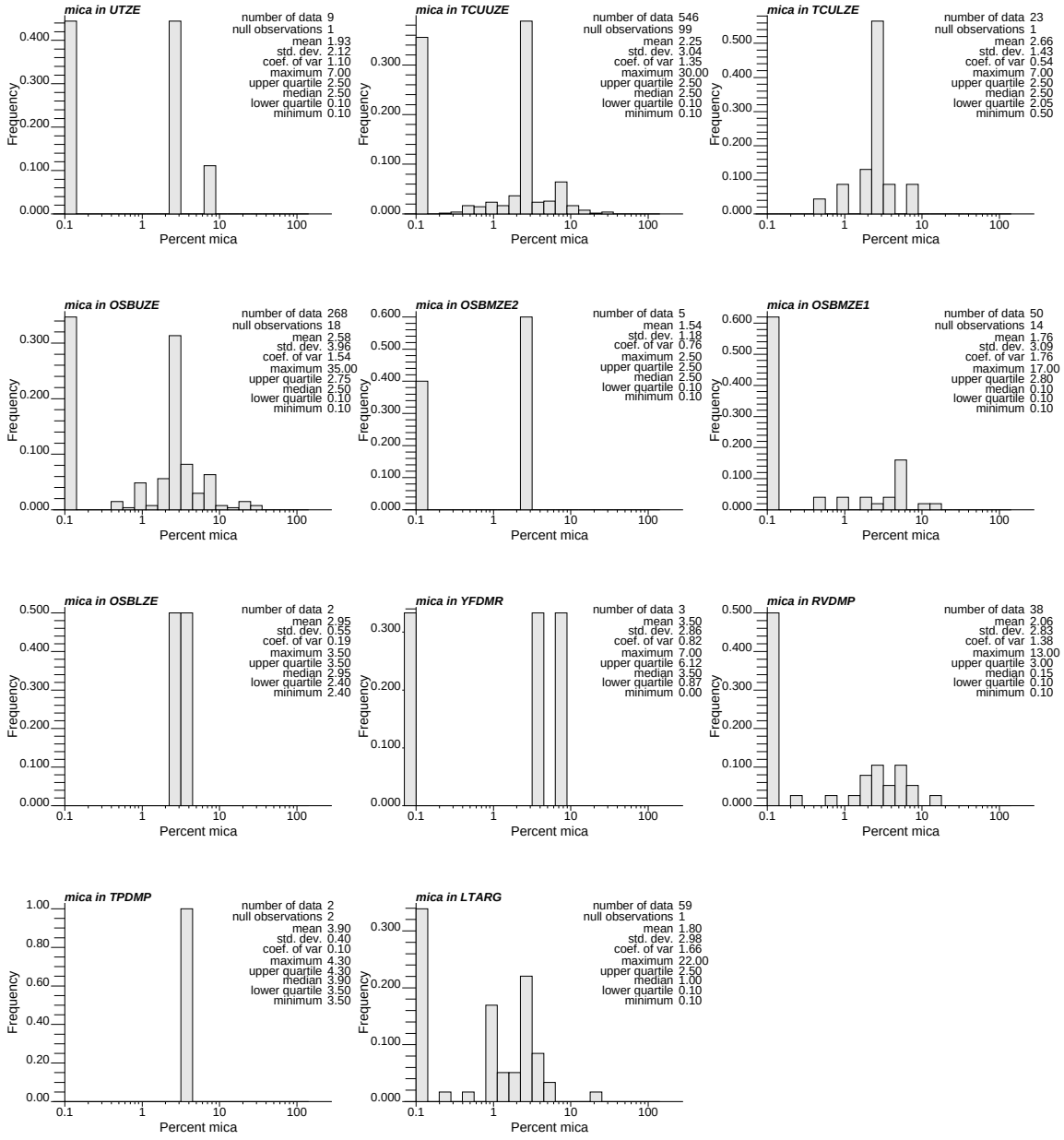

Figure 5-4. Logarithmic scale frequency distributions of mica percentage within RMUs.

5.4 Smectite

Smectite is arguably the most important reactive mineral affecting prediction of radionuclide transport in the TCU for several reasons:

- Smectite is the only reactive mineral that sorbs all 10 radionuclide classes (^{41}Ca, Cs, Sr, Ni, Sm, Eu, Am, Np, Pu, U).

- For 7 of 10 radionuclide classes (Ni, Sm, Eu, Am, Np, Pu, U), smectite is the only sorber that is consistently present in measurable quantities within the TCU.

- Further interpretation of smectite data (Section 7.2) indicates smectite is ubiquitous throughout the TCU and, thus, would sorb all radionuclide classes throughout the entire TCU.

- Although calcite, hematite, or mica have higher capacity than smectite to sorb most radionuclide classes (Sr, Sm, Eu, Am, Np, Pu, and U), greater abundance of smectite in the TCU causes smectite to have more overall impact on radionuclide K_d than any other reactive mineral.

Subsequently, differences in smectite spatial distributions for different RMUs will have strong impact on differences in radionuclide transport properties in the TCU. Figure 5-5 shows frequency distributions of smectite percentage within RMUs. The smectite frequency distributions for different RMUs indicate several characteristics of zonal variability within the TCU:

- Within bedded tuffs, there is a general increase in smectite percentage with depth. Mean smectite percentage increases with depth beginning with the UTZE (1.99) of the UTCU, the TCUUZE (6.61) and TCULZE (4.84) of the LTCU, the OSBUZE (10.97) , OSBMZE2 (8.44), OSBMZE1 (11.62), OSBLZE (8.75) of the OSBCU, the LTARG (39.98)

- With respect to lithology, the lowest overall smectite percentages occur in the devitrified tuffs – YFDMR (3.33), RVDMP (4.94), and TPDMP (8.9). These mean values show increase with depth too, although the differences are not significant because only 3 data are available for YFDMR and 4 data for TPDMP compared to 38 data for RFDMP.

- The devitrified RMUs – YFDMR, RVDMP, and TPDMP - are situated within the OSBCU HSU. Smectite percentages are lower in the devitrified tuffs compared to the zeolitic tuffs in the same HSU.

- Smectite frequency distributions are similar within each HSU, except for the devitrified tuffs. Major depth trends for smectite percentage can be largely captured with zonation based on HSUs .

As for other reactive minerals, differences in frequency distributions for smectite percentage between different RMUs can, in part, be attributed to methods used. Resolution of smectite percentage estimates is limited to varying degrees depending on XRD method. Similar to mica, smectite frequency distributions from RMUs with low smectite percentage tend to show spikes near 2.5 because of numerous “S” method data

with estimates of 2.5 and uncertainty of 2.5 (a range of 0.0 to 5.0). Smectite frequency distributions appear to be tailed toward low percentages, however, low-percentage tails cannot be resolved by the XRD methods used except, possibly, the “F” method. Importantly, even though many XRD data indicate “zero” smectite, small percentages of smectite, such as 1-2%, are likely undetected by all but the “F” method. Yet small percentages of smectite would impart appreciable retardation on all radionuclide classes except Np and U.

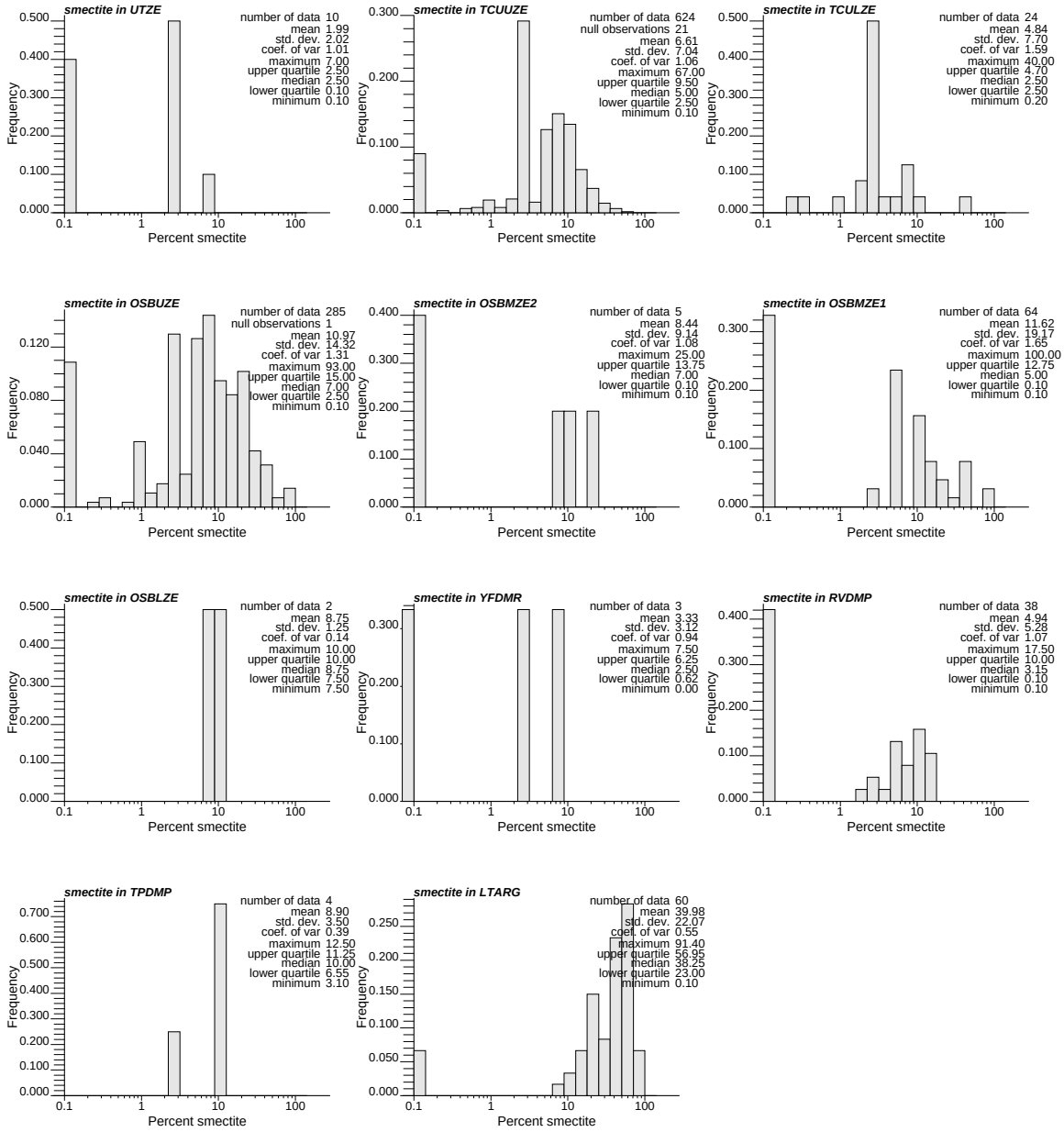

Figure 5-5. Logarithmic scale frequency distributions of smectite percentage within RMUs.

5.5 Zeolite

Zeolite is the most abundant reactive mineral in the TCU. Most of the XRD data are obtained from zeolitic bedded tuffs categorized into zeolitic RMUs - UTZE, TCUUZE, TCULZE, OSBUZE, OSBMZE2, OSBMZE1, and OSBLZE. However, the entire XRD dataset indicates the lower tails of zeolite percentages in the zeolitic RMUs overlap with zeolite frequency distributions in non-zeolitic RMUs – YFDMR, RVDMP, TPDMP, and LTARG.

Although zeolite is abundant through much of the TCU, only 3 of 10 radionuclide classes – ^{41}Ca, Cs, and Sr – sorb to zeolite. The distribution of zeolite in the TCU has no effect on 7 of 10 radionuclide classes – Ni, Sm, Eu, Am, Np, Pu, and U. Smectite has much more overall effect on radionuclide transport in the TCU than zeolite.

Zeolite percentage generally decreases with depth in the TCU in tandem with the general increase in smectite percentage with depth. Figure 5-6 shows frequency distributions of smectite percentage within RMUs. Mean zeolite percentage in RMUs decreases with depth in non-devitrified RMUs beginning with UTZE (70.60) of the UTCU HSU, TCUUZE (53.68) and TCULZE (40.14) of the LTCU HSU, the OSBUZE (42.91) , OSBMZE2 (44.0), OSBMZE1 (35.05), OSBLZE (21.55) of the OSBCU HSU, and LTARG (3.60) of the ATCU HSU. The only exception to the depth-dependent decrease in zeolite percentage is TCULZE, which may be attributed to limited sampling or inclusion of data from devitrified or vitric tuffs. The TCULZE has only 23 data compared to 634 and 285 data in RMUs above and below. Mean percentage in the TCULZE is driven downward by a relatively larger tail of low zeolite percentages compared to other zeolitic RMUs.

Overall the major differences between zeolite frequency distributions for different RMUs are attributed to the major differences in lithology and alteration – zeolitic bedded tuffs, devitrified tuffs, and argillic tuffs and an overall trend of decreasing zeolite with depth.

The main difference in zeolite percentage is between the zeolitic bedded tuffs and the combination of devitrified and argillic tuffs. The devitrified and argillic tuffs have similar zeolite frequency distributions, including large proportions of zero values.

Significant differences between RMUs within zeolitic bedded tuffs within the UTCU (UTZE only) and LTCU (TCUUZE and TCULZE) HSUs are not obvious. Similarly, significant differences between zeolitic bedded tuff RMUs (OSBUZE, OSBMZE2, OSBMZE1, and OSBLZE) within the OSBCU HSU are not obvious. As for other reactive minerals, the differences between different RMUs should not be overanalyzed considering differences in number of data, spatial distribution of sample locations, and XRD method.

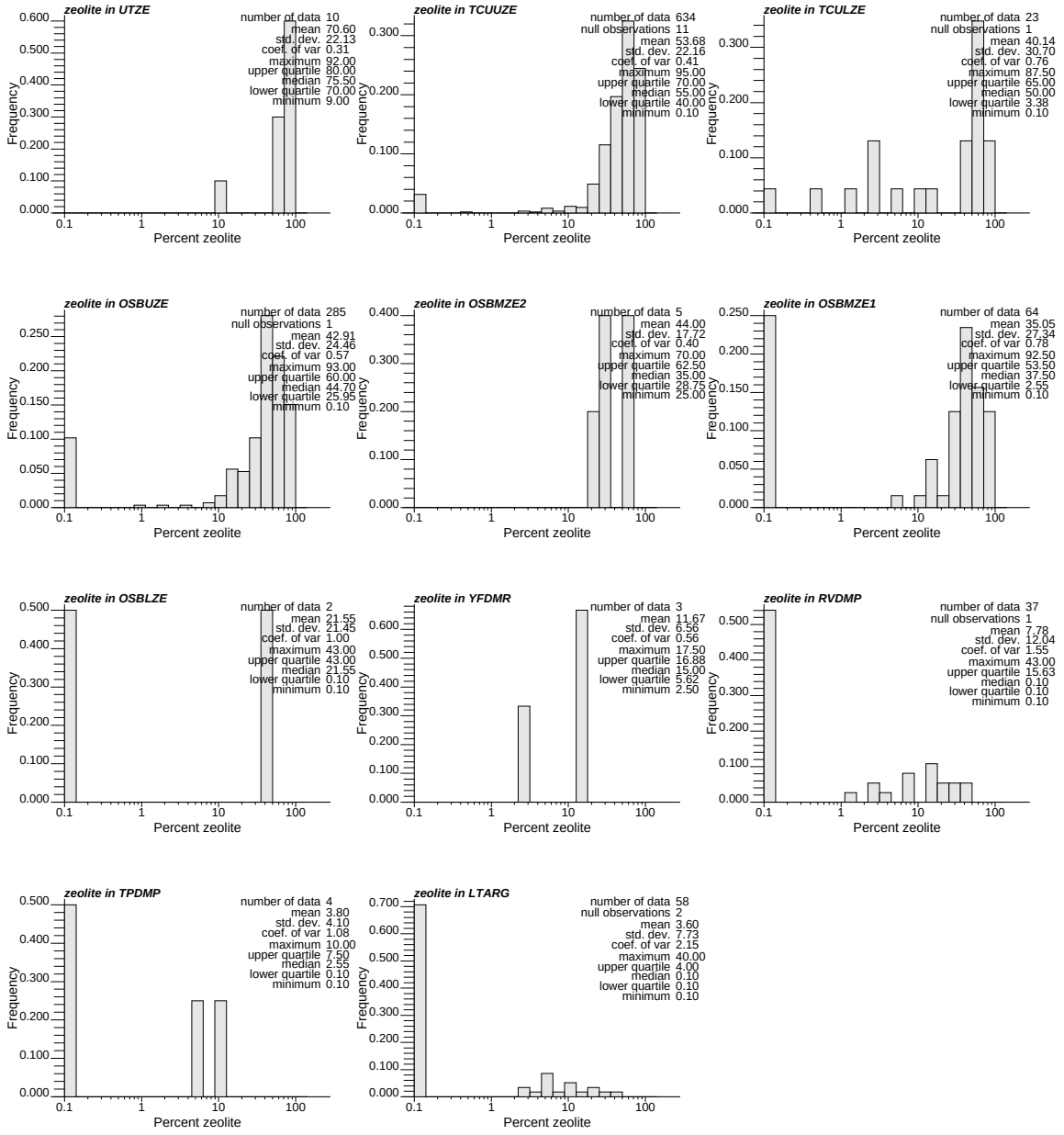

Figure 5-6. Logarithmic scale frequency distributions of smectite percentage within RMUs.

5.6 Reactive Mineral Cross Relationships in RMUs

As discussed in Section 4.3 in analysis of cross relationships of reactive minerals within the RMC framework, smectite and zeolite have the most impact on distinguishing zonal variation of reactive minerals in the TCU. Calcite, hematite, and mica do not show large variations between RMUs, with the possible exception for calcite and hematite in the

ARG RMC or LTARG RMU, which are clearly distinguished by high smectite compared other RMCs and RMUs.

Frequency distributions for reactive minerals appear similar for RMUs within HSUs except for devitrified RMUs, which generally have low smectite and low zeolite relative to the rest of the HSU. Based on the 10 data in the UTZE RMU in the UTCU HSU, reactive mineral distributions in zeolitic bedded tuffs of the UTCU and LTCU HSUs appear similar, particularly if the lower tail of TCULZE RMU is excluded. A logical grouping of RMUs to simplify zonal variation in the TCU to four zones with similar lithologic and reactive mineral distribution characteristics is described and named below in bold:

- **L-UTCU**. Combine the UTZE, TCUUZE, and TCULZE RMUs or, equivalently, combine zeolitic bedded tuffs RMUs within the UTCU and LTCU HSUs.

- **OSBCU.** Combine the OSBUZE, OSBMZE2, OZBMZE1, and OSBLZE RMUs or, equivalently, combine zeolitic bedded tuffs within the OSBCU HSU.

- **DMP-R**. Combine the BFDMP, YFDMR, RVDMP, and TPDMP RMUs or, equivalently, combine devitrified ash flow tuffs of the LTCU and OSBCU HSUs. (note no XRD data are categorized into the BFDMP RMU).

- **LTARG**. Maintain the LTARG RMU (or ATCU HSU) as a distinct zone

Figure 5-7, a cross-plot of smectite and zeolite percentage, illuminates several patterns of reactive mineral zonation within the TCU:

- Smectite and zeolite distributions are similar in the **L-UTCU** and **OSBCU** zones. Some difficulty remains in distinguishing differences in smectite and zeolite distributions between **L-UTCU** and **OSBCU** zones from the composite data set because of differing XRD methods.

- Smectite and zeolite percentages can overlap between devitrified and zeolitic zones, contrary to the RMC framework. For some data ascribed to zeolitic RMU groups, particularly the **L-UTCU** zone, some zeolite and smectite percentages are very similar or even less than typical percentages in the devitrified **DMP-R** zone. Certain intervals of the zeolitic **L-UTCU** and **OSBCU** zones may impart similar reactive mineral characteristics to the **DMP-R** zones

- Smectite and zeolite percentages can overlap between argillic (LTARG) and zeolitic RMUs, particularly where zeolite percentage is less than 10%. Certain intervals of the **OSBCU** zone may impart very similar reactive mineral characteristics to the argillic **LTARG** zone.

- A few data in **LTARG** have high zeolitic percentages that overlap into typical zeolitic zone percentages. It is reasonable to assume this overlap is not only statistical, but related to XRD method. While the LTARG RMU (or ATCU HSU) is distinctively argillized, zeolite is also present.

Figure 5-8 and Figure 5-9, cross plots of smectite and mica percentage and mica and zeolite percentage, are not as revealing as the smectite and zeolite percentage cross plot in Figure 5-7. As discussed previously in Sections 4.2.4 and 4.3, mica percentage frequency distributions exhibit few significant differences throughout the TCU and, subsequently, mica does not help distinguish the **L-UTCU**, **OSBCU**, **DMP-R**, and **LTARG** zones.

5.7 Geostatistical Analysis in a RMU Framework

While the grouped RMUs show promise for distinguishing zones within the TCU having similar distributions of reactive minerals, several problems remain to be resolved for subsequent application of geostatistical analysis:

- Reactive mineral frequency distributions on linear or logarithmic scales do not fit Gaussian assumptions.
- Some RMU reactive mineral frequency distributions show outliers, such as smectite zero values and zeolite in the lower percentage tail of zeolitic RMUs.
- While vitric RMCs are defined, vitric RMUs are not defined. Vitric tuffs have unusually low zeolite and smectite similar to devitrified tuffs, however, lithology differs. Thus, vitric tuffs can be expected to have a distinctive combination of geometric and reactive mineral properties. Distinction of vitric tuffs may also explain some outliers in smectite and zeolite content in RMUs.

To address these problems, a combination of an additive log-ratio (ALR) approach to defining frequency distributions and consideration of ratios between (smectite+zeolite) and felsic minerals is implemented in Chapter 6 to define reactive mineral facies (RMFs). The spatial distribution of RMFs is assumed to be largely tied to RMUs.

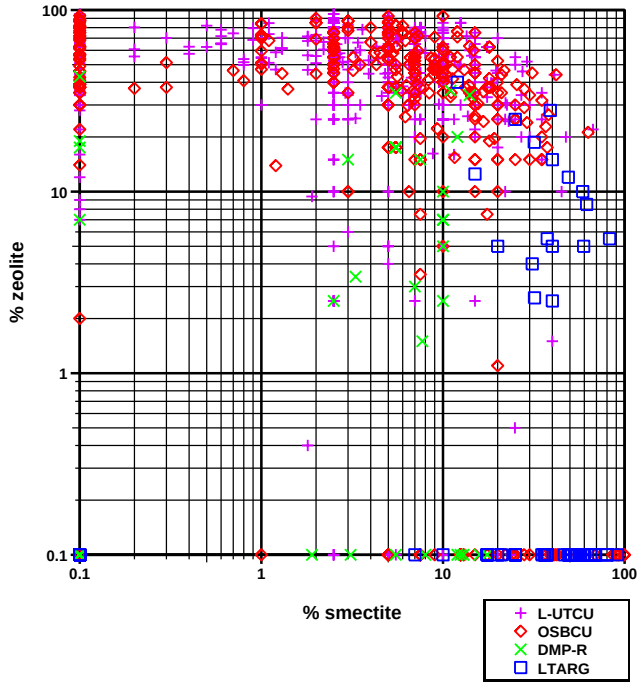

Figure 5-7. Log-scale cross plot of smectite and zeolite percentage sorted by zones defined by grouped RMUs.

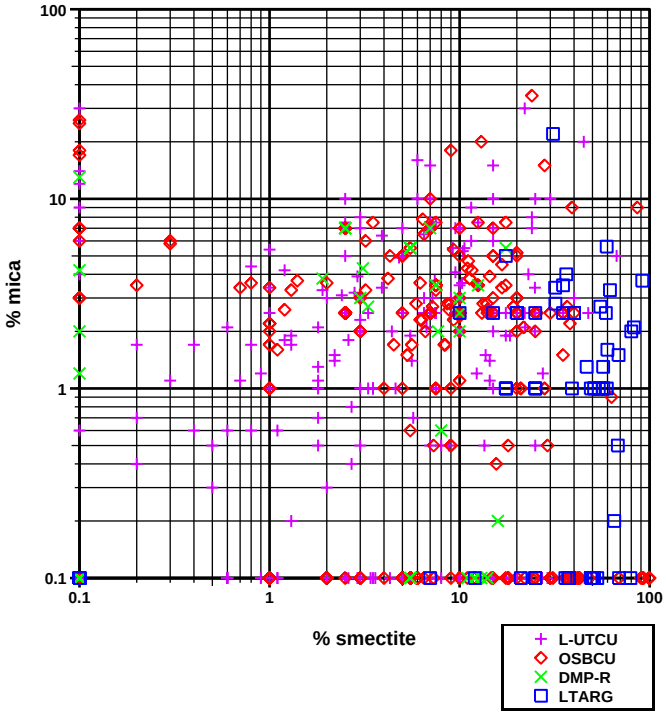

Figure 5-8. Log-scale cross plot of smectite and mica percentage sorted zones defined by grouped RMUs.

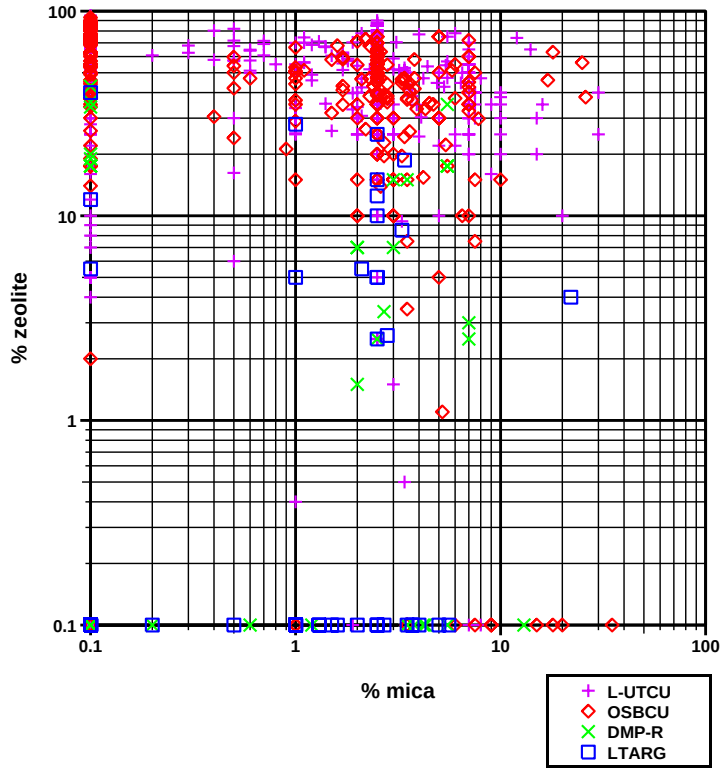

Figure 5-9. Log-scale cross plot of mica and zeolite percentage sorted by zones defined as grouped RMUs.

6. Distinction of Reactive Mineral Facies

A key step in distinction of reactive mineral facies for subsequent geostatistical analysis is interpretation of the logarithm of the ratios (log ratio) between mineralogic percentages or fractions – the additive log ratio transformation. In most cases, compositional data fit a Gaussian assumption better using a log ratio scale compared to linear or logarithmic scales.

6.1 Additive Log Ratio

XRD mineral fractions or percentages constitute compositional variables – vector variables with components that sum to unity (or 100%). The components of compositional variables are bounded between 0 and 1 (or 0 and 100%). As discussed in Section 3.4.3, compositional variables present several difficulties to application of geostatistical methods, which the additive log ratio (ALR) transformation directly confronts:

- ALR transformation of compositional data frequency distributions is better suited to Gaussian assumptions, including symmetry and infinite tailing.
- Cokriging equations formulated by ALR variables are not inherently singular.
- ALR covariances do not suffer from spurious cross-correlations caused by the compositional data summing constraint.
- ALR backtransformation honors summing and bounding constraints.

As discussed in Section 3.4.4, the additive log ratio (ALR) transformation, y_i ,applied to categories defined by reactive minerals can be defined as the logarithm of the ratio between the fraction, $f_{r,i}$, of reactive mineral *i* divided by the fraction, f_{nr}, of non-reactive minerals

$$y_i = \log_{10}\left\{\frac{f_{r,i}}{f_{nr}}\right\}$$

Geostatistical methods, such as variogram calculation and modeling, kriging and cokriging, and simulation, can all be applied to the ALR transformation domain (Pawlosky-Glahn and Olea, 2004). Backtransformation from the ALR, y_i , to the reactive mineral fraction, $f_{r,i}$, is achieved by

$$f_{r,i} = \frac{10^{y_i}}{1.0 + \sum_{k=1}^{N} 10^{y_k}}$$

6.2 Characterization of Reactive Mineral Facies

Three log ratio relationships will be used to characterize reactive mineral facies (RMFs), specifically to distinguish between zeolitic, argillic, devitrified, and vitric facies:

- Smectite/non-reactive and zeolite/non-reactive log ratios
  - to distinguish zeolitic from argillic facies,
- Smectite/felsic and zeolite/felsic log ratios
  - to distinguish devitrified from zeolitic and argillic facies, and
- Smectite/glass and zeolite/glass log ratios
  - to distinguish vitric from zeolitic and argillic facies.

Zeolitic facies will be divided into two zones – L-UTCU and OSBCU – originating from grouped RMUs and corresponding to UTCU-LTCU (combined) and OSBCU HSUs. Thus five RMFs will be distinguished as defined below:

- **L-UTCU Zeolitic** – the more zeolitic portions of Lower and Upper Tuff Confining Units (LTCU and UTCU).
- **OSBCU Zeolitic** – the more zeolitic portions of the Oak Springs Butte Confining Unit (OSBCU).
- **Argillic** – the more argillic portions of the Lower Tuff Argillic and zeolitic RMUs.
- **Devitrified** – devitrified rocks largely within devitrified mafic poor RMUs in the OSBCU and to lesser extent within other zeolitic or argillic RMUs.
- **Vitric** – vitric rocks largely within the Upper Tuff Confining Unit (UTCU).

Cross plots of log ratios involving reactive and felsic minerals and grouped RMUs are used to distinguish RMFs.

6.2.1 Smectite-Zeolite ALR

Cross-plots of the ALR are useful for categorization of different populations (e.g., RMFs) within the composite data. In particular, cross-plots comparing smectite and zeolite abundance are most useful for distinguishing RMFs within the TCU.

Figure 6-1 shows a cross-plot of smectite and zeolite ALR using only "F" method data (highest quality) XRD data, with data sorted by color into zones of grouped RMUs - **L-UTCU**, **OSBCU**, **DMP-R**, and **LTARG** as described in Section 5.6. Considering that the "F" data are the most accurate, this cross-plot suggests clear distinctions between different reactive mineral populations. The zeolitic RMU zones, **L-UTCU** and **OSBCU**, have similar distributions in zeolite and smectite ALR. **L-UTCU** tends to have slightly higher zeolite and, conversely, lower smectite ALR compared to **OSBCU**. The **LTARG** zone has distinctively high smectite ALR and relatively low zeolite ALR. On the cross-plot, "F" data within the **LTARG** zone fall distinctively within the lower right portion of the cross-plot. Some overlap between **LTARG** and **L-UTCU** or **OSBCU** is suggested where zeolite is high in **LTARG** or smectite is high and zeolite is low in **L-UTCU** or **OSBCU**. Devitrified rocks within the **DMP-R** have distinctively low smectite and low zeolite. Where zeolite is zero (plotted on log scale at -3), the distinction between rocks in **DMP-R** and **LTARG** is clear. Where zeolite is low but non-zero, some overlap is evident between **DMP-R** and zeolitic **L-UTCU** and **OSBCU** zones. This overlap could be attributed to several causes:

- Vitric rocks with similar low smectite and low zeolite,
- Outliers within a "zeolitic" distribution,
- Devitrified "mafic-rich" otherwise belonging lithologically and mineralogically to a devitrified facies.

Figure 6-2 shows a cross-plot of smectite and zeolite ALRs for "S" data only. The same general patterns in Figure 6-1 for "F" data are seen in Figure 6-2 for "S" data. However, there is much more overlap between zeolitic **L-UTCU** and **OSBCU** and argillic **LTARG** zones of grouped RMUs. Additionally, devitrified **DMP-R** overlaps considerably with zeolitic **L-UTCU** and **OSBCU** where zeolite and smectite are non-zero and within **LTARG** where zero-valued zeolite data are plotted as log{zeolite/non-reactive = –3}. In addition to the same reasons given for "F" data above, "S" data resolution and uncertainty certainly contributes to overlap of smectite and zeolite ALR distributions between different zones. Notably, "S" data resolve smectite and zeolite ALRs down to about -1.6 compared to -2.4 for "F" data. The limited resolution of the "S" data is also evident in the cross-plots as curved bands of data, which become more pronounced to the left (lower smectite content). Errors from uncertainty in "S" data values increase scatter in frequency distributions and, therefore, increase overlap between different data

populations. Nonetheless, the "S" data are, in most cases, adequate in quality to distinguish RMFs. Since "S" data are most numerous in the TCU, "S" data have potential to provide more extensive reactive mineral characterizations than all other XRD data combined. However, data spacing should be considered in weighing the overall value of "S" data, because much "S" data is collected along closely spaced (5-10 ft) intervals with repetitive data values.

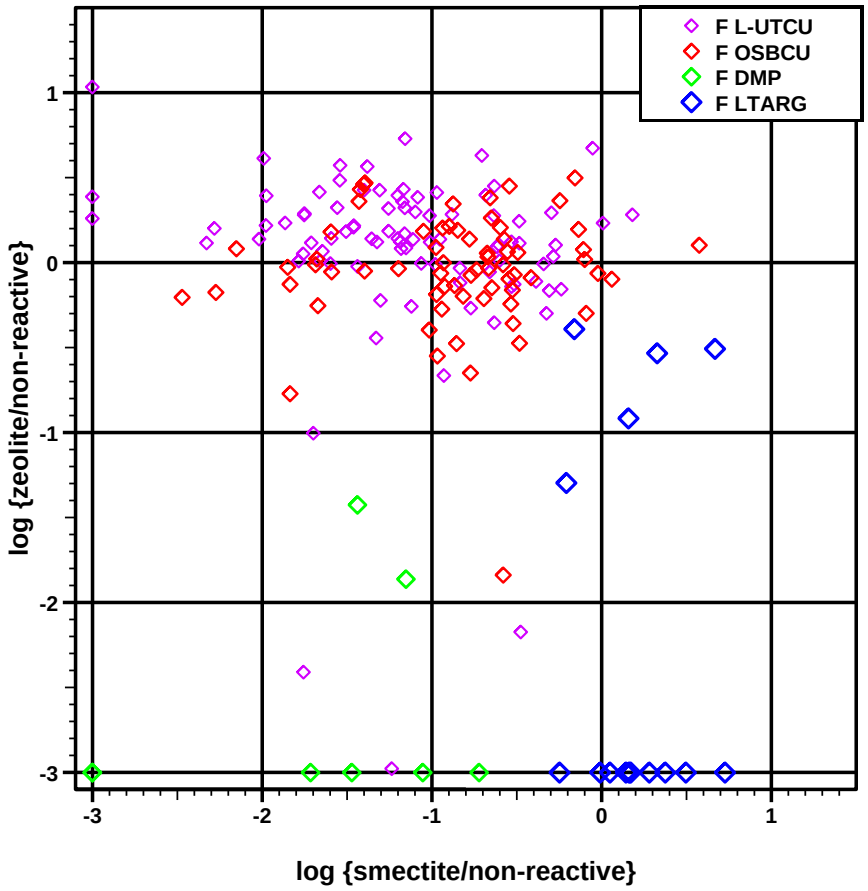

Figure 6-1. Cross-plot of smectite and zeolite ALRs using "F" method data categorized by zones based on grouped RMUs.

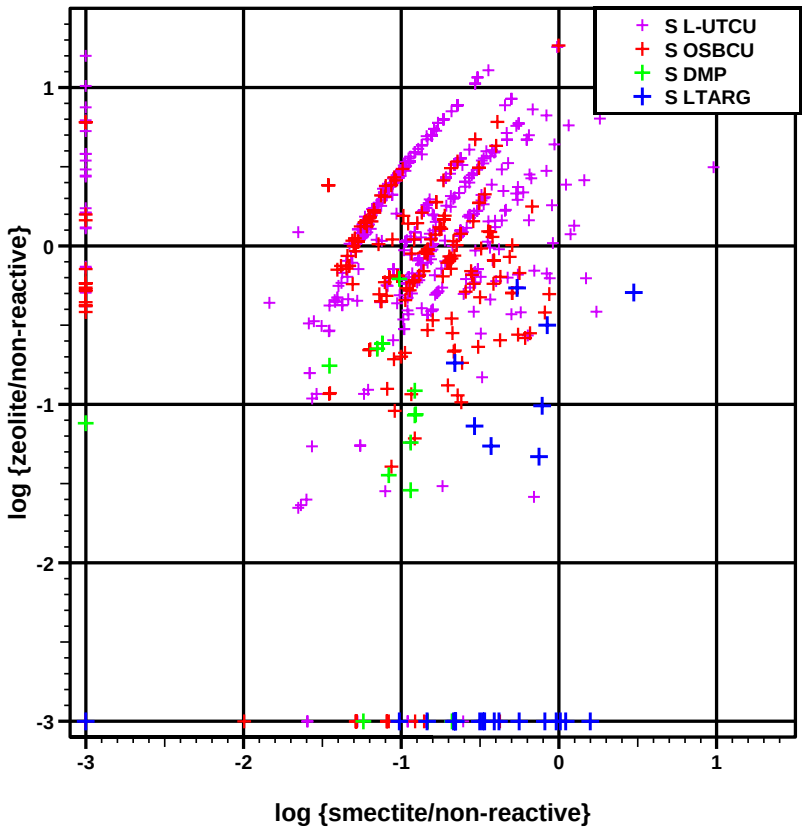

Figure 6-2. Cross-plot of smectite and zeolite ALRs using "S" method data categorized by zones based on grouped RMUs.

Figure 6-3 shows a cross-plot of smectite and zeolite ALRs for "E" data only. Compared to "F" and "S" data, "E" data show the poorest resolution as evident by a high proportion of zero (-3. on log scale) values and general lack of resolution of smectite and zeolite ALRs below about -0.5 to -1.0. Given the "E" data alone, the large proportion of zero values for smectite implies that large proportions of the TCU, particularly zeolitic and devitrified RMUs, have zero smectite. In comparison, the "F" data ALR distribution for smectite clearly implies that the few "zero" smectite XRD measurements are very likely non-zero values below the detection limit. The "E" data could give an impression of patchy smectite occurrence whereas the more accurate "F" data indicate ubiquitous smectite.

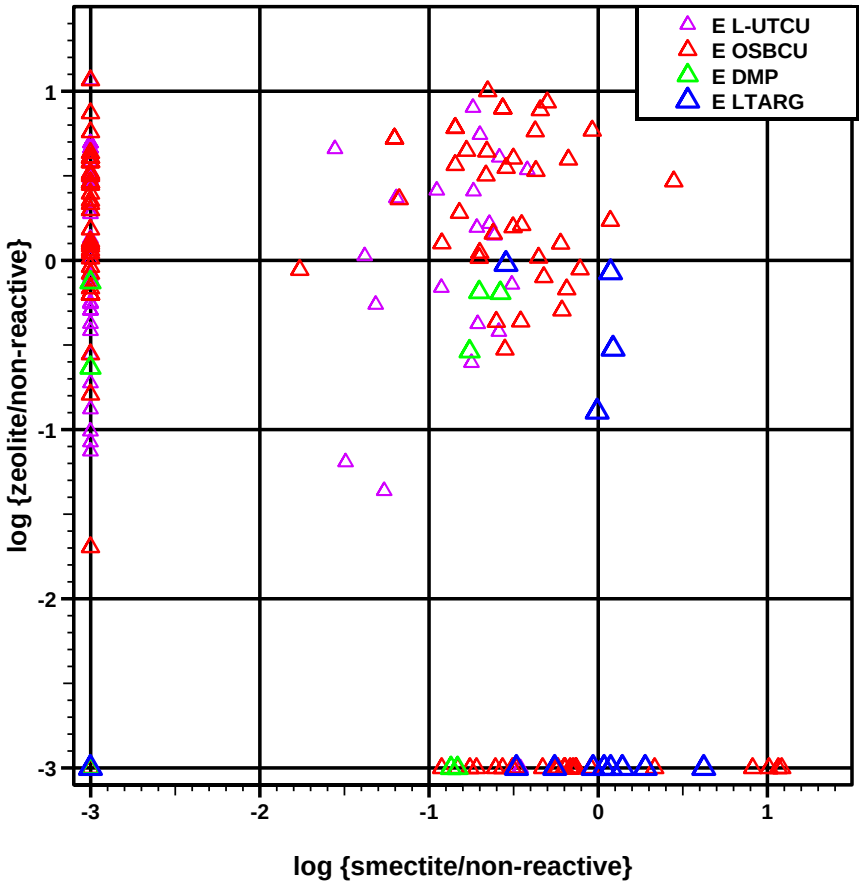

Figure 6-3. Cross-plot of smectite and zeolite ALRs using "E" method data categorized by zones based on grouped RMUs.

Figure 6-4 shows a cross-plot of smectite and zeolite ALRs for the composite of "F", "S", and "I" method data. Only 5 "I" method data are present in the TCU XRD data set, all located within the LTARG RMU. The composite "F", "S", "I" data is recommended for use in reactive mineral facies (RMF) identification. While "S" data lack resolution at low percentages, "S" data resolution is sufficient to resolve between zeolitic and argillic facies unlike "E" data, which has inadequate resolution of low smectite percentage. Sections 6.2.2 and 6.2.3 focus on distinguishing devitrified and vitric facies.

As discussed above, some difficulty arises in distinguishing zeolitic from argillic facies. Cross plots of zeolite and smectite percentages and ALRs overlap between the argillic LTARG RMU and zeolitic **L-UTCU**, and **OSBCU** grouped RMUs. Use of reactive mineral categories (RMCs) is problematic because a portion of zeolitic facies with relatively low zeolite and high smectite can be categorized as "argillic" even though smectite and zeolite percentages within facies can be expected to have tailed distributions. Figure 6-5 shows RMC categorizations of argillic superposed on the cross-plot of smectite and zeolite ALRs. The solid magenta line represents a smectite/zeolite

ratio of 3, which provides criteria for distinguishing "argillic" characteristics mostly occupied by data from the LTARG RMU. Some high zeolite percentages in LTARG RMU data cause overlap above the smectite/zeolite=3 ratio. Three notable exceptions below the magenta line have argillic RMCs and zeolitic RMUs. These data clearly fall within the range of "argillic" smectite and zeolite content. Three data showing as black circles with no RMU categorization are clearly within a range of "argillic" smectite and zeolite content. Data with low zeolite and to the left of the magenta line could be categorized as devitrified or vitric, as discussed below.

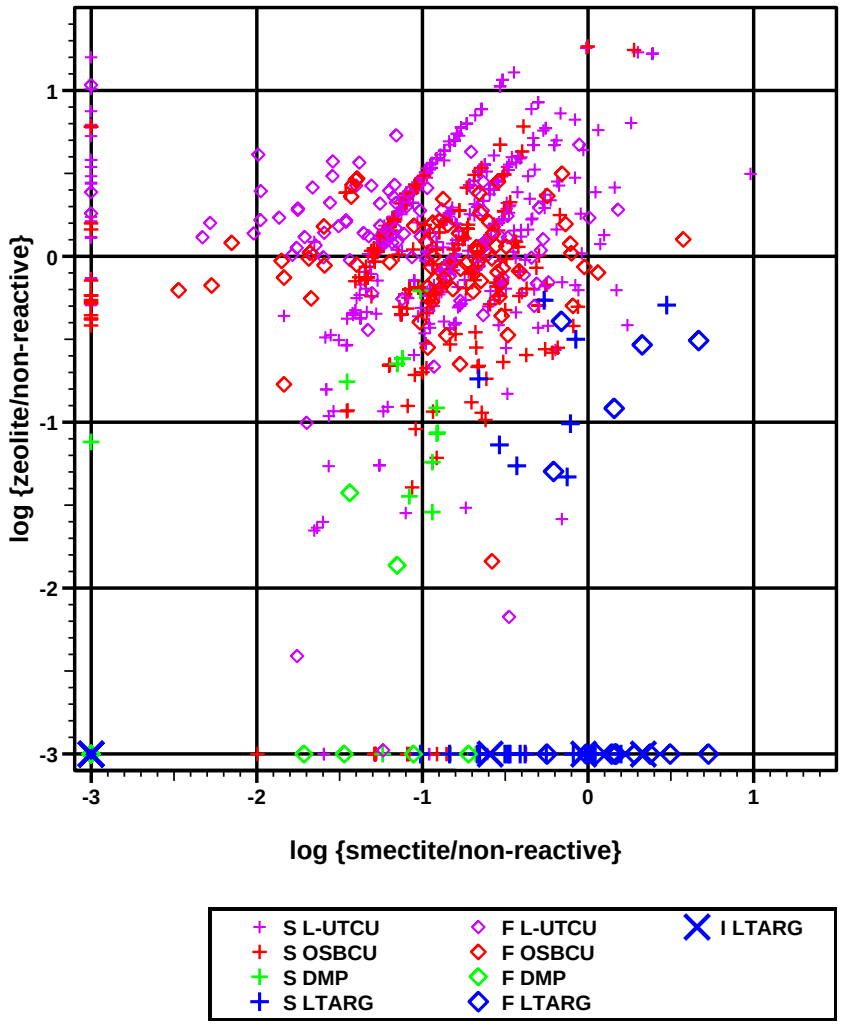

Figure 6-4. Cross-plot of smectite and zeolite ALRs using F, S, and I method data categorized by zones based on grouped RMUs.

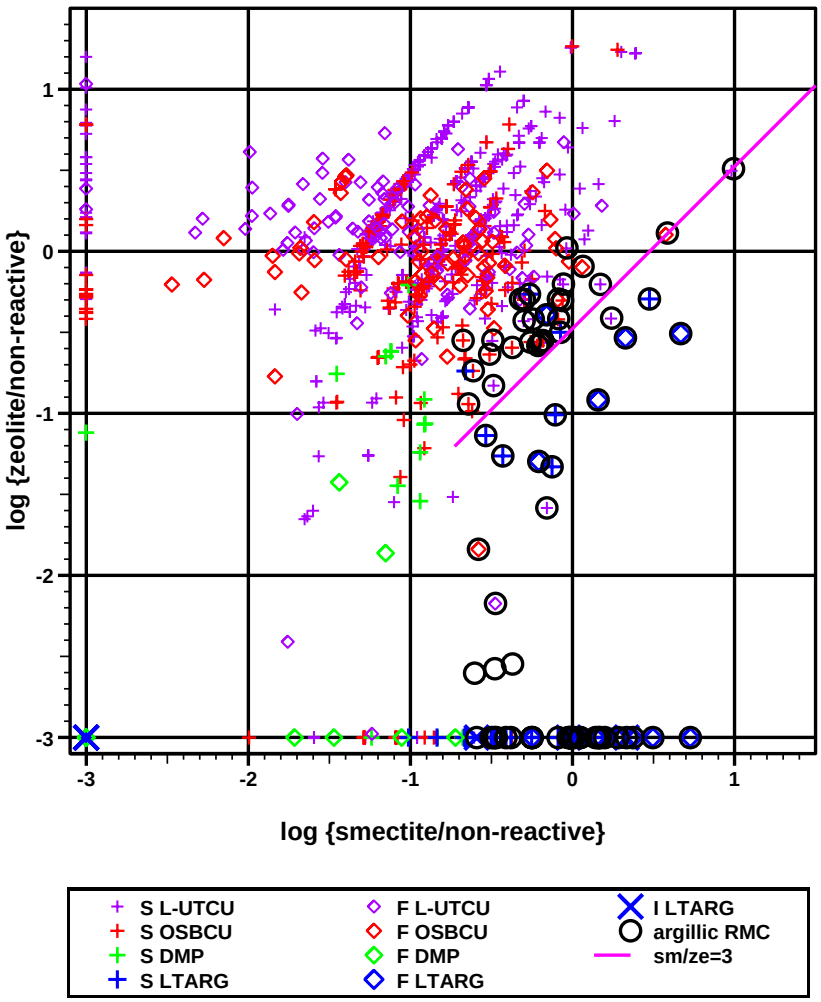

Figure 6-5. Cross-plot of smectite and zeolite ALRs using F, S, and I method data categorized by zones based on grouped RMUs. Data categorized as argillic RMC (ARG) superposed as black circles. Solid magenta line represents smectite:zeolite ratio of 3.

6.2.2 Smectite-Zeolite/Silicate Log Ratio

Devitrified rocks are distinguished by high combined percentages of the felsic minerals including feldspar, quartz, cristobalite, tridymite. In general, feldspar is relatively ubiquitous in devitrified and non-devitrified rocks in the TCU. The combination of silicate minerals quartz, cristobalite, and tridymite content are an indicator of devitrification. The ratio of smectite/(quartz+cristobalite+tridymite) or zeolite/(quartz+cristobalite+tridymite) can be used to distinguish argillic and zeolitic rocks from devitrified rocks.

Evaluation of devitrification in the entire TCU XRD data set is limited because cristobalite and tridymite were usually not analyzed for. Although 77% of XRD samples

have observations for quartz, only 49% of XRD samples analyzed for cristobalite and only 8% for tridymite. Mean quartz percentage (9.78%) is higher than for cristobalite (2.15%) and tridymite (0.70%). Thus, the percentage of quartz largely reflects the (quartz+cristobalite+tridymite) total.

However, for the "F" data set, quartz and cristobalite percentages were observed for all 180 samples and 54 samples for tridymite. Thus, the "F" method data offer a more comprehensive standard for distinguishing devitrified rocks from argillic or zeolitic rocks.

Figure 6-6 shows a cross-plot of the log ratios of zeolite/(quartz+tridymite+cristobalite) and smectite/(quartz+tridymite+cristobalite). Compared to the cross-plot of smectite and zeolite ALR (Figure 6-3), Figure 6-6 better distinguishes devitrified facies from non-devitrified facies. Notably, data categorized in devitrified mafic poor (DMP) RMUs plot more closely to the lower left portion of the graph compared to the smectite and zeolite ALR cross-plot. In particular, much of the overlap between devitrified and zeolitic RMUs attributable to "S" data in Figure 6-3 is eliminated in Figure 6-6.

As discussed previously in Section 5.3 on mica, distinction between "devitrified mafic poor" and "devitrified mafic rich" is largely based on a cutoff value near mean mica percentage. Devitrified rocks, whether "mafic poor" or "mafic rich" have similar distributions of calcite, hematite, smectite, and zeolite. Distinction between "mafic poor" and "mafic rich" devitrified rocks simply divides a distinctly devitrified facies by splitting the bell-shaped mica ALR distribution in half. To apply parametric geostatistical approaches, the "mafic poor" and "mafic rich" categories should be combined.

Figure 6-7 superposes the devitrified RMCs - "devitrified mafic poor" (DMP) as circles and "devitrified mafic rich" (DMR) as squares - onto the cross-plot of the log ratios of zeolite/(quartz+tridymite+cristobalite) and smectite/(quartz+tridymite+cristobalite). The dashed line duplicates the solid line in Figure 6-5 distinguishing a ratio of smectite/zeolite=3. The solid magenta line in Figure 6-7 indicates a (smectite+zeolite)/(quartz+tridymite+cristobalite) equal to ¼, which for simplicity we will call the "silicate" ratio. All "F", "S", or "I" data categorized as "devitrified mafic poor" RMCs have silicate ratios less than ¼. Most data with silicate ratios less than ¼, if not categorized in the DMP, are categorized into DMR RMC. Three data have silicate ratios less than ¼, two of which fall well within the distribution of other data categorized as devitrified, and the remaining datum is borderline argillic. All data with silicate ratios greater than ¼ and categorized in a devitrified RMC are categorized into the DMR RMC. Four of these data are categorized into a DMP RMU, and these data are all "S" data, which are difficult to use for distinction of facies at low smectite and zeolite percentages. The silicate ratio provides simple measure that allows for overlap in smectite and zeolite percentage and ALR frequency distributions for different facies. The silicate ratio

distinguishes a “devitrified” reactive mineral facies (RMF) that corresponds closely to the devitrified mafic poor (DMP) grouped RMUs and combines data categorized into DMP and DMR RMCs with similar silicate ratios. However, the “devitrified” RMF does not include all data categorized as either DMP or DMR RMCs because these data appear to fall within the lower tails of smectite and zeolite abundance within the zeolitic RMUs.

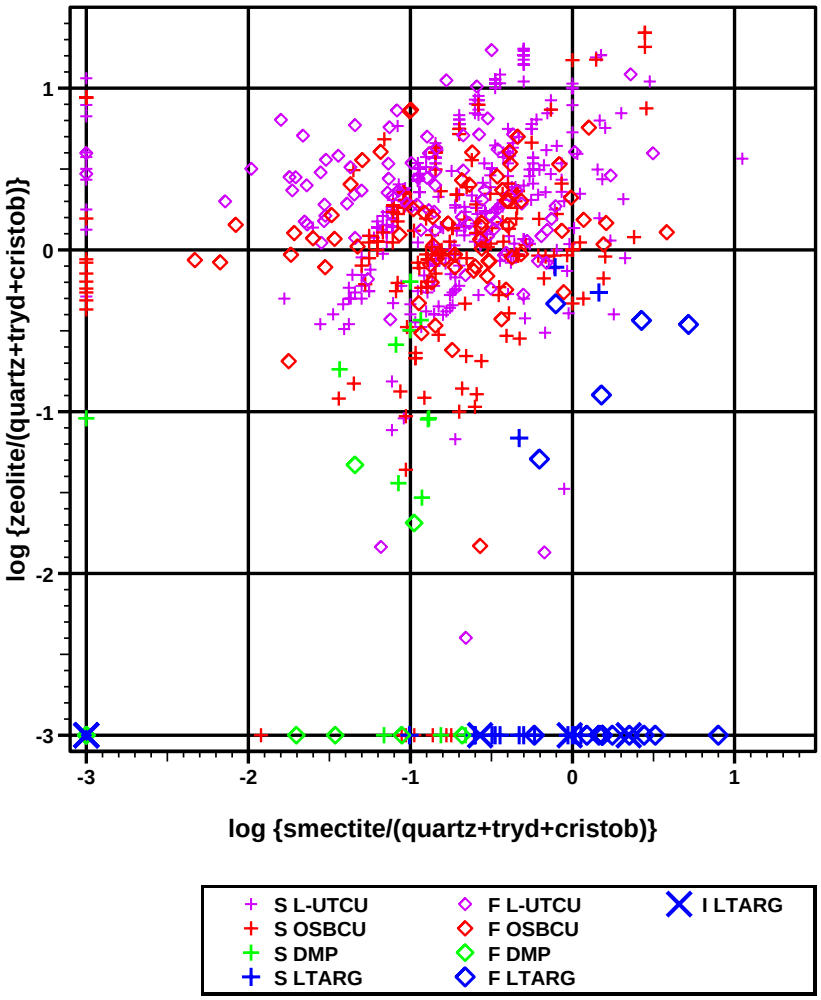

Figure 6-6. Cross-plot of logarithms of smectite/(quartz+tridymite+cristobalite) and zeolite/(quartz+tridymite+cristobalite) ratios using F, S, and I method data categorized by zones based on grouped RMUs.

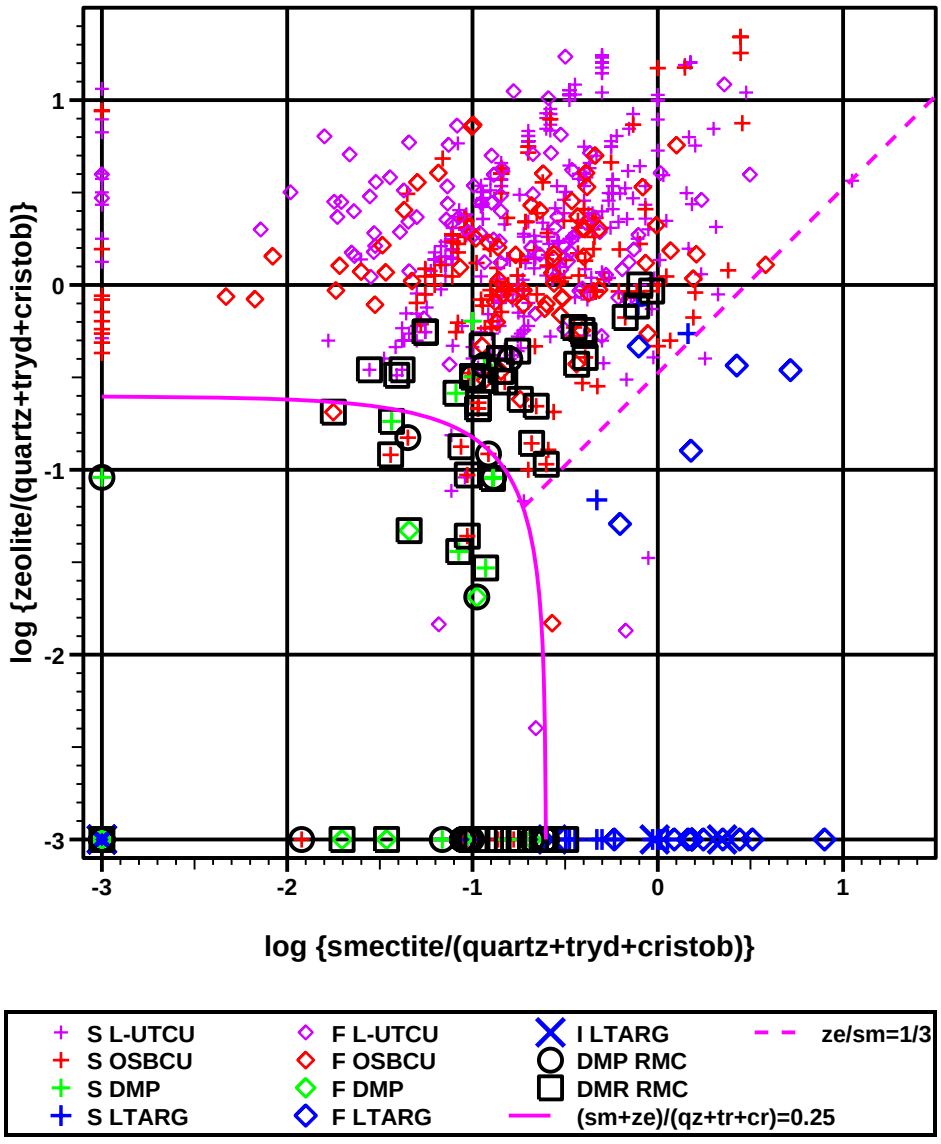

Figure 6-7. Cross-plot of log ratios of smectite/(quartz+tridymite+cristobalite) and zeolite/(quartz+tridymite+cristobalite) to distinguish devitrified RMFs from zeolitic and argillic RMFs. Data are categorized by zones defined by grouped RMUs, XRD method, and devitrified RMC categories (DMP and DMR). Solid line distinguishes devitrified rocks from argillic and zeolitic grouped RMUs or reactive mineral facies (RMFs). Dashed line distinguishes argillic from zeolitic grouped RMUs or RMFs.

6.2.3 Smectite-Zeolite/Glass Log Ratio

Vitric rocks are distinguished by high glass content. No RMUs in the TCU are distinguished as vitric units, however, the vitric mafic poor (VMP) and vitric mafic rich (VMR) RMCs are distinguished as vitric categories. The presence and spatial distribution of vitric rocks in the TCU is potentially significant for prediction of radionuclide transport because of relatively low reactive mineral content, particularly low zeolite and smectite. If vitric rocks are relatively permeable and interconnected, vitric rocks could provide preferential pathways for radionuclide transport. Vitric rocks in the TCU have low smectite and zeolite abundance similar to devitrified tuffs, but similar mica to the zeolitic and argillic tuffs.

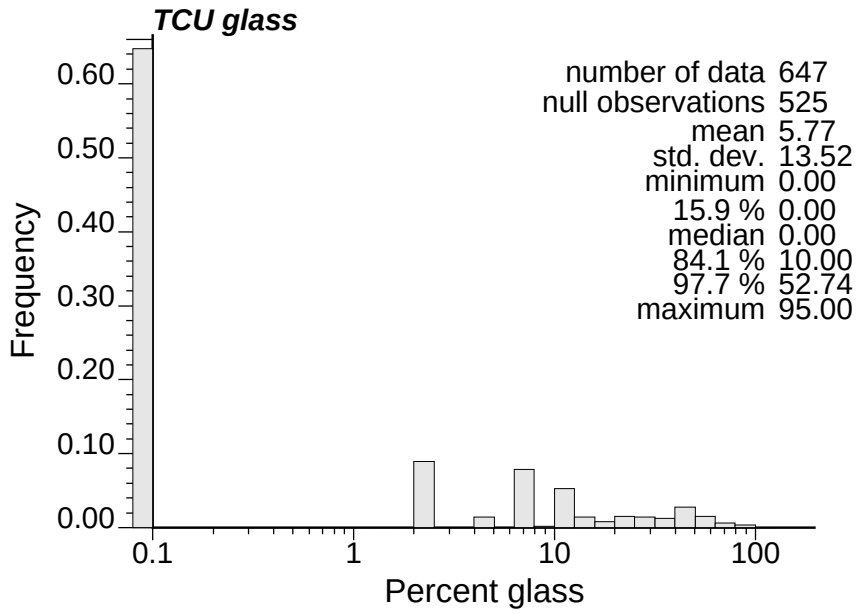

Figure 6-8. Frequency distribution of log percentage of glass for all XRD data in TCU.

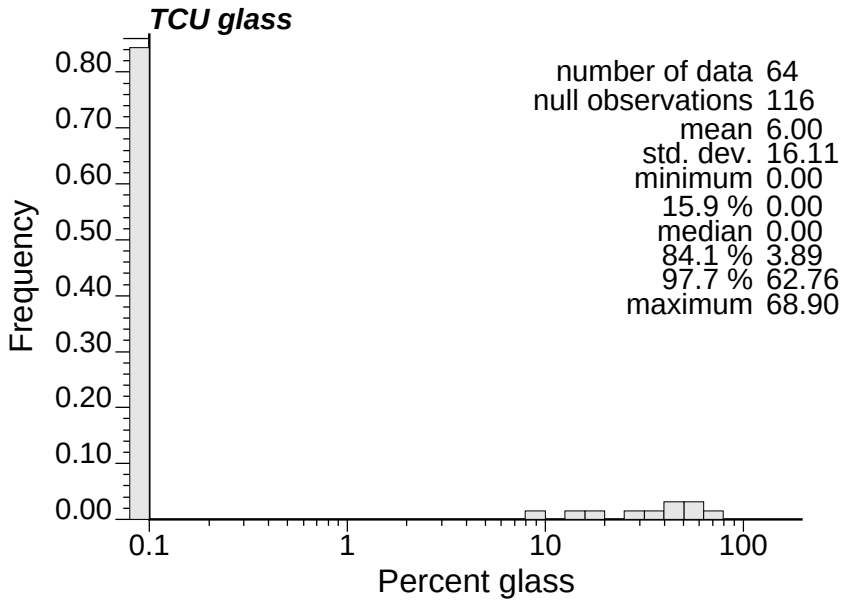

Figure 6-9. Frequency distribution of log percentage of glass for "F" method data in TCU.

Considering that glass is a main parent mineral for clay and zeolite minerals, smectite/glass and zeolite/glass ratios provide a direct measure of degree of argillization and zeolitization. Figure 6-10 shows a cross plot of the logarithm of smectite/glass and zeolite/glass ratios. Data with zero glass, smectite, and zeolite (largely devitrified rocks) are plotted at the 0,0 coordinate for display purposes. Data are sorted by method (symbol shape), grouped RMU (symbol size and color), and vitric RMC (circled in vitric RMC). The cross-plot shows how smectite/glass and zeolite/glass ratios distinguish vitric rocks within the zeolitic **L-UTCU** and **OSBCU Zeolitic** zones. As in Figure 6-5 and Figure 6-7, the dashed magenta line represents a ratio of smectite/zeolite=3. In Figure 6-10, the solid magenta line represents a 2/3 cutoff value for the ratio of (smectite+zeolite)/glass. This cutoff value provides a clean boundary between vitric rocks and non-vitric rocks. It could be argued that this (smectite+zeolite)/glass ratio cutoff could be larger, perhaps 1.0, which would then re-categorize the one outlier **L-UTCU** datum with non-zero, but low zeolite, as "vitric." The dashed magenta line represents a smectite/zeolite ratio of 3.0. Zeolitic rocks generally fall above this dashed line and argillic rocks below. This line divides zeolitic and argillic rocks, although some high zeolite percentages within the LTARG RMU create overlap with the zeolitic zones.

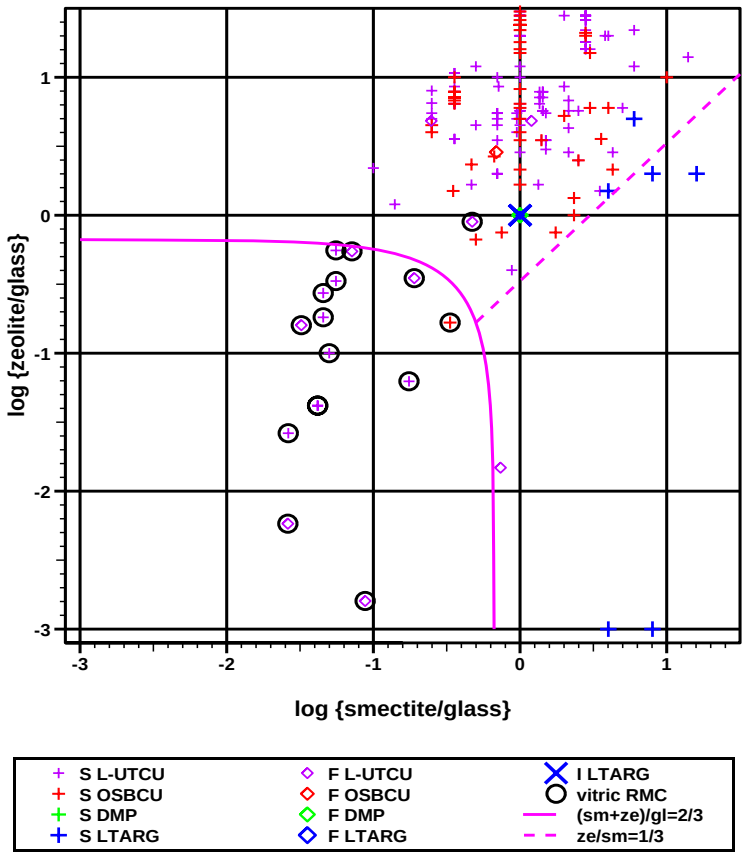

Figure 6-10. Cross-plot of smectite/glass and zeolite/glass log-ratios to distinguish vitric rocks from argillic and zeolitic rocks. Data categorized by zones of grouped RMUs, XRD method, and vitric RMC's. Solid magenta line distinguishes vitric from non-vitric grouped RMUs or reactive mineral facies (RMFs). Dashed line distinguishes argillic from zeolitic grouped RMUs or RMFs.

6.3 Criteria for Distinction of RMFs

The analysis of smectite and zeolite ALR cross-relationships (Figure 6-1 and Figure 6-5) and log ratios for (smectite+zeolite)/(quartz+tridymite+cristobalite) and (smectite+zeolite)/glass (Figure 6-7 and Figure 6-10) described in Section 6.2 leads to the criteria used for distinction of five reactive mineral facies (RMFs) in the TCU. The grouped RMUs or zones – **L-UTCU**, **OSBCU**, **DMP-R**, and **LTARG** – serve as the initial framework for the RMFs. Subsequent cutoff criteria, as follows, are used to define RMFs with Gaussian frequency distributions of mica, smectite, and zeolite ALR:

- Smectite/zeolite=3,
- (smectite+zeolite)/(quartz+tridymite+cristobalite)=1/4, and

- (smectite+zeolite)/glass=2/3

RMFs allow for overlap in reactive mineral frequency distributions while categorizing data into distinctly zeolitic, argillic, vitric, and devitrified facies. These RMFs are

- **L-UTCU Zeolitic.** Only data from zeolitic RMUs within LTCU and UTCU HSUs. If (smectite+zeolite)/ (quartz+tridymite+cristobalite) ratio is less than ¼, the data are categorized into the **Devitrified** RMF. If (smectite+zeolite)/glass ratio is less than 2/3, the data are categorized into the **Vitric** RMF. If the smectite/zeolite ratio is greater than 3 and the data do not qualify as **Devitrified** or **Vitric**, the data are categorized as **Argillic**. The remainder are **L-UTCU Zeolitic**.

- **OSBCU Zeolitic.** Only data from zeolitic RMUs within OSBCU HSU. If (smectite+zeolite)/ (quartz+tridymite+cristobalite) ratio is less than ¼, the data are categorized into the **Devitrified** RMF. If (smectite+zeolite)/glass ratio is less than 2/3, the data are categorized into the **Vitric** RMF. If the smectite/zeolite ratio is greater than 3 and the data do not qualify as **Devitrified** or **Vitric**, the data are categorized as **Argillic**. The remainder are **OSBCU Zeolitic**.

- **Argillic =** Data from LTARG RMU and argillic zeolitic RMUs. All data from LTARG RMU are included unless categorized as **Devitrified** or **Vitric** as described above for zeolitic RMFs.

- **Devitrified =** Data devitrified RMUs and from zeolitic or argillic RMUs where (smectite+zeolite)/ (quartz+tridymite+cristobalite) ratio is less than ¼.

- **vitric =** Data from any RMU where (smectite+zeolite)/glass ratio is less than 2/3.

Different cutoff values for ratios of (smectite+zeolite)/glass and (smectite+zeolite)/(quartz+tridymite+cristobalite) could be used to define the RMFs. The values used were judged to provide a clear division of facies populations within the best quality “F” data while maintaining consistency with combined interpretation of RMU and RMC categorizations. Importantly for this study, the Gaussian characteristics of RMF ALR frequency distributions are suited to parametric approaches to geostatistical analysis of mineral spatial variability.

Table 6-1 summarizes criteria for distinction of RMFs including typical lithologies, relationships to HSUs, RMUs, RMCs, major alteration, reactive mineral presence, and relationships to mineral quantity ratios. The criteria in the last column relating to mineral quantity ratios, RMUs, and RMCs are used to categorize the XRD data into RMFs .

Table 6-1. Criteria for distinction of reactive mineral facies (RMF) in Tuff Confining Unit (TCU), Yucca Flat with respect to lithology, Hydrostratigraphic Units (HSUs), Reactive Mineral Units (RMUs), Reactive Mineral Categories (RMCs), and mineral ratios. "sm"=smectite, "ze"=zeolite, "qz"=quartz, "tr"=tridymite, "cr"=cristobalite, and "gl"=glass.

RMF	Typical Lithologies[1]	HSUs[1]	RMUs[1]	RMCs[1]	Major Alteration[1]	Reactive Minerals[1]	RMF Criteria Relating to Minerals, RMUs and RMCs
L-UTCU Zeolitic	bedded tuffs, nonwelded tuffs	LTCU, UTCU	UT ZE, TCU UZE, TCU LZE	ZEOL, some DMP, DMR	zeolitic, lesser argillic	zeolite, smectite, mica[2]	(sm+ze)/(qz+tr+cr) > ¼ (sm+ze)/gl > 2/3 sm/ze < 3 not in devitrified or vitric RMU
OSBCU Zeolitic	bedded tuffs, nonwelded tuffs, tuffaceous sediments	OSBCU	OSB UZE, OSB MZE2 OSB MZE1 OSB LZE	ZEOL, some DMP, DMR	zeolitic, lesser argillic	zeolite, smectite, mica[2]	(sm+ze)/(qz+tr+cr) > ¼ (sm+ze)/gl > 2/3 sm/ze < 3 not in devitrified or vitric RMU
Argillic	Bedded tuff, colluvium,	ATCU	LT ARG, Some zeolitic	ARG, some ZEOL	argillic, lesser zeolitic	smectite, mica, some zeolite, calcite, and hematite	In LTARG RMU (ATCU HSU) (sm+ze)/(qz+tr+cr) > 1/4 sm+ze)/gl > 2/3; or In LTCU or OSBCU (sm+ze)/(qz+tr+cr) > ¼ sm+ze)/gl > 2/3 sm/ze > 3
Devitrified	Moderately to welded ash-flow tuff	OSBCU, LTCU(?)[3]	BF DMP[3], YF DMR, RV DMP, TP DMP	DMP, DMR, Some ZEOL	devitrification, vapor phase mineralization, quartzo-feldspathic, albitic	smectite, mica[2]	In devitrified RMU or (sm+ze)/(qz+tr+cr) < 1/4
Vitric	Non-welded to partially welded ash-flow tuff, vitrophyric and pumiceous lava	LTCU, OSBCU(?)[4]	TCU Zeolitic, some OSB zeolitic(?)[4]	VMP VMR	None (vitric, glassy)	smectite, mica[2]	In vitric RMC or (sm+ze)/gl < 2/3

[1]Adapted from Chapter 4, Bechtel Nevada (2006) and Table 1-1 and Figure 1-5, Stoller-Navarro (2007)

[2]Calcite and hematite present sporadically in small percentages.

[3]No XRD data in BF DMP RMU within the LTCU HSU.

[4]Only one datum from OSBCU meets "vitric" RMF criteria; this datum could be included in OSBCU Zeolitic RMF.

7. Reactive Mineral Distributions in RMFs

Chapters 4 and 5 evaluated XRD data categorized by reactive mineral categories (RMCs) and reactive mineral units (RMUs) as means to divide the TCU data set into sub-populations with different reactive mineral characteristics. Using grouped RMUs with similar reactive mineral distributions as a starting point, Chapter 6 introduced use of the additive log ratio (ALR) and ratios of reactive to felsic minerals as criteria for distinction of reactive mineral facies (RMFs). This chapter focuses on characterization of reactive mineral ALR frequency distributions in RMFs, including basic statistics, corrections to compensate for data spacing and zero values, consideration of XRD method, and spatial distribution.

Basic statistics (mean, absolute deviation, standard deviation, skewness) of data mineral percentage and ALR data in RMFs illustrate the zonal differences in reactive mineral characteristics within the TCU (Section 7.1). Effects of data spacing and zero values are considered in establishing ALR statistics and frequency distributions (Section 7.2). Comparisons of ALR frequency distributions to Gaussian distributions illustrate how the ALR transformation is well-suited to parametric geostatistical analysis for mica, smectite, and zeolite (Section 7.3). Evaluation of calcite and hematite ALR frequency distributions are separated out from mica, smectite, and zeolite because the preponderance of zero and low-percentage data values (Section 7.4). The spatial distribution of RMFs in Yucca Flat is examined both regionally and locally within the Tuff Pile (Section 7.5).

7.1 Basic Statistics

7.1.1 L-UTCU Zeolitic

Table 7-1 and Table 7-2 show basic statistics for percentages and ALR of reactive minerals in the **L-UTCU Zeolitic** RMF. Compared to other RMFs, the **L-UTCU Zeolitic** RMF shows the highest values for zeolite. Smectite values are lower in the **L-UTCU Zeolitic** RMF than in the **OSBCU Zeolitic** RMF. Mica values are very similar to the **OSBCU Zeolitic**, **Devitrified**, and **Vitric** RMFs and slightly lower than in the **Argillic** RMF.

Although the **L-UTCU Zeolitic** and **OSBCU Zeolitic** RMFs are primarily zeolitized, distinction of these zeolitic RMFs by grouped zeolitic RMUs of the LTCU+UTCU and OSBCU HSUs reflects a depth-dependent trend of decreasing zeolitization and increasing argillization of bedded tuffs (Prothro, 2005). The RMC approach does not distinguish smectite and zeolite depth trends within the zeolitized bedded tuffs that largely compose the UTCU, LTCU, and OSBCU HSUs. Depth trends in zeolite and smectite abundance will affect spatial distributions of K_d in the TCU for all radionuclide classes.

Table 7-1. Basic statistics for reactive mineral percentages in L-UTCU Zeolitic RMF. Values in parenthesis are for non-zero data.

Mineral	Calcite	Hematite	Mica	Smectite	Zeolite
#Data	425 (70)	119 (17)	551 (360)	629 (574)	640 (622)
Mean	0.84 (5.13)	0.32 (2.22)	2.20 (3.37)	6.28 (6.89)	55.34 (56.95)
Abs. Dev.	1.42 (4.37)	0.55 (0.50)	1.76 (1.80)	4.45 (4.36)	17.28 (16.11)
Std. Dev.	3.34 (6.80)	0.83 (0.80)	2.96 (3.08)	6.30 (6.27)	21.21 (19.28)
Skewness	7.36 (3.19)	2.22 (-2.17)	4.09 (4.57)	2.29 (2.35)	-0.55 (-0.32)

Table 7-2. Basic statistics for ALR of mineral percentages in L-UTCU Zeolitic RMF. Zero data values are preliminarily assigned ALR values of -3. Values in parenthesis are for non-zero data.

Mineral	Calcite	Hematite	Mica	Smectite	Zeolite
#Data	425 (70)	119 (17)	551 (360)	629 (574)	640 (622)
Mean	-2.67 (-1.02)	-2.76 (-1.35)	-1.76 (-1.10)	-1.00 (-0.81)	0.15 (0.24)
Abs. Dev.	0.54 (0.34)	0.40 (0.29)	0.87 (0.26)	0.50 (0.32)	0.41 (0.33)
Std. Dev.	0.76 (0.46)	0.61 (0.47)	0.95 (0.35)	0.73 (0.42)	0.67 (0.41)
Skewness	2.06 (0.67)	2.22 (-1.82)	-0.38 (-0.12)	-1.52 (-0.05)	-2.79 (-0.28)

7.1.2 OSBCU Zeolitic

Table 7-3 and Table 7-4 show basic statistics for percentages and ALR of reactive minerals in the **OSBCU Zeolitic** RMF. Compared to the **L-UTCU Zeolitic** RMF, zeolite abundance is slightly lower and smectite abundance is slightly higher in the **OSBCU Zeolitic** RMF. Measured differences in smectite and zeolite frequency distributions are consistent with an overall trend in the TCU of decreasing zeolite and increasing smectite with depth, with the exception of **Devitrified** and **Vitric** RMFs, which have both low smectite and low zeolite (Sections 7.1.4 and 7.1.5).

Statistics of mica distribution are very similar between the **OSBCU Zeolitic** and **L-UTCU Zeolitic** RMFs. Significance of differences in calcite and hematite statistics between the **L-UTCU Zeolitic** and **OSBCU Zeolitic** RMFs is difficult to interpret because of the combined effects of different XRD methods, high proportions of zero values, and numerous null observations, particularly for hematite. Therefore, the **L-UTCU Zeolitic** and **OSBCU Zeolitic** RMFs are distinguished as separate facies in the zeolitic portion of the TCU to characterize depth-dependent trends of decreasing zeolite and increasing smectite without significant differences in calcite, hematite, and mica distributions.

Table 7-3. Basic statistics for reactive mineral percentages in OSBCU Zeolitic RMF. Values in parenthesis are for non-zero data.

Mineral	Calcite	Hematite	Mica	Smectite	Zeolite
#Data	233 (25)	69 (3)	288 (182)	319 (268)	319 (307)
Mean	0.23 (2.15)	0.11 (2.50)	2.20 (3.48)	8.87 (10.55)	46.15 (47.96)
Abs. Dev.	0.41 (0.56)	0.21 (0.00)	1.84 (1.79)	7.36 (7.56)	17.86 (16.83)
Std. Dev.	0.71 (0.73)	0.51 (0.00)	3.09 (3.26)	11.62 (11.95)	22.1 (20.51)
Skewness	2.83 (-1.55)	4.38 (0.00)	4.04 (4.36)	3.84 (3.85)	-0.04 (0.13)

Table 7-4. Basic statistics for ALR of mineral percentages in OSBCU Zeolitic RMF. Zero data values are assigned ALR values of -3. Values in parenthesis are for non-zero data.

Mineral	Calcite	Hematite	Mica	Smectite	Zeolite
#Data	233 (25)	69 (3)	288 (182)	319 (268)	319 (307)
Mean	-2.82 (-1.33)	-2.93 (-1.28)	-1.86 (-1.19)	-1.11 (-0.75)	-0.05 (0.06)
Abs. Dev.	0.32 (0.17)	0.14 (0.09)	0.85 (0.22)	0.70 (0.37)	0.44 (0.33)
Std. Dev.	0.53 (0.27)	0.35 (0.12)	0.91 (0.32)	0.94 (0.49)	0.72 (0.43)
Skewness	2.62 (-2.09)	4.41 (-0.22)	-0.29 (0.84)	-0.96 (0.26)	-2.39 (0.03)

7.1.3 Argillic

Table 7-5 and Table 7-6 show basic statistics for percentages and ALR of reactive minerals in the **Argillic** RMF. Most data in the argillic RMF are derived from the LTARG RMU at the base of the TCU. Distinctively high smectite and low zeolite is consistent with the overall increasing smectite and decreasing zeolite with depth in the TCU. Zeolite abundance in the argillic RMF is comparable, if not lower, than zeolite abundance in **Devitrified** and **Vitric** RMFs (Sections 7.1.4 and 7.1.5). Compared to all other RMFs, calcite, hematite, and mica abundances in the **Argillic** RMF show small increases. Assuming the sample populations are not biased by XRD method and data spacing, the **Argillic** RMF is not only distinguished by argillization, but by slightly higher calcite, hematite, and mica and relatively low zeolite compared to other RMFs in the TCU.

Table 7-5. Basic statistics for reactive mineral percentages in Argillic RMF. Values in parenthesis are for non-zero data.

Mineral	Calcite	Hematite	Mica	Smectite	Zeolite
#Data	78 (22)	20 (12)	84 (55)	85 (85)	83 (22)
Mean	2.03 (7.20)	0.78 (1.31)	2.89 (4.41)	42.09 (42.09)	2.89 (10.90)
Abs. Dev.	3.03 (5.12)	0.79 (0.96)	2.90 (3.49)	17.58 (17.58)	4.40 (7.81)
Std. Dev.	4.51 (5.97)	1.54 (1.82)	5.27 (5.99)	21.75 (21.75)	7.08 (10.22)
Skewness	2.38 (0.61)	3.26 (2.48)	3.81 (3.26)	0.56 (0.56)	3.10 (1.24)

Table 7-6. Basic statistics for ALR of mineral percentages in Argillic RMF. Zero data values are assigned ALR values of -3. Values in parenthesis are for non-zero data.

Mineral	Calcite	Hematite	Mica	Smectite	Zeolite
#Data	78 (22)	20 (12)	84 (55)	85 (85)	83 (22)
Mean	-2.45 (-1.04)	-2.22 (-1.70)	-1.82 (-1.20)	-0.07 (-0.07)	-2.40 (-0.74)
Abs. Dev.	0.79 (0.46)	0.63 (0.24)	0.83 (0.39)	0.38 (0.38)	0.88 (0.51)
Std. Dev.	0.93 (0.54)	0.70 (0.33)	0.96 (0.53)	0.50 (0.50)	1.06 (0.64)
Skewness	1.21 (-0.30)	-0.01 (0.26)	0.01 (0.85)	0.70 (0.70)	1.32 (-0.30)

7.1.4 Devitrified

Table 7-7 and Table 7-8 show basic statistics for percentages and ALR of reactive minerals in the **Devitrified** RMF. Like the **Vitric** RMF, the **Devitrified** RMF is distinguished by low smectite and low zeolite. Based on the limited data, smectite and zeolite abundance is slightly lower in the **Devitrified** RMF compared to the **Vitric** RMF. Otherwise, calcite, hematite, and mica abundance is comparable to other RMFs.

Table 7-7. Basic statistics for reactive mineral percentages in Devitrified RMF. Values in parenthesis are for non-zero data.

Mineral	Calcite	Hematite	Mica	Smectite	Zeolite
#Data	49 (4)	8 (4)	50 (27)	52 (32)	51 (21)
Mean	0.72 (8.80)	0.21 (0.43)	2.25 (4.17)	4.82 (7.82)	6.13 (14.88)
Abs. Dev.	1.32 (7.85)	0.22 (0.23)	2.39 (2.26)	4.41 (3.52)	7.95 (7.82)
Std. Dev.	3.50 (10.06)	0.29 (0.26)	3.00 (2.95)	5.10 (4.29)	10.87 (12.59)
Skewness	5.14 (0.33)	0.73 (0.05)	1.45 (1.05)	0.67 (0.33)	1.92 (1.83)

Table 7-8. Basic statistics for ALR of mineral percentages in Devitrified RMF. Zero data values are assigned ALR values of -3. Values in parenthesis are for non-zero data.

Mineral	Calcite	Hematite	Mica	Smectite	Zeolite
#Data	49 (4)	8 (4)	50 (27)	52 (32)	51 (21)
Mean	-2.87 (-1.35)	-2.71 (-2.41)	-2.16 (-1.44)	-1.83 (-1.09)	-2.13 (-0.88)
Abs. Dev.	0.25 (0.65)	0.29 (0.26)	0.79 (0.31)	0.91 (0.25)	1.03 (0.42)
Std. Dev.	0.50 (0.76)	0.37 (0.30)	0.84 (0.41)	0.97 (0.33)	1.10 (0.50)
Skewness	3.39 (0.08)	0.58 (0.01)	0.14 (-0.93)	-0.27 (-0.72)	0.58 (-0.04)

7.1.5 Vitric

Table 7-9 and Table 7-10 show basic statistics for percentages and ALR of reactive minerals in the **Vitric** RMF. Calcite, hematite, mica, smectite, and zeolite abundances in the **Vitric** RMF are similar to those in the **Devitrified** RMF. Calcite, hematite, and mica abundances are similar to the **L-UTCU Zeolitic** and **OSBCU Zeolitic** RMFs. The **Vitric** RMF will have similar K_d values to the **Devitrified** RMF.

The **Vitric** and **Devitrified** RMFs are separated as facies assuming differences in lithology and morphology between **Vitric** and **Devitrified** RMFs would cause differences in spatial variability including geometry and small-scale variability. Whereas devitrified tuffs are associated with welded ash-flow tuffs or dense stony lavas, vitric tuffs are associated with nonwelded to partially welded ash flow or vitrophyres, unaltered bedded/ash-fall tuffs, or vitrophyric and pumiceous lava. However, considering both **Vitric** and **Devitrified** RMFs are volumetrically small, similar in reactive mineral distributions, and associated lithologically and morphologically, it may be practical to combine the **Vitric** and **Devitrified** RMFs into one reactive mineral facies.

Table 7-9. Basic statistics for reactive mineral percentages in the Vitric RMF. Values in parenthesis are for non-zero data.

Mineral	Calcite	Hematite	Mica	Smectite	Zeolite
#Data	29 (5)	6 (1)	35 (21)	37 (29)	35 (25)
Mean	0.46 (2.64)	0.42 (2.50)	2.16 (3.60)	6.08 (7.75)	6.64 (9.30)
Abs. Dev.	0.75 (0.94)	0.69 (n.a.)	2.32 (3.07)	6.00 (6.43)	6.43 (6.53)
Std. Dev.	1.17 (1.53)	1.02 (n.a.)	4.41 (5.25)	7.72 (7.94)	8.15 (8.27)
Skewness	2.53 (0.32)	1.36 (n.a.)	3.18 (2.37)	1.28 (0.97)	1.28 (0.97)

Table 7-10. Basic statistics for ALR of mineral percentages in Vitric RMF. Zero data values are assigned ALR values of -3. Values in parenthesis are for non-zero data.

Mineral	Calcite	Hematite	Mica	Smectite	Zeolite
#Data	29 (5)	6 (1)	35 (21)	37 (29)	35 (25)
Mean	-2.75 (-1.57)	-2.75 (-1.48)	-2.17 (-1.62)	-1.62 (-1.24)	-1.72 (-1.21)
Abs. Dev.	0.41 (0.19)	0.42 (n.a.)	0.68 (0.34)	0.64 (0.40)	0.86 (0.46)
Std. Dev.	0.56 (0.29)	0.62 (n.a.)	0.78 (0.47)	0.84 (0.46)	0.97 (0.61)
Skewness	1.77 (-0.53)	1.36 (n.a.)	0.28 (0.58)	-0.53 (0.35)	-0.33 (-0.99)

7.2 Data Corrections

The basic statistics of reactive mineral percentages and ALRs given in Section 7.1 were based on raw XRD data and, thus, could be influenced by data spacing and resolution. XRD data spacing and resolution largely depends on the XRD method and sampling objectives.

7.2.1 Correcting for Data Spacing

Some XRD data, particularly "S" method data, were obtained at closely spaced intervals. Preferential sampling in clay-rich zones occurred by design by targeting low-resistivity intervals in geophysical logs (Pawloski, 1983). Low-resistivity zones can also be explained by high percentages of clinoptilolite (Schenkel et al., 1999). As a result, closely-spaced data in low-resistivity zones could bias statistics toward higher smectite or zeolite. Weighting data through moving-window averaging is one approach to reducing bias from closely spaced data. Weights are assigned to a data value for computation of statistics in proportion to the inverse of the number of data within a length interval (window) centered on the data value location. For example, if the moving window is 10 meters and three data are located within ± 5 m of a datum location, then a weight of 1/3 is assigned to the datum.

In processing the TCU XRD data, window sizes of 5 to 100 m were attempted. Reduction of bias from preferential sampling in low-resistivity intervals was expected to be evident by reducing estimates of mean smectite or zeolite percentage. It was found that window sizes of 10 to 50 m had similar effect of slightly lowering mean smectite or zeolite percentage in the overall data set. In this study, a moving-average window size of 10 m is used where weighting factors are applied to statistical analyses.

7.2.2 Correcting for Zero Values

As discussed in Section 3.3, many "zero" values probably represent non-zero mineral percentages as related to variable resolution and uncertainty of the different XRD methods. Zero values present difficulties in applying logarithmic or ALR transformation. The logarithm of zero is negative infinity. If certain minerals are effectively ubiquitous, then zero-valued data erroneously underestimate the logarithmic or ALR value to infinite extent. It is more realistic to assume that zero-valued data for ubiquitous minerals actually represent non-zero positive values that will translate to a relatively low logarithmic or ALR value.

To account for zero values in ALR statistics and distributions, this study will assume the following:

- The ALR frequency distribution is Gaussian for a reactive mineral that is ubiquitous within a RMF.
- The ALR distributions from data can better predict the median than the mean because zero-percentage data bias the mean, while higher percentage data are relatively accurate. The median is unaffected by zero-valued data unless 50% or more of the data are zero values.
- Considering that mean and median values of a Gaussian distribution are equivalent, the estimation of a reasonable ALR value for zero-valued data can be used to adjust the mean to match the median.

The correction for zero values used in this study is designed to match mean and median statistics are the ALR as follows

$$ALR_{zero} = -3.0 + \frac{\left(ALR_{median} - ALR_{mean}\right)}{f_{zero}}, \qquad \text{Equation (7.1)}$$

where:

ALR_{zero} = ALR value to assign to zero-valued data,

-3.0 = Assumed ALR value for zero-valued data prior to correction,

f_{zero} = Fraction of zero-valued data,

ALR_{median} = median of ALR distribution, and

ALR_{mean} = mean of ALR distribution assuming ALR=-3.0 for zero-valued data.

This correction is applied separately to each XRD method for reactive minerals assumed ubiquitous in the RMF, as implemented in Section 7.3.

7.3 Corrected Mica, Smectite, and Zeolite ALR Frequency Distributions

Analysis of reactive mineral frequency distributions in RMFs will begin with mica, smectite, and zeolite, for which the most data and most non-zero data are compiled in the TCU XRD data set. Calcite and hematite frequency distributions are more difficult to analyze because of high proportions of zero-valued data, low-percentage data, and null observations. Analysis of mica, smectite, and zeolite ALR frequency distributions by different XRD methods offers means to assess effects of method resolution, uncertainty, and data spacing on development of parametric descriptions of K_d and reactive mineral percentage distributions in the RMFs.

7.3.1 "F" Data

The full spectrum method or "F" data offer the best resolution and lowest uncertainty of all XRD methods used in the TCU. Figure 7-1shows mica, smectite, and zeolite ALR frequency distributions for "F" data in RMFs. A Gaussian distribution is fitted to the mean and standard deviation statistics of the data. In compiling statistics, zero percentages are assigned ALR values of -3 as a preliminary step to correcting for effects of zero values on characterization of the reactive mineral frequency distributions. In cases where non-zero data are abundant and zero values are few or non-existent, such as smectite and zeolite in the **L-UTCU Zeolitic** and **OSBCU Zeolitic** RMFs and smectite in the **Argillic** RMF, a Gaussian distribution fits the ALR frequency distributions quite well. In other cases, such as mica in the **L-UTCU Zeolitic**, **OSBCU Zeolitic**, and **Argillic** RMFs, a Gaussian distribution could fit the frequency distribution better if the "zero values" were not assigned ALR values of -3. The zeolite ALR distribution in the **Argillic** RMF displays a wide range including a high proportion of ALR values originating from zero-valued data. Frequency distributions in the **Devitrified** and **Vitric** RMFs are not resolved very well by the few "F" data, although all 5 data in the **Vitric** RMF have non-zero zeolite values, whereas 6 of 8 data in the **Devitrified** RMF have zero values.

Figure 7-2 illustrates the same ALR frequency distributions for RMFs as Figure 7-1, but with moving average weights applied for a window size of 10 m. The weights either do not affect or only slightly affect the "F" data statistics and frequency distributions because few "F" data were sampled at close spacings less than 10 m.

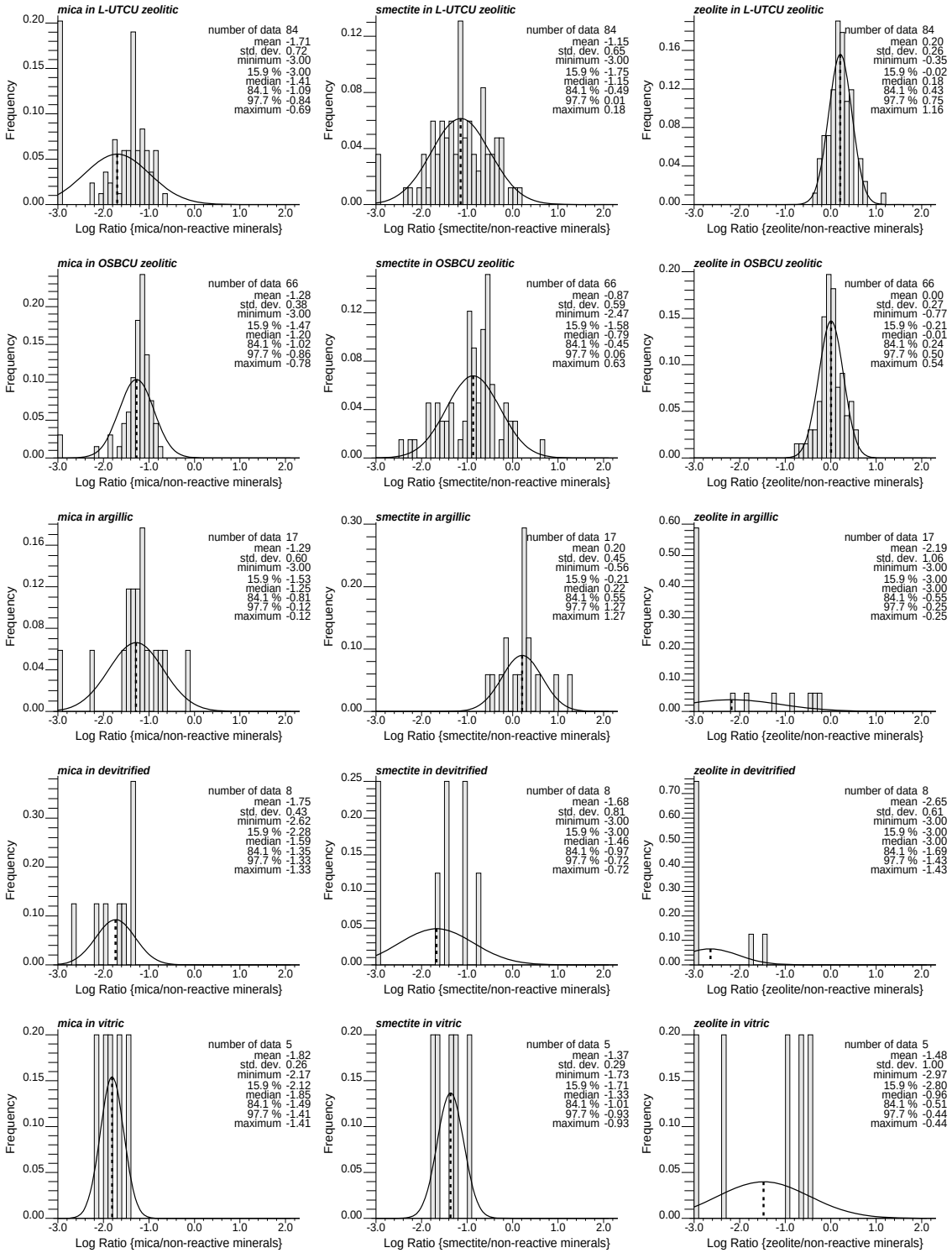

Figure 7-1. Mica, smectite, and zeolite ALR frequency distributions for “F” data in RMFs.

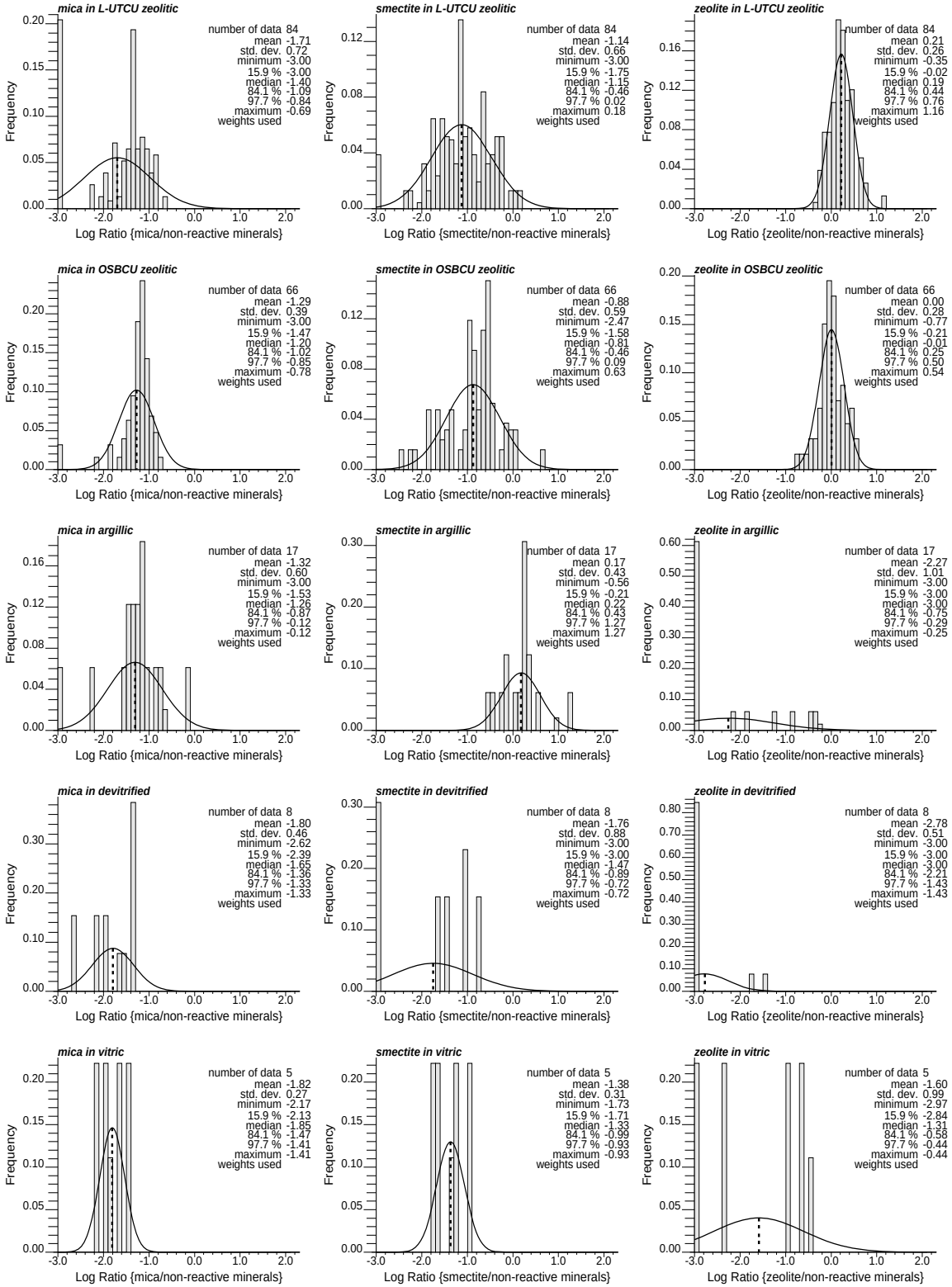

Figure 7-2. Mica, smectite, and zeolite ALR frequency distributions for “F” data in RMFs, with weighting based 10 m vertical moving average.

Figure 7-3 shows mica, smectite, and zeolite ALR frequency distributions for RMFs using the Equation (7.1) correction for zero values applied to smectite. The "F" data have zero smectite values only in the **L-UTCU Zeolitic** and **Devitrified** RMFs. The corrections closely match mean and median zeolite ALRs in the **L-UTCU Zeolitic** (-1.15, -1.15) and **devitrified** (-1.49, -1.47) RMFs. A slight mismatch between corrected mean and median occurs as a result of the moving window weighting, which is not accounted for in corrections for zero values.

Corrections for zero values of mica and zeolite are not applied to the "F" data. Correction for zero values is not applied to mica "F" data because some peralkaline tuff beds mainly in the LTCU are known to have zero mica. Most of the zero-valued mica data are located within the LTCU. A correction for zero values is not applied to zeolite "F" data because no zero-valued data occur in the **L-UTCU** and **OSBCU Zeolitic** and **Vitric** RMFs, while the **Argillic** and **Devitrified** RMFs are characterized by a majority of zero-valued zeolite data.

7.3.2 "S" Data

Compared to "F" method data in the TCU, the semi-quantitative method or "S" data are more numerous but have lower resolution and higher uncertainty resulting in more zero-valued data. Figure 7-4 shows mica, smectite, and zeolite ALR frequency distributions for "S" data in RMFs. As described for the "F" data, zero percentages are initially assigned ALR values of -3 as a preliminary step to correcting for effects of zero values on characterization of the reactive mineral frequency distributions. A Gaussian distribution is fitted to the mean and standard deviation statistics of the data. In the sole case of abundant "S" data with no zero values for a reactive mineral in the RMF, smectite in the **Argillic** RMF, a Gaussian distribution fits the ALR frequency distribution quite well. In other cases, some zero-valued data are present and a Gaussian distribution would appear to fit the frequency distribution well if the ALR value for zero-valued data were adjusted, such as smectite and zeolite in the **L-UTCU Zeolitic** and **OSBCU Zeolitic** RMFs, smectite in **Devitrified**, and mica in all RMFs but **Vitric**. The zeolite ALR distributions in **Argillic** and **Devitrified** RMFs display a combination of zero-valued data and relatively low zeolite ALR values similar to "F" data. Zeolite ALRs are low but non-zero for "S" data in the **Vitric** RMF, as was observed for the "F" data.

Figure 7-5 illustrates the same ALR frequency distributions in RMFs as shown in Figure 7-4, but with moving average weights applied for a window size of 10 m. The weights change the frequency distributions for "S" data more than for "F" data because "S" data were sampled at closer spacings – as small as 1.73 m (5 ft). However, the weighting affects "S" data ALR statistics only slightly.

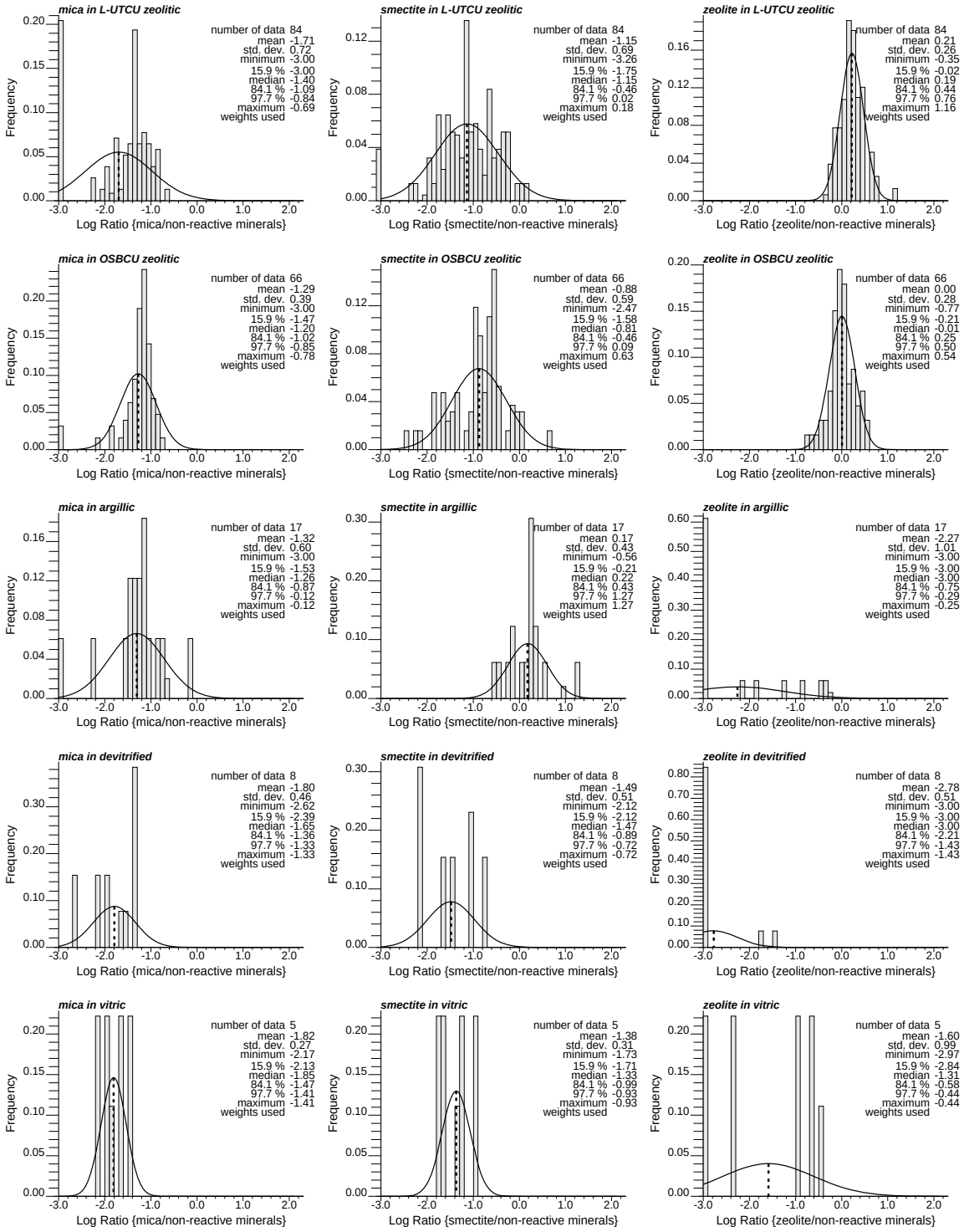

Figure 7-3. Mica, smectite, and zeolite ALR frequency distributions for "F" data in RMFs with zero-valued smectite data and mica data not in L-UTCU corrected to balance median and mean ALR.

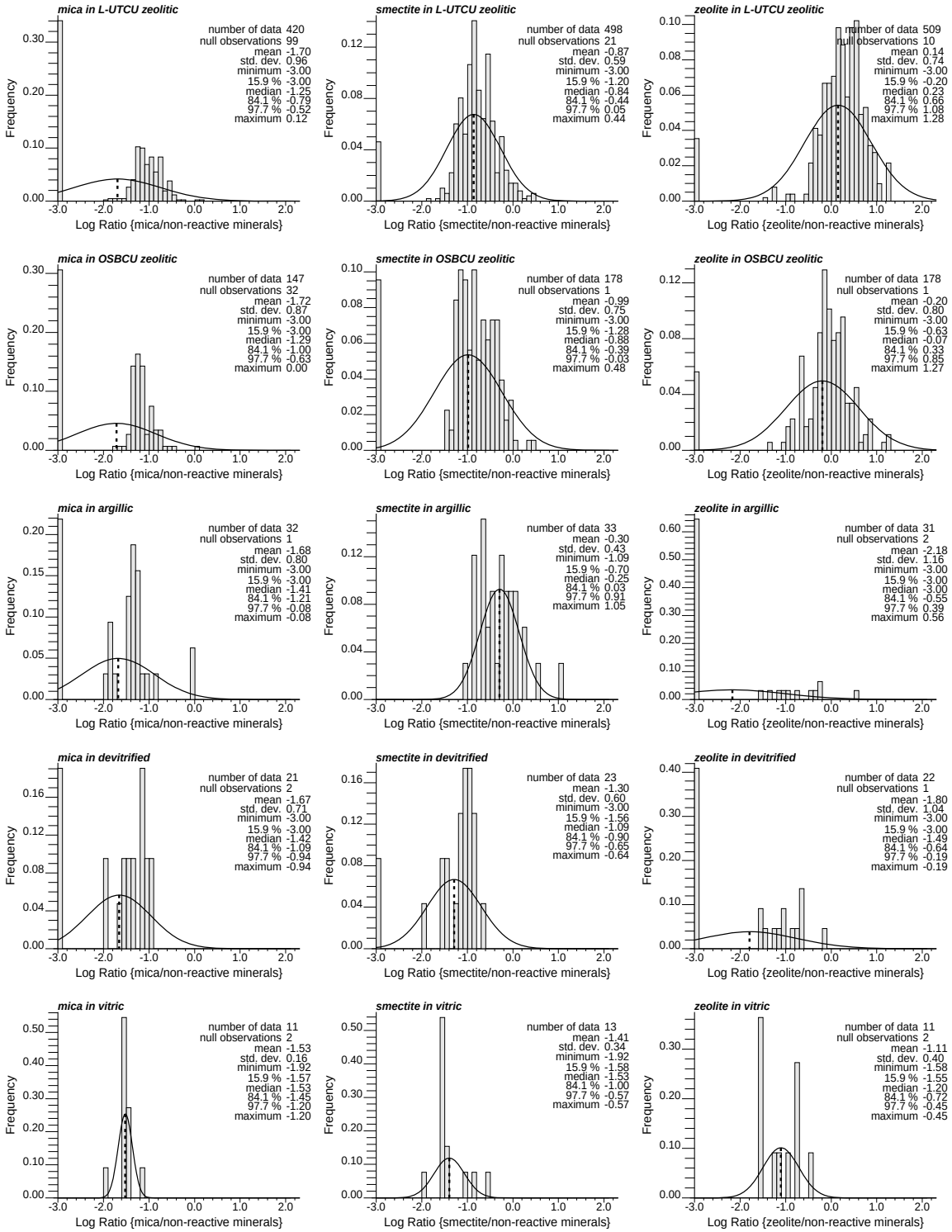

Figure 7-4. Mica, smectite, and zeolite ALR frequency distributions for “S” data in RMFs.

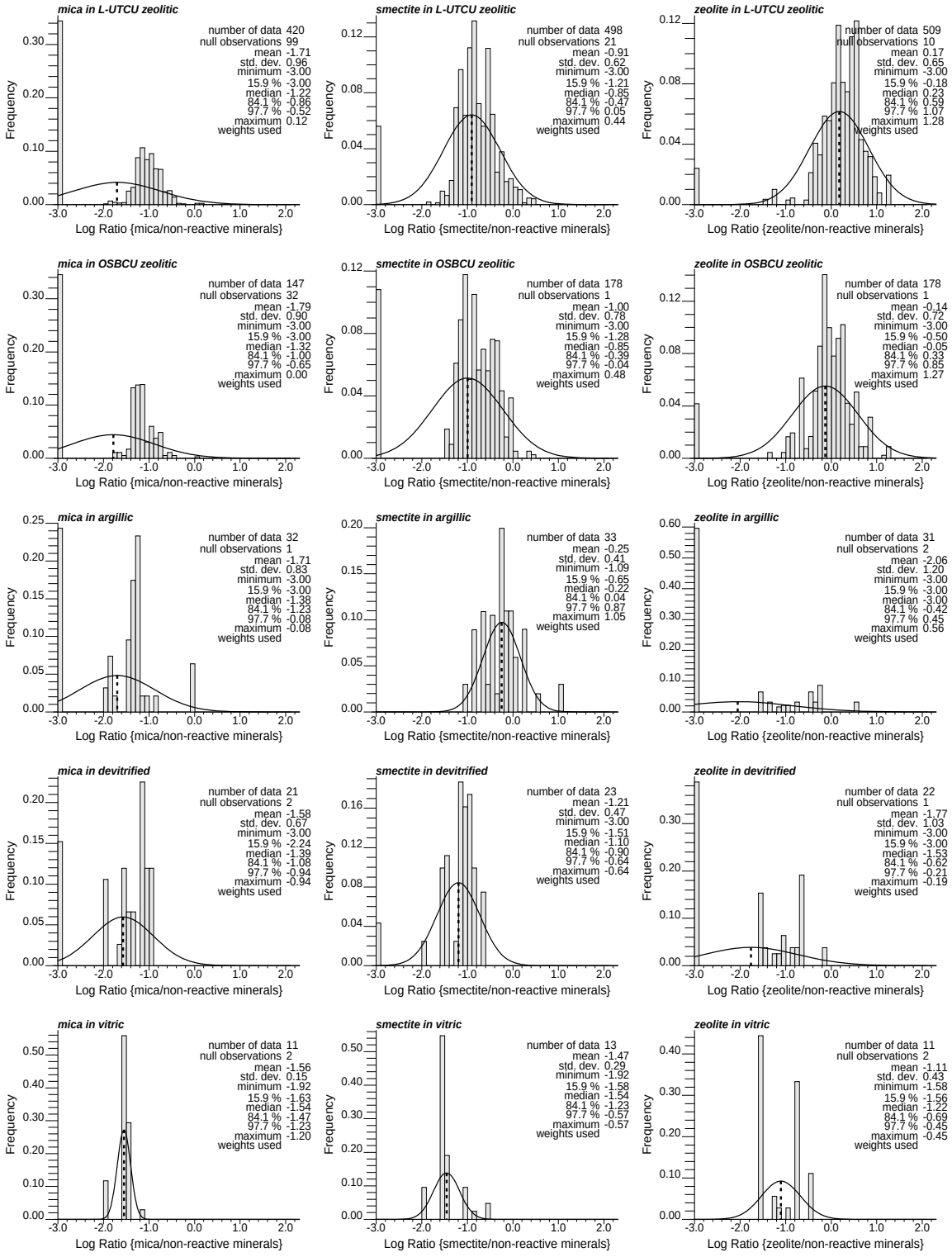

Figure 7-5. Mica, smectite, and zeolite ALR frequency distributions for "S" data in RMFs, with weighting based 10 m vertical moving average.

Using Equation (7.1), corrections for zero values of mica, smectite, and zeolite were applied to the "S" data for all RMFs with zero values except mica in **L-UTCU Zeolitic** and zeolite in the **argillic** and **devitrified** RMFs. The "S" data have proportionately far more zero values in mica than "F" data, particularly in the **OSBCU Zeolitic**, **argillic**, **devitrified**, and **vitric** RMFs, suggesting many zero values for mica in the "S" data more likely represent non-zero percentages of mica. Zero value corrections for mica were not applied to **L-UTCU Zeolitic** "S" data because the proportion of zero-valued mica data in **L-UTCU Zeolitic** for "S" data (0.34) is comparable to "F" data (0.20), and zero-values of mica are expected in the **L-UTCU Zeolitic** because of peralkaline tuff beds.

Small proportions of zero-valued "S" smectite data occur in the **L-UTCU Zeolitic**, **OSBCU Zeolitic** and **Devitrified** RMFs. Comparison to "F" data smectite distributions suggests smectite is ubiquitous in all RMFs. Therefore, the assumption that zero-valued "S" smectite data represent low non-zero smectite percentages is plausible.

Small proportions of zero-valued zeolite "S" data occur in the **L-UTCU Zeolitic** and **OSBCU Zeolitic** RMFs. It is possible that these "S" data are misclassified because of lack of quartz, tridymite, or cristobalite data to distinguish **Devitrified** RMF or lack of glass data to distinguish **Vitric** RMF.

Figure 7-6 shows "S" data ALR frequency distributions with zero-value corrections compared to Gaussian distributions based on ALR mean and standard deviation. Gaussian distributions fit ALR frequency distributions more closely with the zero value corrections.

7.3.3 "E" Data

Although the external standard XRD method or "E" data offer more comprehensive mineralogic analysis than the "S" data, the "E" data present difficulties in implementing the ALR approach to RMFs because of a high proportion of zero-value mica and smectite percentages. Figure 7-7 shows mica, smectite, and zeolite ALR frequency distributions in each RMF for "E" data. While "F" data strongly indicate ubiquity for mica and smectite in all RMFs (Section 7.3.1), "E" data show greater than 50% zero values for mica in all RMFs and 42%-75% zero values for smectite in all RMFs except the **Argillic**.

Given that the "E" method data do not resolve mica distributions in all five RMFs and smectite distributions in 4 of 5 RMFs, deleting "E" method data from the geostatistical analysis of reactive mineral variability is recommended. Deleting the "E" method data removes a large proportion of the zero valued reactive mineral percentage data from the XRD data set. Mica and smectite frequency distributions are better resolved by "F" and "S" data.

The “E” data do produce zeolite frequency distributions in the **L-UTCU Zeolitic** and **OSBCU Zeolitic** RMFs comparable to the “S” data, but not as narrow as for the “F” data. This suggests uncertainties for non-zero “E” zeolite data are greater than for “F” data and comparable to “S” data.

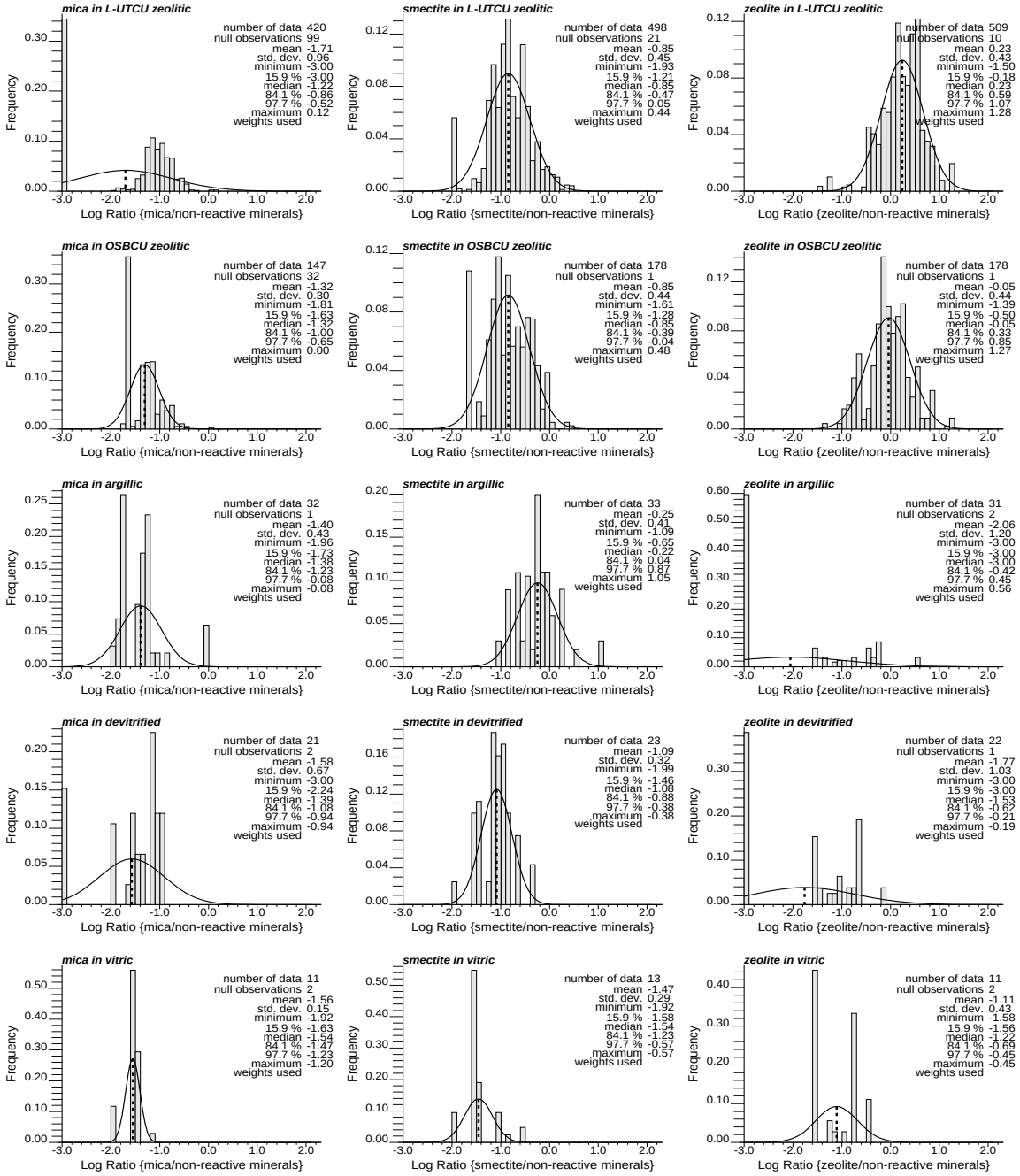

Figure 7-6. Mica, smectite, and zeolite ALR frequency distributions for “S” data in RMFs, with zero-valued smectite data and mica data corrected to balance median and mean ALR.

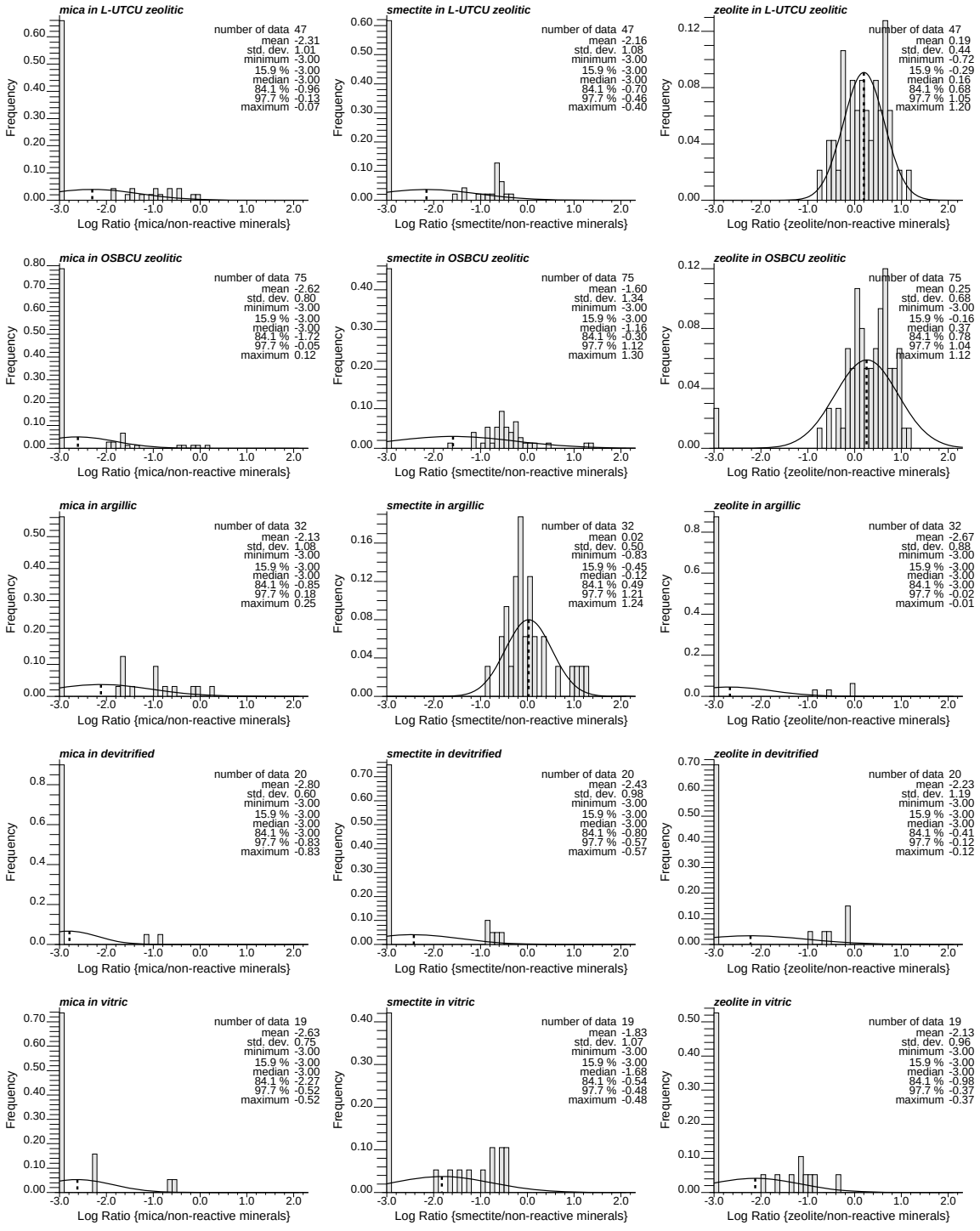

Figure 7-7. Mica, smectite, and zeolite ALR frequency distributions for "E" data in RMFs.

7.3.4 Comparison of Estimated RMF ALR Mean and Standard Deviations by XRD Method

The different XRD methods yield different frequency distributions of reactive mineral ALRs in RMFs. Table 7-11 gives Gaussian parameters for each RMF as inferred by the "F", "S", and "E" XRD methods for mica, smectite, and zeolite. In general, the "F" and "S" methods yield similar Gaussian parameters after correction for zero values as detailed in Section 7.2.2. Inference of reactive mineral ALR Gaussian parameters is problematic for "E" data mainly because of higher proportions (~50% or more) of zero-valued data particularly for smectite as detailed in Section 7.3.3. The "E" data do not resolve low reactive mineral percentages as well as "F" and "S" data. Where "E" data have adequate resolution, such as for zeolite in the **LTCU Zeolitic** and **OSBCU Zeolitic** RMFs, Gaussian ALR parameters are comparable to the "F" and "S" data parameters. Much of the zero valued mica and smectite data in the composite data frequency distributions (Figure 3-14 and Figure 3-15, Section 3.5.2) can be attributed to the "E" data.

Comparisons for internal standard ("I") data are not shown because only 5 "I" data are present in the TCU, all from the LTARG RMU. It may reasonable to pool "F", "S", and "I" method XRD data in the TCU for statistical analysis under the following assumptions:

- Characterization of reactive mineral ALR frequency distributions is acceptable using "S" and "F" data.
- "I" data are of similar or better accuracy than "S" data.
- "E" data are not adequate to characterize most of the reactive mineral ALR frequency distributions because of limited resolution.

However, as will be discussed in Chapter 8, it is problematic to include "S" data into variogram analyses because the "S" data percentages as inferred from ranges of values do not reflect actual spatial variability of reactive mineral distributions. Given only 5 "I" data, only the "F" data provide sufficient numbers of accurate data needed to implement parametric geostatistical analysis of spatial variability of reactive mineral distributions in the TCU.

Table 7-11. Comparisons of mica, smectite, and zeolite ALR mean and standard deviation in RMFs for different XRD methods. Italicized values are inaccurate or not analyzable (NA) as described in footnotes.

RMF	Method	ALR Mean ± Standard Deviation		
		Mica	Smectite	Zeolite
L-UTCU zeolitic	"F"	*-1.71 ± 0.72*[1]	-1.15 ± 0.69	0.21 ± 0.26
	"S"	*-1.71 ± 0.96*[1]	-0.85 ± 0.45	0.23 ± 0.43
	"E"	*NA*[2]	*NA*[2]	0.23 ± 0.44
OSBCU zeolitic	"F"	-1.29 ± 0.39	-0.88 ± 0.59	0.00 ± 0.28
	"S"	-1.32 ± 0.30	-0.85 ± 0.44	-0.05 ± 0.44
	"E"	*NA*[2]	*NA*[2]	0.24 ± 0.55
argillic	"F"	-1.32 ± 0.60	0.17 ± 0.43	*-2.27 ± 1.01*[3]
	"S"	-1.40 ± 0.43	-0.25 ± 0.41	*-2.06 ± 1.20*[3]
	"E"	*NA*[2]	-0.02 ± 0.42	*-2.37 ± 1.14*[3]
devitrified	"F"	-1.80 ± 0.46	-1.49 ± 0.51	*-2.78 ± 0.51*[3]
	"S"	-1.58 ± 0.67	-1.09 ± 0.32	*-1.77 ± 1.03*[3]
	"E"	*NA*[2]	*NA*[2]	*-2.20 ± 1.14*[3]
vitric	"F"	-1.82 ± 0.27	-1.38 ± 0.31	-1.60 ± 0.99
	"S"	-1.56 ± 0.15	-1.47 ± 0.29	-1.11 ± 0.43
	"E"	*NA*[2]	*NA*[2]	*NA*[2]

[1]A significant proportion of the L-UTCU Zeolitic RMF actually has zero mica content because of presence of peralkaline tuff beds.

[2]Estimate of median is inaccurate because proportion of zero-valued data is greater than 50% or median value is at extreme lower tail of non-zero values. Zero-value correction cannot be applied.

[3]Correction for zero-valued data is feasible, however, high proportion of zero-valued data suggests the estimate of the median is inaccurate and, therefore, zero-value correction is inaccurate.

7.4 Corrected Calcite and Hematite Frequency Distributions

The preponderance of null observations and zero values for calcite and hematite data cause difficulty in characterization of frequency distributions for calcite and hematite. Unlike mica or smectite, there is no indication that calcite or hematite minerals are ubiquitous in any of the RMFs. Figure 7-8 and Figure 7-9 show calcite and hematite ALR frequency distributions for "F" and "S" method data. The "F" data show largely zero values, with only the **Argillic** RMF showing a significant proportion of non-zero calcite and hematite data. The "S" data show a similar pattern for calcite. Interpretation of the "S" data for hematite is problematic because very few observations are available. In general, the combined effects of assessing zero values, null observations, resolution, and uncertainty question the usefulness of using the "S" data to characterize hematite distributions in the TCU.

While calcite and hematite may be more abundant in the **Argillic** RMF, as indicated by the "F" data, smectite will still dominate estimation of sorption parameters. Locally where calcite and/or hematite are present within an RMF, calcite and hematite could be a stronger sorber than smectite for Am, Eu, Np, Pu, Sm, and U as indicated by the component additivity methodology parameters (Section 7.1). However, overall sorption properties in the TCU, particularly for ^{41}Ca, Cs, Ni, and Sr, are more likely dominated by mica, smectite, and zeolite distributions.

If calcite and hematite spatial distributions are to be accounted for in geostatistical analysis within the TCU, an indicator (categorical) approach would be recommended to distinguish zones of existence and non-existence of calcite and hematite. However, as will be shown in Chapter 8, the effects of calcite and hematite on K_d spatial variability are relatively small for all radionuclide classes. In characterization of the effects of reactive mineral spatial distributions on radionuclide transport in the TCU, focus should be on characterization of mica, smectite, and zeolite distributions and spatial variability.

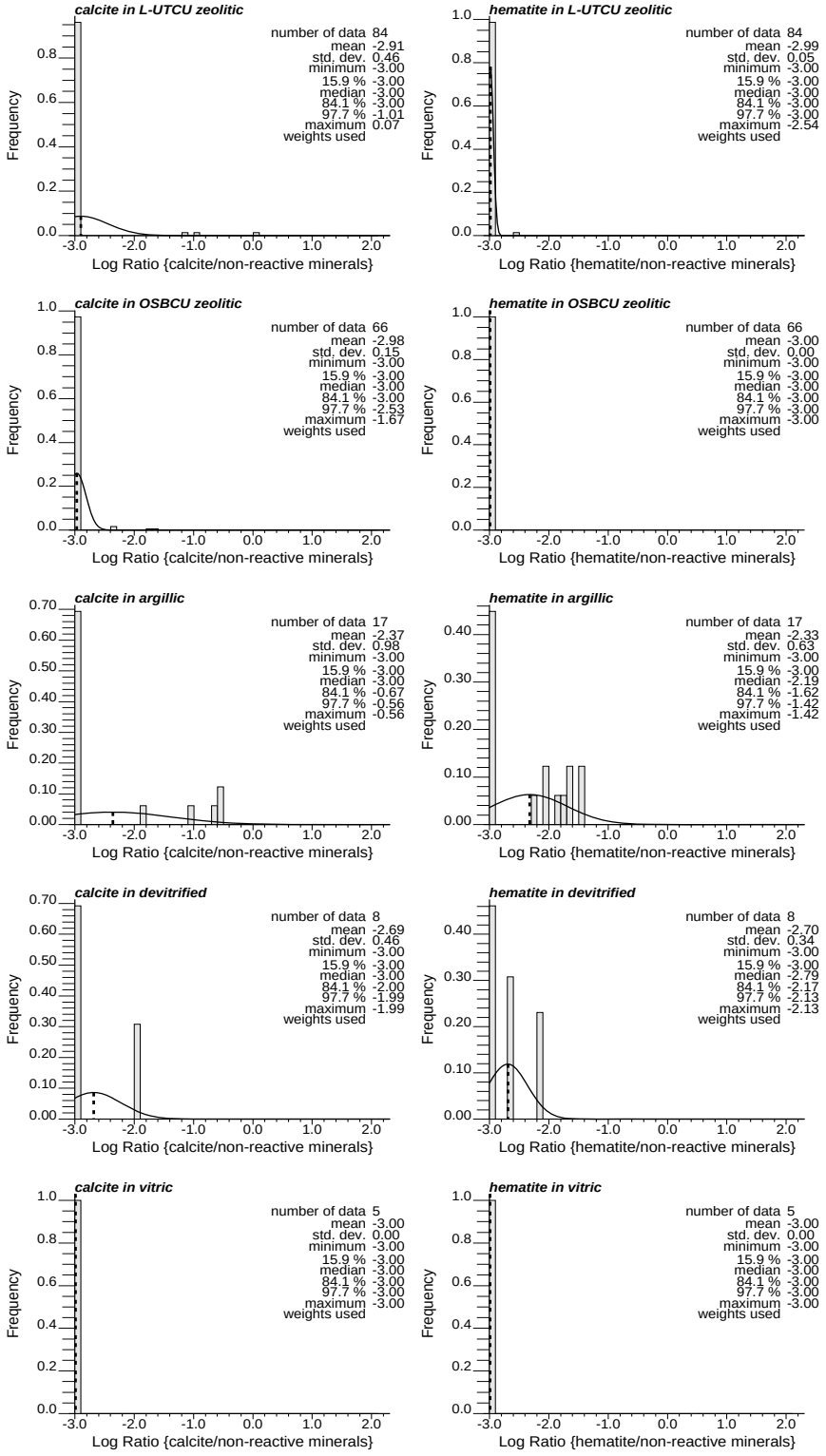

Figure 7-8. Calcite and hematite ALR frequency distributions for “F” data in RMFs.

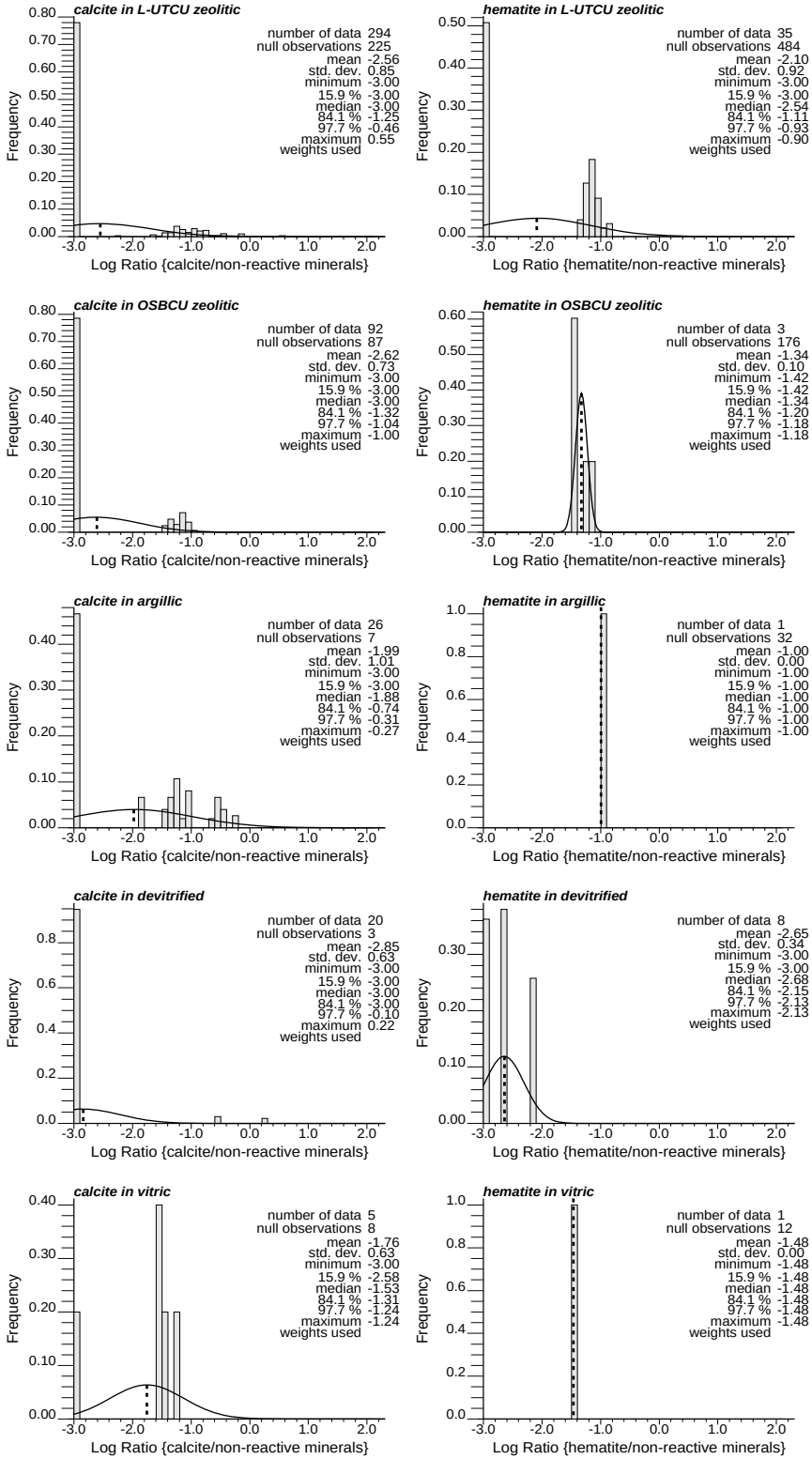

Figure 7-9. Calcite and hematite ALR frequency distributions for “S” data in RMFs.

7.5 Spatial Distribution of Reactive Mineral Facies in Yucca Flat

Reactive mineral facies (RMFs) use hydrostratigraphic units (HSU) and reactive mineral units (RMU) as the geometric framework for characterizing zonal variations in the spatial distribution of reactive minerals in the TCU. This section examines the spatial distribution of XRD data categorized as RMFs throughout the TCU in Yucca Flat. At this regional scale, the spatial distribution of RMFs will control larger-scale vertical and lateral variations in sorption properties of the TCU.

7.5.1 Regional Distribution

Figure 7-10 and Figure 7-11 show cutaway block-perspective views of the spatial distribution of XRD data categorized by XRD method and reactive mineral facies (RMFs) superposed over TCU hydrostratigraphic units in northern and southern Yucca Flat. Since RMFs are largely correlated to HSUs and RMU subunits within HSUs, the complex HSU geometry will control the regional-scale zonal spatial variations in reactive mineral content in the TCU. The three RMFs with most lateral continuity, **L-UTCU Zeolitic**, **OSBCU Zeolitic**, and **Argillic**, form a vertical sequence that dominates regional-scale zonal variations of reactive mineral content in the TCU, particularly in central and eastern Yucca Flat. The remaining two RMFs, **Devitrified** and **Vitric**, are thin and discontinuous. The **Devitrified** RMF largely occurs within the OSBCU HSU, and the **Vitric** RMF usually occurs in and near the base of the LTCU HSU and rarely in the OSBCU HSU. A few **Argillic** RMF occur within the OSBCU.

Most of central and eastern Yucca Flat will show a consistent vertical succession of the **L-UTCU Zeolitic**, **OSBCU Zeolitic**, and **Argillic** RMFs because LTCU, OSBCU, and ATCU (LTARG RMU) HSUs are laterally continuous. Toward the south, the UTCU forms a thin sheet above the Topapah Springs Aquifer (TSA) HSU. The western basin of northern Yucca Flat (includes drill holes U-2cr, U-2cv, UE-2co, and UE-4ac) shows an incomplete vertical section of RMFs. In the western basin, the OSBCU HSU is completely absent, and the LTCU HSU is largely absent. Zeolitic RMFs are less prevalent in the western basin of Yucca Flat. Indeed, most XRD data in the western basin of Yucca Flat are categorized either as **Argillic**, **Devitrified**, or **Vitric** RMFs – much different the main basin of Yucca Flat, which is dominated by the **L-UTCU Zeolitic** and **OSBCU Zeolitic** RMFs.

By associating zonal differences in reactive mineral content to HSUs and RMUs, the RMF framework accounts for regional-scale vertical and lateral variations in reactive mineral properties, including major differences between central-eastern and western Yucca Flat. Without consideration of RMUs and HSUs or reactive mineral zonations in the TCU (e.g. Prothro, 2005), subsequent geostatistical analysis of reactive mineral

distributions and K_d will suffer from issues related "nonstationarity" of the mean and variogram or covariance. The depth-dependent trends of increasing smectite and decreasing zeolite with depth are obvious examples of nonstationary mean that will directly influence characterization of spatial variability of K_d in the TCU.

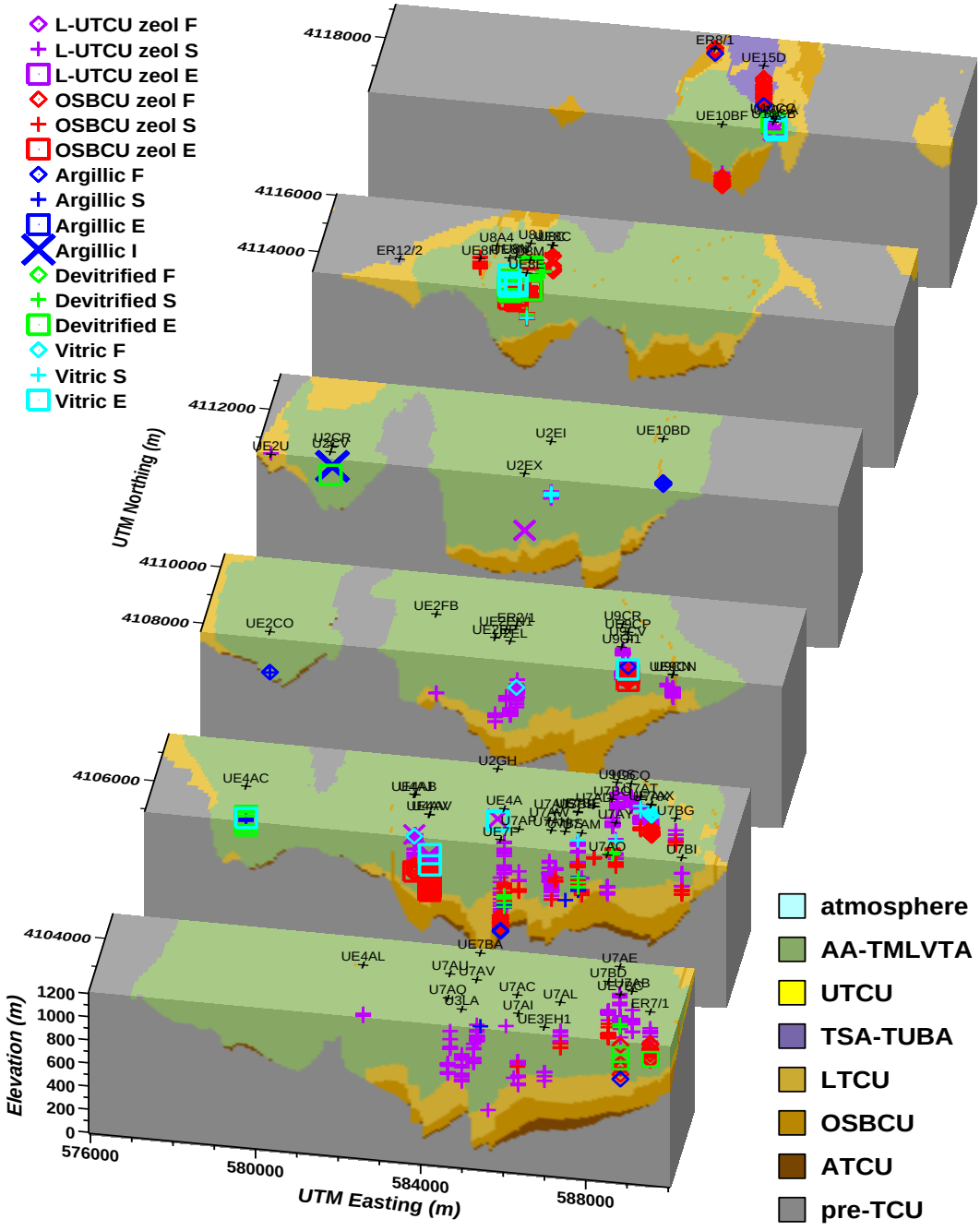

Figure 7-10. Spatial distribution of XRD data categorized by reactive mineral facies (RMFs) superposed over TCU hydrostratigraphic units in northern Yucca Flat.

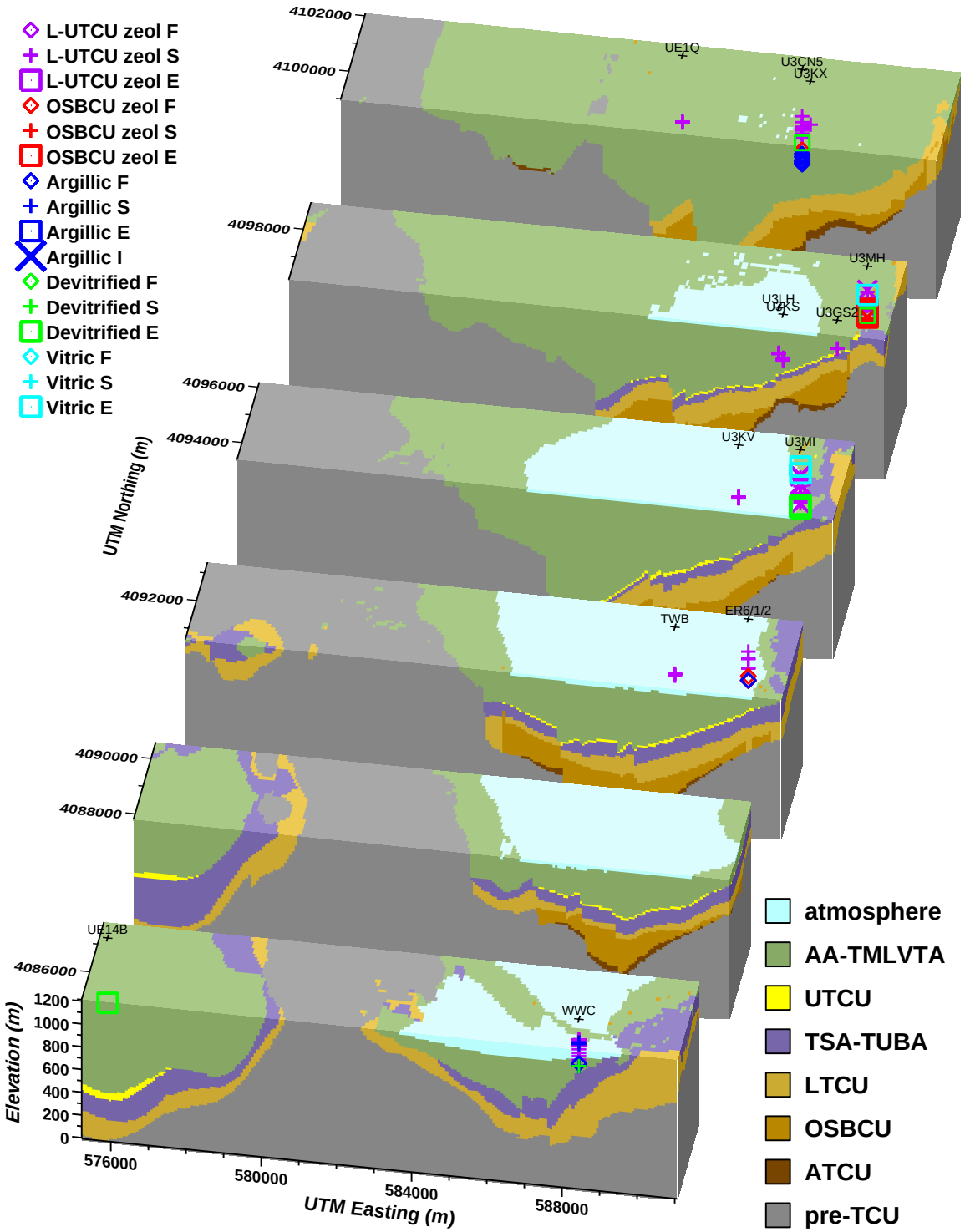

Figure 7-11. Spatial distribution of XRD data categorized by reactive mineral facies (RMFs) superposed over TCU hydrostratigraphic units in southern Yucca Flat.

7.5.2 Tuff Pile

The Tuff Pile is a north-south trending fault block within central Yucca Flat bounded by the Topgallant Fault on the west and the Yucca Fault on the east. Groundwater levels in the Tuff Pile have been elevated to hundreds of meters by pore-fluid pressurization resulting from compaction of water-saturated rock from stresses caused by underground nuclear tests (Halford et al., 2005). Rises and subsequent declines of groundwater elevations associated with underground test detonations, which ceased in 1992, have been interpreted using both simple and complex hydrogeologic conceptual models for the Tuff Pile. In the northern portion of the Tuff Pile, Halford et al. (2005) assumed a homogeneous and isotropic conceptual model of the bedded tuff sequence and calibrated a numerical groundwater model to groundwater level changes over time. Halford et al. (2005) mentioned that welded tuffs would have higher permeability, which would quickly dissipate fluid pressures. In analysis of groundwater elevation changes in the southern Tuff Pile, Wolfsberg et al. (2007) developed a highly heterogeneous conceptual model with laterally-continuous lenticular high-permeability zones sandwiched within low-permeability bedded tuff and calibrated a numerical groundwater model to observed water level changes.

Considering the unusual hydrogeologic conditions of the Tuff Pile and importance of understanding flow and transport mechanisms in Yucca Flat, XRD data are examined here for insights on the distribution flow and transport properties within the Tuff Pile. Figure 7-12 shows a cutaway block-perspective view of the spatial distribution of XRD data categorized by XRD method and reactive mineral facies (RMFs) superposed over TCU hydrostratigraphic units in the vicinity of the southern portion of the Tuff Pile studied by Wolfsberg et al. (2007). The solid black lines on top of each block represent surface traces of the Topgallant Fault to the west and the Yucca Fault on the east separated by about 1.5 km. This block-perspective view covers a south-to-north distance of 5 km.

HSUs within the Tuff Pile portion of the TCU include UTCU, LTCU, OSBCU, and ATCU. All five RMFs could be present within the Tuff Pile, however, XRD data coverage is not particularly dense. Presence of the **Devitrified** RMF would indicate presence of moderately to welded ash flow tuffs, which could be expected to have higher permeability than bedded tuffs (Halford et al., 2005). Moreover, **Devitrified** RMFs would have lower smectite and lower zeolite content and, thus, would typically have lower K_d for most radionuclide classes. Presence of **Devitrified** RMFs within the TCU would indicate a possibility for strong contrasts of flow and transport properties within the Tuff Pile.

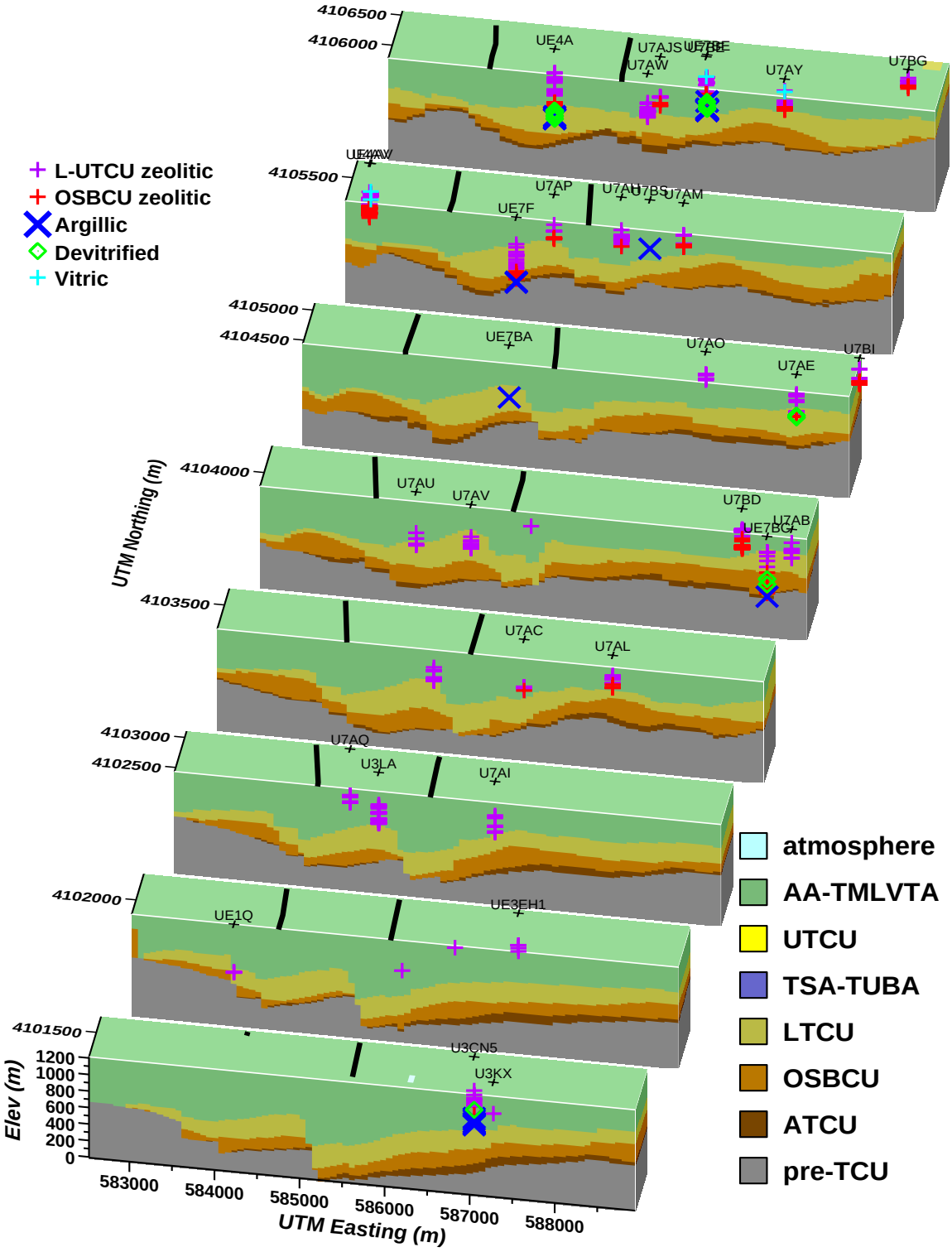

Figure 7-12. Spatial distribution of XRD data categorized by reactive mineral facies (RMFs) superposed over TCU hydrostratigraphic units in Tuff Pile area of Yucca Flat.

Upon careful examination of data shown in Figure 7-12 within the portion of the Tuff Pile examined by Wolfsberg et al. (2007), this study categorizes most XRD data as **L-UTCU Zeolitic** RMF situated within the LTCU HSU. Four boreholes toward the northern end of the Wolfsberg et al. (2007) Tuff Pile study area include data below the LTCU:

- UE7BA has one datum situated in the **Argillic** RMF.
- UE7F has closely-spaced data in the **L-UTCU Zeolitic**, **OSBCU Zeolitic**, and **Argillic** RMFs.
- U7AP has three data, two in the **L-UTCU Zeolitic** RMF and one in the **OSBCU Zeolitic** RMF.
- UE4A has data categorized into the **L-UTCU Zeolitic**, **OSBCU Zeolitic**, **Argillic**, and **Devitrified** RMFs. Importantly, UE4A is the only borehole within the Tuff Pile showing data in the **Devitrified** RMF.

XRD data from boreholes UE4A and UE7F potentially offer insights to interpretation of lateral heterogeneity of reactive mineral distributions within the Tuff Pile for several reasons:

- UE4A and UE7F are the only boreholes in the Tuff Pile that have XRD data spanning a complete cross section of the TCU.
- UE7F primarily consists of full spectrum XRD (“F”) method data, while UE4A consists entirely of semi-quantitative XRD (“S”) method data.
- UE4A and UE7F are located less than 1 km apart along a north-south alignment of the Tuff Pile fault block, presumably in a direction that would favor detection of lateral correlation of lithology and mineralogy.

The UE4A and UE7F data indicate all LTCU mineralogy falls entirely into the **L-UTCU Zeolitic** RMF, and most mineralogy in the OSBCU falls into the **OSBCU Zeolitic** RMF. However, some data in UE4A fall into the **Devitrified** RMF where stratigraphic units are identified as welded ash-flow tuff.

Figure 7-13shows a stratigraphic column for Yucca Flat by Prothro (2005). Lithologic variability is more prevalent within the OSBCU than the LTCU. Three welded ash-flow tuff stratigraphic units occur within the volcanics of Oak Springs Butte – Yucca Flat Tuff (**toy**), Redrock Valley Tuff (**tor**), and Tuff of Twin Peaks (**tot**). The UE4A XRD data identifies two welded ash-flow units, **toy** and **tor**, and the UE7F data identifies one welded ash-flow unit, **tor**.

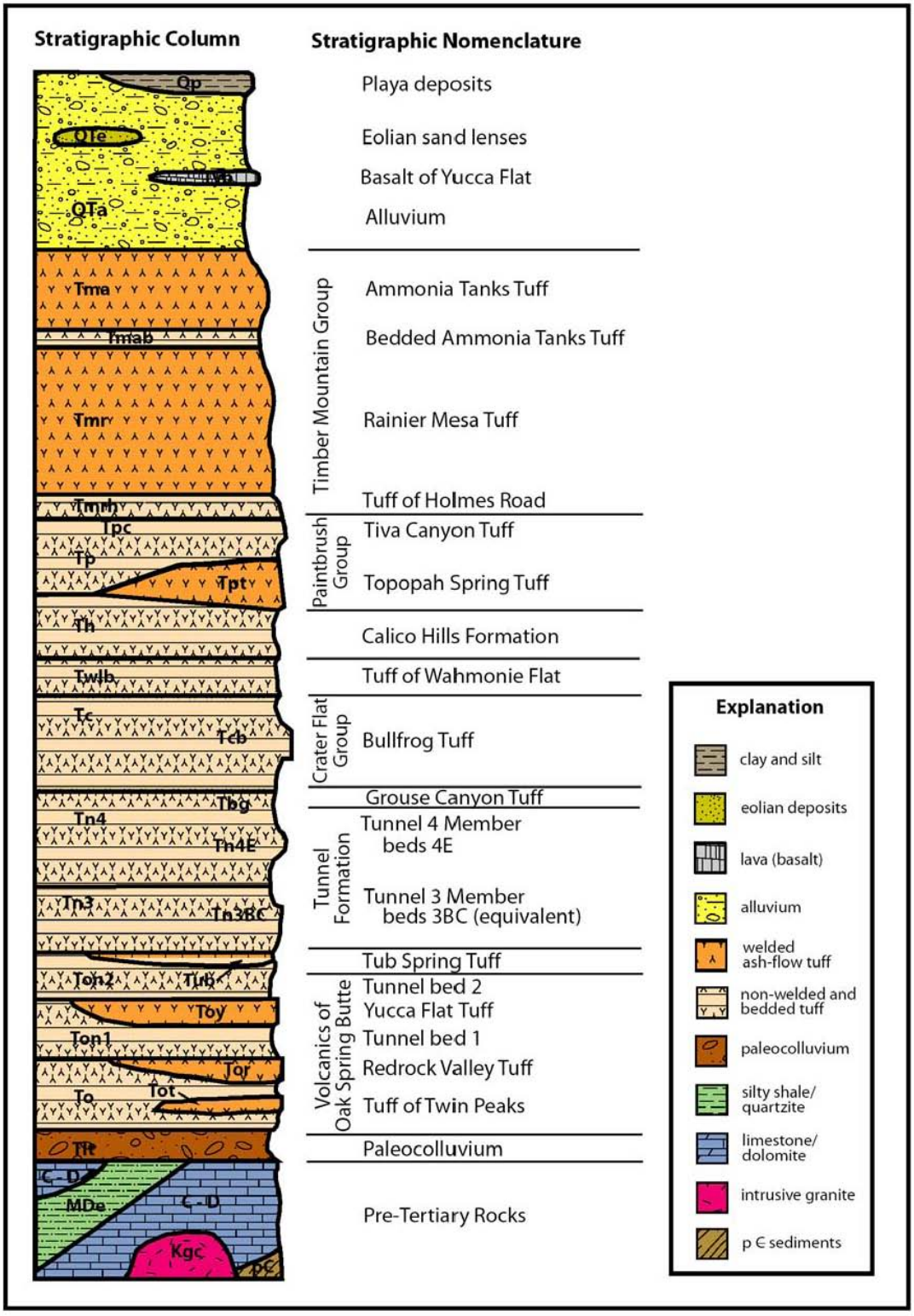

Figure 7-13. Stratigraphic column for Yucca Flat (Prothro, 2005).

Table 7-12 and Table 7-13 compare UE4A and UE7F smectite, zeolite, quartz, and cristobalite mineral percentages with elevation, stratigraphic unit, lithology, RMC, RMU, and RMF for XRD data within welded ash-flow tuff stratigraphic units. Uncertainties in mineral percentage given by Warren et al. (2007) are added to the UE4A semiquantitative ("S") method XRD data. These uncertainties lead to a range of $\frac{sm + ze}{qz + tr + cr}$ as given in the second-to-last column of Table 7-12 and Table 7-13 . For all but one of the UE4A data with devitrified RMUs (YFDMR and RVDMP), the lower range of the $\frac{sm + ze}{qz + tr + cr}$ ratio is below ¼, indicating **toy** and **tor** stratigraphic units could be considered as "devitrified" under the RMF criteria. Comparing data percentages for **tor** stratigraphic units, the $\frac{sm + ze}{qz + tr + cr}$ ratios are generally lower in UE4A than UE7F because quartz is more abundant in UE4A, and zeolite is more abundant in UE7F. The differences in quartz and zeolite percentage can be related to differences in cooling rates during ash-flow deposition and subsequent differences in zeolitization of glass.

This comparison of XRD data for welded ash flow stratigraphic units between UE4A and UE7F illustrates many complexities to interpreting and correlating mineralogic and lithologic data to flow and transport properties:

- Differences in XRD methods lead to uncertainties in correlating lithologic and mineralogic data between different boreholes.
- Uncertainty in the XRD methods leads to uncertainty in identification of major alteration and subsequent categorization of RMCs, RMUs, and RMFs.
- While stratigraphic units are associated with a lithology and major alteration (e.g. welded ash-flow tuffs and devitrification) petrographic analysis often indicates a different lithology (e.g. nonwelded or bedded) or mineralization (e.g. zeolitic or argillic).

Overall, the differences and uncertainties in the XRD methods cause difficulty in distinguishing between actual heterogeneity of mineralogic properties and data uncertainty.

Table 7-12. UE4A XRD mineral percentage data for welded ash-flow stratigraphic units within TCU including lithology, RMC, RMU, and RMF interpretations, with ratio used to distinguish devitrified RMF. Lithologies: BED=bedded tuff, NWT=non-welded tuff, PWT=partially welded tuff. For these data, all cristobalite (cr) percentages are zero and all tridymite (tr) percentages are null observations.

Elevation	Stratigraphic	Lithology	RMC	RMU	XRD Method	Zeolite (ze)	Smectite (sm)	Quartz (qz)	$\frac{sm + ze}{qz + tr + cr}$	RMF
494.84	Toy	NWT	DMP	YFDMR	"S"	17.5 ± 7.5	0	37.5 ± 12.5	$\frac{10}{50}$ to $\frac{25}{25}$	devirified
478.84	Toy	BED	ZEOL	OSBUZE	"S"	37.5 ± 12.5	5.5 ± 4.5	50 ± 25	$\frac{26}{75}$ to $\frac{60}{25}$	OSBCU zeolitic
453.24	Tor	BED	DMR	RVDMP	"S"	17.5 ± 7.5	5.5 ± 4.5	37.5 ± 12.5	$\frac{11}{50}$ to $\frac{35}{25}$	devirified
446.84	Tor	BED	ZEOL	RVDMP	"S"	35 ± 15	5.5 ± 4.5	37.5 ± 12.5	$\frac{21}{50}$ to $\frac{60}{25}$	devirified
443.65	Tor	PWT	DMR	RVDMP	"S"	17.5 ± 7.5	5.5 ± 4.5	37.5 ± 12.5	$\frac{11}{50}$ to $\frac{35}{25}$	devirified
435.56	Tor	NWT	DMR	RVDMP	"S"	0.0	17.5 ± 7.5	62.5 ± 12.5	$\frac{10}{70}$ to $\frac{25}{50}$	devirified
424.28	Tor	BED	DMP	RVDMP	"S"	17.5 ± 7.5	5.5 ± 4.5	30.0 ± 20.0	$\frac{11}{50}$ to $\frac{35}{10}$	devirified
418.80	Tor	BED	ARG	OSBMZE1	"S"	17.5 ± 7.5	37.5 ± 12.5	37.5 ± 12.5	$\frac{35}{50}$ to $\frac{75}{25}$	OSBCU zeolitic

Table 7-13. UE7F XRD mineral percentage data for welded ash-flow stratigraphic units within TCU including lithologic, RMC, RMU, and RMF interpretations, with ratio used to distinguish devitrified RMF. For these data, all cristobalite (cr) percentages are zero except for 0.2 at 488.75 elevation, and all tridymite (tr) percentages are null observations.

Elevation	Stratigraphic	Lithology	RMC	RMU	XRD Method	Zeolite (ze)	Smectite (sm)	Quartz (qz)	$\frac{sm + ze}{qz + tr + cr}$	RMF
488.75	Tor	NWT	ARG	OSBUZE	"F"	22.8	36.8	7.0	$\frac{59.6}{9.0}$	OSBCU zeolitic
476.11	Tor	NWT	ZEOL	OSBUZE	"F"	58	4.2	8.8	$\frac{62.2}{8.8}$	OSBCU zeolitic
447.01	Tor	BED	ZEOL	OSBUZE	"F"	44	8.9	20.8	$\frac{52.9}{20.8}$	OSBCU zeolitic

8. K_d Distributions in Reactive Mineral Facies

The distribution coefficient, K_d (mg/L units), is used in contaminant transport models to measure moles of contaminant sorbed per mass of the porous medium relative to the moles of contaminant per solution volume. The component additivity methodology by Zavarin et al. (2004) is used to estimate K_d for radionuclide classes based on reactive mineral fractions and a given groundwater chemistry. The component additivity methodology assumes K_d for each radionuclide class can be estimated as a linear combination of linear coefficients associated with each reactive mineral fraction. These linear coefficients are derived from mechanistic model calculations calibrated to laboratory sorption data (Zavarin et al., 2004; Zavarin and Bruton, 2004a,b). Each radionuclide has a different set of linear coefficients. Since each reactive mineral facies (RMFs) has different distributions of reactive minerals, each RMF will have different K_d distributions. This chapter applies the component additivity methodology to RMF reactive mineral distributions to obtain estimates of radionuclide class K_d distributions in each RMF.

8.1 Component Additivity Methodology

Based on the component additivity methodology (Zavarin et al., 2004), $K_{d,rn}$ for a particular radionuclide, *rn*, is related to the reactive mineral fraction, x_i, by

$$K_{d.rn} = \sum_{i=1}^{N_{r,rn}} x_i 10^{c(rn,i)} \qquad \text{Equation (8.1)}$$

where $c(rn,i)$ are the exponential coefficients relating degree of sorption of radionuclides to reactive minerals, and $N_{r,rn}$ is the number of reactive minerals for the radionuclide, *rn*.

Table 8-1 lists predicted values and uncertainties in the exponential coefficients used in application of Equation (8.1) to estimate K_d of ten radionuclide classes in the TCU within Yucca Flat. The K_ds were calculated using average water chemistries from seven wells completed within the tuffaceous units of Yucca Flat (ER-2-1, Test Well #7 (HTH), U-2bs, UE-10ITS#3 1926 ft, ER-2-1, UE-14b, and USGS Test Well B) (SNJV, 2006) and mechanistic model parameters identified in Carle et al. (2007). The uncertainties pertain to the variability in $\log\{K_d\}$ resulting from a range of water chemistries. Additional uncertainties associated with the mechanistic model parameters may also be relevant but have not been addressed here.

Table 8-1. Component additivity exponential coefficients and uncertainties associated with groundwater chemistry variability for ten radionuclide classes in the TCU of Yucca Flat.

RadionuclideClass	Reactive Minerals				
	Calcite	Hematite	Mica	Smectite	Zeolite
^{41}Ca(II)	3.19 ± 0.32	3.99 ± 0.38	2.82 ± 0.32	0.96 ± 0.38	-
Cs(I)	3.11 ± 0.18	3.75 ± 0.20	5.58 ± 0.18	-	-
Sr(II)	2.79 ± 0.33	3.77 ± 0.38	2.83 ± 0.32	-0.96 ± 0.38	-0.17 ± 0.70
Ni(II)	3.94 ± 0.12	-	-	0.86 ± 0.40	1.21 ± 0.11
Sm(III)	3.85 ± 0.40	-	-	5.11 ± 0.63	2.94 ± 0.51
Eu(III)	3.69 ± 0.39	-	-	4.58 ± 0.65	2.77 ± 0.52
Am(III)	4.45 ± 0.39	-	-	4.79 ± 0.55	3.17 ± 0.52
Np(V)	1.17 ± 0.24	-	-	2.10 ± 0.56	1.77 ± 0.67
Pu[a]	2.72 ± 0.40	-	-	3.09 ± 0.87	3.03 ± 0.43
U(VI)	0.73 ± 0.70	-	-	-2.27 ± 1.90	1.64 ± 0.66

[a]Pu estimated K_ds were based on a solution with O_2(g) fugacity of 10^{-20} bars. Under these conditions, Pu(IV) is the predominant aqueous species in solution.

8.2 Addressing Uncertainty in Component Additivity Methodology

As indicated in Table 8-1, the component additivity methodology coefficients for each radionuclide class have uncertainty relating to variability in groundwater chemistry in the TCU. This uncertainty, $e(rn,i)$, could be added to the true exponential term, $c(rn,i)$, in Equation (8.1)

$$Kd_{rn} = \sum_{i=1}^{N_{r,rn}} x_i 10^{c(rn,i)+e(rn,i)} \qquad \text{Equation (8.2)}$$

Other uncertainties associated with component additivity and mechanistic model parameters could also be incorporated in this fashion. However, we do not address these other uncertainties here. Notably in Table 8-1, the uncertainty associated with groundwater chemistry in the component additivity coefficients for each radionuclide class is similar for mica, smectite, and zeolite – the largely ubiquitous reactive minerals

in the TCU that dominate sorption. Assuming that for a given radionuclide, the error in the component additivity coefficients is identically *e(rn)* for each reactive mineral *i*, Equation (8.2) with error reduces to

$$K_{d,rn} = 10^{e(rn)} \sum_{i=1}^{N_{r,rn}} x_i 10^{c(rn,i)}$$

For the logarithm of K_d, Equation (8.2) reduces to

$$\log\{K_{d,rn}\} = e(rn) + \log\left\{ \sum_{i=1}^{N_{r,rn}} x_i 10^{c(rn,i)} \right\}$$

Therefore, assuming identical uncertainty in the component additivity coefficients for different reactive minerals simplifies prediction of uncertainty in $\log\{K_d\}$ distributions. A single distribution of component additivity coefficient uncertainty can simply be added directly to the uncertainty of the mean $\log\{K_d\}$.

Assuming Gaussian distributions for component additivity coefficient uncertainty and $\log\{K_d\}$ distributions, the variance, $\sigma^2[\log\{K_d\}]$, of estimated XRD sample-scale $\log\{K_d\}$ distribution including component additivity uncertainty can be estimated by

$$\sigma^2\left[\log\{K_{d,rn}\}\right] = e(rn)^2 + \sigma^2\left[\log\left\{ \sum_{i=1}^{N_{r,rn}} x_i 10^{c(rn,i)} \right\} \right]$$

where $\sigma^2\left[\log\left\{ \sum_{i=1}^{N_{r,rn}} x_i 10^{c(rn,i)} \right\} \right]$ is the square of the standard deviation of the Gaussian distribution fit to the $\log\{K_d\}$ distribution.

K_d for ^{41}Ca, Cs, and Sr will be dominated by zeolite, smectite, and mica fractions. The uncertainties in component additivity coefficients Table 8-1 range only from 0.32–0.38 for ^{41}Ca, 0.18-0.20 for Cs, and 0.32-0.38 for Sr. Therefore, reasonable estimates for uncertainty in mean $\log\{K_d\}$ for ^{41}Ca, Cs, and Sr are 0.35, 0.19, and 0.35, respectively. From the logarithmic scale to a linear scale, these uncertainties translate to multiplication factors of 2.2 for ^{41}Ca, 1.5 for Cs, and 2.2 for Sr.

K_d for Ni, Sm, Eu, Am, Np, Pu, and U will be dominated by smectite except in rare cases where calcite or hematite are present. Uncertainty in the component additivity coefficients for smectite will have the largest effect on uncertainty in mean K_d for Ni, Sm, Eu, Am, Np, Pu, and U. Therefore, reasonable estimates for uncertainty in mean $\log\{K_d\}$

are 0.12 for Ni, 0.40 for Sm, 0.39 for Eu, 0.39 for Am, 0.24 for Np, 0.40 for Pu, and 0.70 for U. These uncertainties translate to the linear scale as multiplication factors of 1.3 for Ni, 2.5 for Sm, 2.5 for Eu, 2.5 for Am, 1.7 for Np, 2.5 for Pu, and 5.0 for U.

Uncertainties for calcite and hematite component additivity coefficients are consistently higher than for smectite. However, contribution to $\log\{K_d\}$ uncertainty from calcite and hematite is expected to be secondary because the mineralogic data indicate calcite and hematite are more abundant in argillic zones where smectite is far more prevalent.

Alternatively, uncertainty in component additivity coefficients could be addressed by adding normally distributed deviates with standard deviation $e_{rn,i}$ to exponential coefficients in application of Equation (8.1) to mineralogic data.

8.3 K_d Distributions for Radionuclide Classes

Application of Equation (8.1) to reactive mineral fractions will produce distributions of K_d. In this section, Equation (8.1) is applied to the "F" and "S" method XRD reactive mineral fraction data for each RMF. Mica and smectite zero values are corrected as described in Sections 7.2.2 and 7.3.1. The zero value correction helps avoid unrealistic left tailing to extremely small K_d values, which can also unrealistically exaggerate the variance of $\log\{K_d\}$.

The resulting K_d distributions tend to be more closely fit by a log-normal distribution than a normal distribution. Accordingly, the K_d distributions are plotted on a logarithmic scale. Each $\log\{K_d\}$ distribution is compared to a Gaussian distribution with the same mean and standard deviation. In general, a log-normal distribution provides a reasonable fit to the sample distribution of $\log\{K_d\}$ for the radionuclide classes in each RMF.

The $\log\{K_d\}$ distributions presented in this chapter are pertinent to the scale of XRD data and probably represent a wider distribution of $\log\{K_d\}$ compared to a grid block scale as indicated by K_d upscaling studies (Zavarin et al., 2004). Considering that the component additivity methodology parameters themselves are uncertain as indicated in Table 8-1 , a comprehensive evaluation of uncertainty in K_d for transport models would need to consider a distribution of K_d regardless of K_d upscaling properties.

In the following subsections, $\log\{K_d\}$ distributions are estimated from application of Equation (8.1) using mean values of component additivity coefficients in Table 8-1 and reactive mineral percentage data for each RMF from "F" and "S" XRD data with corrections for zero values and data spacing (Section 7.2). Gaussian distributions are fit to mean and standard deviation of the $\log\{K_d\}$ distributions for each RMF. These

$\log\{K_d\}$ distributions represent variability of $\log\{K_d\}$ associated with variability within RMFs and uncertainty in XRD method. Lower uncertainty in "F" method data generally translates to narrower $\log\{K_d\}$ distributions compared to "S" method data. Additional uncertainty associated with component additivity coefficients can be superposed as discussed in Section 8.2.

8.3.1 ^{41}Ca

^{41}Ca is a strong sorber to zeolite, smectite, and mica. Figure 8-1 and Figure 8-2 show estimated XRD sample-scale ^{41}Ca $\log\{K_d\}$ distributions in the RMFs for "F" and "S" data. In **L-UTCU Zeolitic** and **OSBCU Zeolitic** RMFs, $\log\{K_d\}$ for ^{41}Ca is highest and dominated by the narrow zeolite frequency distribution. ^{41}Ca $\log\{K_d\}$ in the **Argillic** RMF is lower than in the zeolitic RMFs, but the ^{41}Ca $\log\{K_d\}$ distribution remains narrow. ^{41}Ca $\log\{K_d\}$ in the **Devitrified** and **Vitric** RMFs relatively low but more variable. Trends in ^{41}Ca $\log\{K_d\}$ reflect trends in zeolite abundance. Uncertainty in ^{41}Ca $\log\{K_d\}$ attributed to groundwater chemistry variability is estimated at 0.38 based on uncertainty in the zeolite component additivity coefficient (Table 8-1).

Table 8-2 shows estimates of mean $\log\{K_d\}$ for ^{41}Ca from "F" and "S" XRD data with standard deviation (σ) of $\log\{K_d\}$ derived from XRD data and attributed to groundwater chemistry variability. Mean $\log\{K_d\}$ in RMFs are similar for ^{41}Ca $\log\{K_d\}$ distributions derived from "F" and "S" data except for the **Devitrified** RMF, where the mean ^{41}Ca $\log\{K_d\}$ is estimated at 1.98 from "F" data and 2.55 from "S" data. This difference can be attributed to lower estimates of zeolite, smectite, and mica percentage from "F" data (Figure 7-3) compared to "S" data (Figure 7-6) in the **Devitrified** RMF. Standard deviations are greater in the "S" data, except for the **Vitric** RMF which have only 5 "F" data. Larger standard deviations are expected for "S" data as a result of uncertainty derived from estimation ranges.

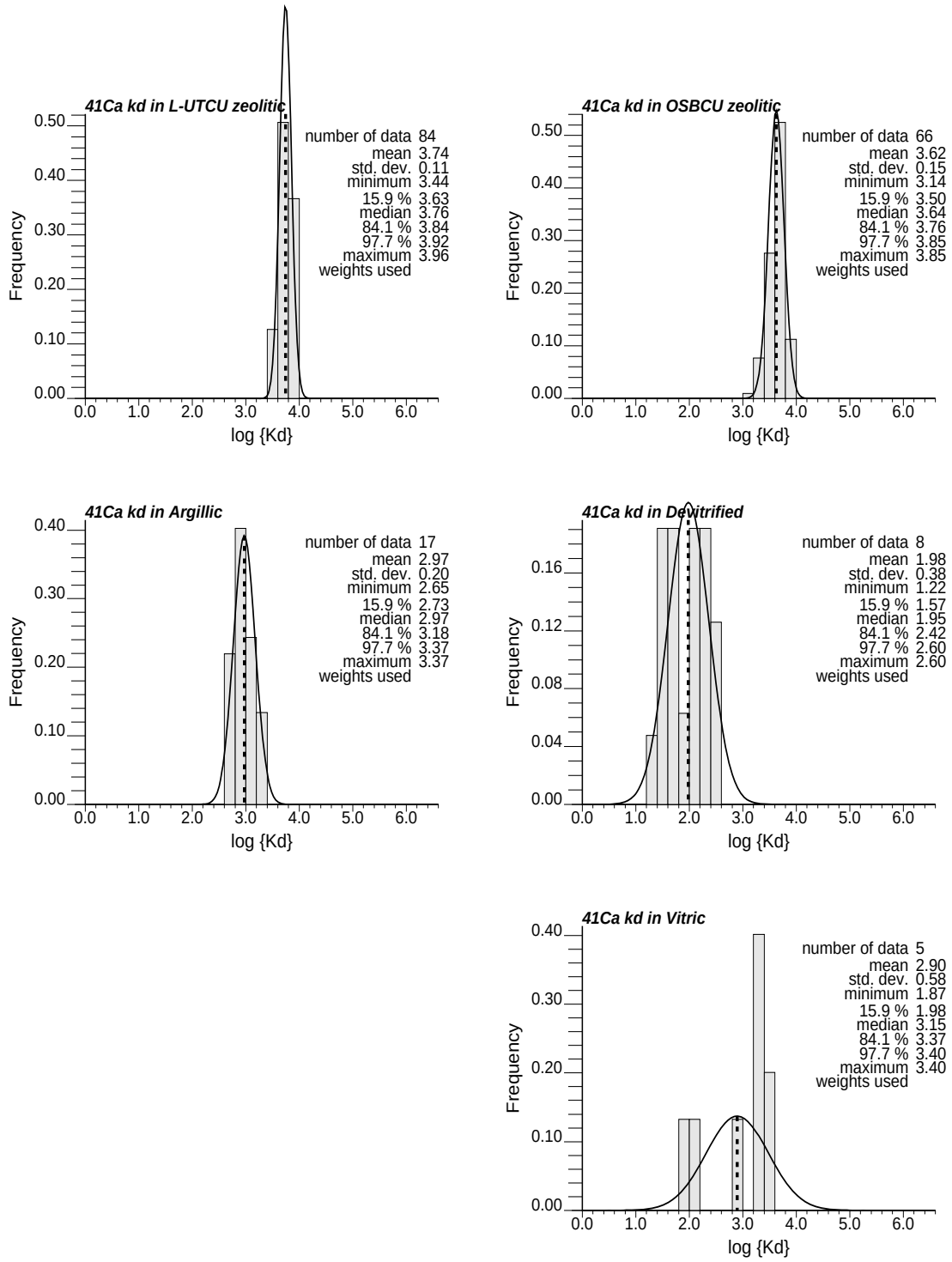

Figure 8-1. $\log\{K_d\}$ distributions for ^{41}Ca in TCU RMFs as determined from "F" data and application of mean component additivity coefficients.

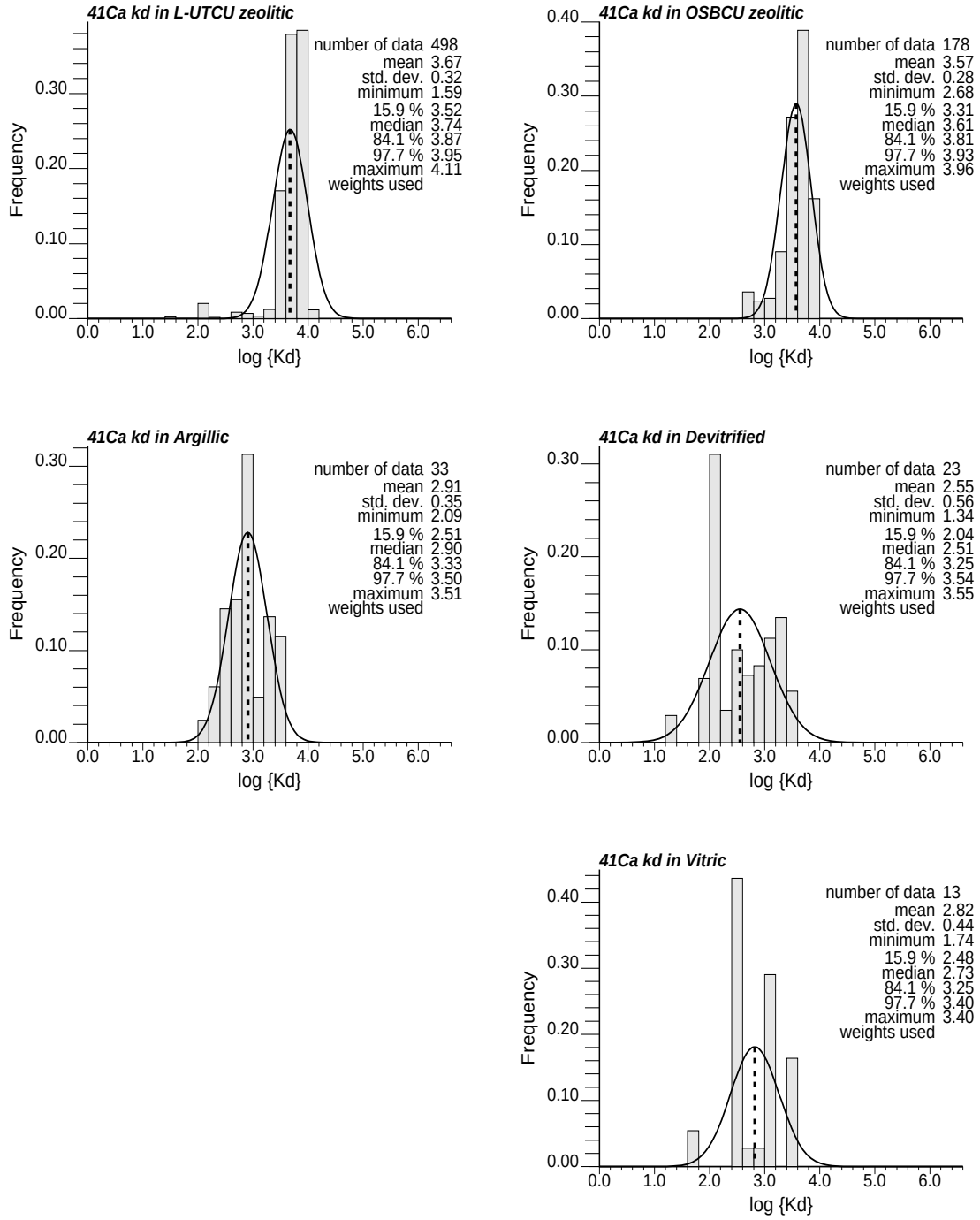

Figure 8-2. $\log\{K_d\}$ distributions for ^{41}Ca in TCU RMFs as determined from "S" data and application of mean component additivity coefficients.

Table 8-2. Estimates of mean $\log\{K_d\}$ for ^{41}Ca from "F" and "S" XRD data with standard deviation (σ) of $\log\{K_d\}$ derived from XRD data and attributed to groundwater chemistry variability.

RMF	Mean ^{41}Ca $\log\{K_d\}$		σ ^{41}Ca $\log\{K_d\}$ derived from XRD data		Uncertainty in ^{41}Ca $\log\{K_d\}$ attributed to groundwater chemistry variability
	"F"	"S"	"F"	"S"	
L-UTCU Zeolitic	3.74	3.67	0.11	0.32	0.38 based on zeolite coefficient (Table 8.1)
OSBCU Zeolitic	3.62	3.57	0.15	0.28	
Argillic	2.97	2.91	0.20	0.35	
Devitrified	1.98	2.55	0.38	0.56	
Vitric	2.90	2.82	0.58	0.44	

8.3.2 Am

Am is a strong sorber to smectite, calcite, and hematite. Figure 8-3 and Figure 8-4 show estimated XRD sample-scale Am $\log\{K_d\}$ distributions in the RMFs for "F" and "S" data. In the **Argillic** RMFs, $\log\{K_d\}$ for Am is highest and dominated by the smectite frequency distribution. Mean $\log\{K_d\}$ increases with the depth-dependent increase in smectite between **L-UTCU Zeolitic**, **OSBCU Zeolitic**, and **Argillic** RMFs. Mean $\log\{K_d\}$ distributions for Am in the **OSBCU Zeolitic**, **Devitrified**, and **Vitric** RMFs are similar, suggesting a single distribution of K_d could be applied to Am for the OSBCU HSU. Trends in Am $\log\{K_d\}$ reflect trends in smectite abundance. Uncertainty in Am $\log\{K_d\}$ attributed to groundwater chemistry variability is estimated at 0.39 based on uncertainty for the smectite component additivity coefficient (Table 8-1).

Table 8-3 shows estimates of mean $\log\{K_d\}$ for Am from "F" and "S" XRD data with standard deviation (σ) of $\log\{K_d\}$ derived from XRD data and attributed to groundwater chemistry variability. Mean $\log\{K_d\}$ and standard deviation are similar for Am $\log\{K_d\}$ distributions derived from "F" and "S" data. This suggests for radionuclide classes with K_d dominated by smectite, both the "F" and "S" data provide similar characterization quality.

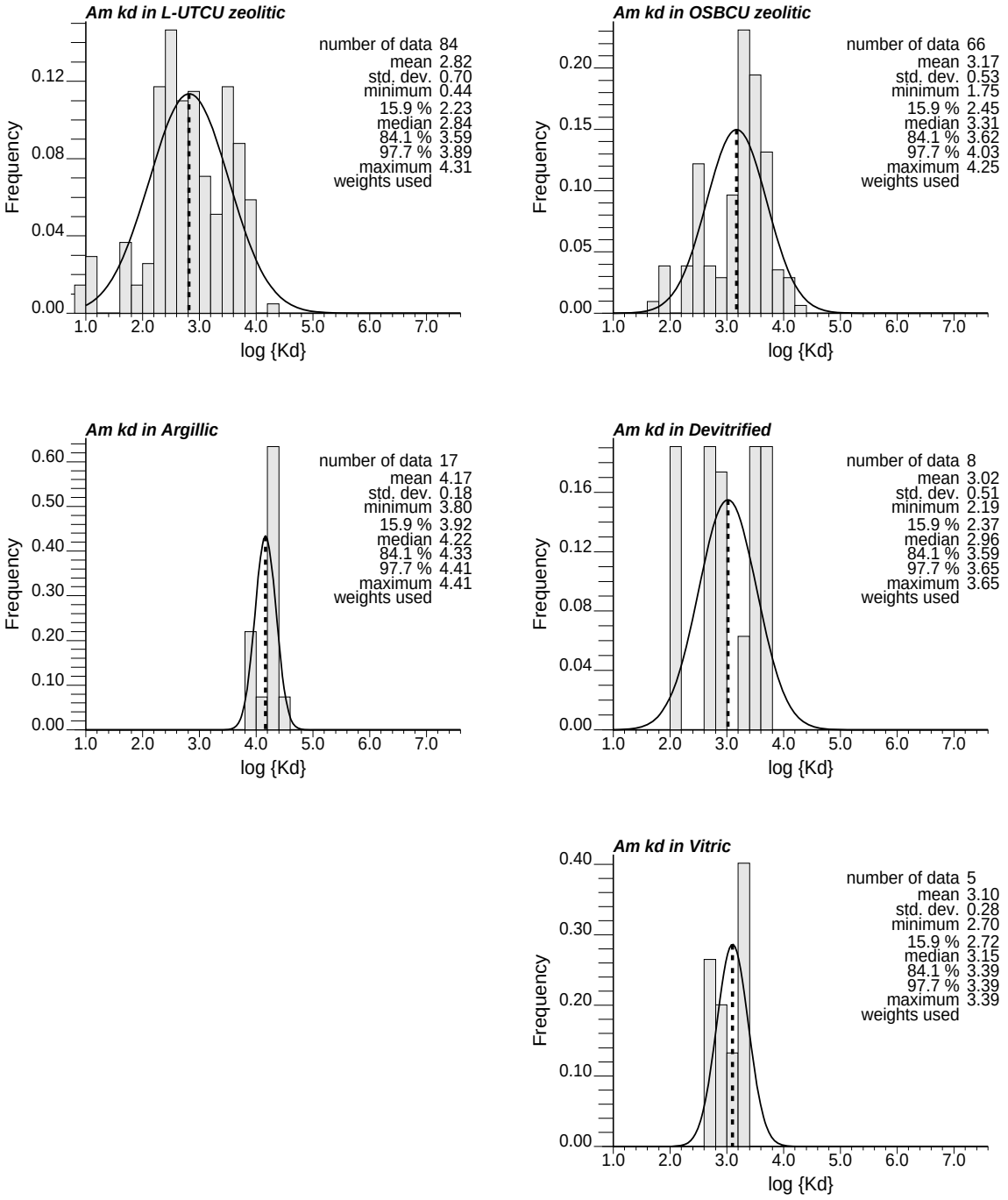

Figure 8-3. $\log\{K_d\}$ distributions for Am in TCU RMFs as determined from "F" data and application of mean component additivity coefficients.

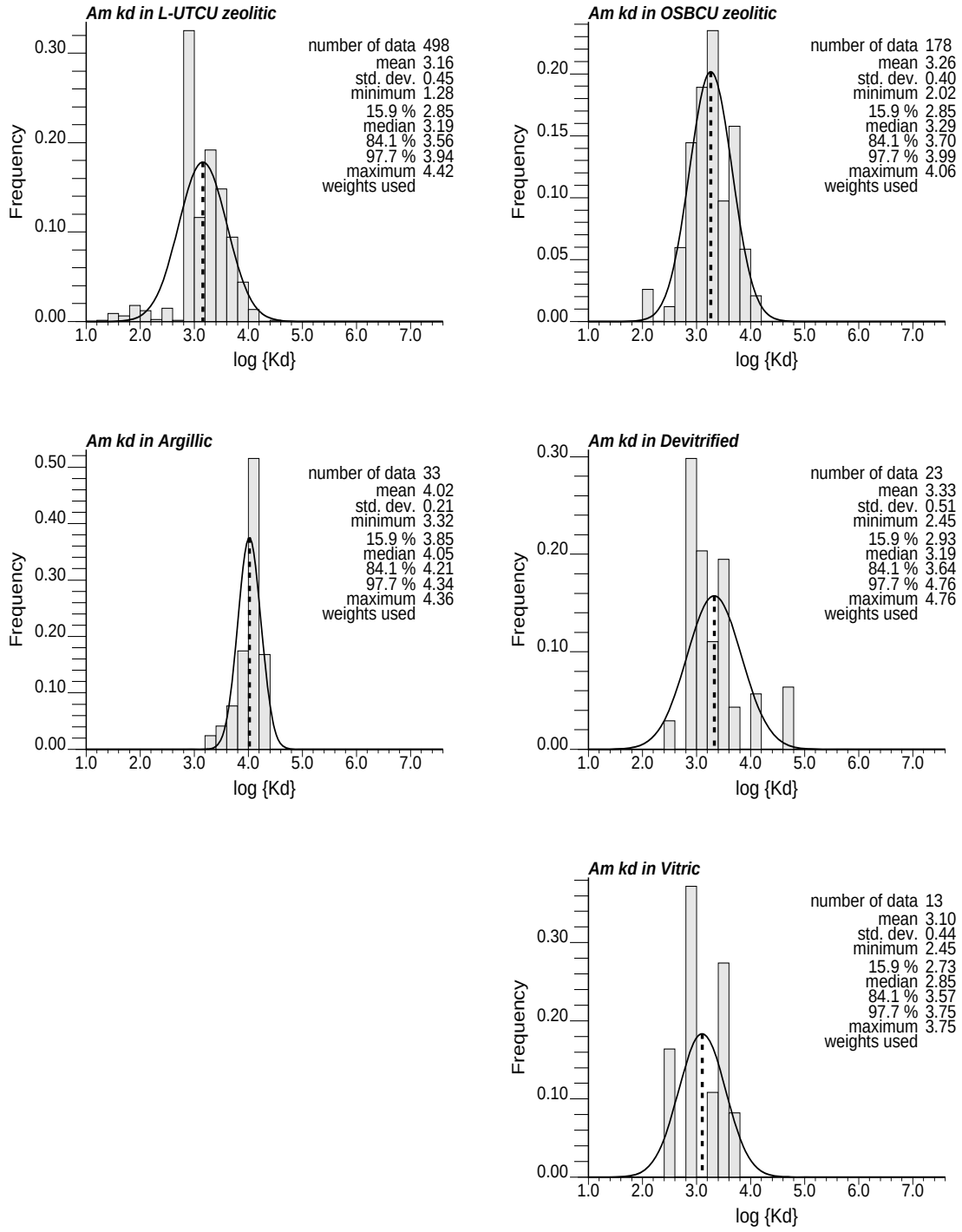

Figure 8-4. $\log\{K_d\}$ distributions for Am in TCU RMFs as determined from "S" data and application of mean component additivity coefficients.

Table 8-3. Estimates of mean $\log\{K_d\}$ for Am from "F" and "S" XRD data with standard deviation (σ) of $\log\{K_d\}$ derived from XRD data and attributed to groundwater chemistry variability.

RMF	Mean Am $\log\{K_d\}$		σ Am $\log\{K_d\}$ derived from XRD data		Uncertainty in Am $\log\{K_d\}$ attributed to groundwater chemistry variability
	"F"	"S"	"F"	"S"	
L-UTCU Zeolitic	2.82	3.16	0.70	0.45	0.39 based on smectite coefficient (Table 8-1)
OSBCU Zeolitic	3.17	3.26	0.53	0.40	
Argillic	4.17	4.02	0.18	0.21	
Devitrified	3.02	3.33	0.51	0.51	
Vitric	3.10	3.10	0.28	0.44	

8.3.3 Cs

Cs is a strong sorber to smectite and zeolite, and a particularly strong sorber to mica. Figure 8-5 and Figure 8-6 show estimated XRD sample-scale Cs $\log\{K_d\}$ distributions in the RMFs for "F" and "S" data. Mean Cs $\log\{K_d\}$ is uniformly high in all RMFs, reflecting the ubiquity and uniformity of mica throughout the TCU. Standard deviations in $\log\{K_d\}$ for **L-UTCU Zeolitic** are greater than **OSBCU Zeolitic** because of zero-valued mica associated with peralkaline tuffs. Trends in Cs $\log\{K_d\}$ reflect trends in mica abundance. Mica abundance varies little throughout the TCU and, correspondingly mean Cs $\log\{K_d\}$ is relatively uniform throughout the TCU. Uncertainty in Cs $\log\{K_d\}$ attributed to groundwater chemistry variability is estimated at 0.18 based on uncertainty for the mica component additivity coefficient (Table 8-1).

Table 8-4 shows estimates of mean $\log\{K_d\}$ for Cs from "F" and "S" XRD data with standard deviation (σ) of $\log\{K_d\}$ derived from XRD data and attributed to the component additivity methodology. Mean $\log\{K_d\}$ are similar for Cs $\log\{K_d\}$ distributions derived from "F" and "S" data. Standard deviations of Cs $\log\{K_d\}$ are higher from "S" data than "F" data largely because uncertainty in "S" data mica percentage estimates is greater. The "F" data provide more accurate estimates of the $\log\{K_d\}$ distribution for Cs that "S" data because "F" data have better resolution of mica percentage, which is typically near 2% throughout the TCU.

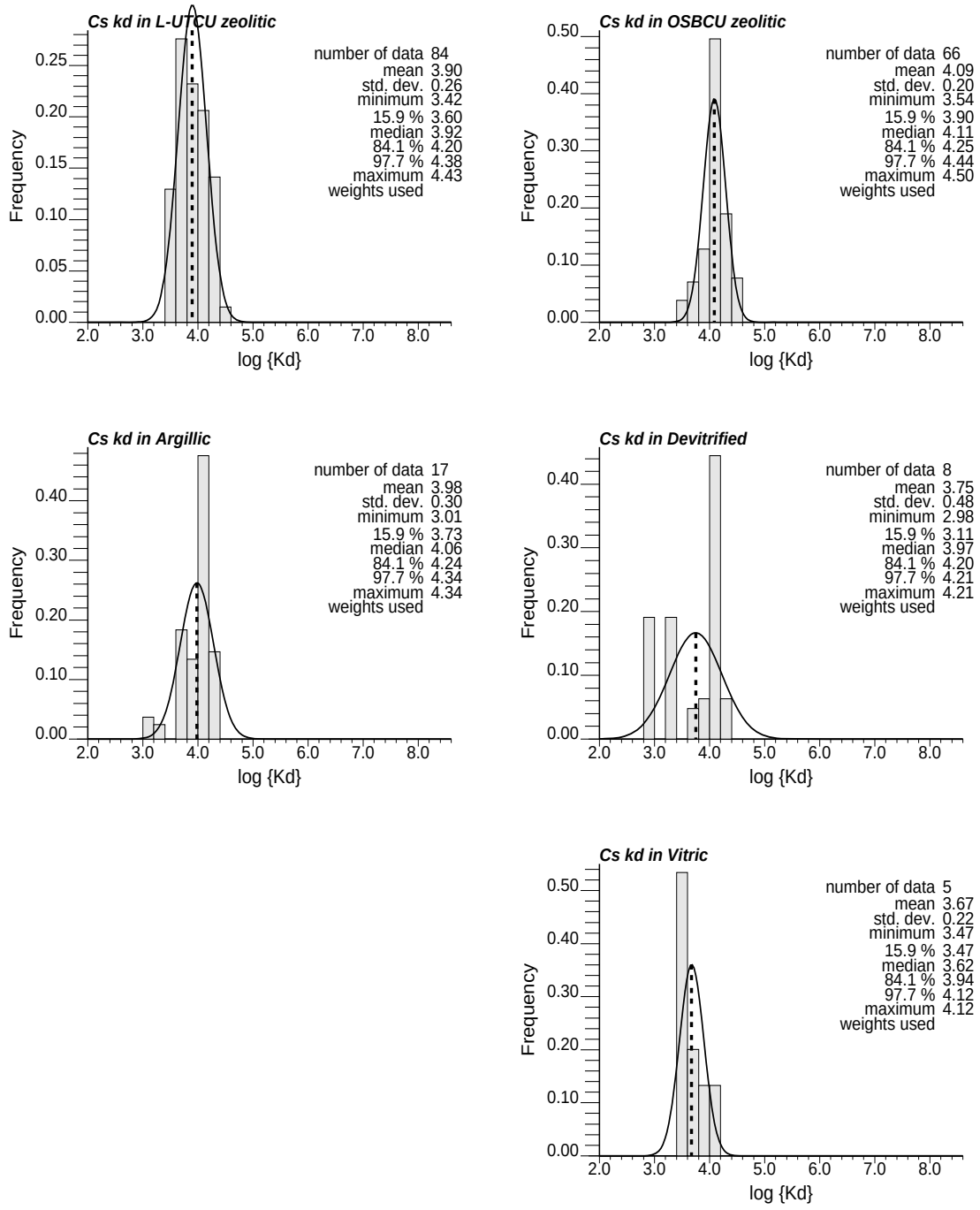

Figure 8-5. $\log\{K_d\}$ distributions for Cs in TCU RMFs as determined from "F" data and application of mean component additivity coefficients.

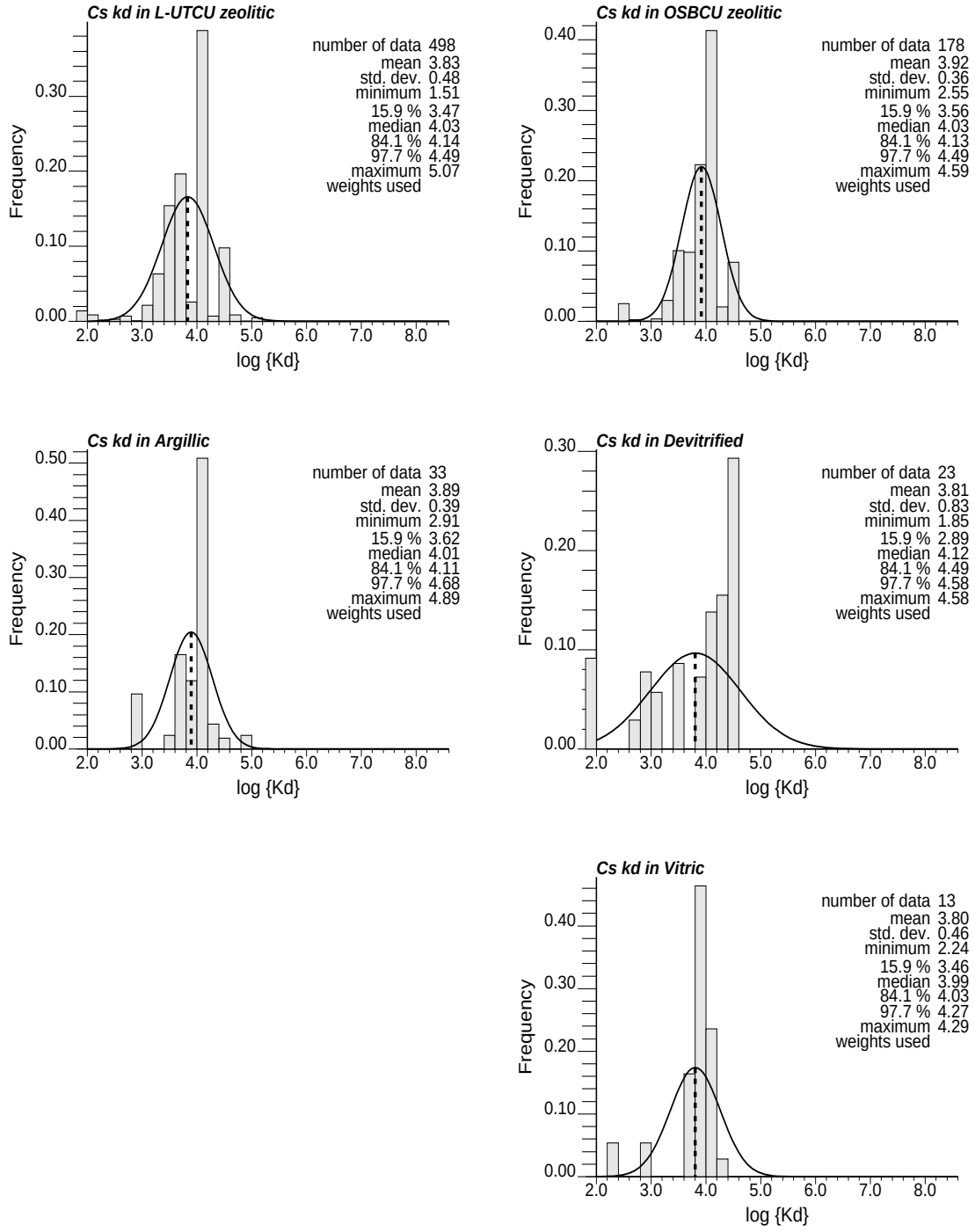

Figure 8-6. $\log\{K_d\}$ distributions for Cs in TCU RMFs as determined from "S" data and application of mean component additivity coefficients.

Table 8-4. Estimates of mean $\log\{K_d\}$ for Cs from "F" and "S" XRD data with standard deviation (σ) of $\log\{K_d\}$ derived from XRD data and attributed to groundwater chemistry variability.

RMF	Mean Cs $\log\{K_d\}$		σ Cs $\log\{K_d\}$ derived from XRD data		Uncertainty in Cs $\log\{K_d\}$ attributed to groundwater chemistry variability
	"F"	"S"	"F"	"S"	
L-UTCU Zeolitic	3.90	3.83	0.26	0.48	0.18 based on mica coefficient (Table 8-1)
OSBCU Zeolitic	4.09	3.92	0.20	0.36	
Argillic	3.98	3.89	0.30	0.39	
Devitrified	3.75	3.81	0.48	0.83	
Vitric	3.67	3.80	0.22	0.46	

8.3.4 Eu

Eu is a strong sorber to smectite and calcite and a moderate sorber to hematite. Figure 8-7 and Figure 8-8 show estimated XRD sample-scale Eu $\log\{K_d\}$ distributions in the RMFs for "F" and "S" data. In the **Argillic** RMF, $\log\{K_d\}$ for Eu is highest and dominated by the smectite frequency distribution. Mean Eu $\log\{K_d\}$ increases with the depth-dependent increase in smectite between **L-UTCU Zeolitic**, **OSBCU Zeolitic**, and **Argillic** RMFs. Eu $\log\{K_d\}$ distributions in the **OSBCU Zeolitic**, **Devitrified**, and **Vitric** RMFs are similar, suggesting a single distribution of K_d could be applied to Eu for the OSBCU HSU. Trends in Eu $\log\{K_d\}$ reflect trends in smectite abundance. Uncertainty in Eu $\log\{K_d\}$ attributed to groundwater chemistry variability is estimated at 0.39 based on uncertainty for the smectite component additivity coefficient (Table 8-1).

Table 8-5 shows estimates of mean $\log\{K_d\}$ for Eu from "F" and "S" XRD data with standard deviation (σ) of $\log\{K_d\}$ derived from XRD data and groundwater chemistry variability. As with other smectite-dominated sorbers in the TCU, mean $\log\{K_d\}$ and standard deviation are similar for Eu $\log\{K_d\}$ distributions derived from "F" and "S" data. This suggests for radionuclide classes with K_d dominated by smectite, both the "F" and "S" data provide similar characterization quality. Although Eu is a stronger sorber to calcite, smectite dominates trends in $\log\{K_d\}$distribution between different RMFs because calcite is distributed sporadically at relatively low percentages throughout the TCU.

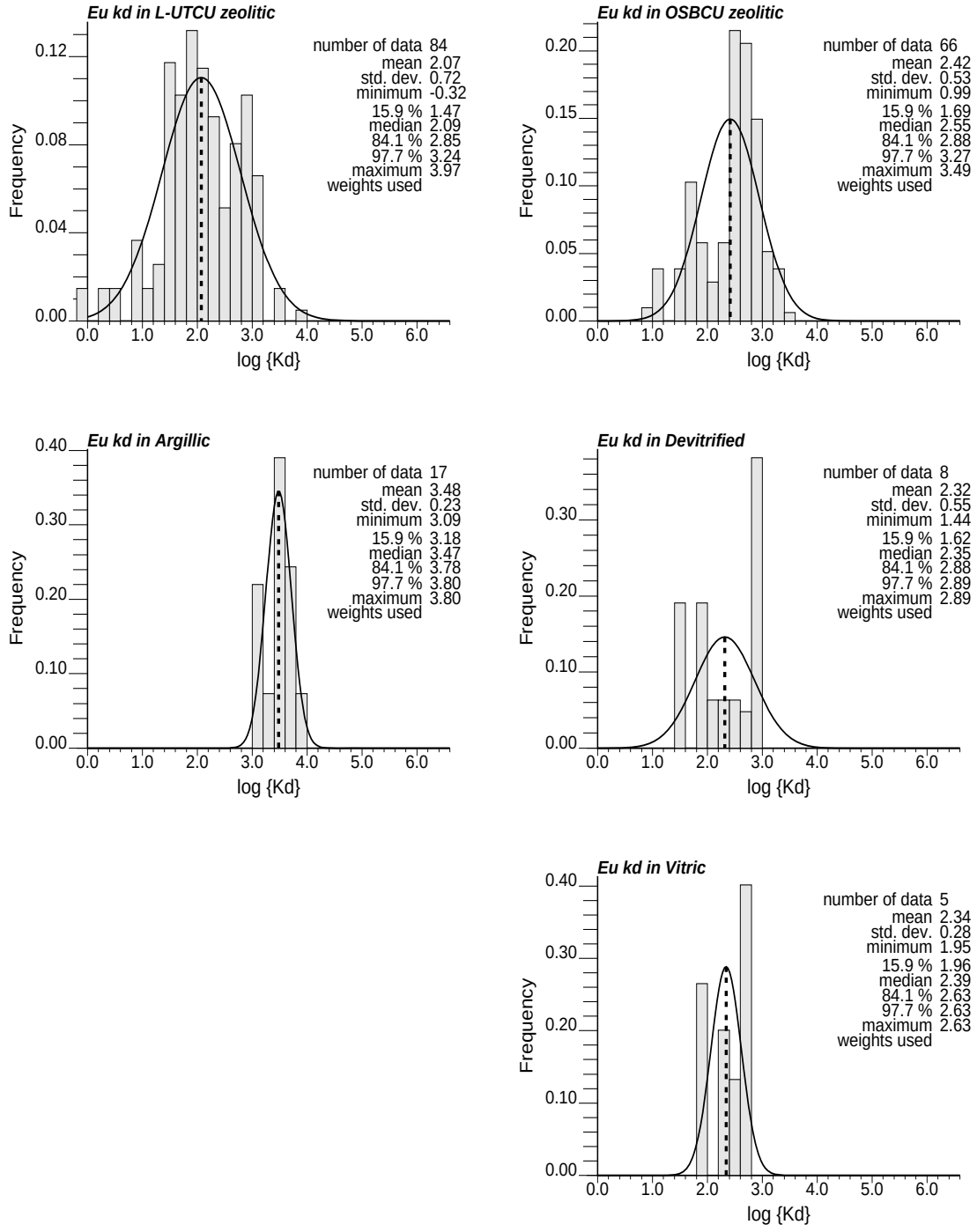

Figure 8-7. $\log\{K_d\}$ distributions for Eu in TCU RMFs as determined from "F" data and application of mean component additivity coefficients.

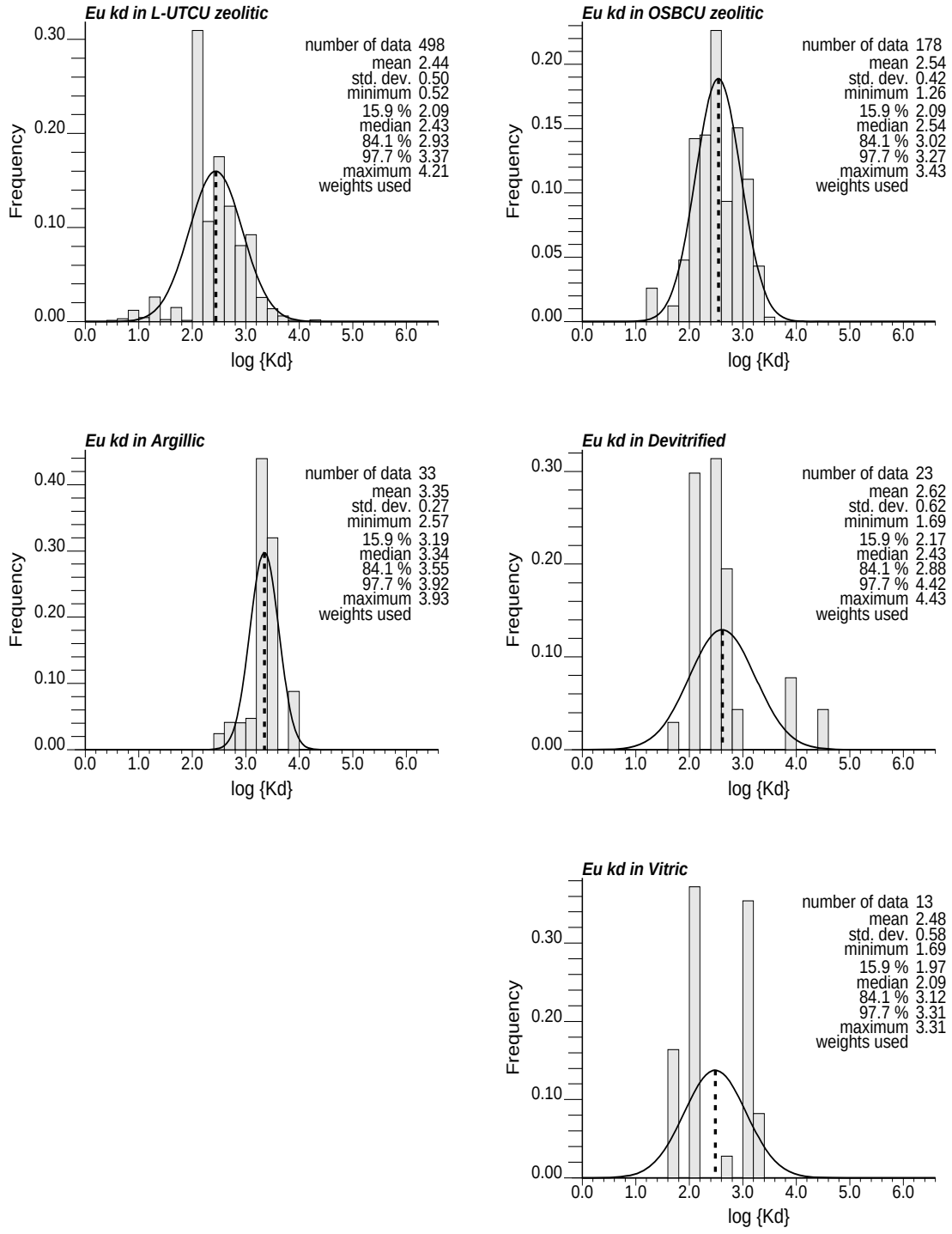

Figure 8-8. $\log\{K_d\}$ distributions for Eu in TCU RMFs as determined from "S" data and application of mean component additivity coefficients.

Table 8-5. Estimates of mean $\log\{K_d\}$ for Eu from "F" and "S" XRD data with standard deviation (σ) of $\log\{K_d\}$ derived from XRD data and attributed to groundwater chemistry variability.

RMF	Mean Eu $\log\{K_d\}$		σ Eu $\log\{K_d\}$ derived from XRD data		Uncertainty in Eu $\log\{K_d\}$ attributed to groundwater chemistry variability
	"F"	"S"	"F"	"S"	
L-UTCU Zeolitic	2.07	2.44	0.72	0.50	0.39 based on smectite coefficient (Table 8-1)
OSBCU Zeolitic	2.42	2.54	0.53	0.42	
Argillic	3.48	3.35	0.23	0.27	
Devitrified	2.32	2.62	0.55	0.62	
Vitric	2.34	2.48	0.28	0.58	

8.3.5 Ni

Ni is a strong sorber to smectite and a weak sorber to calcite and hematite. Figure 8-9 and Figure 8-10 show estimated XRD sample-scale Ni $\log\{K_d\}$ distributions in the RMFs for "F" and "S" data. In the **Argillic** RMF, $\log\{K_d\}$ for Ni is highest and dominated by the smectite frequency distribution. Mean Ni $\log\{K_d\}$ increases with the depth-dependent increase in smectite between **L-UTCU Zeolitic**, **OSBCU Zeolitic**, and **Argillic** RMFs. Ni $\log\{K_d\}$ distributions in the **OSBCU Zeolitic**, **Devitrified**, and **Vitric** RMFs are similar, suggesting a single distribution of K_d could be applied to Ni for the OSBCU HSU. Trends in Ni $\log\{K_d\}$ reflect trends in smectite abundance. Uncertainty in Ni $\log\{K_d\}$ attributed to groundwater chemistry variability is estimated at 0.12 based on uncertainty for the smectite component additivity coefficient (Table 8-1).

Table 8-6 shows estimates of mean $\log\{K_d\}$ for Ni from "F" and "S" XRD data with standard deviation (σ) of $\log\{K_d\}$ derived from XRD data and attributed to groundwater chemistry variability. As with other smectite-dominated sorbers in the TCU, mean $\log\{K_d\}$ and standard deviation for "F" and "S" data are similar for Ni. For radionuclide classes with K_d dominated by smectite, both the "F" and "S" data provide similar characterization quality. Notably, Ni is a far weaker sorber to calcite and hematite compared to other smectite-dominated sorbers such as Am, Eu, Sm, and Pu. Nonetheless, the prevalence of smectite and lack of variation in calcite and hematite content in different RMFs result in similar trends in $\log\{K_d\}$ distribution for Ni, Am, Eu, Sm, and Pu between different RMFs.

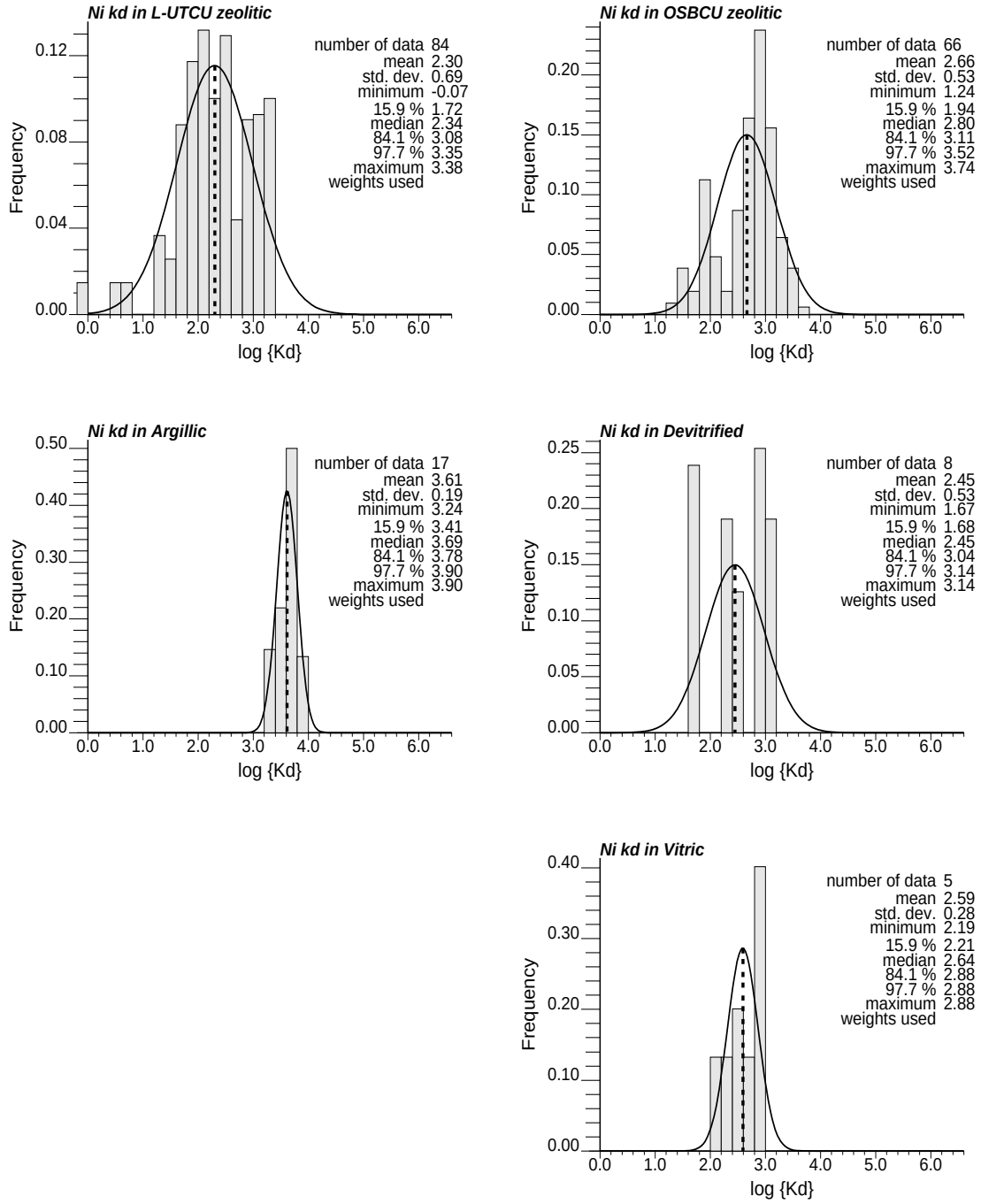

Figure 8-9. $\log\{K_d\}$ distributions for Ni in TCU RMFs as determined from "F" data and application of mean component additivity coefficients.

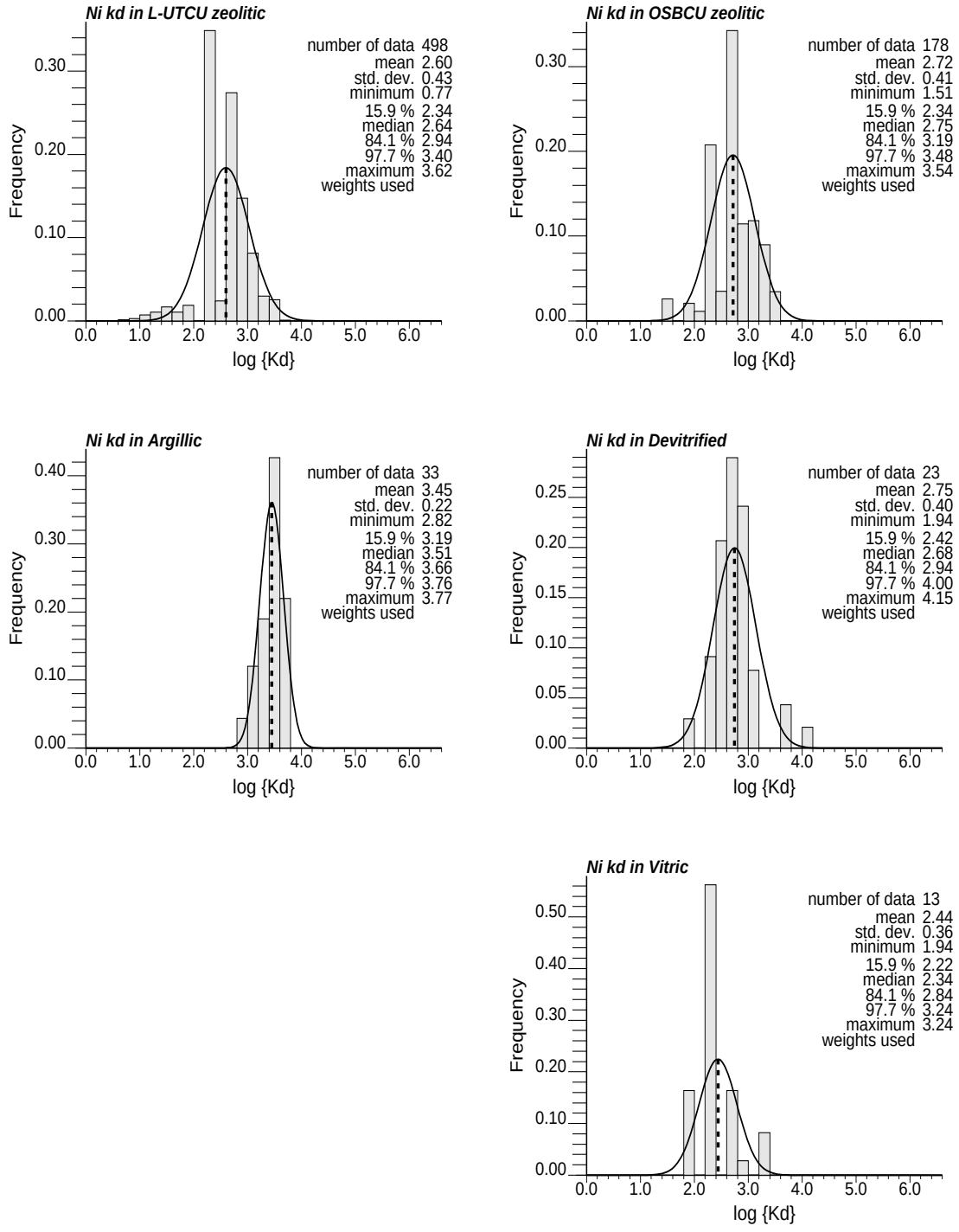

Figure 8-10. $\log\{K_d\}$ distributions for Ni in TCU RMFs as determined from "S" data and application of mean component additivity coefficients.

Table 8-6. Estimates of mean $\log\{K_d\}$ for Ni from "F" and "S" XRD data with standard deviation (σ) of $\log\{K_d\}$ derived from XRD data and attributed to groundwater chemistry variability.

RMF	Mean Ni $\log\{K_d\}$		σ Ni $\log\{K_d\}$ derived from XRD data		Uncertainty in Ni $\log\{K_d\}$ attributed to groundwater chemistry variability
	"F"	"S"	"F"	"S"	
L-UTCU Zeolitic	2.30	2.60	0.69	0.43	0.12 based on smectite coefficient (Table 8-1)
OSBCU Zeolitic	2.66	2.72	0.53	0.41	
Argillic	3.61	3.45	0.19	0.22	
Devitrified	2.45	2.75	0.53	0.40	
Vitric	2.59	2.44	0.28	0.36	

8.3.6 Np

Np is a weak sorber to smectite and a moderate sorber to calcite and hematite. Figure 8-11 and Figure 8-12 show estimated XRD sample-scale Np $\log\{K_d\}$ distributions in the RMFs for "F" and "S" data. In the **Argillic** RMF, $\log\{K_d\}$ for Np is highest and dominated by the smectite frequency distribution. Mean Np $\log\{K_d\}$ increases with the depth-dependent increase in smectite between **L-UTCU Zeolitic**, **OSBCU Zeolitic**, and **Argillic** RMFs. Np $\log\{K_d\}$ distributions in the **OSBCU Zeolitic**, **Devitrified**, and **Vitric** RMFs are similar, suggesting a single distribution of K_d could be applied to Np for the OSBCU HSU. Trends in Np $\log\{K_d\}$ reflect trends in smectite abundance. Uncertainty in Np $\log\{K_d\}$ attributed to groundwater chemistry variability is estimated at 0.24 based on uncertainty for the smectite component additivity coefficient (Table 8-1).

Table 8-7 shows estimates of mean $\log\{K_d\}$ for Np from "F" and "S" XRD data with standard deviation (σ) of $\log\{K_d\}$ derived from XRD data and attributed to groundwater chemistry variability. As with other smectite-dominated sorbers in the TCU, mean $\log\{K_d\}$ and standard deviation for "F" and "S" data are similar for Np. For radionuclide classes with $\log\{K_d\}$ dominated by smectite, both the "F" and "S" data provide similar characterization quality. Notably, Np is a far weaker sorber to smectite compared to calcite and hematite. Nonetheless, smectite dominates trends in Np $\log\{K_d\}$ distribution between different RMFs because calcite and hematite are distributed sporadically at low percentages throughout the TCU.

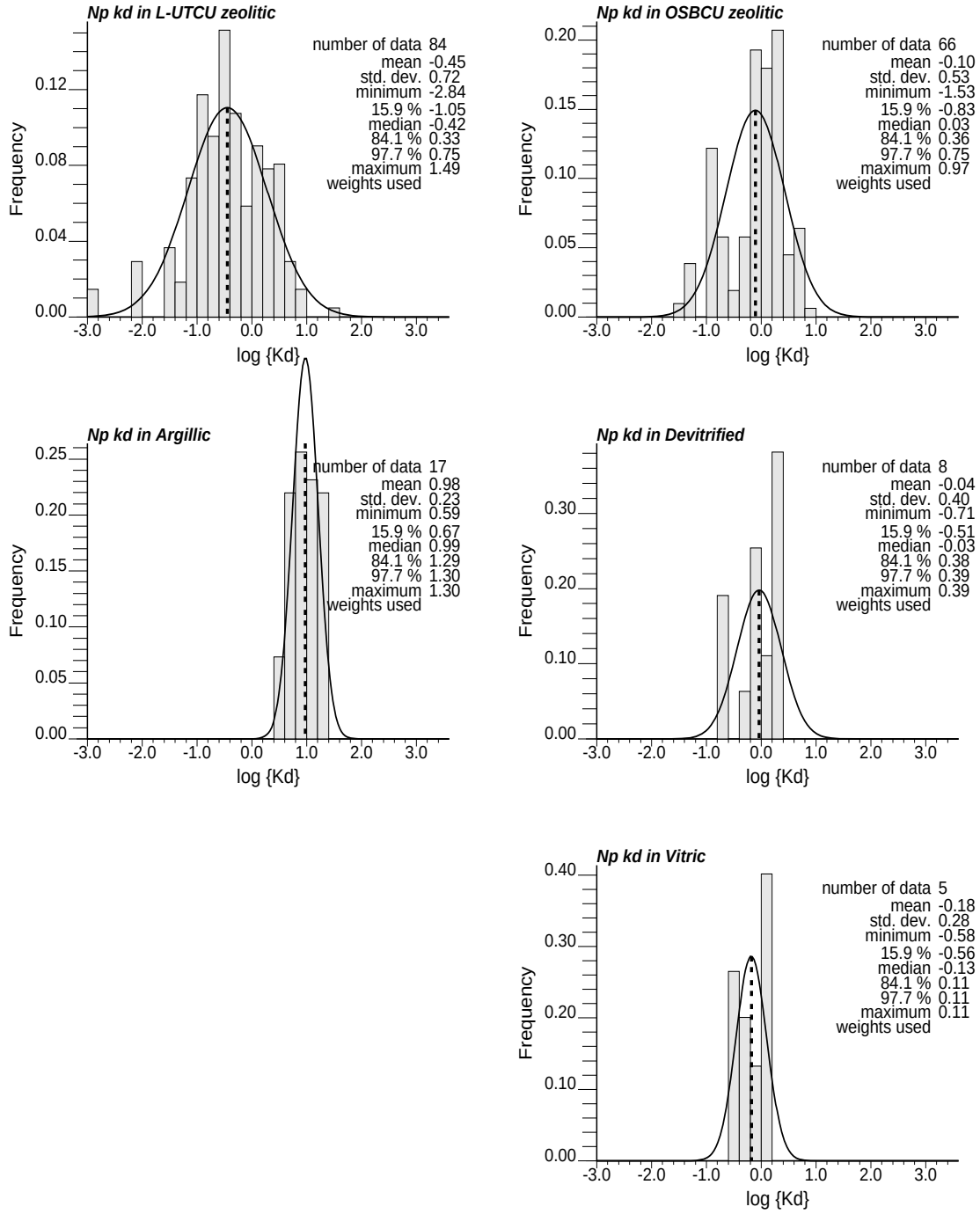

Figure 8-11. $\log\{K_d\}$ distributions for Np in TCU RMFs as determined from "F" data and application of mean component additivity coefficients.

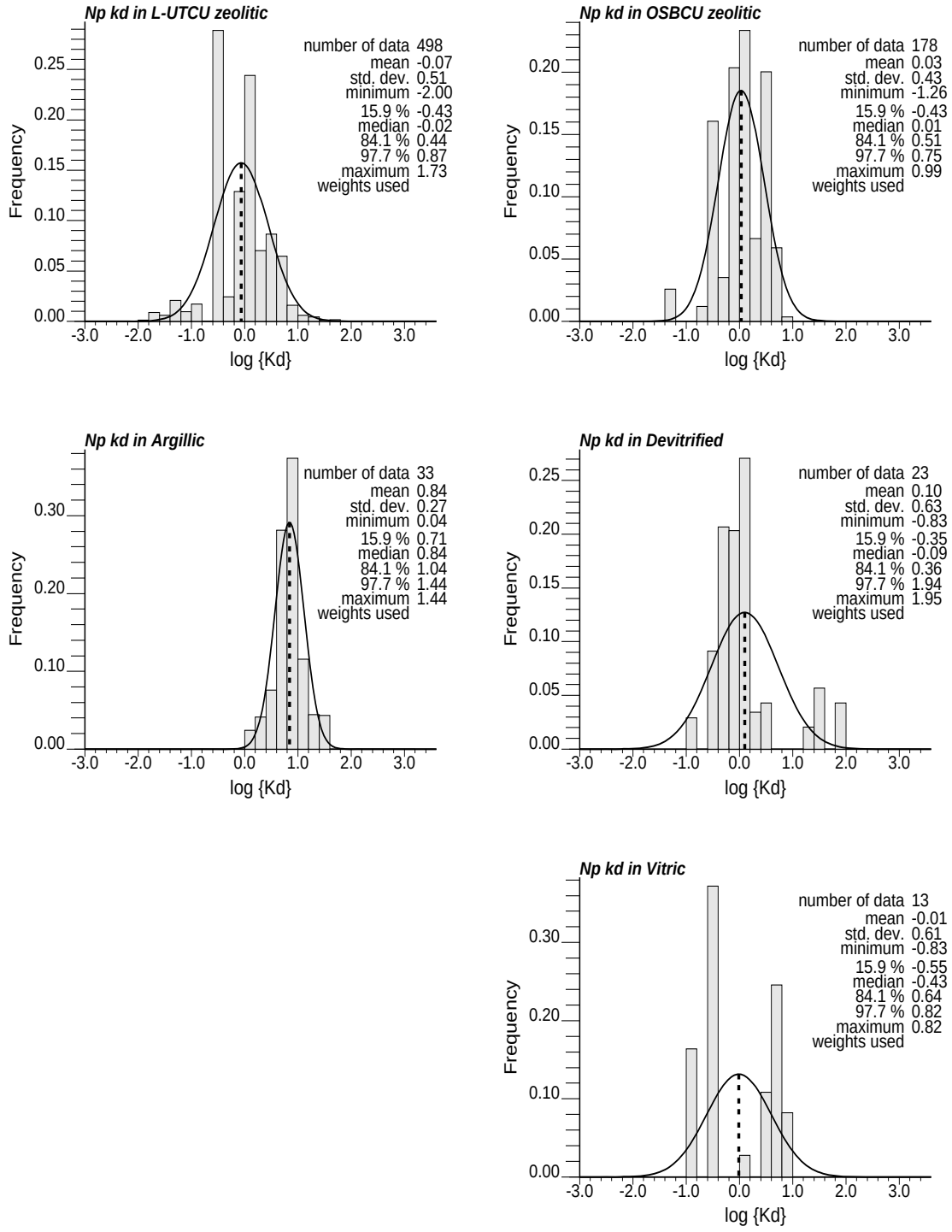

Figure 8-12. $\log\{K_d\}$ distributions for Np in TCU RMFs as determined from "S" data and application of mean component additivity coefficients.

Table 8-7. Estimates of mean $\log\{K_d\}$ for Np from "F" and "S" XRD data with standard deviation (σ) of $\log\{K_d\}$ derived from XRD data and attributed to groundwater chemistry variability.

RMF	Mean Np $\log\{K_d\}$		σ Np $\log\{K_d\}$ derived from XRD data		Uncertainty in Np $\log\{K_d\}$ attributed to groundwater chemistry variability
	"F"	"S"	"F"	"S"	
L-UTCU Zeolitic	–0.45	–0.07	0.72	0.51	0.24 based on smectite coefficient (Table 8-1)
OSBCU Zeolitic	–0.10	0.03	0.53	0.43	
Argillic	0.98	0.84	0.23	0.27	
Devitrified	–0.04	0.10	0.40	0.63	
Vitric	–0.18	–0.01	0.28	0.61	

8.3.7 Pu

Pu is a moderately strong sorber to smectite, calcite, and hematite. Figure 8-13 and Figure 8-14 show estimated XRD sample-scale Pu $\log\{K_d\}$ distributions in the RMFs for "F" and "S" data. In the **Argillic** RMF, $\log\{K_d\}$ for Pu is highest and dominated by the smectite frequency distribution. Mean Pu $\log\{K_d\}$ increases with the depth-dependent increase in smectite between **L-UTCU Zeolitic**, **OSBCU Zeolitic**, and **Argillic** RMFs. Pu $\log\{K_d\}$ distributions in the **OSBCU Zeolitic**, **Devitrified**, and **Vitric** RMFs are similar, suggesting a single distribution of K_d could be applied to Pu for the OSBCU HSU. Trends in Pu $\log\{K_d\}$ reflect trends in smectite abundance. Uncertainty in Pu $\log\{K_d\}$ attributed to groundwater chemistry variability is estimated at 0.40 based on uncertainty for the smectite component additivity coefficient (Table 8-1).

Table 8-8shows estimates of mean $\log\{K_d\}$ for Pu from "F" and "S" XRD data with standard deviation (σ) of $\log\{K_d\}$ derived from XRD data and attributed to groundwater chemistry variability. As with other smectite-dominated sorbers in the TCU, mean $\log\{K_d\}$ and standard deviation are similar for Pu $\log\{K_d\}$ distributions derived from "F" and "S" data. Although Pu is a stronger sorber to calcite and hematite, smectite dominates trends in $\log\{K_d\}$distribution between different RMFs because calcite and hematite are distributed sporadically at low percentages throughout the TCU.

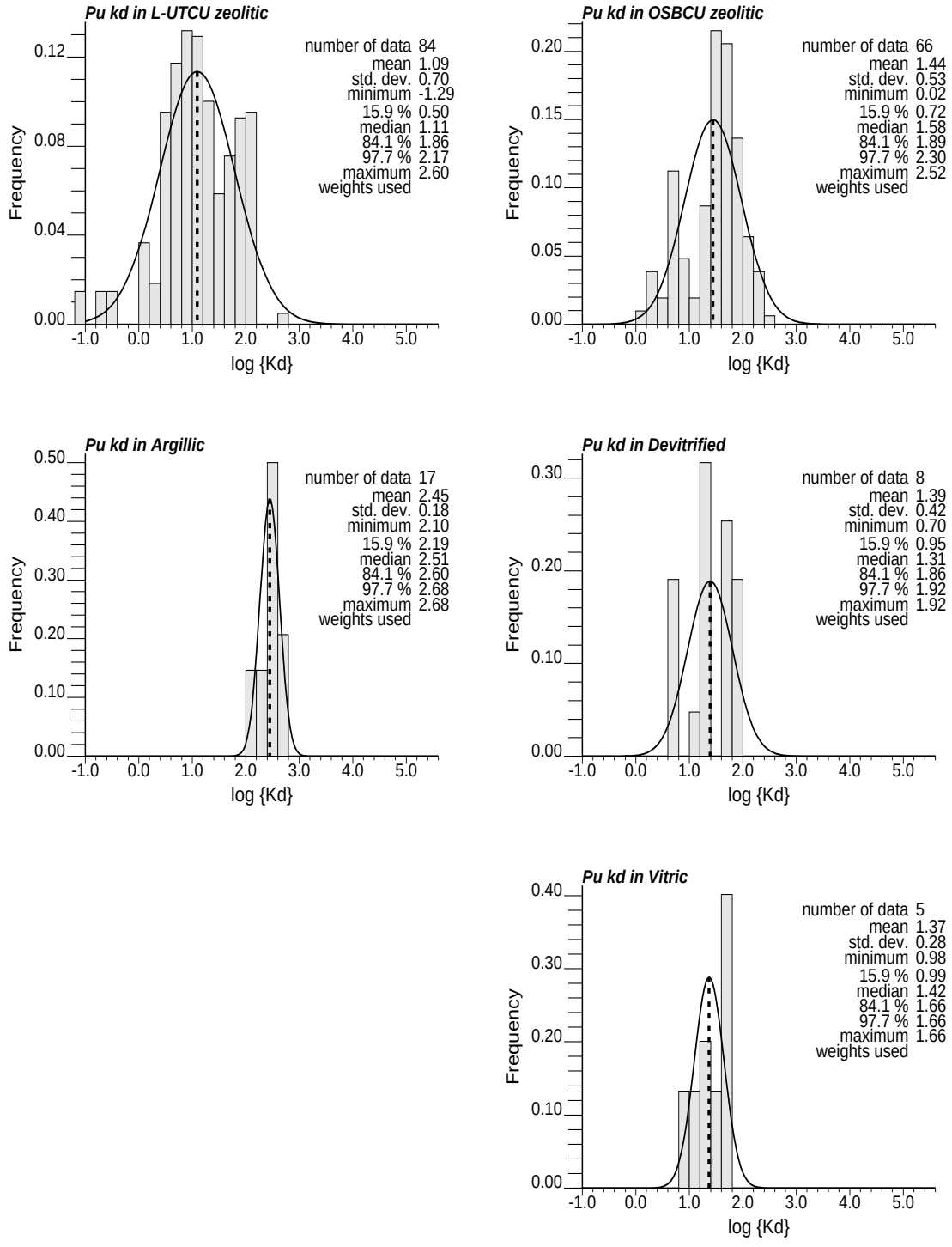

Figure 8-13. $\log\{K_d\}$ distributions for Pu in TCU RMFs as determined from "F" data and application of mean component additivity coefficients.

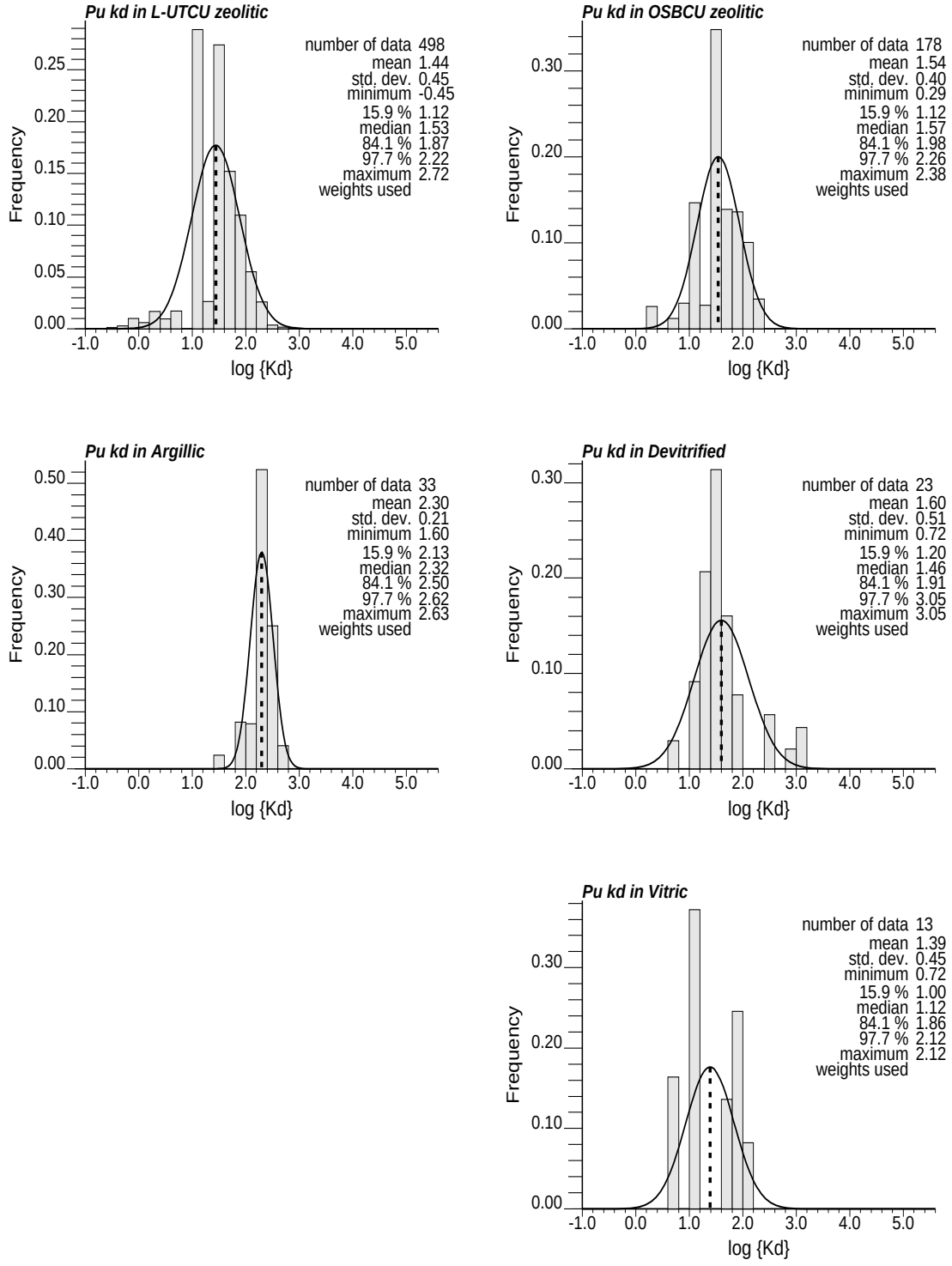

Figure 8-14. $\log\{K_d\}$ distributions for Pu in TCU RMFs as determined from "S" data and application of mean component additivity coefficients.

Table 8-8. Estimates of mean $\log\{K_d\}$ for Pu from "F" and "S" XRD data with standard deviation (σ) of $\log\{K_d\}$ derived from XRD data and attributed to groundwater chemistry variability.

RMF	Mean Pu $\log\{K_d\}$		σ Pu $\log\{K_d\}$ derived from XRD data		Uncertainty in Pu $\log\{K_d\}$ attributed to groundwater chemistry variability
	"F"	"S"	"F"	"S"	
L-UTCU Zeolitic	1.09	1.44	0.70	0.45	0.40 based on smectite coefficient (Table 8-1)
OSBCU Zeolitic	1.44	1.54	0.53	0.40	
Argillic	2.45	2.30	0.18	0.21	
Devitrified	1.39	1.60	0.42	0.51	
Vitric	1.37	1.39	0.28	0.45	

8.3.8 Sm

Sm is a strong sorber to smectite and hematite and a very strong sorber to calcite. Figure 8-15 and Figure 8-16 show estimated XRD sample-scale Sm $\log\{K_d\}$ distributions in the RMFs for "F" and "S" data. In the **Argillic** RMF, $\log\{K_d\}$ for Sm is highest and dominated by the smectite frequency distribution. Mean Sm $\log\{K_d\}$ increases with the depth-dependent increase in smectite between **L-UTCU Zeolitic**, **OSBCU Zeolitic**, and **Argillic** RMFs. Sm $\log\{K_d\}$ distributions in the **OSBCU Zeolitic**, **Devitrified**, and **Vitric** RMFs are similar, suggesting a single distribution of K_d could be applied to Sm for the OSBCU HSU. Trends in Sm $\log\{K_d\}$ reflect trends in smectite abundance and correlate strongly with Eu and Am $\log\{K_d\}$ distribution among the various RMFs. The similarity in sorptive behavior of Sm, Eu, and Am, reflects the similar chemical properties of these trivalent actinides/lanthanides. Uncertainty in Sm $\log\{K_d\}$ attributed to groundwater chemistry variability is estimated at 0.40 based on uncertainty for the smectite component additivity coefficient (Table 8-1).

Table 8-9 shows estimates of mean $\log\{K_d\}$ for Sm from "F" and "S" XRD data with standard deviation (σ) of $\log\{K_d\}$ derived from XRD data and attributed to groundwater chemistry variability. As with other smectite-dominated sorbers in the TCU, mean $\log\{K_d\}$ and standard deviation are similar for Sm $\log\{K_d\}$ distributions derived from "F" and "S" data. Although Sm is a stronger sorber to calcite, smectite dominates trends in $\log\{K_d\}$distribution between different RMFs because calcite is distributed sporadically at relatively low percentages throughout the TCU.

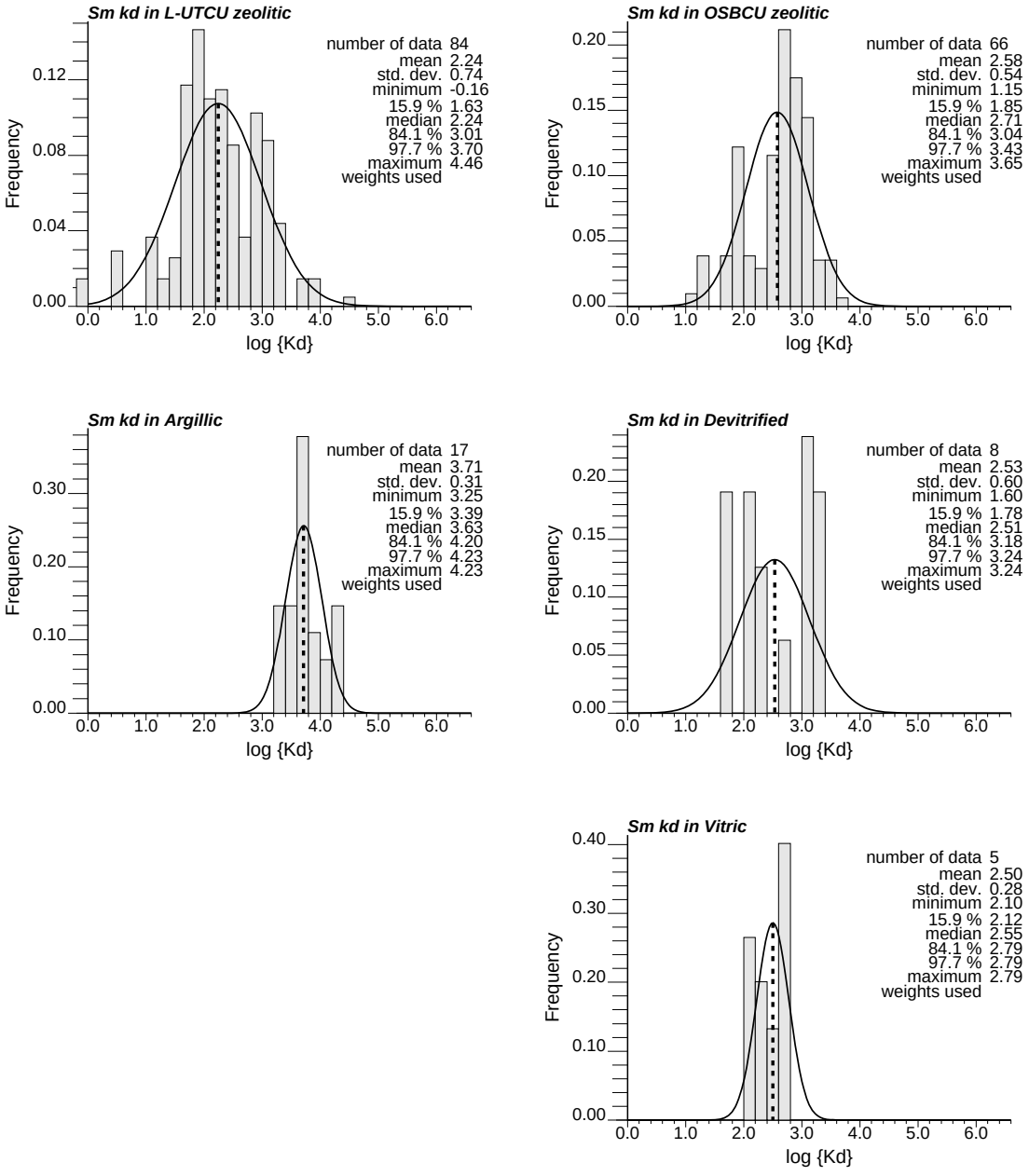

Figure 8-15. $\log\{K_d\}$ distributions for Sm in TCU RMFs as determined from "F" data and application of mean component additivity coefficients.

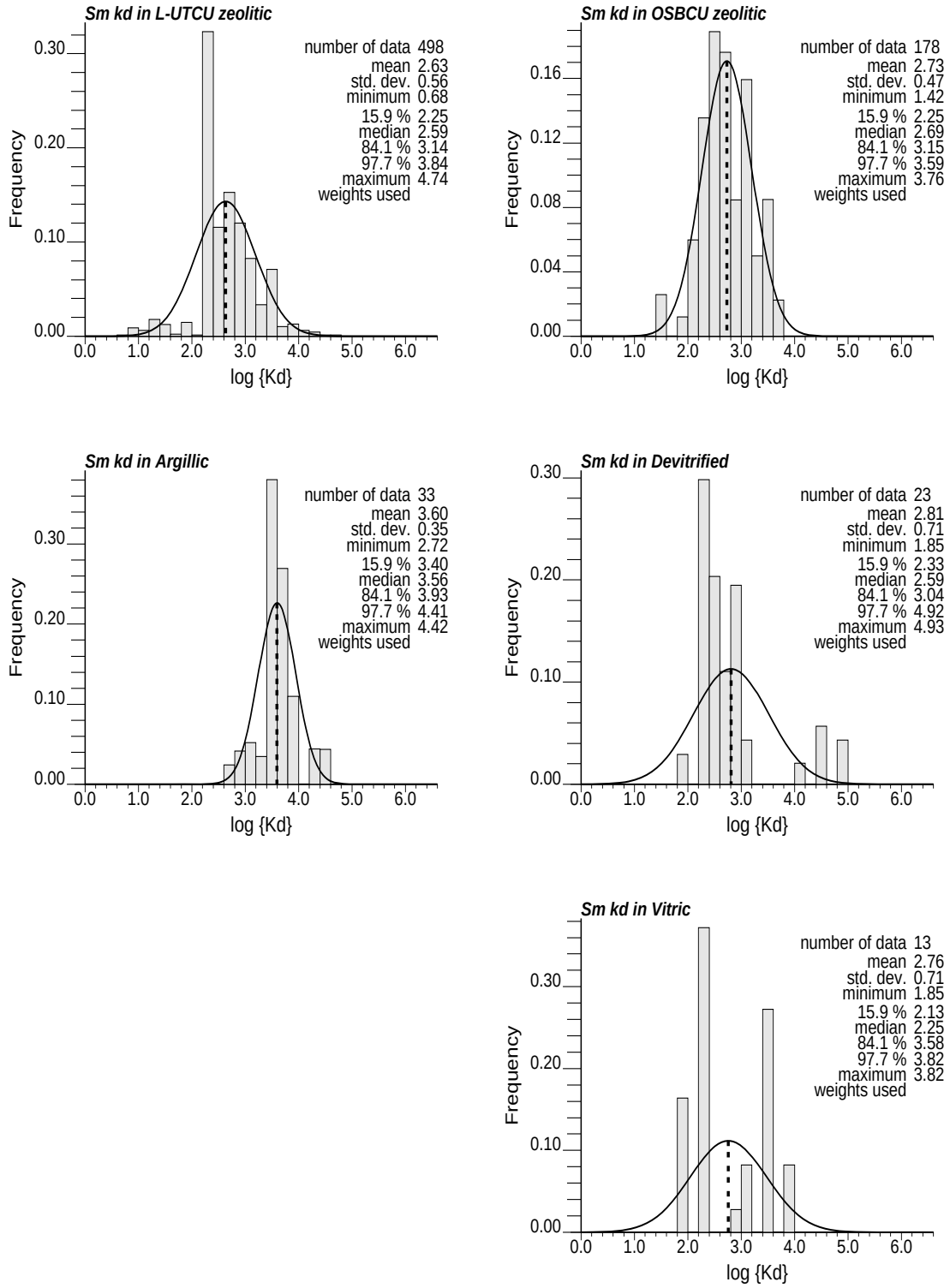

Figure 8-16. $\log\{K_d\}$ distributions for Sm in TCU RMFs as determined from "S" data and application of mean component additivity coefficients.

Table 8-9. Estimates of mean $\log\{K_d\}$ for Sm from "F" and "S" XRD data with standard deviation (σ) of $\log\{K_d\}$ derived from XRD data and attributed to groundwater chemistry variability.

RMF	Mean Sm $\log\{K_d\}$		σ Sm $\log\{K_d\}$ derived from XRD data		Uncertainty in Sm $\log\{K_d\}$ attributed to groundwater chemistry variability
	"F"	"S"	"F"	"S"	
L-UTCU Zeolitic	2.24	2.63	0.74	0.56	0.40 based on smectite coefficient (Table 8-1)
OSBCU Zeolitic	2.58	2.73	0.54	0.47	
Argillic	3.71	3.60	0.31	0.35	
Devitrified	2.53	2.81	0.60	0.71	
Vitric	2.50	2.76	0.28	0.71	

8.3.9 Sr

Like ^{41}Ca, Sr is a strong sorber to smectite, zeolite, and mica. Sr is a very weak sorber to calcite and hematite. Figure 8-17 and Figure 8-18 show estimated XRD sample-scale Sr $\log\{K_d\}$ distributions in the RMFs for "F" and "S" data. In **L-UTCU Zeolitic** and **OSBCU Zeolitic** RMFs, $\log\{K_d\}$ for Sr is highest and dominated by the narrow zeolite frequency distribution. $\log\{K_d\}$ in the **Argillic** RMF is lower than in the zeolitic RMFs, but the $\log\{K_d\}$ distribution remains narrow. $\log\{K_d\}$ for ^{41}Ca in the **Devitrified** and **Vitric** RMFs are lower but more variable. Trends in Sr $\log\{K_d\}$ reflect trends in zeolite abundance. Uncertainty in Sr $\log\{K_d\}$ attributed to groundwater chemistry variability is estimated at 0.38 based on uncertainty for the zeolite component additivity coefficient (Table 8-1).

Table 8-10 shows estimates of mean $\log\{K_d\}$ for Sr from "F" and "S" XRD data with standard deviation (σ) of $\log\{K_d\}$ derived from XRD data and attributed to groundwater chemistry variability. Mean $\log\{K_d\}$ in RMFs are similar for Sr $\log\{K_d\}$ distributions derived from "F" and "S" data except for the **Devitrified** RMF, where the mean Sr $\log\{K_d\}$ is estimated at 1.74 from "F" data and 2.30 from "S" data. This difference can be attributed to lower estimates of zeolite, smectite, and mica percentage from "F" data compared to "S" data in the **Devitrified** RMF. Standard deviations of Sr $\log\{K_d\}$ are greater in the "S" data, except for the **Vitric** RMF which have only 5 "F" data.

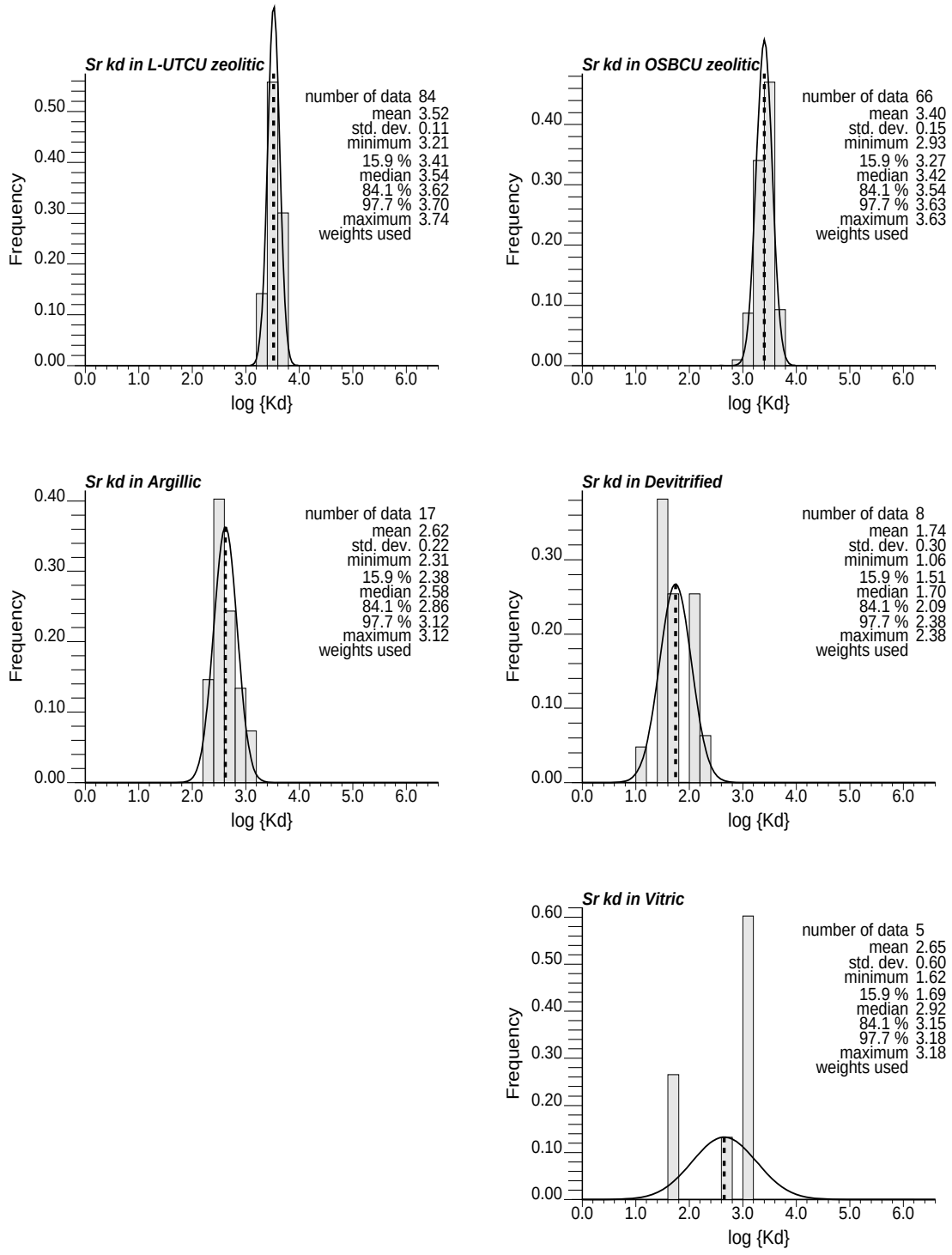

Figure 8-17. $\log\{K_d\}$ distributions for Sr in TCU RMFs as determined from "F" data and application of mean component additivity coefficients.

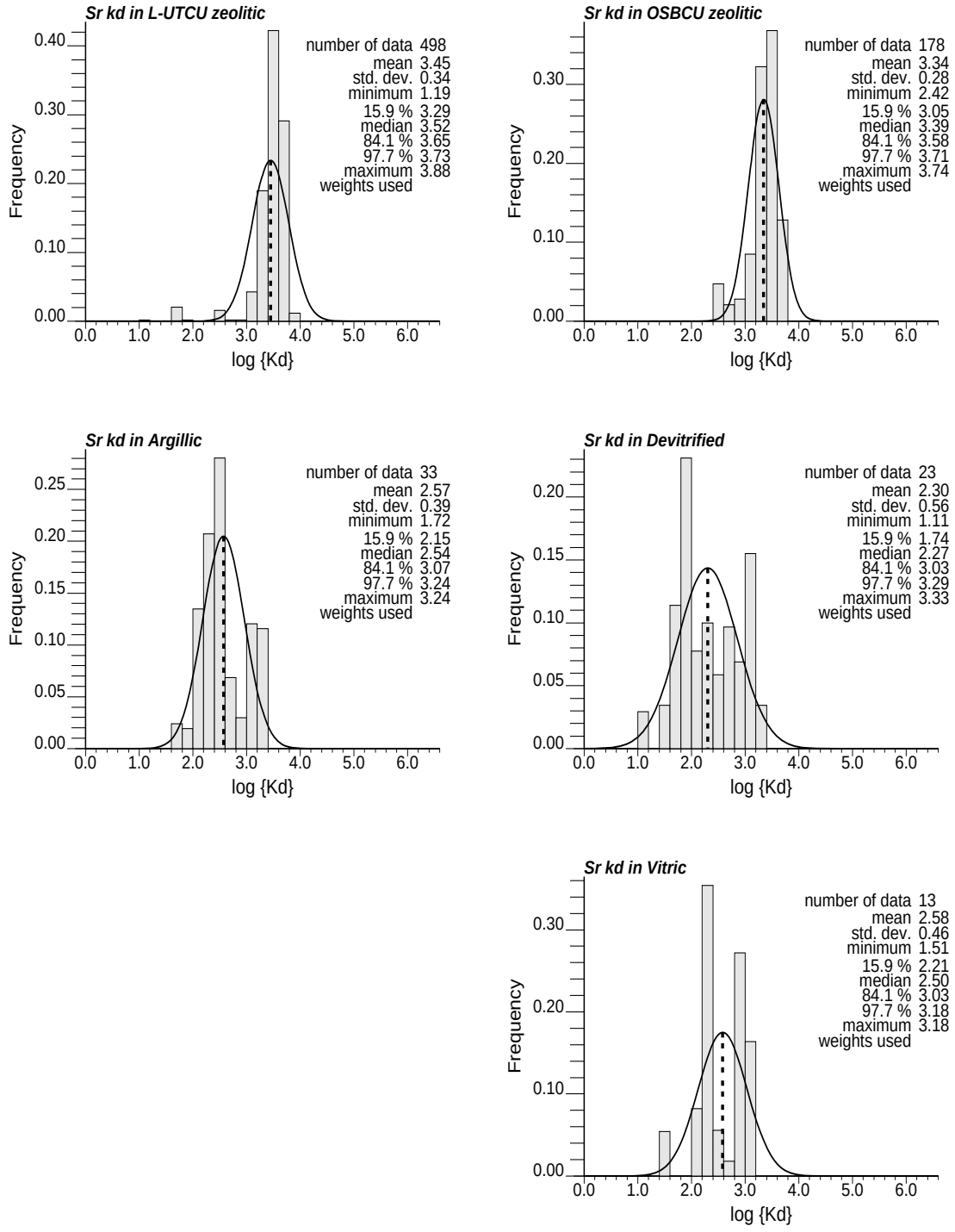

Figure 8-18. $\log\{K_d\}$ distributions for Sr in TCU RMFs as determined from "S" data and application of mean component additivity coefficients.

Table 8-10. Estimates of mean $\log\{K_d\}$ for Sr from "F" and "S" XRD data with standard deviation (σ) of $\log\{K_d\}$ derived from XRD data and attributed to groundwater chemistry variability.

RMF	Mean Sr $\log\{K_d\}$		σ Sr $\log\{K_d\}$ derived from XRD data		Uncertainty in Sr $\log\{K_d\}$ attributed to groundwater chemistry variability
	"F"	"S"	"F"	"S"	
L-UTCU Zeolitic	3.52	3.45	0.11	0.34	0.38 based on zeolite coefficient (Table 8-1)
OSBCU Zeolitic	3.40	3.34	0.15	0.28	
Argillic	2.62	2.57	0.22	0.39	
Devitrified	1.74	2.30	0.30	0.56	
Vitric	2.65	2.58	0.60	0.46	

8.3.10 U

U is a moderately weak sorber to hematite, weak sorber to smectite and a very weak sorber to calcite. Figure 8-19 and Figure 8-20 show estimated XRD sample-scale U $\log\{K_d\}$ distributions in the RMFs for "F" and "S" data. In the **Argillic** RMF, $\log\{K_d\}$ for U is highest and dominated by the smectite frequency distribution. Mean U $\log\{K_d\}$ increases with the depth-dependent increase in smectite between **L-UTCU Zeolitic**, **OSBCU Zeolitic**, and **Argillic** RMFs. U $\log\{K_d\}$ distributions in the **OSBCU Zeolitic**, **Devitrified**, and **Vitric** RMFs are similar, suggesting a single distribution of K_d could be applied to U for the OSBCU HSU. Trends in U $\log\{K_d\}$ reflect trends in smectite abundance. Uncertainty in U $\log\{K_d\}$ attributed to groundwater chemistry variability is estimated at 0.70 based on uncertainty for the smectite component additivity coefficient (Table 8-1).

Table 8-11 shows estimates of mean $\log\{K_d\}$ for U from "F" and "S" XRD data with standard deviation (σ) of $\log\{K_d\}$ derived from XRD data and attributed to groundwater chemistry variability. As with other smectite-dominated sorbers in the TCU, mean $\log\{K_d\}$ and standard deviation for "F" and "S" data are similar for U. For radionuclide classes with $\log\{K_d\}$ dominated by smectite, both the "F" and "S" data provide similar characterization quality. Notably, U is a weaker sorber to smectite compared to hematite. Nonetheless, smectite dominates trends in U $\log\{K_d\}$ distribution between different RMFs because hematite is distributed sporadically at low percentages throughout the TCU.

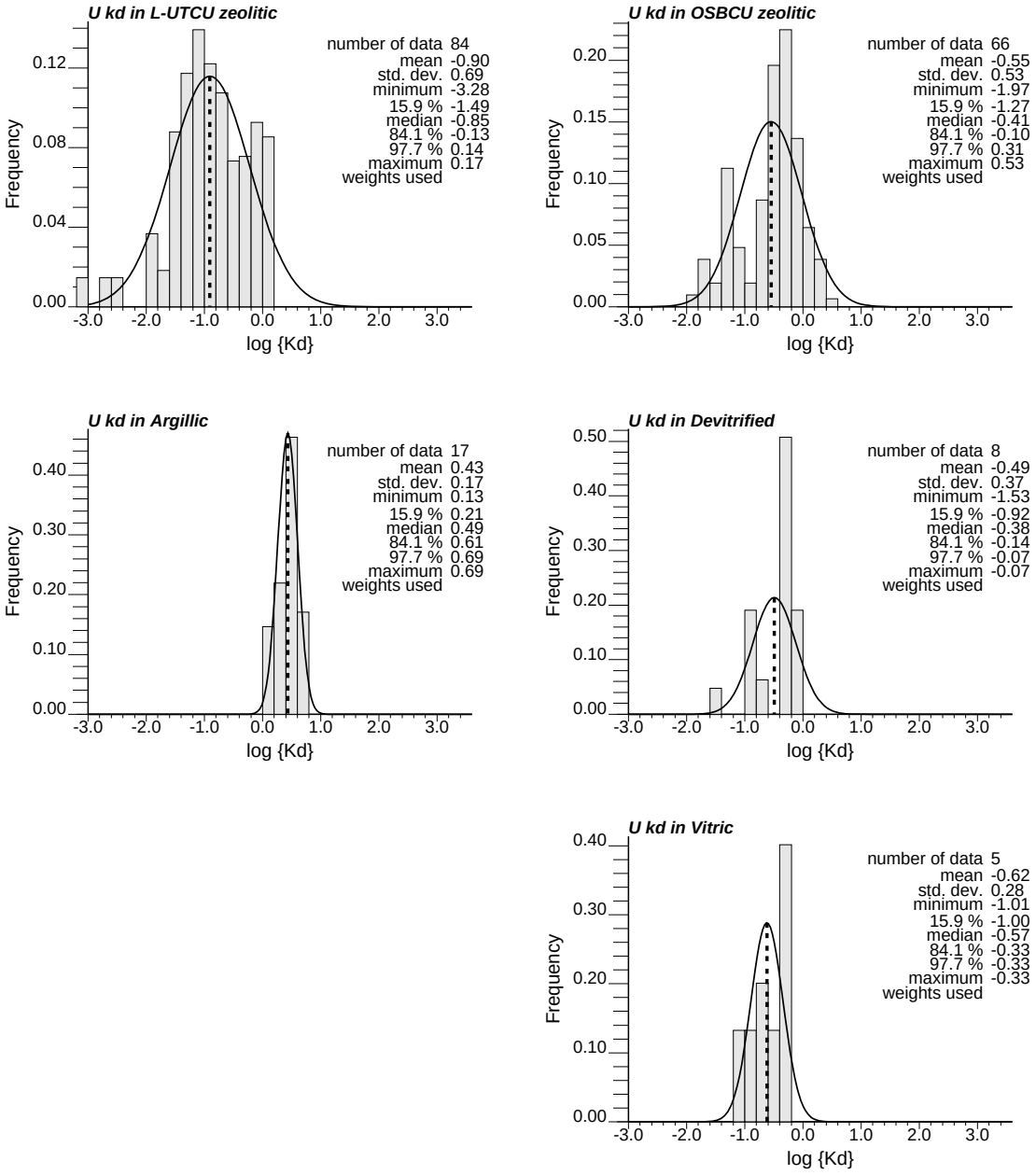

Figure 8-19. $\log\{K_d\}$ distributions for U in TCU RMFs as determined from "F" data and application of mean component additivity coefficients.

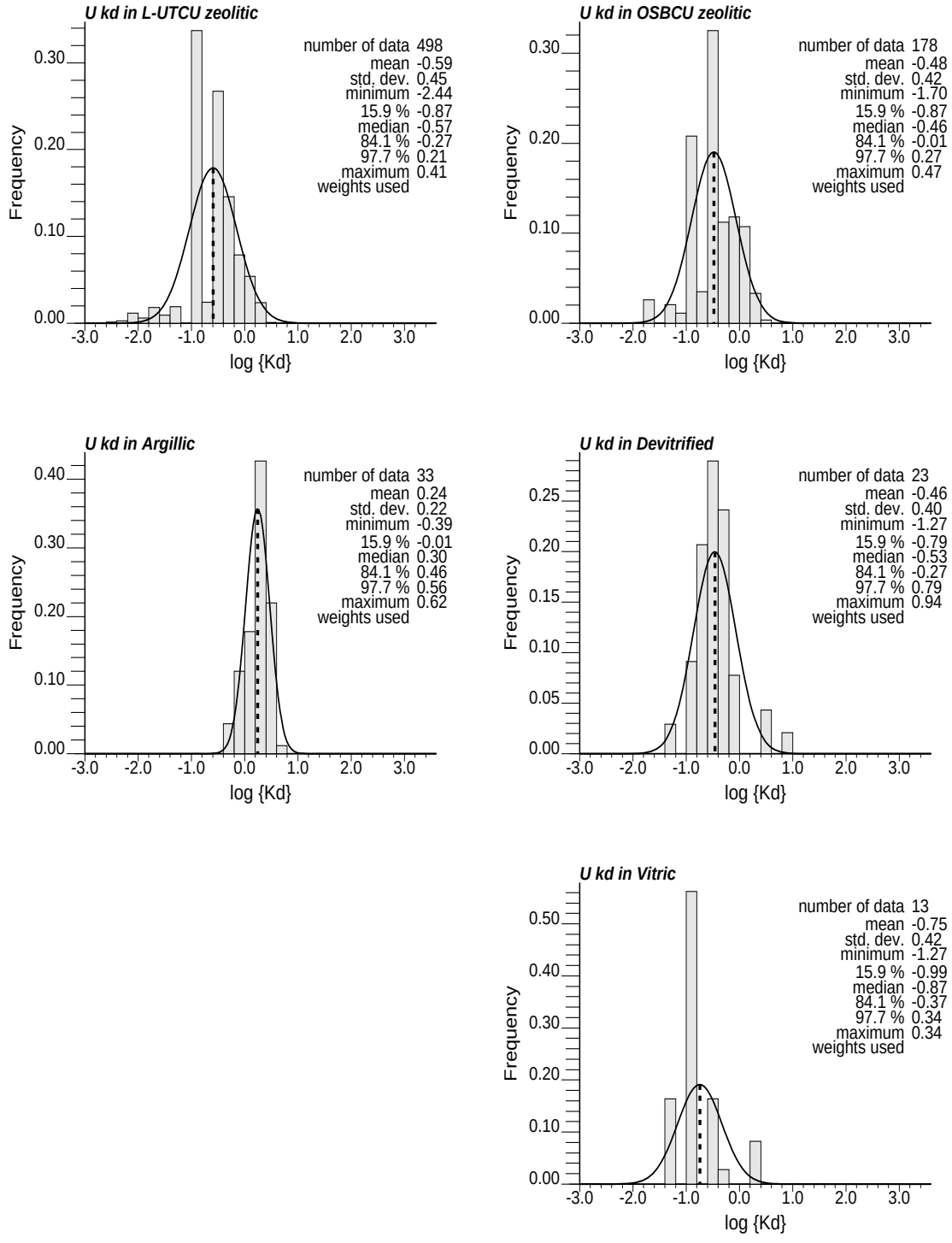

Figure 8-20. $\log\{K_d\}$ distributions for U in TCU RMFs as determined from "S" data and application of mean component additivity coefficients.

Table 8-11. Estimates of mean $\log\{K_d\}$ for U from "F" and "S" XRD data with standard deviation (σ) of $\log\{K_d\}$ derived from XRD data and attributed to groundwater chemistry variability.

RMF	Mean U $\log\{K_d\}$		σ U $\log\{K_d\}$ derived from XRD data		Uncertainty in U $\log\{K_d\}$ attributed to groundwater chemistry variability
	"F"	"S"	"F"	"S"	
L-UTCU Zeolitic	–0.90	–0.59	0.69	0.45	0.70 based on smectite coefficient (Table 8-1)
OSBCU Zeolitic	–0.55	–0.48	0.53	0.42	
Argillic	0.43	0.24	0.17	0.22	
Devitrified	–0.49	–0.46	0.37	0.40	
Vitric	–0.62	–0.75	0.28	0.42	

9. Variogram Analysis of K_d Spatial Variation

The variogram is a geostatistical measure of spatial variability defined as

$$\gamma(\mathbf{h}) = \frac{1}{2} E\left[v(\mathbf{x}+\mathbf{h}) - v(\mathbf{x})\right]^2$$

where $v(\mathbf{x})$ is a random variable at location **x**, and **h** is a lag (separation) vector. Variogram values typically range from near zero at small lags to data variance or greater at large lags beyond the range of correlation. The term "range" used in variogram analysis corresponds to the range of correlation. In practice, variogram values are typically averaged from lag vectors spaced $\mathbf{h} \pm \frac{1}{2}\Delta\mathbf{h}$ apart, where $\Delta\mathbf{h}$ is a finite lag vector spacing. In practice, a large number of data pairs spaced $\Delta\mathbf{h}$ apart are needed to obtain good estimates of variogram values.

One advantage of using the variogram over covariance to measure spatial correlation is that the variogram "filters out" the local mean, which can vary as a result of spatial trends in the data. "Intrinsic stationarity" is a fundamental assumption to variogram analysis with the following properties:

- Spatial variability of the random variable throughout the region being analyzed is characterized by a single variogram.
- While the mean may vary in the region, the variogram is constant.

A variogram-based geostatistical model assumes the pattern of spatial variability consists of a gradually varying mean superposed by a stochastic component characterized by the variogram.

In this chapter, $\log\{K_d\}$ is treated as a random variable for variogram analysis. Mineral percentage data are combined with the mean component additivity exponential coefficients (Section 8.1) to produce estimated $\log\{K_d\}$ values for each radionuclide class at XRD sample location. Variogram analyses are performed in vertical and lateral directions to evaluate vertical and lateral spatial continuity in K_d, which could result from stratification or other forms of spatial continuity in mineral distributions. Variograms are constructed in each RMF assuming intrinsic stationarity within RMFs, with the expectation that spatial statistics could be different in different RMFs.

9.1 Vertical Direction

Variograms for $\log\{K_d\}$ will be analyzed in the vertical direction because typical subsurface data obtained from boreholes offer better characterization of vertical (or stratigraphic upward) spatial variability. Borehole samples are aligned along linear transects of the "stratigraphic upward" direction.

9.1.1 L-UTCU RMF

Figure 9-1 shows calculated vertical direction variograms $\log\{K_d\}$ in the **L-UTCU Zeolitic** RMF using "F" data only and a 1.524-m (5 ft) vertical lag spacing or larger based on a minimum of 5 pairs per lag. These vertical $\log\{K_d\}$ variograms in the **L-UTCU Zeolitic** RMF show several patterns that will be evident in other vertical variograms using the highest quality "F" XRD data:

- None of the $\log\{K_d\}$ variograms show evidence of vertical spatial continuity. Variogram values at the smallest non-zero lag (~8 m) are similar in magnitude to variogram values at larger lags. If spatial continuity exists, the range of vertical spatial correlation is less than 8 m.

- Some radionuclide classes share similar $\log\{K_d\}$ variogram structures. ^{41}Ca and Sr $\log\{K_d\}$variograms are nearly identical, with small magnitudes, because zeolite dominates K_d for ^{41}Ca and Sr, and variability of zeolite log{percentage} is small in the **L-UTCU Zeolitic** RMF. Overall variogram structures for the smectite-dominated sorbers Ni, Sm, Eu, Am, Np, Pu, and U are similar, with differences attributable to differences between component additivity coefficients for calcite and smectite. Radionuclides with similar *differences* [in brackets] between component additivity coefficients for calcite and smectite (see Table 8-1) have similar variograms at all lags, for example: (1) Ni and U [-3.08, -3.00], (2) Eu and Np [0.89, 0.93], and (3) Am and Pu [0.34, 0.37].

- Variogram structure for Cs is intermediate between the zeolite-dominated sorbers, ^{41}Ca and Sr, and the smectite dominated sorbers, Ni, Sm, Eu, Am, Np, Pu, and U, because Cs is also a very strong sorber to mica, which is nearly ubiquitous in the **L-UTCU Zeolitic** RMF.

- Variogram values for the smectite-dominated sorbers differ most at lags of 8, 12, and 27 m, suggesting that calcite occurs in the data at spacings of about 8, 12, and 27 m apart.

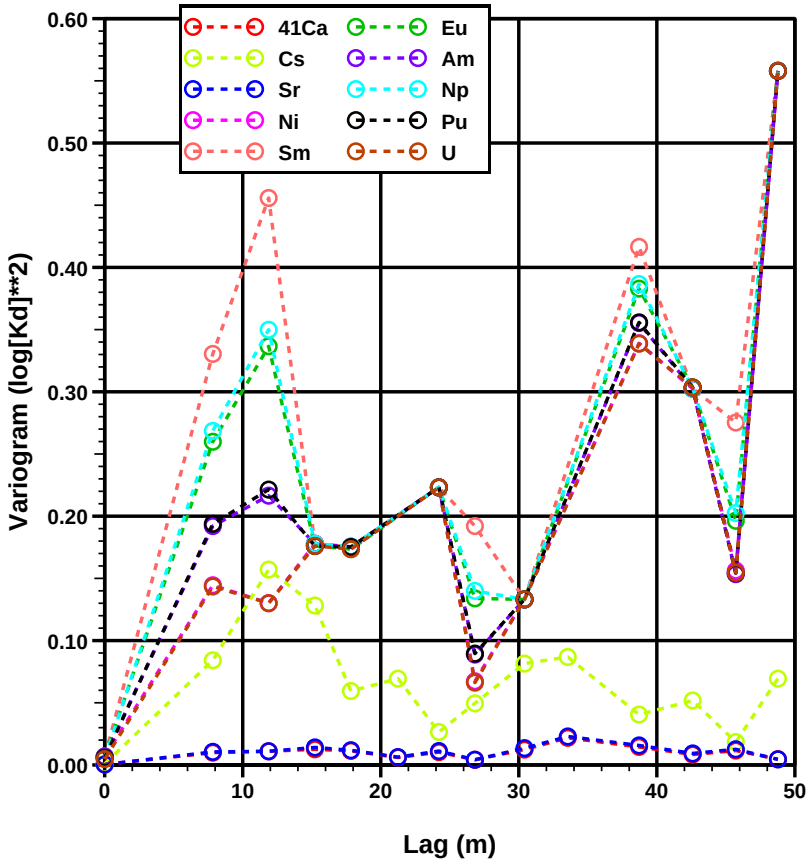

Figure 9-1. Vertical direction variogram analysis of K_d in L-UTCU RMF using "F" data with minimum 1.524-m lag spacing and minimum of 5 pairs per lag.

Figure 9-2 shows calculated vertical direction variograms $\log\{K_d\}$ in the **L-UTCU Zeolitic** RMF using "S" data only and a 1.524-m (5 ft) vertical lag spacing or larger based on a minimum of 5 pairs per lag. With the numerous "S" data, more lag spacings achieve the minimum 5 pairs per lag. Differences in the "S" data variograms compared to "F" data variograms in Figure 9-1 are explained as follows:

- The "S" data variograms show an apparent cyclicity at alternating lag intervals. This is caused by more variability in 1.524 m (5 ft)-spaced data. Subsequently, variogram values at lags of 15 ft, 25 ft, 35 ft, etc. show higher magnitudes than variogram values at lags of 10 ft, 20 ft, 30 ft, etc. Data with 5 ft spacing, far less common than data with 10 ft spacing, may have been preferentially obtained in zones with lower electrical resistivity and, thus, higher smectite or zeolite content. Notably, the Cs variogram, dominated by mica, does not show much cyclicity.

- The "S" data variogram values at 3.28 m (10 ft) spacing suggest spatial continuity within a range of about 10 m. However, this apparent spatial continuity is an artifact of the "S" data. Variograms constructed from "S" data mineral percentages are subject to spurious spatial correlation caused by translation of mineral percentage ranges into fixed mineral percentage values that persist over spatial intervals.

- As for the "F" data variograms, variograms are nearly identical for the smectite sorbers that have similar differences between smectite and calcite component additivity methodology exponential coefficients.

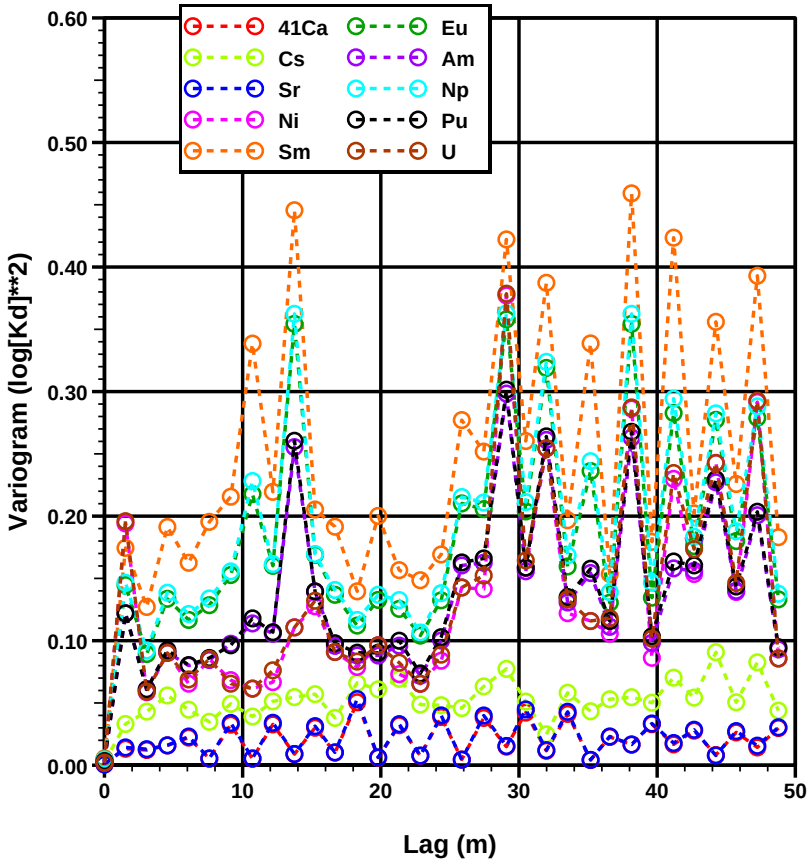

Figure 9-2. Vertical direction variogram analysis of K_d in L-UTCU RMF using "S" data with 1.524-m lag spacing and minimum of 5 pairs per lag.

Figure 9-3 shows calculated vertical direction variograms $\log\{K_d\}$ in the **L-UTCU Zeolitic** RMF using "S" data only and 3.048 m (10 ft) vertical lag spacing or larger based on a minimum of 100 pairs per lag. This larger variogram lag spacing and increased lag

pair minimum results in more averaging of variogram values. The resulting variograms indicate existence of vertical spatial continuity in $\log\{K_d\}$, with a range of correlation of about 10 m. However, this apparent vertical spatial correlation remains spurious because of translation of "S" data into fixed mineral percentage values that persist over spatial intervals.

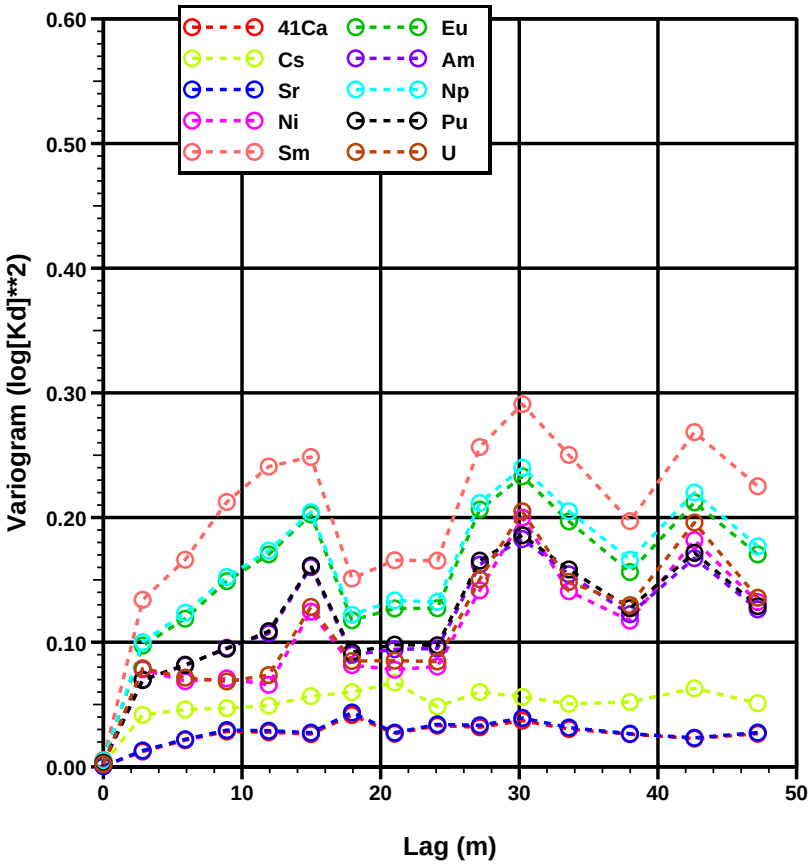

Figure 9-3. Vertical direction variogram analysis of K_d in L-UTCU RMF using "S" data with minimum 3.048 m lag spacing and minimum of 100 pairs per lag.

9.1.2 OSBCU RMF

Figure 9-4 shows calculated vertical direction variograms of $\log\{K_d\}$ in the **OSBCU Zeolitic** RMF using "F" data only and a 1.524-m (5 ft) vertical lag spacing or larger based on a minimum of 5 pairs per lag. The "F" data $\log\{K_d\}$ variograms for the **OSBCU Zeolitic** RMF show wider lag spacing than for the **L-UTCU Zeolitic** RMF because of less data (only 66 "F" data compared to 178 "S" data in **OSBCU Zeolitic** and

84 "F" data compared to 498 "S" in **L-UTCU Zeolitic**). Variogram patterns in **OSBCU Zeolitic** are similar to those in the **L-UTCU Zeolitic**:

- None of the $\log\{K_d\}$ variograms show evidence of vertical spatial continuity. Variogram values at the smallest non-zero lag (~ 8 m) are similar in magnitude to variogram values at larger lags. If spatial continuity exists, the range of vertical spatial correlation is less than 8 m.

- Similarities in $\log\{K_d\}$ in variogram structures for different radionuclide classes are even greater for **OSBCU Zeolitic** than **L-UTCU Zeolitic** because of less calcite. As in the **L-UTCU Zeolitic** RMF, ^{41}Ca and Sr $\log\{K_d\}$ has nearly identical small-magnitude variogram values because zeolite dominates K_d for ^{41}Ca and Sr, and variability of zeolite percentage is small in the **L-UTCU Zeolitic** RMF. Overall variogram structures for the smectite-dominated sorbers Ni, Sm, Eu, Am, Np, Pu, and U are nearly identical because of lack of calcite and hematite in the **OSBCU Zeolitic** RMF.

- Cs variogram structure is strongly influenced by mica followed by zeolite and smectite. Cs variogram magnitudes are smaller in the **OSBCU Zeolitic** compared to the **L-UTCU Zeolitic** because mica percentage variability is less in the **OSBCU Zeolitic**, particularly as a result of a lesser proportion of zero values.

- Variogram values for the smectite-dominated sorbers only differ at a lags of 35 m, suggesting that some calcite occurs in the **OSBCU Zeolitic** data about 35 m apart.

Figure 9-5 shows calculated vertical direction variograms $\log\{K_d\}$ in the **OSBCU Zeolitic** RMF using "S" data only and a 1.524-m (5 ft) vertical lag spacing or larger based on a minimum of 5 pairs per lag. With the numerous "S" data, more lag spacings achieve a minimum 5 pairs per lag. Differences in vertical variograms for "S" data in **OSBCU Zeolitic** compared to "F" data in Figure 9-4 and "S" data for **L-UTCU Zeolitic** in Figure 9-2 are explained as follows:

- As for **L-UTCU Zeolitic** in Figure 9-2, the "S" data K_d variograms show an apparent cyclicity at alternating lag intervals caused by more variability in 1.524 m (5 ft)-spaced data.

- The **OSBCU Zeolitic** K_d vertical variograms show smaller magnitudes for smectite and mica sorbers compared to **L-UTCU Zeolitic**. Variogram magnitudes are smaller for the smectite sorbers (Ni, Sm, Eu, Am, Np, Pu, and U) because the "S" data indicate proportionately less non-zero values for calcite in **OSBCU Zeolitic** compared to **L-UTCU Zeolitic** (Figure 7-9). Mica

percentage variability is less in the **OSBCU Zeolitic**, hence the Cs K_d variogram magnitudes are less than in the **L-UTCU Zeolitic**.

- The "S" data K_d variogram values for smectite-sorbers (Ni, Sm, Eu, Am, Np, Pu, and U) suggest spatial continuity within a range of about 25 m. However, as for the **L-UTCU Zeolitic**, variograms constructed from "S" data mineral percentages are subject to spurious spatial correlation caused by translation of mineral percentage ranges given by the semi-quantitative method into fixed mineral percentage values that persist over spatial intervals.

- Figure 7-8 that very few "F" data in the **OSBCU Zeolitic** have non-zero calcite percentages. Consequently, "F" data variograms in **OSBCU Zeolitic** (Figure 9-4) are nearly identical for the smectite sorbers Ni, Sm, Eu, Am, Np, Pu, and U.

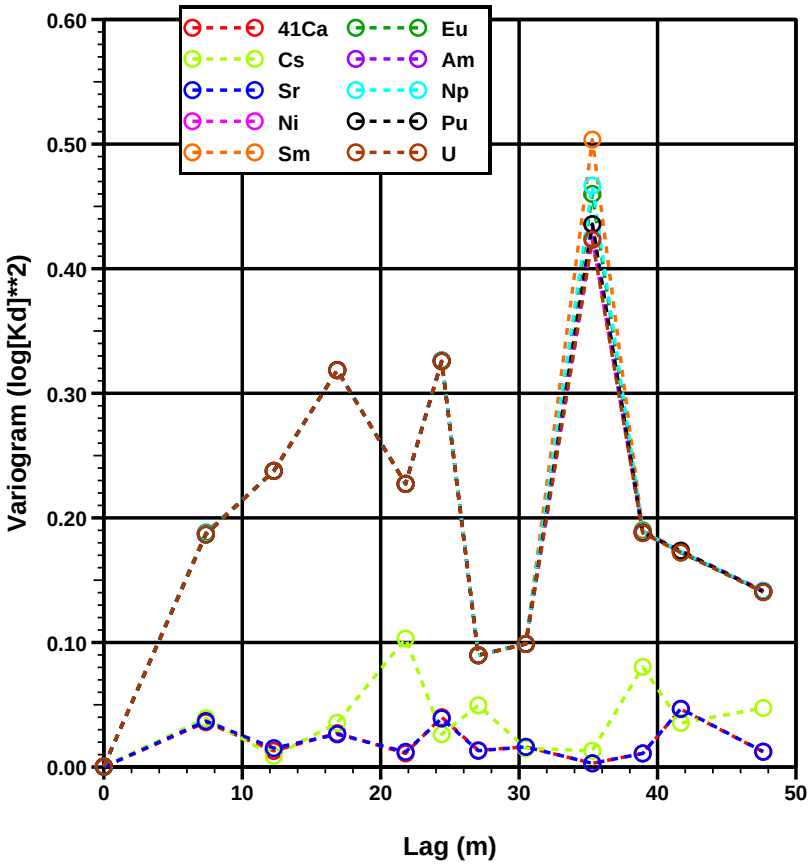

Figure 9-4. Vertical direction variogram analysis of K_d in OSBCU RMF using "F" data with minimum 1.524 m lag spacing and minimum of 5 pairs per lag.

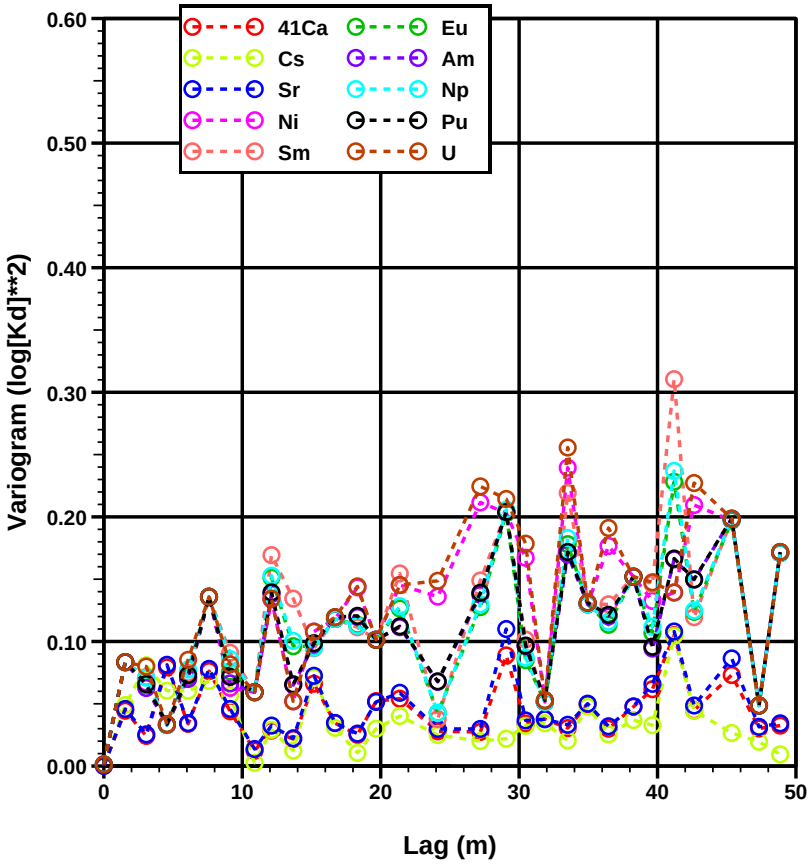

Figure 9-5. Vertical direction variogram analysis of K_d in OSBCU RMF using "S" data with minimum 1.524 m lag spacing and minimum of 5 pairs per lag.

Figure 9-6 shows calculated vertical direction variograms $\log\{K_d\}$ in the **OSBCU Zeolitic** RMF using "S" data only and 3.048 m (10 ft) vertical lag spacing or larger based on a minimum of 100 pairs per lag. This larger variogram lag spacing and increased lag pair minimum results in more averaging of variogram values. Less variogram lags result from less "S" data (179) in the **OSBCU Zeolitic** compared to the **L-UTCU Zeolitic** (519). The resulting variograms indicate existence of vertical spatial continuity in $\log\{K_d\}$, with a range of correlation of about 10–25 m. However, as for the **L-UTCU Zeolitic** "S" data, this apparent vertical spatial correlation remains spurious because of translation of "S" data into fixed mineral percentage values that persist over spatial intervals.

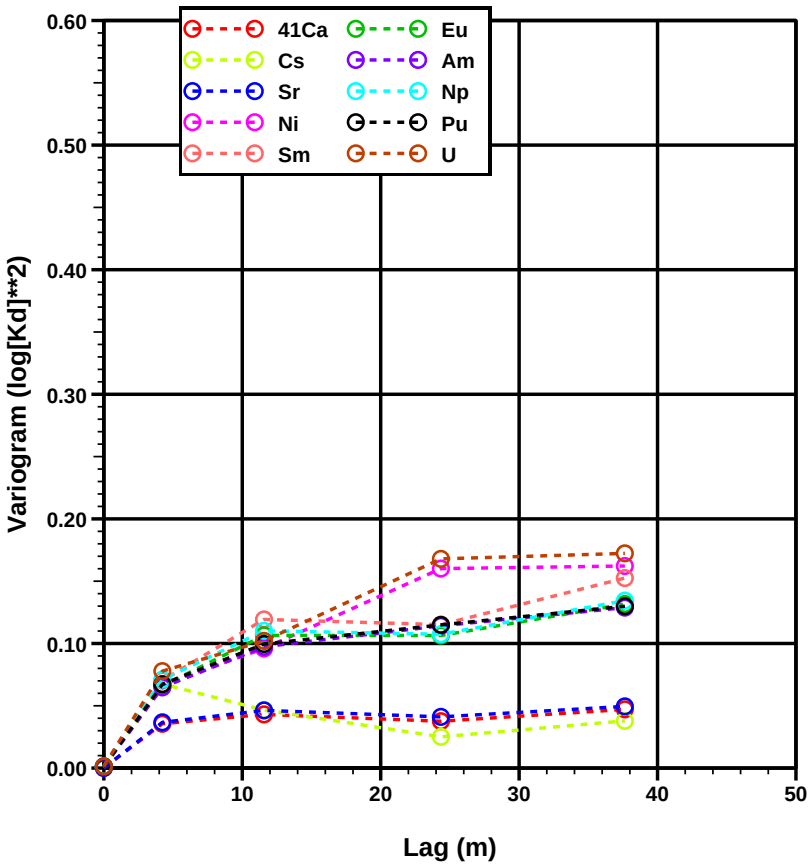

Figure 9-6. Vertical direction variogram analysis of K_d in OSBCU RMF using "S" data with variable lag spacing and minimum of 100 pairs per lag.

9.1.3 Argillic RMF

Figure 9-7 shows calculated vertical direction variograms $\log\{K_d\}$ in the **Argillic** RMF using "F" data only and a 1.524-m (5 ft) vertical lag spacing or larger based on a minimum of 5 pairs per lag. Because only 17 "F" data are located within the **Argillic** RMF, the variogram has only three lags. For lack of data, differences in the "F" data K_d vertical variograms in the **Argillic** RMF are not interpretable.

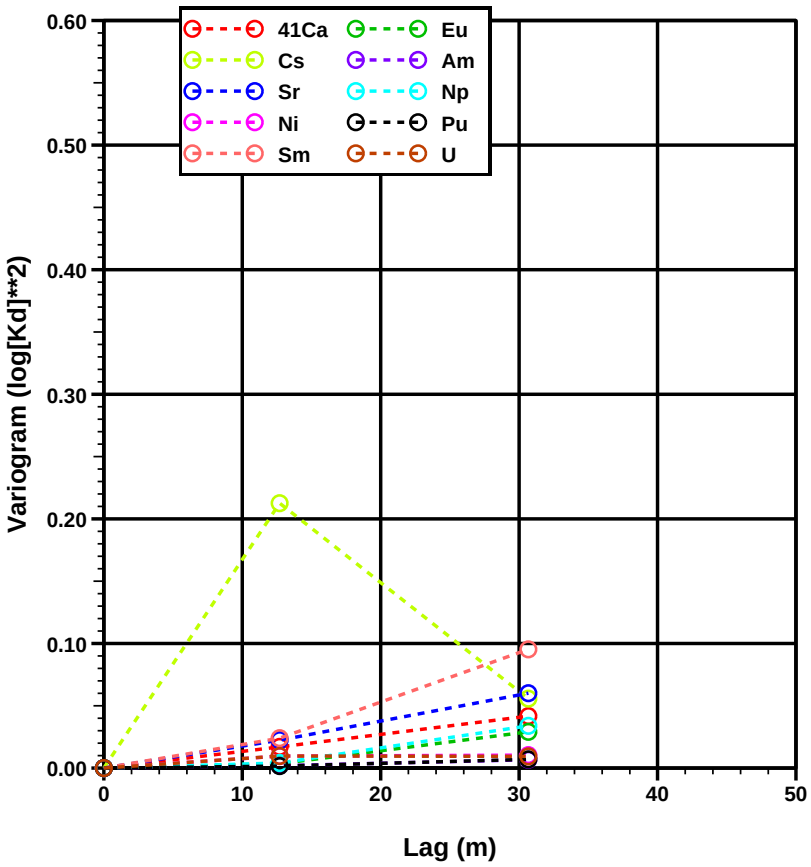

Figure 9-7. Vertical direction variogram analysis of K_d in Argillic RMF using "F" data with 1.524 m lag spacing and minimum of 5 pairs per lag.

The **Argillic** RMF has more "S" data (33) than "F" data (17). Figure 9-8shows calculated vertical direction variograms $\log\{K_d\}$ in the **Argillic** RMF using "S" data only and a 1.524-m (5 ft) vertical lag spacing or larger based on a minimum of 5 pairs per lag. Although the **Argillic** RMF is high in smectite, and all radionuclide classes sorb to smectite, the $\log\{K_d\}$variograms show differences:

- Of the smectite-dominated sorbers (Am, Eu, Ni, Np, Pu, Sm, U), variograms for Sm, Eu, and Np have higher variogram values with similar shapes attributed to greater dependence on calcite. The higher variogram values are proportionate to the differences between the calcite and smectite component additivity coefficients (+1.26 for Sm, +0.89 for Eu, and +0.93 for Np).

- Variograms for ^{41}Ca and Sr are very similar because smectite, zeolite, and mica exponential coefficients are similar.

- As in the **L-UTCU Zeolitic** and **OSBCU Zeolitic** RMFs, variograms are similar for radionuclide classes with similar differences in component additivity coefficients (Am and Pu; U and Ni).
- The variogram values for Cs have small magnitude because component additivity coefficients depend strongly on smectite and mica (and not calcite), which are ubiquitous with relatively small variability in the **Argillic** RMF.
- As in previous interpretations of "S" data variograms, indications of spatial continuity are spurious.

The number of "S" data was not sufficient to calculate vertical $\log\{K_d\}$ variograms at high numbers of pairs per lag (e.g., 100) as was done for the **L-UTCU Zeolitic** and **OSBCU Zeolitic** RMFs

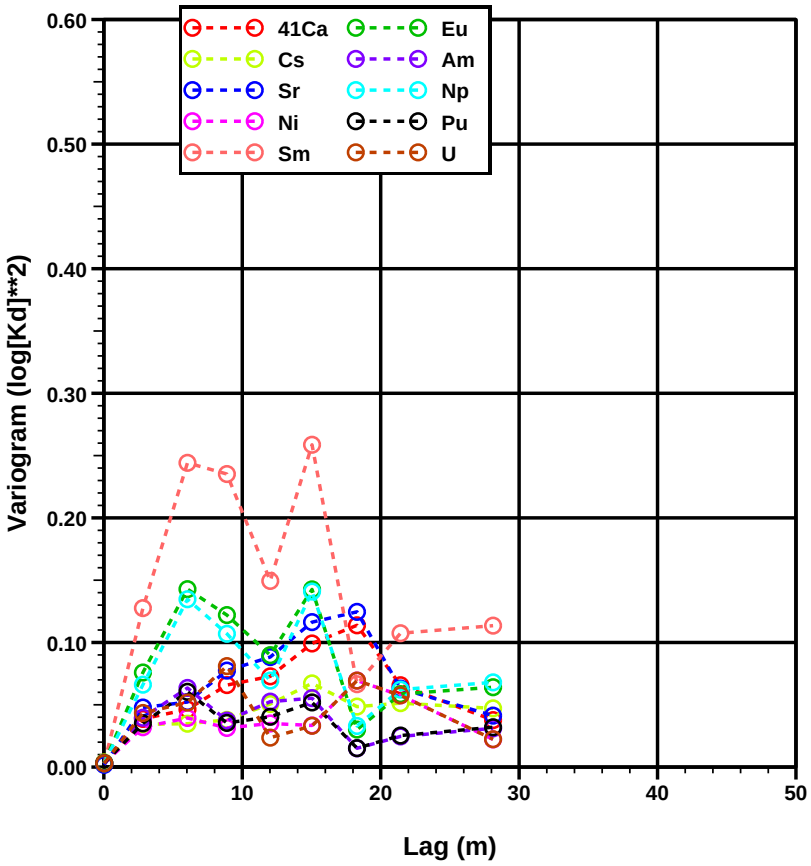

Figure 9-8. Vertical direction variogram analysis of K_d in argillic RMF using "S" data with 1.524-m lag spacing and minimum of 5 pairs per lag.

9.1.4 Devitrified RMF

As for the **Argillic** RMF, variogram analysis of $\log\{K_d\}$ is problematic in the **Devitrified** RMF mainly because of few "F" data (8) and "S" data (23). Figure 9-9 shows calculated vertical direction variograms $\log\{K_d\}$ in the **Devitrified** RMF using "S" data only and a vertical lag spacing based on a minimum of 5 pairs per lag. Although the number of data are limiting, the following interpretations can be made:

- Magnitudes of variogram values are high in the **Devitrified** RMF. Although reactive mineral abundance is low in the Devitrified RMF, variability of reactive mineral abundance is larger on a logarithmic scale relative to the **L-UTCU Zeolitic**, **OSBCU Zeolitic** and **Argillic** RMFs.

- As in the **L-UTCU Zeolitic** and **OSBCU Zeolitic**, and **Argillic** RMFs, variograms are similar for radionuclide classes with similar patterns component additivity coefficients, such as similar smectite, zeolite, and mica coefficients (^{41}Ca and Sr) and for similar calcite and smectite differences (Np and Eu; Am and Pu; U and Ni).

- Mica causes relatively more variability in $\log\{K_d\}$ for Cs because zeolite and smectite are much less abundant in the **Devitrified** RMF than in the **L-UTCU Zeolitic** and **OSBCU Zeolitic**, and **Argillic** RMF.

- As for other RMFs, spatial continuity indicated in "S" data $\log\{K_d\}$ variograms is spurious.

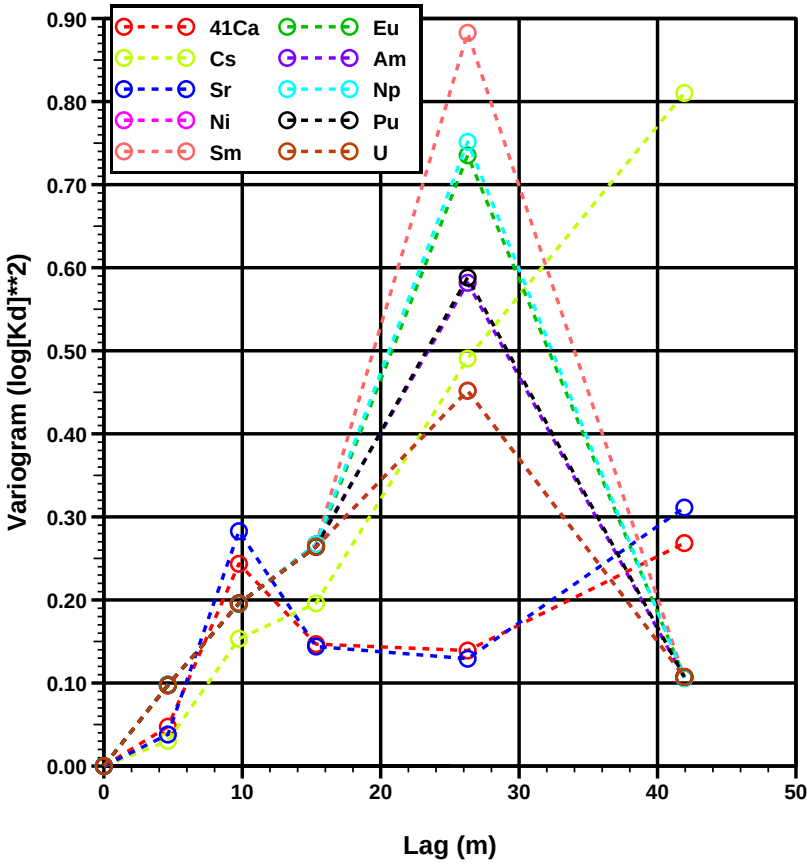

Figure 9-9. Vertical direction variogram analysis of K_d in Devitrified RMF using "S" data, 1.524-m lag spacing, and minimum of 5 pairs per lag.

9.1.5 Vitric RMF

As for the **Argillic** and **Devitrified** RMFs, variogram analysis of $\log\{K_d\}$ in the **Vitric** RMF is problematic mainly because of few "F" data (5) and "S" data (13). Figure 9-10 shows calculated vertical direction variograms $\log\{K_d\}$ in the **Vitric** RMF using "S" data only and a vertical lag spacing based on a minimum of 5 pairs per lag.

- Similar to the **Devitrified** RMF, magnitudes of variogram values are high in the **Vitric** RMF. Although reactive mineral abundance is low in the **Vitric** RMF, variability of reactive mineral abundance is larger on a logarithmic scale relative to the **L-UTCU Zeolitic**, **OSBCU Zeolitic** and **Argillic** RMFs.

- As in the **L-UTCU Zeolitic** and **OSBCU Zeolitic**, **Argillic**, and **Devitrified** RMFs, variograms are similar for radionuclide classes with similar patterns in the component additivity coefficients, such as for similar smectite, zeolite, and mica

coefficients (^{41}Ca and Sr) and for similar calcite and smectite differences (Np and Eu; Am and Pu; U and Ni).

- As in the **Devitrified** RMF, mica causes relatively more variability in $\log\{K_d\}$ for Cs because zeolite and smectite are much less abundant in the **Vitric** RMF than in the **L-UTCU Zeolitic** and **OSBCU Zeolitic**, and **Argillic** RMF.
- As for other RMFs, spatial continuity indicated in the "S" data $\log\{K_d\}$ variograms is spurious.

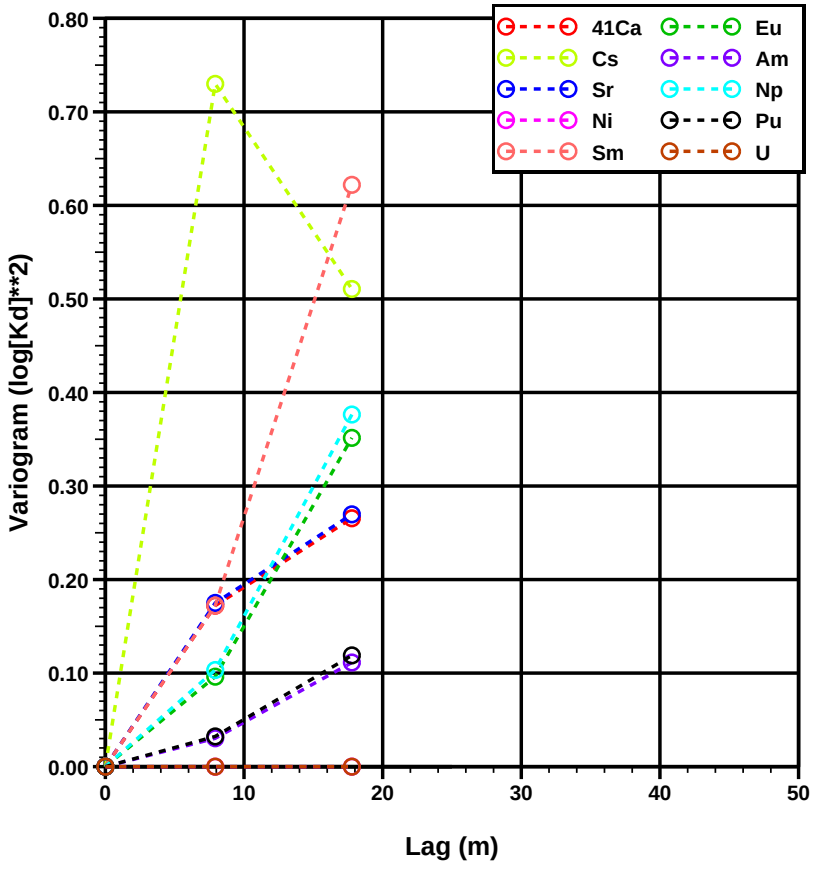

Figure 9-10. Vertical direction variogram analysis of K_d in Vitric RMF using "S" data, 1.524-m lag spacing, and minimum of 5 pairs per lag.

9.2 Lateral Direction

Ideally with enough data at locations spaced within the range of correlation, variogram analysis can be applied in all directions. As mentioned previously, borehole data usually provide, at best, adequate data to evaluate spatial variability in the vertical direction. Evaluation of spatial variability in non-vertical directions is also hampered by inevitable variations in dip angle and vertical displacements, such as faults or errors in vertical control. Lateral variogram data at small lags is most reliable if vertical control of data locations is not a large source of error.

This section constructs variograms of $\log\{K_d\}$ in the "lateral" direction under the highly simplified assumptions that bedding is horizontal and patterns of spatial variability are isotropic in the horizontal plane. Assuming horizontal bedding and isotropy, the variogram for the "lateral" direction can be composed of variogram values with the same range of horizontal distances independent of azimuth. Ideally, the data pairs should be obtained along the true bedding plane. Despite these simplifications, km-scale lateral variations in $\log\{K_d\}$, if accompanied by vertical correlation scales on the order of 50 m or more, should be detectable. However, as we have seen in vertical direction $\log\{K_d\}$ variogram analysis, vertical correlation scales in $\log\{K_d\}$ are, at most, 10 m.

Obtaining enough data pairs for variogram lag vector for the lateral (or any non-vertical) direction remains difficult in the TCU. Figure 9-11 tallies data pairs as a function of lateral distance and RMF for "F" data. The "F" data provide only one lateral variogram lag with distance less than 3,000 m, and this lag is only within the **L-UTCU Zeolitic** RMF.

Figure 9-12 tallies data pairs as a function of lateral distance and RMF for "S" data. The "S" data provide at least 5 lag pairs at 18 lateral distances in the **L-UTCU Zeolitic** RMF and 5 lateral distances in the **OSBCU Zeolitic** RMF. Of the different XRD methods, only the "S" method data are sufficiently numerous and closely-spaced to possibly detect spatial continuity of properties related to reactive minerals, including K_d. However, the "S" data are only sufficient in number and spacing for lateral variogram analysis within the **L-UTCU Zeolitic** and **OSBCU Zeolitic** RMFs.

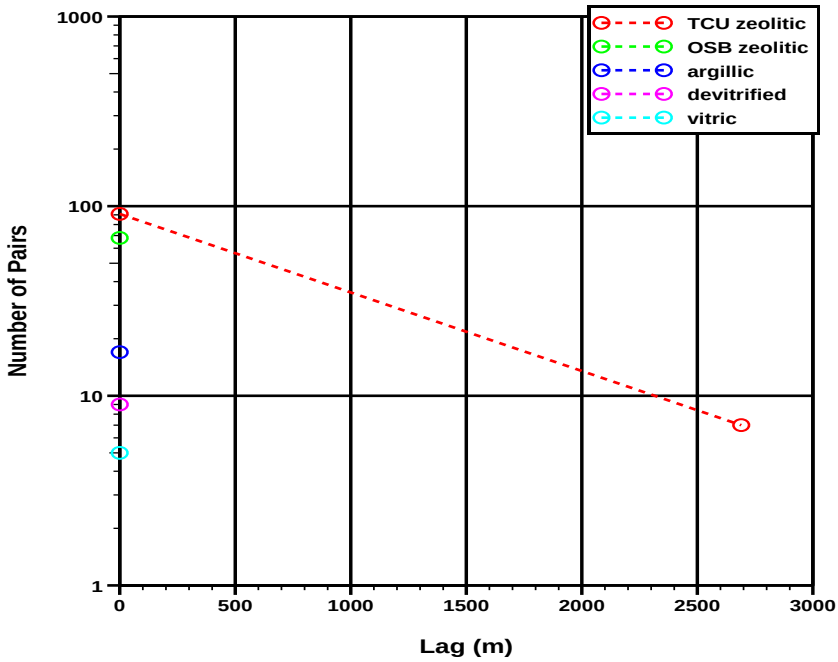

Figure 9-11. Number of data pairs for lateral direction lags using "F" data and 5 pair minimum.

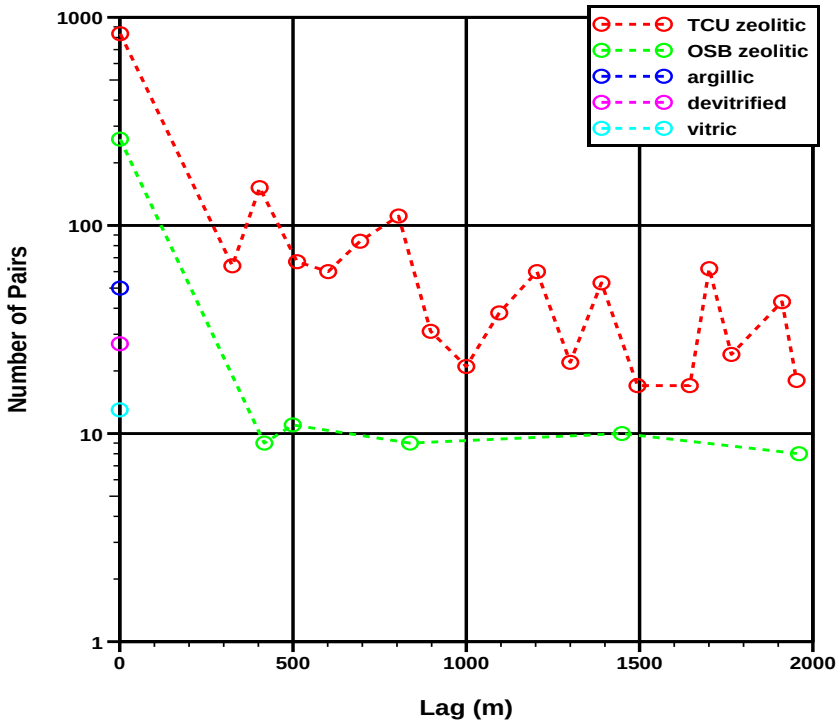

Figure 9-12. Number of data pairs for lateral direction lags using "S" data, 100 m lag spacing, and 5 pair minimum.

9.2.1 L-UTCU Zeolitic RMF

Figure 9-13 shows calculated lateral direction variograms for $\log\{K_d\}$ in the **L-UTCU Zeolitic** RMF using "S" data only and a minimum of 100 m (328 ft) horizontal lag spacing or larger based on a minimum of 5 pairs per lag. The smallest non-zero lateral lag is about 320 m. These lateral direction $\log\{K_d\}$ variograms from "S" data should not be over-interpreted beyond the limitations of the data as follows:

- Magnitude of $\log\{K_d\}$ variogram values are not appreciably smaller at the 320 m lag compared to larger distance lags, indicating that lateral spatial continuity is not detected. If lateral spatial continuity exists, the variograms indicate the range of lateral spatial correlation is less than 320 m.

- As seen with vertical $\log\{K_d\}$ variograms, some radionuclide classes share similar $\log\{K_d\}$ variogram structures. Zeolite dominates K_d for ^{41}C and Sr. Variability of zeolite log{percentage} is small in the **L-UTCU Zeolitic** RMF. Overall variogram structures for the smectite-dominated sorbers Ni, Sm, Eu, Am, Np, Pu, and U are similar, with differences attributable to differences between component additivity coefficients for calcite and smectite as described in more detail for the vertical $\log\{K_d\}$ variograms.

- Lateral $\log\{K_d\}$ variogram magnitudes for Cs in the **L-UTCU Zeolitic** RMF are larger than for the other two zeolite sorbers, ^{41}Ca and Sr, because of the large component additivity coefficient for mica.

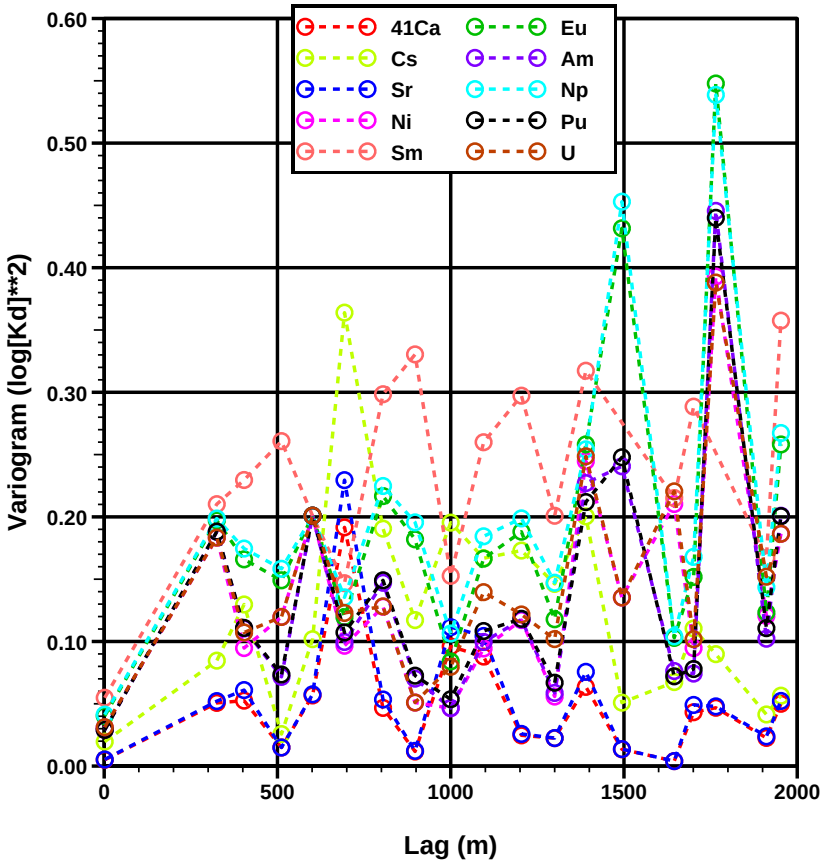

Figure 9-13. Lateral direction variogram analysis of K_d in L-UTCU RMF using "S" data, 100-m lag spacing, and minimum of 5 pairs per lag.

9.2.2 OSBCU RMF

Figure 9-14 shows calculated lateral direction variograms $\log\{K_d\}$ in the **OSBCU Zeolitic** RMF using "S" data only and a minimum of 100 m (328 ft) horizontal lag spacing or larger based on a minimum of 5 pairs per lag. The smallest non-zero lateral lag is about 410 m. As for the **L-UTCU Zeolitic** RMF, these lateral direction $\log\{K_d\}$ variograms from "S" data should not be over-interpreted beyond the limitations of the data as follows:

- As indicated by Figure 9-14, the lateral $\log\{K_d\}$ variogram values for the **OSBCU Zeolitic** RMF rely on fewer data pairs than for the **L-UTCU Zeolitic** RMF.
- Magnitude of $\log\{K_d\}$ variogram values at the 410-m lag are large for the smectite-dominated sorbers (Ni, Sm, Eu, Am, Np, Pu, and U), and small for the

zeolite-dominated sorbers (^{41}Ca and Sr) compared to larger distance lags. If the variograms values were accurate, this would indicate zeolitized zones are more laterally continuous than argillized zones. However, the uncertainty of the variogram values is high.

- As seen with vertical $\log\{K_d\}$ variograms and in the **L-UTCU Zeolitic** RMF, some radionuclide classes share similar $\log\{K_d\}$ variogram structures. Zeolite dominates K_d for ^{41}Ca and Sr. Variability of zeolite log{percentage} is small in the **L-UTCU Zeolitic** RMF. Variogram structures for the smectite-dominated sorbers Ni, Sm, Eu, Am, Np, Pu, and U are nearly identical because calcite is not very abundant in the **OSBCU Zeolitic** RMF.

- As for the **L-UTCU Zeolitic** RMF, lateral $\log\{K_d\}$ variogram magnitudes for Cs in the **OSBCU Zeolitic** RMF are larger than for the other two zeolite sorbers, ^{41}Ca and Sr, because of the large component additivity coefficient for mica.

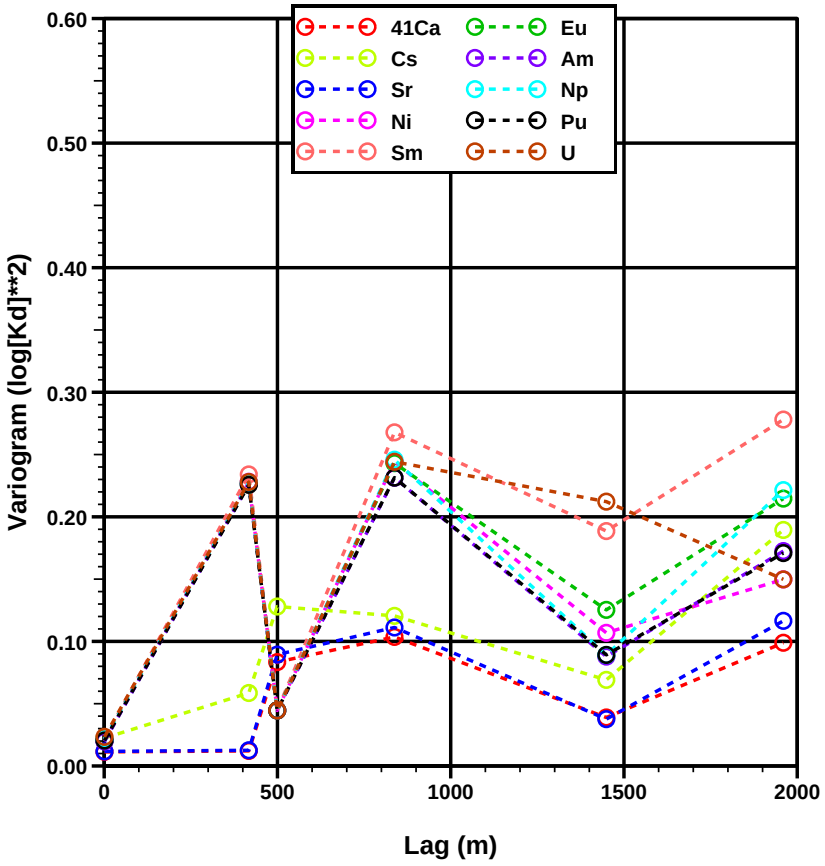

Figure 9-14. Lateral direction variogram analysis of K_d in OSBCU RMF using "S" data, 100-m lag spacing, and minimum of 5 pairs per lag.

9.3 Insights from log{K_d} Variogram Analysis in the TCU

9.3.1 Variogram Structure

Variogram analysis of $\log\{K_d\}$ using the component additivity methodology applied to the TCU XRD data set suffers from two main issues: (1) the full spectrum "F" method data are not sufficiently numerous and closely spaced to develop accurate variograms, and (2) the semi-quantitative "S" data ,while numerous, produce spurious impressions of spatial correlation from use of fixed values derived from data given as ranges of values. Nonetheless, the variogram analysis provides general insights that will be useful to develop models of spatial variability:

- Smectite is the dominant sorber for seven of the ten radionuclide classes, Am, Eu, Ni, Np, Pu, Sm, and U. Therefore, a $\log\{K_d\}$variogram range can be expected to be similar for all of the smectite-dominated sorbers. Presence of calcite can add to the variogram magnitude, and this depends largely on the difference between calcite and smectite component additivity methodology coefficients.

- ^{41}Ca and Sr $\log\{K_d\}$ are dominated by zeolite, particularly in the more zeolitic RMFs – **L-UTCU Zeolitic** and **OSBCU Zeolitic**. ^{41}Ca and Sr $\log\{K_d\}$variogram range and magnitude can be expected to be similar.

- Cs $\log\{K_d\}$, though influenced by zeolite and smectite, can be dominated by mica. Cs $\log\{K_d\}$ variogram structures may be unique compared to other radionuclide classes.

- Variogram magnitudes (sills) for $\log\{K_d\}$ are likely higher in **Devitrified** and **Vitric** RMFs because reactive mineral abundance, while relatively small, varies more greatly on a logarithmic scale. However, considering in Section 8.3 that the smectite-dominated sorbers - Am, Eu, Ni, Np, Pu, Sm, and U – showed similar $\log\{K_d\}$ distributions throughout the OSBCU HSU, it would be reasonable to assume a similar pattern of spatial variability of $\log\{K_d\}$ through out the OSBCU HSU for all smectite sorbers.

9.3.2 Simulation of log{*Kd*} Spatial Variability

Shortcomings in modeling $\log\{K_d\}$ variogram structure preclude simulation of $\log\{K_d\}$ spatial variability. Only the full spectrum "F" XRD data provide suitable accuracy to characterize spatial distributions of $\log\{K_d\}$ within RMFs of the TCU. However, the "F" data are not sufficiently numerous and closely spaced to detect spatial continuity by

variogram analysis. The scale of spatial variability of $\log\{K_d\}$ remains undetected within RMFs of the TCU.

The major differences in $\log\{K_d\}$ within the TCU are attributable to the zonal differences associated with different RMFs (or RMUs). Most of this spatial variability can be accounted for by deterministic mapping of the major HSUs within the TCU – LTCU and UTCU, OSBCU, ATCU. Smaller heterogeneities are associated with the devitrified RMUs and vitric tuffs. However, these smaller sub-HSU heterogeneities may only affect the zeolite dominated sorbers – ^{41}Ca and Sr because smectite and mica content is similar throughout the OSBCU HSU. The sub-HSU scale heterogeneities will be the most difficult to map or conceptualize, particularly in regard to lateral continuity.

Several scaling issues remain for translating $\log\{K_d\}$ inferred from XRD data to simulation of spatial distributions of $\log\{K_d\}$:

- The scale of the XRD measurement differs from simulation grid blocks or cells.
- Upscaling of $\log\{K_d\}$ may have non-linear dependencies from cross-correlation between $\log\{K_d\}$ and $\log\{permeability\}$.
- Depending on the size of the grid blocks, spatial variability of effective $\log\{K_d\}$ values for grid blocks could be expected within RMFs.

The combination of data insufficiencies and scaling issues preclude application of geostatistical simulation to $\log\{K_d\}$ within the RMFs. Assumptions can be made, however, on how to upscale XRD measurements and conceptualize spatial variability of $\log\{K_d\}$ within RMFs to produce realizations of $\log\{K_d\}$ for each radionuclide class. A more promising (and less tedious) approach may be to simulate spatial variability of reactive mineral percentage, then apply the component additivity methodology to realizations of reactive mineral percentage as will be discussed in Chapter 10.

10. Simulation of Mineralogic Spatial Variability

Another approach to addressing K_d or $\log\{K_d\}$ spatial variability is to simulate spatial distributions or "realizations" of reactive mineral percentages, then generate realizations of K_d values on a cell-by-cell basis from the mineral percentage realizations using the component additivity methodology, for example. This approach has several advantages of direct simulation of K_d:

- Different K_d model parameters or modeling approaches (in addition to the component additivity methodology) can be applied to the same realizations of mineralogic percentage.
- Uncertainty analysis in K_d model parameters can be assessed empirically, such as through Monte Carlo approaches. This is advantageous for assessing uncertainty in the component additivity methodology because analytical approaches to assessing uncertainty in $\log\{K_d\}$ are not feasible if the component additivity methodology parameters depend on more than one reactive mineral (see Section 8.2).
- Realizations can be conditioned to mineralogic percentage observations, whereas field-based K_d observations are not readily available.
- Realizations can be constructed that honor cross-correlations between different reactive mineralogic quantities.
- K_d distributions need not be assumed log-normal.
- Generation of independent parametric representations for each K_d frequency distribution of each radionuclide class is not necessary.

10.1 Scaling Issues

As in previous discussion in Section 9.3.2 for direct simulation of $\log\{K_d\}$, a main difficulty in simulation of reactive mineral spatial variability is in relating scales of spatial correlation for the reactive mineral distributions to the scales of K_d values implemented in transport simulation (Shaw, 2003). Differences in scale arise between XRD measurements, XRD sample spacing, the component additivity methodology, and effective K_d values in transport simulation grid blocks or cells.

This study addresses only scaling issues related to XRD sample spacing. If XRD sampling spacing is greater than scales of spatial correlation of reactive mineral

variability, the data will indicate a condition of "no spatial correlation" suggesting mineralogic spatial variability is only related to variance in the reactive mineral distribution. Although spatial correlation may exist at a scale less than the sample spacing, for practical purposes this may represent effectively "no spatial correlation" relevant to the scale of a reactive transport model grid block. If, however, spatial correlations of reactive mineral distributions are comparable or greater then transport model grid blocks, such spatial correlation would contribute to uncertainty of grid block scale K_d values.

Using geostatistical realizations of $\log\{K_d\}$ spatial variation in Frenchman Flat alluvium, Zavarin et al. (2004) conducted numerical radionuclide transport experiments with Gaussian random field spatial variation of $\log\{K_d\}$ and permeability fields correlated, negatively correlated, and positively correlated permeability fields $\log\{K_d\}$. These numerical experiments indicated effective $\log\{K_d\}$ was approximated by mean $\log\{K_d\}$ regardless of correlation to permeability. Dispersion was increased by spatial variability of $\log\{K_d\}$. Similar numerical experiments could be implemented in the TCU using $\log\{K_d\}$ distributions for RMFs to estimate effective K_d in RMUs.

10.2 Simulation with "No Spatial Correlation"

The term "no spatial correlation" will refer to the condition where spatial variability of reactive mineral distributions occurs at a very small scale without evidence of spatial continuity at measurement scale. Under an assumption of no spatial correlation in reactive mineral distributions and application of the component additivity methodology, K_d or $\log\{K_d\}$ would also have effectively no spatial correlation. Assuming no spatial correlation in reactive mineral distributions, effective K_d values for grid blocks could be estimated under an assumption that spatial variability of K_d is much smaller than the scale of the grid block. The effective grid-block scale K_d values can then be predicted from averages of K_d values obtained by applying the component additivity methodology to the reactive mineral distribution.

A complete characterization of correlation between different mineral distributions includes characterization of cross-correlation. If there is no spatial correlation, only the correlation matrix at lag zero will have non-zero auto- and cross-correlation values. However, compositional data produce spurious cross-correlations that do not necessarily represent spatial continuity.

10.2.1 ALR Approach

Parametric geostatistical approaches typically assume Gaussian distributions in evaluation of the (cross-)covariance matrix. Transformation of the mineralogic percentage data to the additive log-ratio (ALR) fits the Gaussian conceptual model better than raw percentage or log transform. The diagonal entries in a cross-correlation matrix of the ALR represent the auto-correlations (variances) of the ALR for each reactive mineral, and the off-diagonal entries represent the cross-correlations of ALR between different reactive minerals. The geostatistical framework of simulation can be implemented in the ALR domain, and the mineralogic percentages needed for the component additivity methodology can be obtained by back-transformation of the ALR.

The reactive mineral percentage simulation approach uses the following steps:

1. Compute each entry $C_{ij}(0)$ in the correlation matrix $\mathbf{C}(0)$ of ALR for *N* reactive minerals for lag zero, where $ALR_i(\mathbf{x})$ is the additive log ratio of the percentage of mineral *i* at location **x**.

   $$C_{ij}(0) = E\{ALR_i(\mathbf{x})ALR_j(\mathbf{x})\} - E\{ALR_i(\mathbf{x})\}E\{ALR_j(\mathbf{x})\}$$

2. Compute a Cholesky decomposition of $C(0)$

   $$\mathbf{C}(0) = \mathbf{B}\mathbf{B}^T$$

3. To generate a random field of ALR vectors $\mathbf{r}(x)$ with uniform spatial correlation of $\mathbf{C}(0)$ at all lags, the ALR vector of mean values is added to a vector obtained by multiplying **B** by a vector **g** of standard normal deviates
   $\mathbf{r}(\mathbf{x}) = \mathbf{B}\mathbf{g}$
   This relationship holds because the expected value of $\mathbf{g}\mathbf{g}^{\mathbf{T}}$ is the identity matrix and, consequently, the covariance matrix for **Bg** is $\mathbf{C}(0)$ because
   $Cov\{\mathbf{Bg}\} = E\{\mathbf{BgBg} - 0\} = E\{\mathbf{Bgg}^T\mathbf{B}^T\} = E\{\mathbf{B}\mathbf{B}^T\} = \mathbf{C}(0)$

4. Back transform $\mathbf{r}(x)$ from ALR values to mineralogic percentage vector $\mathbf{p}(\mathbf{x})$ with components $p_j(\mathbf{x})$

   $$p_j(\mathbf{x}) = 100\% \times \frac{10^{ALR_j(\mathbf{x})}}{1.0 + \sum_{k=1}^{N} 10^{ALR_k(\mathbf{x})}}$$

Under the reactive mineral facies (RMF) framework, a separate ALR correlation matrix is developed for each RMF because the reactive mineral distributions are assumed unique to each RMF.

10.2.2 Application to L-UTCU Zeolitic RMF

The next two subsections detail simulation of reactive mineral distributions based on a zero-lag ALR covariance matrix with application to the **L-UTCU Zeolitic** and **OSBCU Zeolitic** RMFs using "F" data. These two RMFs provide the best quality data for predicting K_d distributions in the TCU. For simplicity, calcite and hematite will be ignored in analysis of spatially cross-correlated ALR variables because of non-ubiquity indicated by large proportions of zero-valued or low-percentage data and subsequent low impact on K_d. Only the mica, smectite, and zeolite components of ALR cross-covariance will be examined.

Figure 10-1 shows the covariance matrix of mica, smectite, and zeolite ALRs as a function of vertical lag using "F" data from the **L-UTCU Zeolitic** RMF. Beyond lag zero, the spatial covariance fluctuates near zero for all components. Significant non-zero covariance appears only at lag zero, indicating that ALR is spatially uncorrelated over the scales of 6 m or more. The zero-lag covariance matrix $\mathbf{C}_{\mathrm{ALR}}(0)$ can be used to simulate frequency distributions of ALRs and, subsequently, frequency distributions of mineralogic percentages. For the L-UTCU, a symmetric $\mathbf{C}_{\mathrm{ALR}}(0)$ for mica, smectite, and zeolite components is computed as

$$\mathbf{C}_{ALR}(0) = \begin{bmatrix} 0.1165 & 0.04275 & -0.0096 \\ 0.04275 & 0.2980 & -0.0272 \\ -0.0096 & -0.0272 & -0.0640 \end{bmatrix},$$

where off-diagonal entries were averaged from computed covariance values on opposing sides of the matrix assuming symmetry. The vector of mean ALR values, $E\{ALR(\mathbf{x})\}$, for the L-UTCU is

$$E\{ALR(\mathbf{x})\} = \begin{bmatrix} -1.37 \\ -1.06 \\ 0.21 \end{bmatrix}.$$

From the Cholesky decomposition of $\mathbf{C}_{\mathrm{ALR}}(0)$, an ALR vector with the above specified mean and covariance can be simulated by

$$ALR(\mathbf{x}) = \begin{bmatrix} -1.37 \\ -1.06 \\ 0.21 \end{bmatrix} + \begin{bmatrix} 0.3413 & 0.1252 & -0.0281 \\ 0.1252 & 0.5313 & -0.0445 \\ -0.0281 & -0.0446 & 0.2474 \end{bmatrix} \begin{bmatrix} g_1 \\ g_2 \\ g_3 \end{bmatrix}$$

where g_1, g_2, and g_3 are random values obtained as normal deviates of a Gaussian distribution with mean zero.

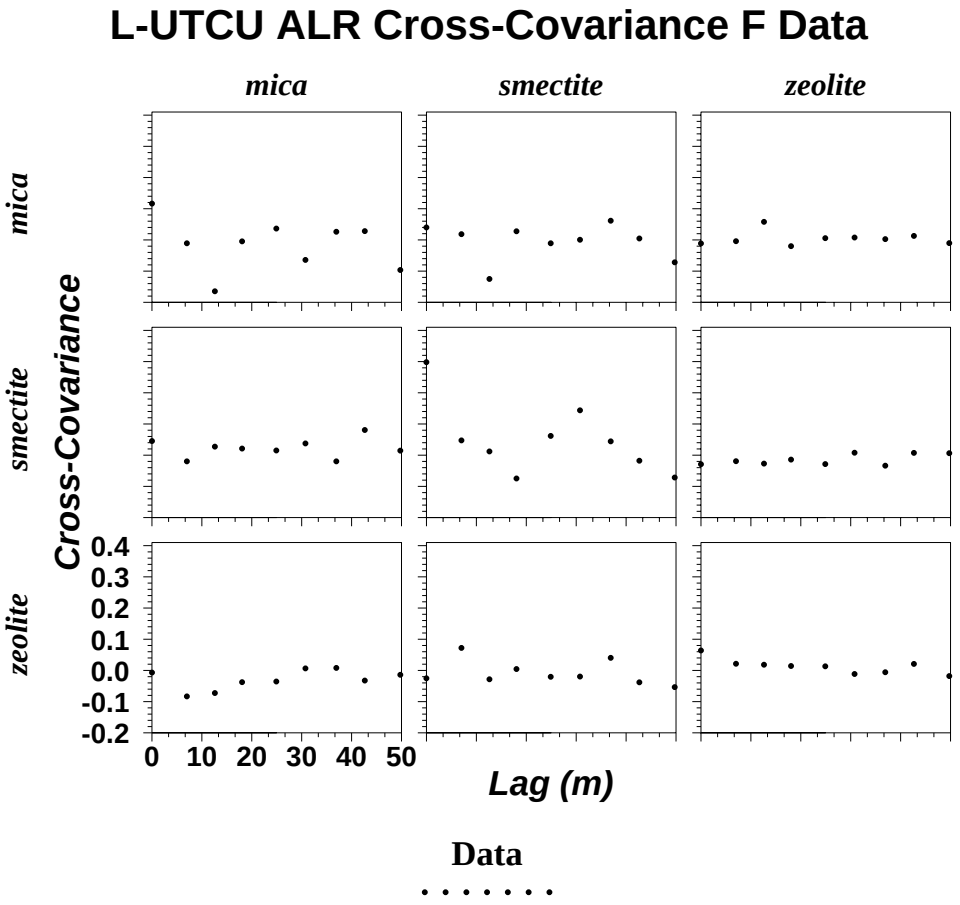

Figure 10-1. Cross covariance matrix of ALR for mica, smectite, and zeolite in L-UTCU Zeolitic RMF with dependence on vertical lag.

Figure 10-2 compares measured and simulated ALRs and reactive mineral percentage frequency distributions for mica, smectite, and zeolite in the **L-UTCU Zeolitic** RMF. This comparison shows several advantages of using the ALR for parametric representation of frequency distributions for compositional variables:

- The ALR-transformed distributions are bell-shaped, symmetric, and not bounded and, therefore, a Gaussian distribution is a plausible model for the measured frequency distributions.

- The simulated distributions (second row) replicate Gaussian distribution properties specified in the fits to the measured ALR frequency distributions (first row).

- The log-scaled simulated reactive mineral percentage distributions (fourth row) are consistent with the observed reactive mineral percentage distributions (third row), including asymmetric properties such as left-skewed tailing and finite upper bounds (particularly for mica and zeolite).

- The simulated reactive mineral percentage distributions maintain the vital compositional variable properties of bounding of values and sums between 0 and 100 (finite tails).

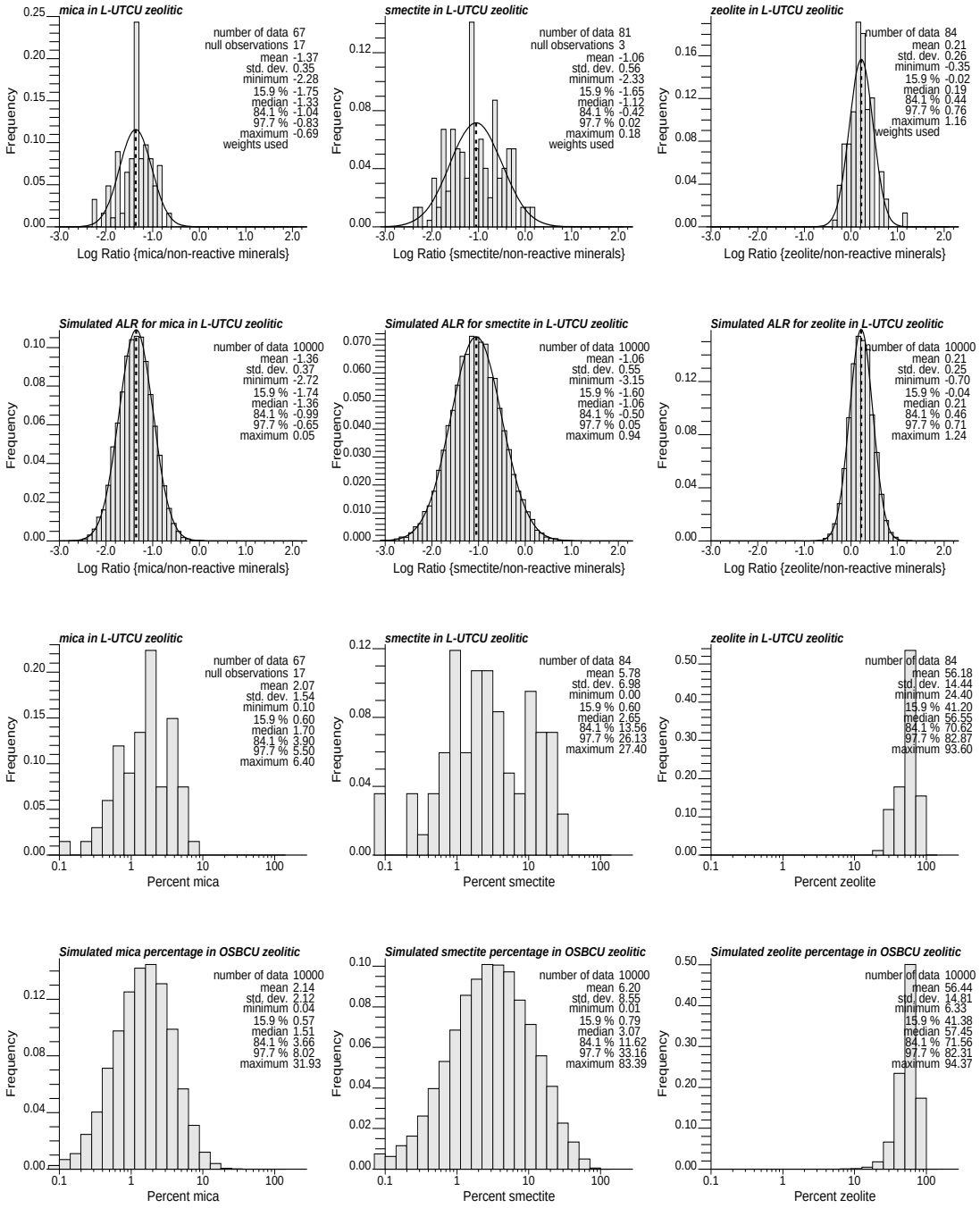

Figure 10-2. Comparison of measured and simulated ALR and reactive mineral percentage frequency distributions for mica, smectite, and zeolite in the L-UTCU Zeolitic RMF. Top row is measured ALR, which is compared to 10,000 simulated ALRs in second row. Third and fourth rows compare measured and simulated log{reactive mineral percentage}.

10.2.3 Application to OSBCU RMF

Figure 10-3 shows the covariance matrix of mica, smectite, and zeolite ALRs as a function of vertical lag using "F" data from the **OSBCU Zeolitic** RMF. Beyond lag zero, the spatial covariance fluctuates near zero for all components. With the possible exception of smectite auto covariance, significant non-zero covariance appears only at lag zero, indicating that the ALR, in general, is not spatially correlated over the scales of 6 m or more within the **OSBCU Zeolitic**. With or without spatial correlation, the zero-lag covariance matrix $\mathbf{C}_{ALR}(0)$ can be used to simulate frequency distributions of ALRs and, subsequently, frequency distributions of mineralogic percentages. For the **OSBCU Zeolitic** RMF, the symmetric $\mathbf{C}_{ALR}(0)$ for mica, smectite, and zeolite components is computed as

$$\mathbf{C}_{ALR}(0) = \begin{bmatrix} 0.1449 & -0.0343 & -0.01365 \\ 0.0343 & 0.2980 & 0.01865 \\ -0.01365 & -0.01865 & -0.0640 \end{bmatrix}$$

Off-diagonal entries were averaged from computed covariance values on opposing sides of the matrix assuming symmetry. The vector of mean ALR values, $E\{ALR(\mathbf{x})\}$, for the OSBCU is

$$E\{ALR(\mathbf{x})\} = \begin{bmatrix} -1.29 \\ -0.88 \\ 0.00 \end{bmatrix}$$

From the Cholesky decomposition of $\mathbf{C}_{ALR}(0)$, an ALR vector with the above specified mean and covariance can be simulated by

$$ALR(\mathbf{x}) = \begin{bmatrix} -1.29 \\ -0.88 \\ 0.00 \end{bmatrix} + \begin{bmatrix} 0.3807 & -0.0901 & -0.0359 \\ -0.0901 & 0.5313 & 0.0267 \\ -0.0359 & 0.0267 & 0.2474 \end{bmatrix} \begin{bmatrix} g_1 \\ g_2 \\ g_3 \end{bmatrix}$$

where g_1, g_2, and g_3 are random values obtained as normal deviates of a Gaussian distribution with mean zero.

Like Figure 10-2 for the **L-UTCU Zeolitic** RMF, Figure 10-4 compares measured and simulated ALRs and reactive mineral percentage frequency distributions for mica, smectite, and zeolite in the **OSBCU Zeolitic** RMF. This comparison echoes the advantages of using the ALR for parametric representation of frequency distributions for compositional variables listed at the end of Section 10.2.2.

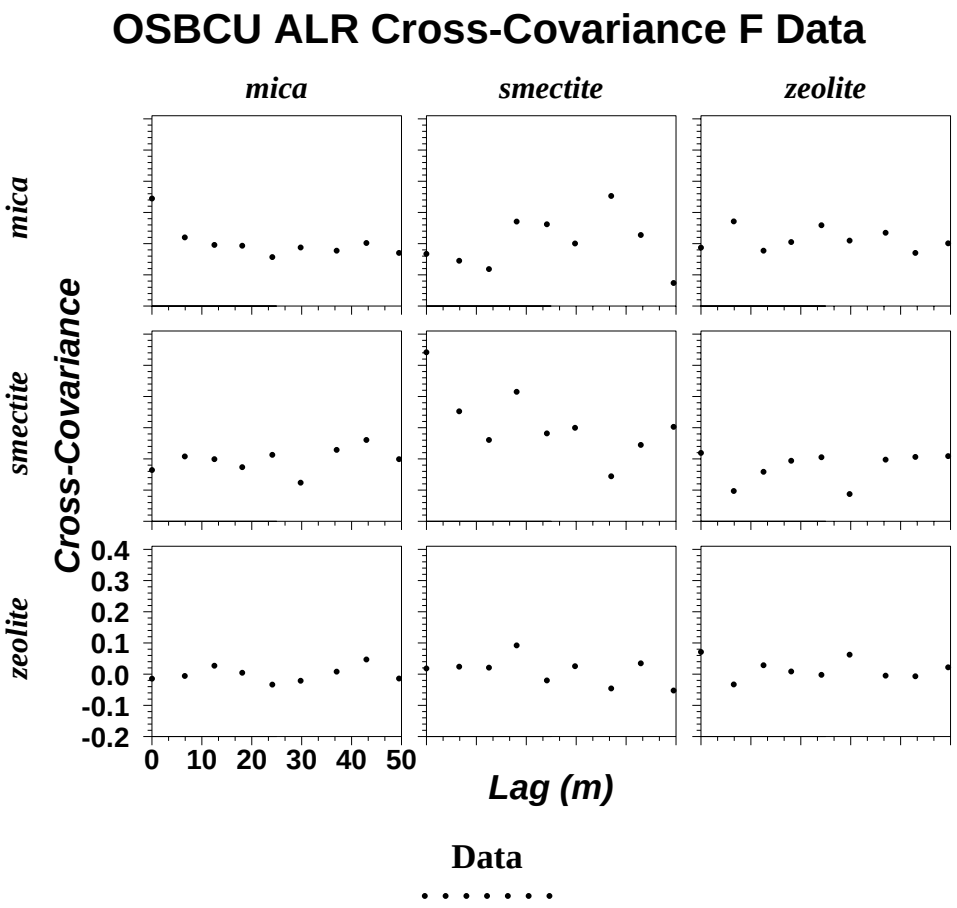

Figure 10-3. Cross covariance matrix of ALR for mica, smectite, and zeolite in OSBCU Zeolitic RMF with dependence on vertical lag.

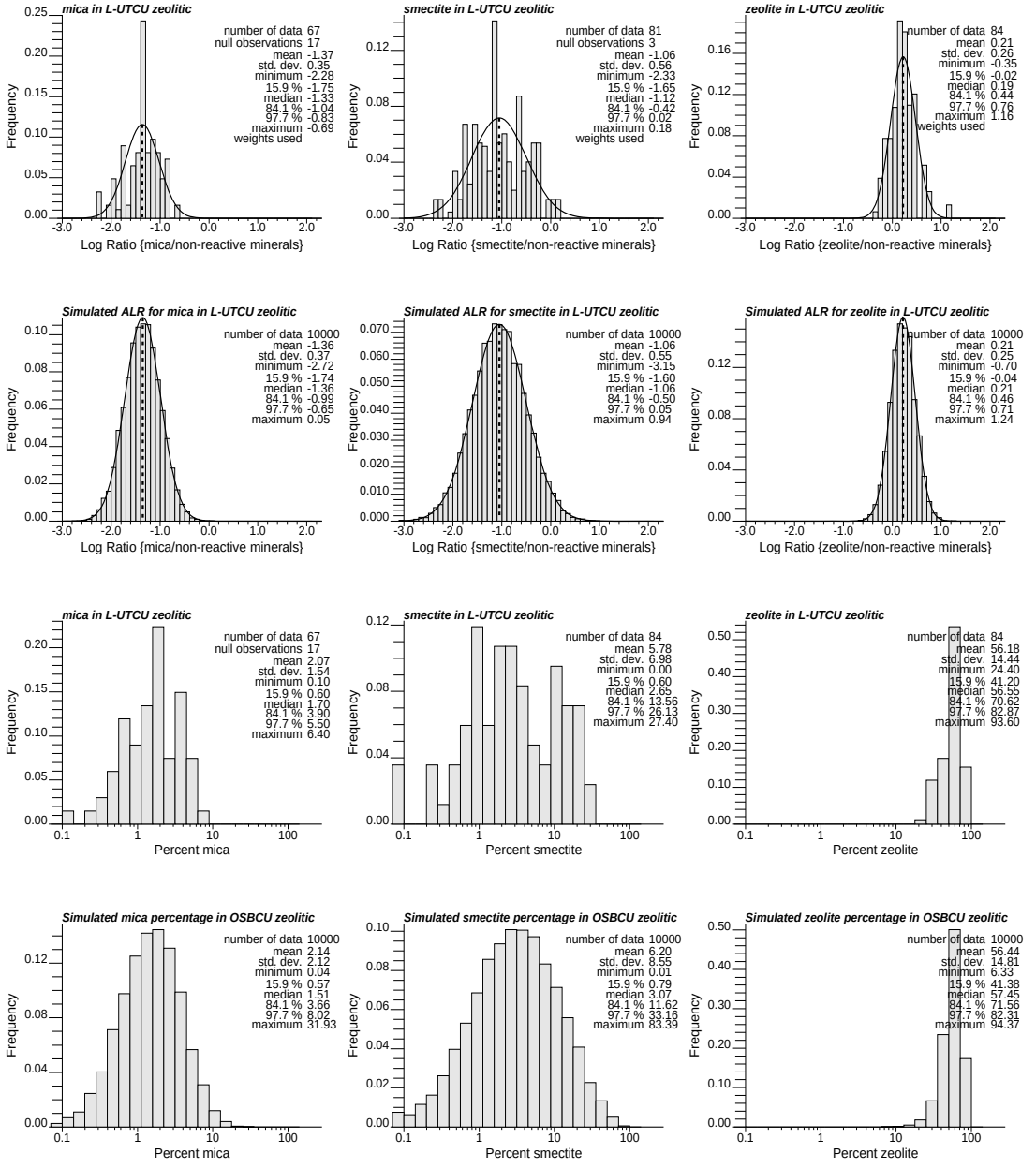

Figure 10-4. Comparison of measured and simulated ALR and reactive mineral percentage frequency distributions for mica, smectite, and zeolite in the OSBCU Zeolitic RMF. Top row is measured ALR, which is compared to 10,000 simulated ALRs in second row. Third and fourth rows compare measured and simulated log{reactive mineral percentage}.

10.3 Simulation With Spatial Correlation

If reactive mineralogic percentages are spatially (cross-) correlated, then an algorithm for simulation of mineralogic variability would need to replicate the spatial (cross-) correlations.

10.3.1 Data Limitations

However, detection of spatial (cross-) correlation of reactive mineral properties is not definitive within reactive mineral facies in the TCU. Lack of detectable spatial correlation is attributed to several limiting factors of the TCU XRD reactive mineral data set:

- The number of data usable for evaluating spatial correlation is far less than the total number of data available. The most numerous semi-quantitative “S” data impart false indications of spatial correlation because fixed modal values derived from mineral percentage ranges produce inaccurate constant data values over vertical intervals.
- Much of the external standard “E” data do not resolve low percentages, resulting in excessive zero values that are particularly problematic to logarithmic transformations including the ALR.
- The best quality data - full spectrum “F” data - are far less numerous and more widely spaced, both vertically and laterally, than “S” data.
- Although the data indicate possible vertical spatial auto-correlation for smectite ALR, detection of lateral spatial variability from the existing data is not possible because of wide spacing between wells with “F” data.

Despite data limitations, characterization of mineralogic spatial variability for reactive transport modeling still may require generation of a three-dimensional (3-D) geostatistical model. If spatial (cross-) correlation of the reactive mineralogic properties can be detected in 3-D, the next challenge would be to model and honor the full spatial cross-covariance matrix. However, simulation of spatially cross-correlated random fields remains a theoretical challenge for the following reasons:

- Geostatistical modeling approaches for multivariate cross-covariance matrices are uncommon and data intensive.
- Existing geostatistical simulation approaches for multivariate cross-correlated variables do not fully consider cross-correlations.

- Direct modeling and simulation of compositional variables leads to multiple difficulties caused by non-Gaussian frequency distributions and singularity caused by the summing constraint. The ALR approach does bypass these difficulties.

Considering that the TCU XRD data are insufficient to support geostatistical modeling of 3-D spatial cross-covariances, simulation of spatially (cross-) correlated reactive mineralogic properties is not pursued in this study.

10.3.2 A Simulation Algorithm

If XRD data were collected at spacing sufficiently small in both vertical and lateral directions to characterize spatial (cross-) covariance of reactive mineral distributions, particularly the ALR, then the following geostatistical approach would be suggested:

- Use the additive log ratio (ALR) as the reactive mineralogic property, where the denominator is the percentage of non-reactive minerals. Based on experience with existing XRD data, the ALR transformation produces a random variable characterized by Gaussian distributions within each of the reactive mineral facies (RMFs).

- Measure spatial (cross-) covariance between ALRs in each RMF.

- Model spatial (cross-) covariance with linear combinations of exponential or other positive-definite functions – one for each reactive mineral. If the linear coefficient matrices are positive-definite, the spatial (cross-) correlation model will be positive definite.

- Alternatively, use autoregressive cross-covariance modeling approaches, which provide a general modeling approach that encompasses the linear approach described above for exponential functions.

- Re-formulate the sequential Gaussian simulation (sGs) algorithm (Deutsch and Journel, 1992) into a sequential Gaussian “co-simulation” algorithm. To accomplish this, the kriging equations would need to be modified to cokriging equations, and the estimation step would need to be modified to account for cross-covariances. The existing sGs estimation step uses a random number drawn from a Gaussian distribution based on the kriging estimate and kriging variance. This step would be generalized by Cholesky decomposition the simulation procedure described in Section 10.2 using the cokriging estimate and “cokriging covariance” matrix multiplied by a vector of standard normal deviates.

- Back-transform simulated cross-correlated ALR random field vectors to reactive mineralogic percentages and use the component additivity methodology to formulate K_d distributions from the reactive mineralogic percentages.

This approach would yield a parametric model for K_d distributions rooted from parameters representing both mineralogic spatial variability and the coefficients of the component additivity methodology. The frequency distributions and spatial variability of K_d for all radionuclides would be characterized by component additivity coefficients multiplied by the cross-correlated Gaussian vector random fields of ALR components consisting of the logarithm of the reactive/non-reactive mineral ratios.

10.4 Assessing Uncertainty and Scaling Effects

With or without spatial correlation, the approach of simulating mineralogic variability first then assigning K_d values based on the component additivity methodology provides a reasonable framework for assessing uncertainty in K_d. Several contributions to uncertainty in radionuclide transport behavior can be addressed individually or in combination in a stochastic framework by simulating mineralogic variability:

- Uncertainty in the distribution of reactive mineral percentages.
- Uncertainty related to spatial correlation and structure, including heterogeneity, of reactive mineral properties.
- Uncertainty in component additivity coefficients.

Currently, the XRD data appear to be insufficient in number and spatial resolution to characterize spatial covariance of reactive mineral properties within RMUs or RMFs of the TCU.

Without sufficient data to characterize spatial covariance of reactive mineral properties, the scale of mineralogic variability within RMUs or RMFs remains unknown. The data suggest correlation scales less than about 6 m in the vertical (except, possibly, for smectite in the OSBCU Zeolitic RMF) and undetermined scales in the lateral directions. It would be useful to conduct fine-scale sampling (e.g. 1 m or less) to determine spatial correlations. From this, it would be useful to determine how the scales of variability of reactive mineral percentages effect transport properties within RMUs or RMFs. Numerical experiments could be carried out at fine resolution to assess effects of spatial variability of reactive mineral properties on prediction of radionuclide transport behavior (Viswanathan et al., 2003; Zavarin et al., 2004). Such numerical experiments could be used to provide effective K_d distributions at larger scales.

10.5 Simulation of K_d Distributions from ALR Parameterizations of Reactive Mineral Distributions

Simulation of spatial distributions of K_d could be accomplished by simulation of the spatial distributions of mineralogic percentage with transformation to K_d using the component additivity methodology. Considering that spatial correlation is undetectable for all reactive minerals except, possibly, smectite in the **OSBCU Zeolitic** RMF (Section 9.2.3), it is possible that mineralogic spatial variability is effectively uncorrelated within RMFs. Furthermore, under this "no spatial correlation" assumption examined in Section 10.2, K_d distributions at grid block scales could be characterized by averages of K_d values derived from mineralogic frequency distributions.

As demonstrated in Section 10.2, ALR mean and variance provide parameters for simulating measured mica, smectite, and zeolite frequency distributions with bounding between 0 and 100%. Assuming the sporadic occurrences of typically low percentages of calcite and hematite have minimal impact on K_d in the TCU, K_d can be assumed to be dominated by mica, smectite, and zeolite.

In this section, component additivity methodology parameters for mica, smectite, and zeolite are applied to the simulated frequency distributions of mica, smectite, and zeolite from Section 10.2 to generate "simulated K_d" distributions. The resulting $\log\{K_d\}$ distributions for the 10 radionuclide classes in the L-UTCU and OSBCU Zeolitic RMFs (see Figure 10-5 through Figure 10-14) can be compared to the $\log\{K_d\}$ frequency distributions in RMFs generated directly from the "F" mineralogic data, including calcite and hematite, shown in Figures 8-1, 8-3, 8-5, 8-7, 8-9, 8-11, 8-13, 8-15, 8-17, and 8-19 in Section 8.3. Table 10-1 and Table 10-2 compare mean and standard deviation of $\log\{K_d\}$ in the LTCU and OSBCU RMF as computed directly from "F" data and simulated from ALR covariance matrix for mica, smectite, and zeolite based on "F" data. These results show ALR parameterizations of mineralogic frequency distributions yield very similar $\log\{K_d\}$distributions compared to $\log\{K_d\}$ distributions generated from the raw mineral percentage data.

Compared to typical log-normal K_d distribution assumptions, several advantages of ALR mineral-percentage approach for characterization of K_d distributions are:

- K_d and $\log\{K_d\}$ distributions based on ALR of reactive minerals have upper bounds, as expected, whereas Gaussian $\log\{K_d\}$ distributions have infinite upper tails.
- $\log\{K_d\}$ distributions based on ALR of reactive minerals can represent asymmetry, whereas Gaussian $\log\{K_d\}$ distributions are assumed symmetric.

- The ALR K_d approach relies on a single set of statistical parameters to characterize only mineralogic variability rather than using separate sets of statistics for each K_d distribution.

- The ALR K_d approach relies on statistical parameters of properties that are measurable in the field, mineralogic variability, whereas K_d is difficult to measure in the field.

These results indicate a viable approach to simulating K_d variability within the TCU is to focus efforts on characterizing mean and covariance of reactive mineral ALRs within RMFs. The TCU data set indicates reactive mineral ALRs within RMFs are readily characterized by mean and covariance statistics (unlike the raw percentages or log percentages) and, therefore, ALR statistics alone can be used to predict realistic K_d distributions.

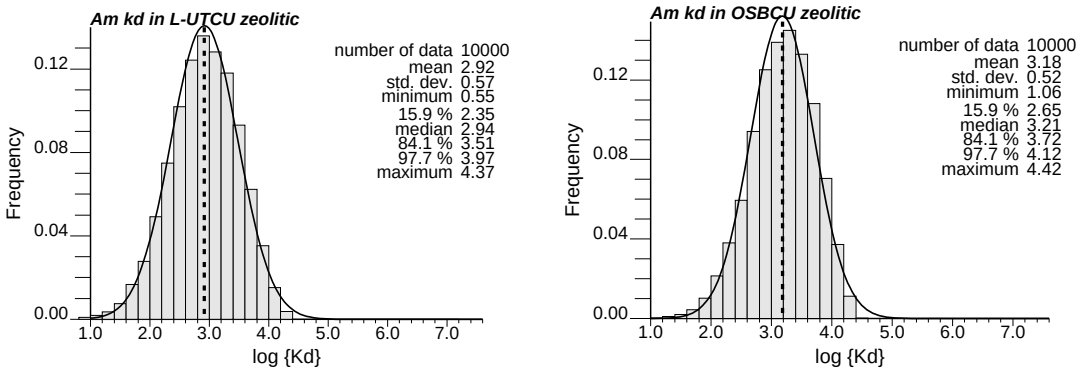

Figure 10-5. Simulated Am $\log\{K_d\}$ distributions in L-UTCU Zeolitic and OSBCU Zeolitic RMFs using mean component additivity methodology parameters applied to 10,000 simulated mica, smectite, zeolite ALR vectors described in Section 10.2.

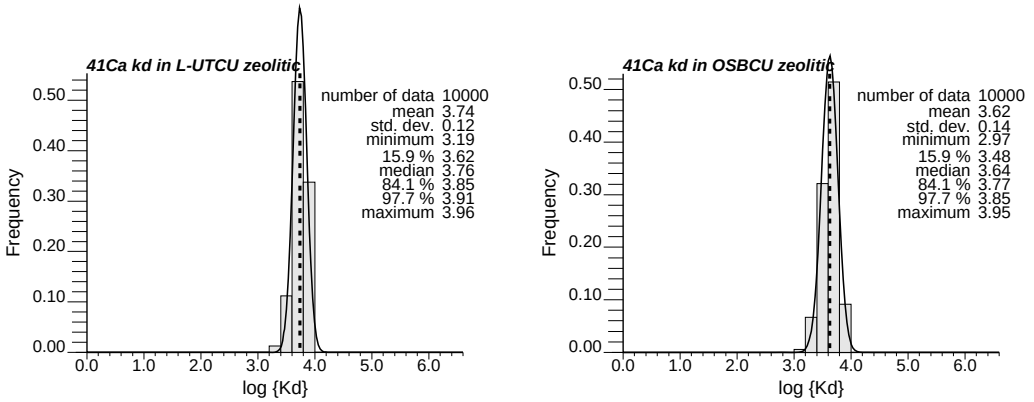

Figure 10-6. Simulated ^{41}Ca $\log\{K_d\}$ distributions in L-UTCU Zeolitic and OSBCU Zeolitic RMFs using mean component additivity methodology parameters applied to 10,000 simulated mica, smectite, zeolite ALR vectors described in Section 10.2.

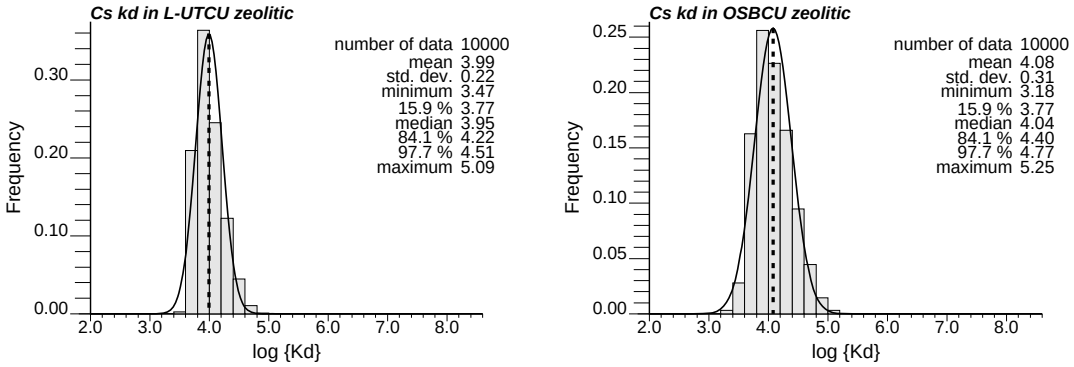

Figure 10-7. Simulated Cs $\log\{K_d\}$ distributions in L-UTCU Zeolitic and OSBCU Zeolitic RMFs using mean component additivity methodology parameters applied to 10,000 simulated mica, smectite, zeolite vectors ALR described in Section 10.2.

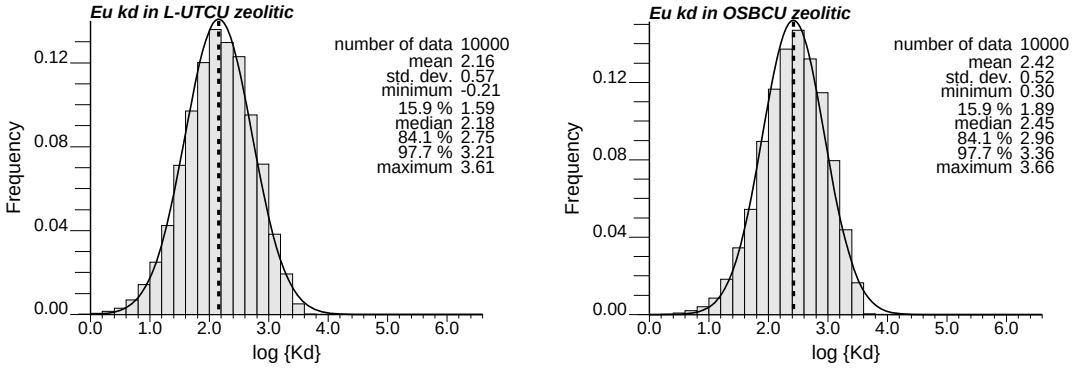

Figure 10-8. Simulated Eu $\log\{K_d\}$ distributions in L-UTCU Zeolitic and OSBCU Zeolitic RMFs using mean component additivity methodology parameters applied to 10,000 simulated mica, smectite, zeolite vectors described in Section 10.2.

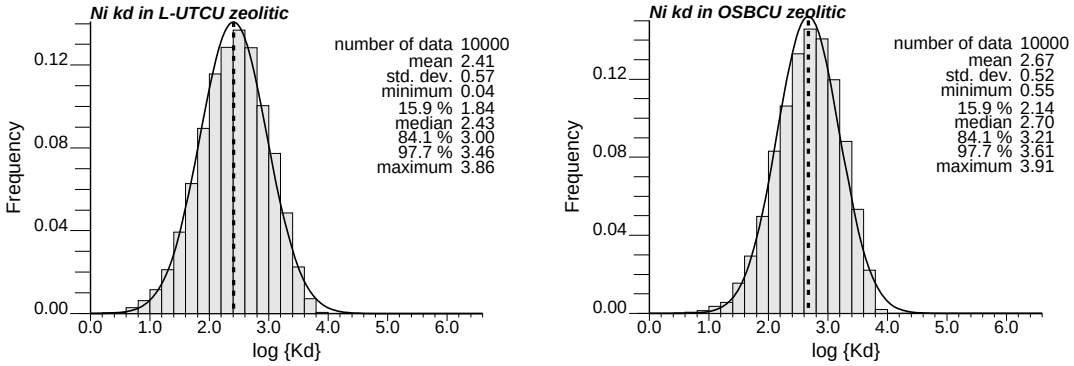

Figure 10-9. Simulated Ni $\log\{K_d\}$ distributions in L-UTCU Zeolitic and OSBCU Zeolitic RMFs using mean component additivity methodology parameters applied to 10,000 simulated mica, smectite, zeolite vectors described in Section 10.2.

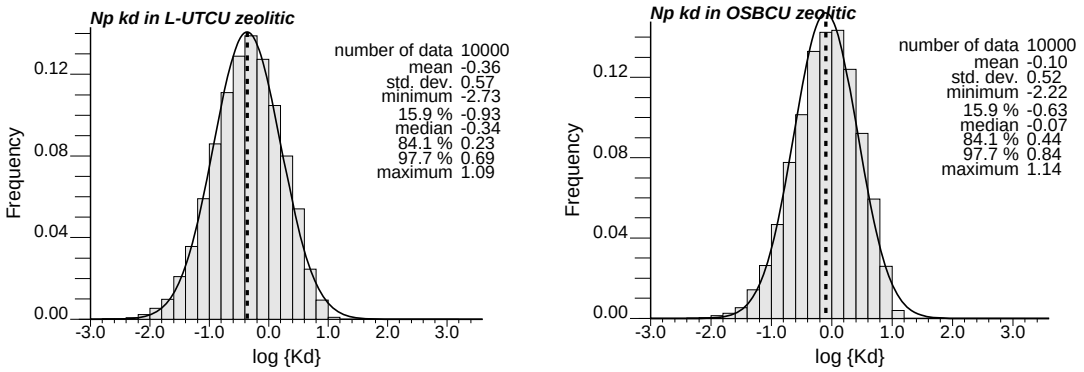

Figure 10-10Simulated Np $\log\{K_d\}$ distributions in L-UTCU Zeolitic and OSBCU Zeolitic RMFs using mean component additivity methodology parameters applied to 10,000 simulated mica, smectite, zeolite vectors described in Section 10.2.

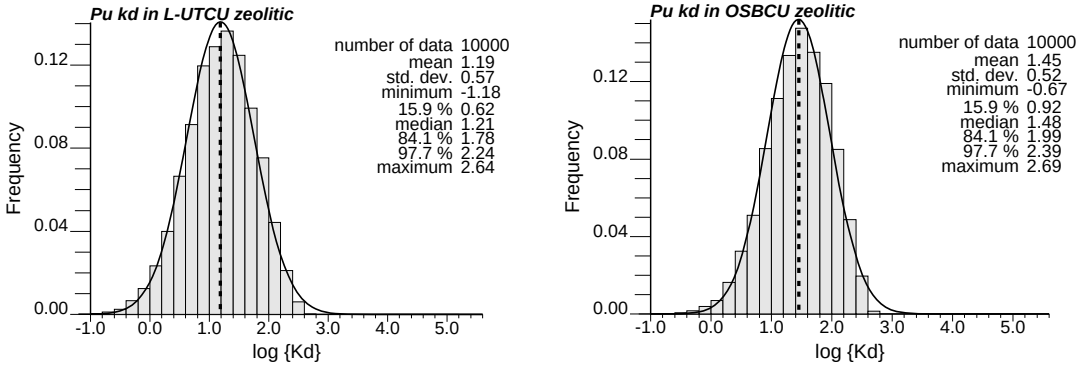

Figure 10-11.Simulated Pu $\log\{K_d\}$ distributions in L-UTCU Zeolitic and OSBCU Zeolitic RMFs using mean component additivity methodology parameters applied to 10,000 simulated mica, smectite, zeolite vectors described in Section 10.2.

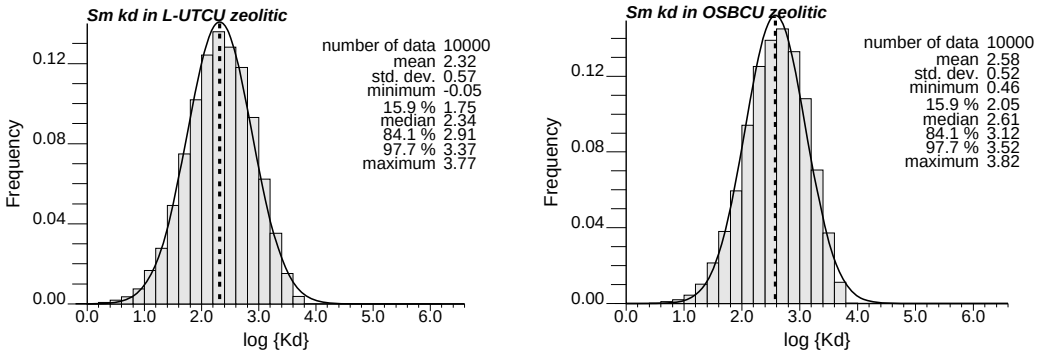

Figure 10-12.Simulated Sm $\log\{K_d\}$ distributions in L-UTCU Zeolitic and OSBCU Zeolitic RMFs using mean component additivity methodology parameters applied to 10,000 simulated mica, smectite, zeolite vectors described in Section 10.2.

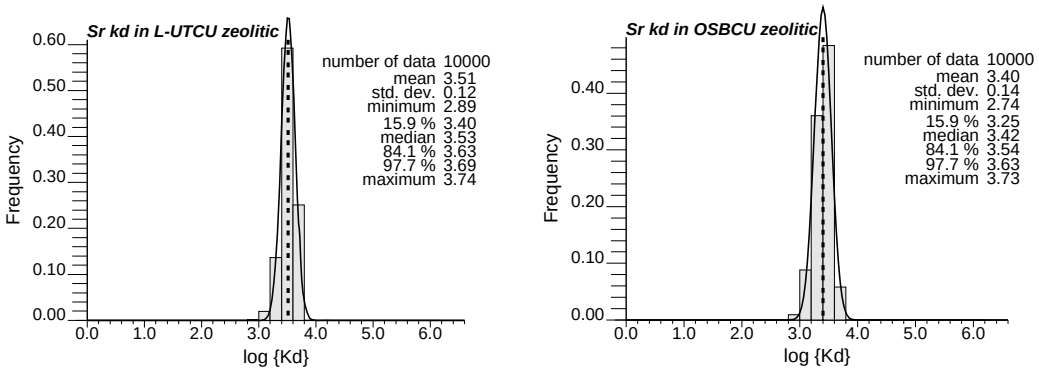

Figure 10-13.Simulated Sr $\log\{K_d\}$ distributions in L-UTCU Zeolitic and OSBCU Zeolitic RMFs using mean component additivity methodology parameters applied to 10,000 simulated mica, smectite, zeolite vectors described in Section 10.2.

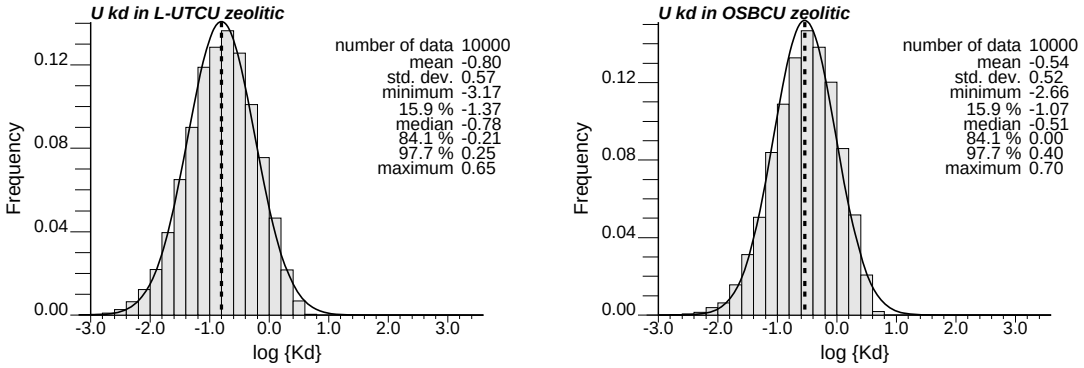

Figure 10-14.Simulated U $\log\{K_d\}$ distributions in L-UTCU Zeolitic and OSBCU Zeolitic RMFs using mean component additivity methodology parameters applied to 10,000 simulated mica, smectite, zeolite vectors described in Section 10.2.

Notably, Table 10-1 and Table 10-2 indicate the ALR simulation approach to generating K_d distributions produces identical standard deviations for Am, Eu, Ni, Np, Pu, Sm, and U because only smectite is included in the simulated K_d calculation. Simulated K_d standard deviations for ^{41}Ca and Sr are similar because the component additivity coefficients for mica, smectite, and zeolite are similar, particularly for zeolite which dominates K_d for ^{41}Ca and Sr. K_d for Cs is also strongly dependent on zeolite, but has a higher K_d standard deviation than for ^{41}Ca and Sr because of the large component additivity coefficient for mica. Differences in simulated and calculated means and standard deviations are mainly attributed to calcite and hematite. The differences are greater in the **L-UTCU Zeolitic** compared to **OSBCU Zeolitic** because more non-zero calcite and hematite percentages occur in the **L-UTCU Zeolitic**.

Table 10-1. Comparison of mean and standard deviation (σ) of log{ K_d } in L-UTCU Zeolitic RMF computed directly from "F" data and simulated from ALR covariance matrix for mica, smectite, and zeolite. The difference between simulated values relative to data values is shown in parenthesis.

RN Class	Mean $\log\{K_d\}$ From "F" data	σ $\log\{K_d\}$ From "F" data	Mean $\log\{K_d\}$ Simulated	σ $\log\{K_d\}$ Simulated
Am	2.82	0.70	2.92 (+0.10)	0.57 (–0.13)
^{41}Ca	3.74	0.11	3.74 (0.00)	0.12 (+0.01)
Cs	3.90	0.26	3.99 (+0.09)	0.22 (–0.04)
Eu	2.07	0.72	2.16 (+0.09)	0.57 (–0.15)
Ni	2.30	0.69	2.41 (+0.11)	0.57 (–0.12)
Np	–0.45	0.72	–0.36 (+0.09)	0.57 (–0.15)
Pu	1.09	0.70	1.19 (+0.10)	0.57 (–0.13)
Sm	2.24	0.74	2.32 (+0.08)	0.57 (–0.17)
Sr	3.52	0.11	3.51 (-0.01)	0.12 (0.01)
U	–0.90	0.69	–0.80 (+0.10)	0.57 (+0.10)

Table 10-2. Comparison of mean and standard deviation (σ) of $\log\{K_d\}$ in OSBCU Zeolitic RMF computed directly from "F" data and simulated from ALR covariance matrix for mica, smectite, and zeolite. The difference between simulated values relative to data values is shown in parenthesis.

RN Class	Mean $\log\{K_d\}$ From "F" data	σ $\log\{K_d\}$ From "F" data	Mean $\log\{K_d\}$ Simulated	σ $\log\{K_d\}$ Simulated
Am	3.17	0.53	3.18 (+0.01)	0.52 (–0.01)
^{41}Ca	3.62	0.15	3.62 (+0.00)	0.14 (–0.01)
Cs	4.09	0.20	4.08 (–0.01)	0.31 (+0.11)
Eu	2.42	0.53	2.42 (0.00)	0.52 (–0.01)
Ni	2.66	0.53	2.67 (0.01)	0.52 (–0.01)
Np	–0.10	0.53	–0.10 (0.00)	0.52 (–0.01)
Pu	1.44	0.53	1.45 (+0.01)	0.52 (–0.01)
Sm	2.58	0.54	2.58 (0.00)	0.52 (–0.02)
Sr	3.40	0.15	3.40 (0.00)	0.14 (–0.01)
U	–0.55	0.53	–0.54 (+0.01)	0.52 (–0.01)

11. Conclusions and Recommendations

11.1 Conclusions

Conclusions of this study separate out into subjects related to (1) XRD method, (2) comparison to previous reactive mineral distribution interpretation frameworks involving mineral zonation, reactive mineral category (RMC), and reactive mineral unit (RMU) frameworks, (3) distinction of reactive mineral facies (RMFs) including use of the additive log ratio (ALR) transformation, (4) prediction of reactive mineral and $\log\{K_d\}$ distributions within different RMFs, and (5) analysis of spatial variability of reactive mineral and $\log\{K_d\}$ distributions.

11.1.1 XRD Methods

Recognition of different limitations for the different XRD methods is a critical step in interpreting the XRD data on mineral percentages in the southwestern Nevada volcanic field (Warren, 2007). Full spectrum ("F"), internal standard ("I"), external spectrum ("E"), and semi-quantitative ("S") XRD methods were used to generate the 1,172 XRD data within the TCU. The "F" data provide the highest accuracy. Importantly, the "F" data indicate smectite, which sorbs all ten radionuclide classes (^{41}Ca, Am, Cs, Eu, Ni, Np, Pu, Sm, Sr, U), is ubiquitous throughout the TCU. The "F" data also indicate mica is ubiquitous, except for a few thin peralkaline beds mainly within the LTCU HSU. The "F" data provide the most accurate estimates of reactive mineral distributions within different RMCs, RMUs, or RMFs. Where feasible, "F" data should be used to estimate realistic $\log\{K_d\}$ distributions.

"S" data are most numerous but are inherently uncertain because the original mineral percentage estimates were given as ranges. Mineral percentage values for "S" data given in Warren (2007) actually represent modal values of ranges. "S" data are relatively more certain at higher mineral percentages but do not resolve low mineral percentages as well as "F" or "I" data. Recognizing differences in XRD method ability to resolve low mineral percentages, "zero" values as likely to be assigned to actual non-zero percentages particularly for smectite, mica, and zeolite. Interpretation of "zero" value is problematic for statistical analysis involving logarithmic transformation. This study recommends replacing zero values with non-zero values for ubiquitous reactive minerals by balancing mean and median ALR statistics specifically to each XRD method. With correction for zero values, "S" and "F" data frequency distributions are largely consistent, although "S" data generally show more variance attributed to estimation uncertainty (ranges).

While the "E" data appear to have accuracy comparable or better than "S" data, the "E" data have poor resolution of low reactive mineral percentages. "E" data usually resolve only half or less of the frequency distribution for zones with ubiquitous mica, smectite, and zeolite as indicated by "F" data. This is problematic to characterization of reactive mineral frequency and $\log\{K_d\}$ distributions and in most RMUs and RMFs.

Only 5 "I" data are present in the TCU all within the ATCU HSU, so the "I" data alone cannot be used to analyze spatial variability.

The XRD methods also vary in extent of minerals analyzed for. For example, although "S" data are most numerous, hematite was rarely analyzed for in "S" data. Such "null observations" must not be treated as zero values in characterization of hematite (or any important reactive mineral) frequency distributions.

11.1.2 Use of RMC and RMU Frameworks

Reactive mineral category (RMC) and reactive mineral unit (RMU) frameworks were developed by Stoller-Navarro (2007) to address spatially variable K_d in CAU-scale transport models. The RMC framework relies on various reactive mineral cutoff values to distinguish categories with ranges of reactive mineral percentages. Use of cutoff values for categorization is the main drawback of the RMC framework for typical parametric Gaussian-based geostatistical analysis.

The RMU framework divides HSUs into subunits having distinctive reactive mineral characteristics largely related to stratigraphic units and lithology. The RMU framework is more conducive to typical parametric geostatistical approaches because reactive mineral distributions within RMUs are more Gaussian, particularly through use of ALR transformation. Reactive mineral facies (RMFs) are formed primarily by individual RMUs or RMUs grouped by similarity in reactive mineral characteristics. An advantage of the RMU approach is that it already provides a geometric framework for delineating zones of distinctive reactive mineral properties within the TCU.

11.1.3 Use of ALR Transformation

Mineral percentages constitute a compositional variable – the components sum to a fixed value of 100%. Compositional variables present unique difficulties to standard statistical and geostatistical analysis. Gaussian assumptions are violated by the finite limits of 0 to 100%. The summing constraint produces singularities in cokriging systems of equations and non-sensical spurious correlations. Mineral percentage distributions do not consistently fit either normal or log-normal distributions.

The additive log ration (ALR) transformation examines logarithms of ratios of components where one component is placed in the denominator. In this study, the components are chosen to be the reactive mineral percentages in the numerator and the sum of the non-reactive mineral percentages in the denominator. The ALR transformation was found to consistently produce Gaussian distributions in RMFs with ubiquitous reactive minerals.

11.1.4 Distinction of Reactive Mineral Facies

The concept of "reactive mineral facies" (RMF) is a zone of rock distinguished by its reactive mineral distribution characteristics. This study introduces RMFs for characterization of spatial variability of reactive minerals and K_d within the TCU for the following interrelated reasons:

- While RMUs are conducive to geostatistical analysis, some RMUs with similar reactive mineral properties can be grouped together to pool data into one RMF. For example, zeolitic RMUs in the lower and upper tuff confining units (LTCU and UTCU) HSUs are pooled into the **L-UTCU Zeolitic** RMF, and four devitrified RMUs are pooled into the **Devitrified** RMF. Pooling of the limited XRD data, where appropriate, produces better characterizations distinct zones with unique mineral percentage and K_d distributions.

- In some exceptional cases, some XRD data categorized into RMUs have mineral distributions characteristic of other RMUs, such as argillic or devitrified characteristics within a zeolitic RMU. The RMF framework re-categorizes exceptional data only where the mineral distributions are clearly outside the main population. Re-categorization of exceptional data was found to remove outliers from RMU or grouped RMU reactive mineral frequency distributions to produce more Gaussian-like RMF frequency distributions using ALR transformation.

- Gaussian ALR distributions characterize smectite in all RMFs, mica in all RMFs except for the **L-UTCU Zeolitic** (because of occasional occurrences of thin peralkaline mica-free tuff beds), and zeolite in the **L-UTCU Zeolitic** and **OSBCU Zeolitic** RMFs. With Gaussian distributions established for ALR transformations, variogram analysis and Gaussian-based geostatistical simulation of reactive mineral distributions are justifiable.

- By pooling data and carefully sorting out uncertainties related to XRD method, the RMF framework minimizes spread in the distributions of reactive minerals and K_d that characterize different zones of the TCU. This will reduce the range of uncertainty in prediction of radionuclide transport.

11.1.5 Reactive Mineral and K_d Distributions within RMFs

The three most voluminous RMFs, **L-UTCU Zeolitic**, **OSBCU Zeolitic**, and **Argillic**, largely correspond spatially with the four HSUs, UTCU, LTCU, OSBCU, and ATCU. Thus, vertical and lateral trends in reactive mineral and $\log\{K_d\}$ spatial distribution within the TCU largely correspond to the HSUs. Exceptions to this trend are the **Devitrified** and **Vitric** RMFs which introduce low zeolite percentages relative to typical vertical zonation of decreasing zeolite and increasing smectite with depth (Prothro, 2005).

Through application of the component additivity methodology (Zavarin et al., 2004), $\log\{K_d\}$ distributions for seven of 10 radionuclide classes (Am, Eu, Ni, Np, Pu, Sm, and U) are dominated by smectite. Because the **Devitrified** and **Vitric** RMFs are located mainly within the OSBCU HSU or near the base of the LTCU HSU, decreased zeolite in **Devitrified** and **Vitric** RMFs does not change $\log\{K_d\}$distributions much relative to the **OSBCU** Zeolitic RMF. For smectite-dominated sorbers, $\log\{K_d\}$ distributions will consistently increase in magnitude with depth in the TCU except in isolated argillic zones that occur within zeolitic zones.

^{41}Ca and Sr $\log\{K_d\}$ distributions are largely dominated by zeolite and, thus, show different depth-related trends than the smectite sorbers. Zeolite abundance generally decreases with depth. However, since ^{41}Ca and Sr are also moderately strong sorbers to mica and smectite, depth-decreasing trends in $\log\{K_d\}$for ^{41}Ca and Sr are damped except in **Devitrified** and **Vitric** RMFs which are low in both smectite and zeolite abundance.

Cs $\log\{K_d\}$ is dominated by mica, which is nearly ubiquitous and uniformly distributed throughout the TCU. As a result, Cs shows the least zonal spatial variation in $\log\{K_d\}$ among the ten radionuclide classes.

11.1.6 Spatial Variability of Reactive Mineral and $\log\{K_d\}$ Distributions within RMFs

While the RMFs subdivide reactive mineral and $\log\{K_d\}$ distributions into zones largely corresponding to individual or groups of RMUs, it is possible that reactive mineral and $\log\{K_d\}$ distributions could be spatially correlated within RMFs. Variogram analysis of $\log\{K_d\}$ derived from "F" data in different RMUs consistently produced no spatial correlation in either vertical or lateral directions. These variogram analyses suggest spatial correlation scales of $\log\{K_d\}$ must be less than approximately 6 m in the vertical direction. "F" data were not sufficiently numerous and closely spaced to measure lateral spatial variability. While "S" data are more numerous and capable of producing both vertical and lateral variograms of $\log\{K_d\}$ in some RMFs, the "S" data suffer from

uncertainty related to the original quantification by ranges. Use of modal values from ranges imparts apparent spatial correlations in variogram analysis that are not real.

Parametric geostatistical analysis can also be applied to ALR transformed reactive mineral percentages where the major reactive minerals, mica, smectite, and zeolite, are ubiquitous, which occurs in the **L-UTCU Zeolitic** (for non-peralkaline tuff beds) and **OSBCU Zeolitic** RMFs. Cross-covariances between mica, smectite, and zeolite ALRs can be measured as a function of vertical lag. No non-zero spatial correlation beyond lag zero was detected except, possibly, for smectite in the **OSBCU Zeolitic** RMF. Fitted Gaussian distributions of mica, smectite, and zeolite ALRs can be used in stochastic simulation of $\log\{K_d\}$ distributions through a Cholesky decomposition technique. Advantages of this ALR-based approach over direct analysis of $\log\{K_d\}$ are

- Only one geostatistical model is developed for the reactive mineral distribution rather than ten separate models for $\log\{K_d\}$ distributions of the ten radionuclide classes.
- The resulting $\log\{K_d\}$ distributions are bounded above zero and below a finite value and can also characterize asymmetry unlike a Gaussian distribution.
- The approach has the potential to account for a matrix of spatial auto- and cross-correlations in mineral abundance through a cokriging-based extension of sequential Gaussian simulation (Deutsch and Journel, 1992). However, this concept was not pursued because only a single vertical ALR auto-correlation and no ALR spatial cross-correlations were detectable in the TCU XRD data.

11.1.7 Use of Indicator Geostatistical Methods

Although study recommends use of a parametric geostatistical approaches applied to either $\log\{K_d\}$ ALR-transformed reactive mineral percentages, non-parametric or "indicator" geostatistical methods could be applied. The main drawbacks of indicator approaches are twofold (1) considerably more variogram analysis and modeling and (2) difficulty in defining tails of distributions.

One possible advantage of employing indicator geostatistics to the TCU mineral data set is to address the main weakness of the numerous "S" data – data values given as ranges of mineralogic percentages (Warren, 2007). An indicator approach could be applied with cutoff values corresponding to the limits of the "S" data ranges. An indicator approach applied to "S" data would avoid problems of producing spurious indications of spatial correlation caused by data values assigned by the mode the "S" data range.

11.2 Comparison with Yucca Flat/Climax Mine Matrix K_d Distributions

Stoller-Navarro (2007) includes estimates of HSU-specific K_d distributions for radionuclide classes. These K_d distributions were obtained by applying the component additivity methodology (Section 8.1) to the composite XRD data set. This section focuses on the differences that RMF-based interpretation of K_d distributions could provide for assessing transport processes in the TCU relative to K_d distributions presented in Stoller-Navarro (2007).

As discussed in Section 11.1.5, several important geochemical factors affect estimation of $\log\{K_d\}$ distributions for the 10 radionuclide classes:

- $\log\{K_d\}$ distributions for seven of 10 radionuclide classes (Am, Eu, Ni, Np, Pu, Sm, and U) are dominated by smectite, which generally increases with depth.
- ^{41}Ca and Sr $\log\{K_d\}$ distributions are largely dominated by zeolite, which generally decreases with depth.
- Cs $\log\{K_d\}$ distribution is dominated by mica, which is nearly ubiquitous and uniformly distributed throughout the TCU.
- Magnitudes of $\log\{K_d\}$ for smectite or zeolite sorbers will be relatively low in devitrified and vitric rocks, which are associated with distinct lithologies. Devitrified tuffs are associated with welded ash-flow tuffs or dense stony lavas, and vitric tuffs are associated with nonwelded to partially welded ash flow or vitrophyres, unaltered bedded/ash-fall tuffs, or vitrophyric and pumiceous lava.
- Variability in groundwater chemistry increases variability of $\log\{K_d\}$.

Additionally, prediction of $\log\{K_d\}$ distributions is affected by the accuracy and spatial distribution of the XRD data, as discussed in Sections 3.4.1, 7.2, 7.3, and 11.1.1.

The RMF approach attempts to improve consideration of both geochemical and data accuracy and spatial distribution factors in estimation of spatial distribution of $\log\{K_d\}$ distributions in the TCU. The benefit of the RMF approach is to increase the accuracy, decrease the range of uncertainty, and improve prediction of the spatial distribution of $\log\{K_d\}$ within the TCU. Importantly, the RMF approach pays close attention to treatment of data that govern estimation of low $\log\{K_d\}$ within the TCU, considering the spatial distribution of low $\log\{K_d\}$ can dominate transport predictions.

11.2.1 Smectite-Dominated Sorbers - Am, Eu, Ni, Np, Pu, Sm, and U

Figure 11-1 shows histograms from Stoller-Navarro (2007) of estimated Eu $\log\{K_d\}$ distributions in the UTCU, LTCU, OSBCU, and ATCU HSUs of the TCU. The histogram of Eu $\log\{K_d\}$ distribution is similar to other radionuclides with sorption dominated by smectite percentage (Am, Ni, Np, Pu, Sm, and U), although magnitudes are different. While the majority of the $\log\{K_d\}_d$ estimates fall within a bell-shaped curve, a significant proportion of (over 10%) of the $\log\{K_d\}$ estimates are effectively zero. As summarized in Section 11.1.1, the highest quality full-spectrum ("F") XRD data indicate smectite is ubiquitous in the TCU. The zero K_d values in Figure 11-1 are associated with lower quality XRD data lacking resolution of low smectite percentage. Accordingly, zero K_d values for Am, Eu, Ni, Np, Pu, Sm, and U are unrealistic. Moreover, some of the spread in $\log\{K_d\}$ is also caused by uncertainty, error, or lack of resolution in the XRD data. Use of "F" data will decrease variability of estimated $\log\{K_d\}$ distribution attributed to data uncertainty.

Many of the lowest non-zero K_d values in Figure 11-1 are also associated with vitric and devitrified tuffs. Distinction of the **Vitric** and **Devitrified** RMFs within HSUs will better pinpoint locations in the TCU where K_d can be expected to be relatively low and, consequently, mobility of Am, Eu, Ni, Np, Pu, Sm, and U can potentially be higher. Conversely, distinction of **Vitric** and **Devitrified** RMFs leads to higher magnitude and less-variability in prediction of $\log\{K_d\}$ distributions in the zeolitic portions of the UTCU, LTCU, and OSBCU. Distinction of **L-UTCU Zeolitic, OSBCU Zeolitic**, **Vitric,** and **Devitrified** RMFs combined with use of full-spectrum "F" XRD data will provide a more accurate prediction of the spatial distribution of TCU $\log\{K_d\}$ spatial distributions, particularly zones of extreme highs and lows, for smectite-dominated sorbing radionuclide classes compared to resolving spatial variability of $\log\{K_d\}$ compositely within HSUs.

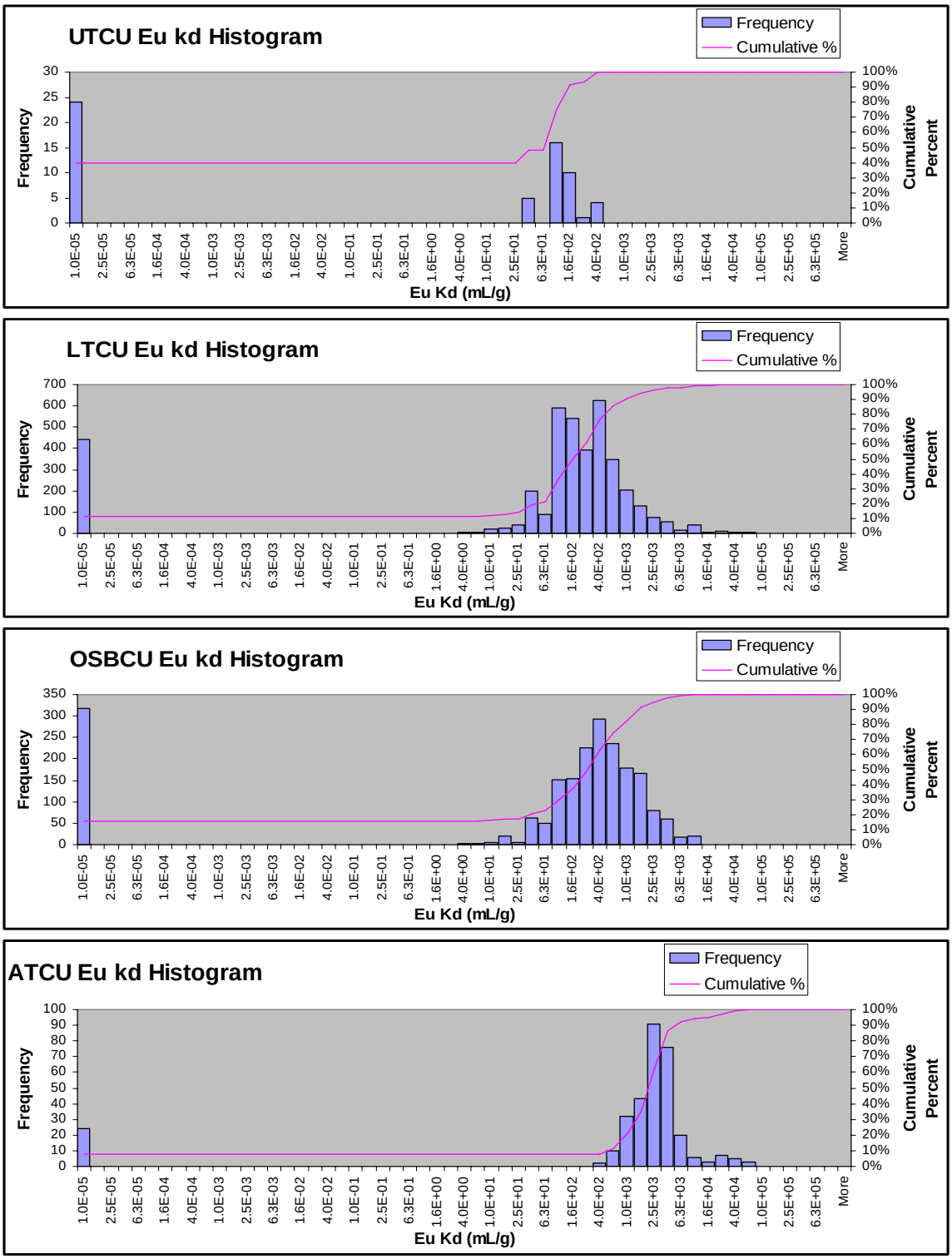

Figure 11-1. Histograms of Eu $\log\{K_d\}$ in TCU HSUs estimated by applying component additivity method variability considering composite XRD data set and variability of groundwater chemistry (Stoller-Navarro, 2007).

11.2.2 Zeolite/Smectite Dominated Sorbers – ^{41}Ca and Sr

Based on the component additivity exponential coefficients (Table 8-1), ^{41}Ca and Sr $\log\{K_d\}$ distributions are dominated firstly by zeolite percentage and secondarily by smectite. Because the differences in zeolite and smectite component additivity exponential coefficients for ^{41}Ca and Sr are similar, the shape of estimated ^{41}Ca and Sr $\log\{K_d\}$ distributions will be similar. Full spectrum "F" XRD data indicate smectite is ubiquitous throughout the TCU. Therefore, zero-valued ^{41}Ca and Sr $\log\{K_d\}$ are unrealistic.

Figure 11-2 shows histograms from Stoller-Navarro (2007) of estimated ^{41}Ca distributions in the UTCU, LTCU, OSBCU, and ATCU HSUs of the TCU. The ^{41}Ca $\log\{K_d\}$ in the UTCU and LTCU are similar, except for left-tailing in the LTCU. As discussed in Chapters 6 and 7, the zeolitic portion of the LTCU and UTCU show very similar reactive mineral distributions and, thus, can be combined as the **L-UTCU Zeolitic** RMF. The left tailing and zero values in the LTCU and OSBCU ^{41}Ca $\log\{K_d\}$ is attributed a combination of vitric and devitrified rocks lower quality XRD data that do not resolve low smectite or zeolite percentages. ^{41}Ca and Sr $\log\{K_d\}$ in the ATCU is more influenced by smectite percentage in addition to zeolite percentage. As for the smectite-sorbing radionuclide classes, use of the RMF approach with "F" data will eliminate left-tailing and unrealistic zero-valued K_ds and will more specifically characterize the spatial distribution of low values of ^{41}Ca and Sr $\log\{K_d\}$ as occurring in devitrified ash-flow and vitric ash-fall tuffs.

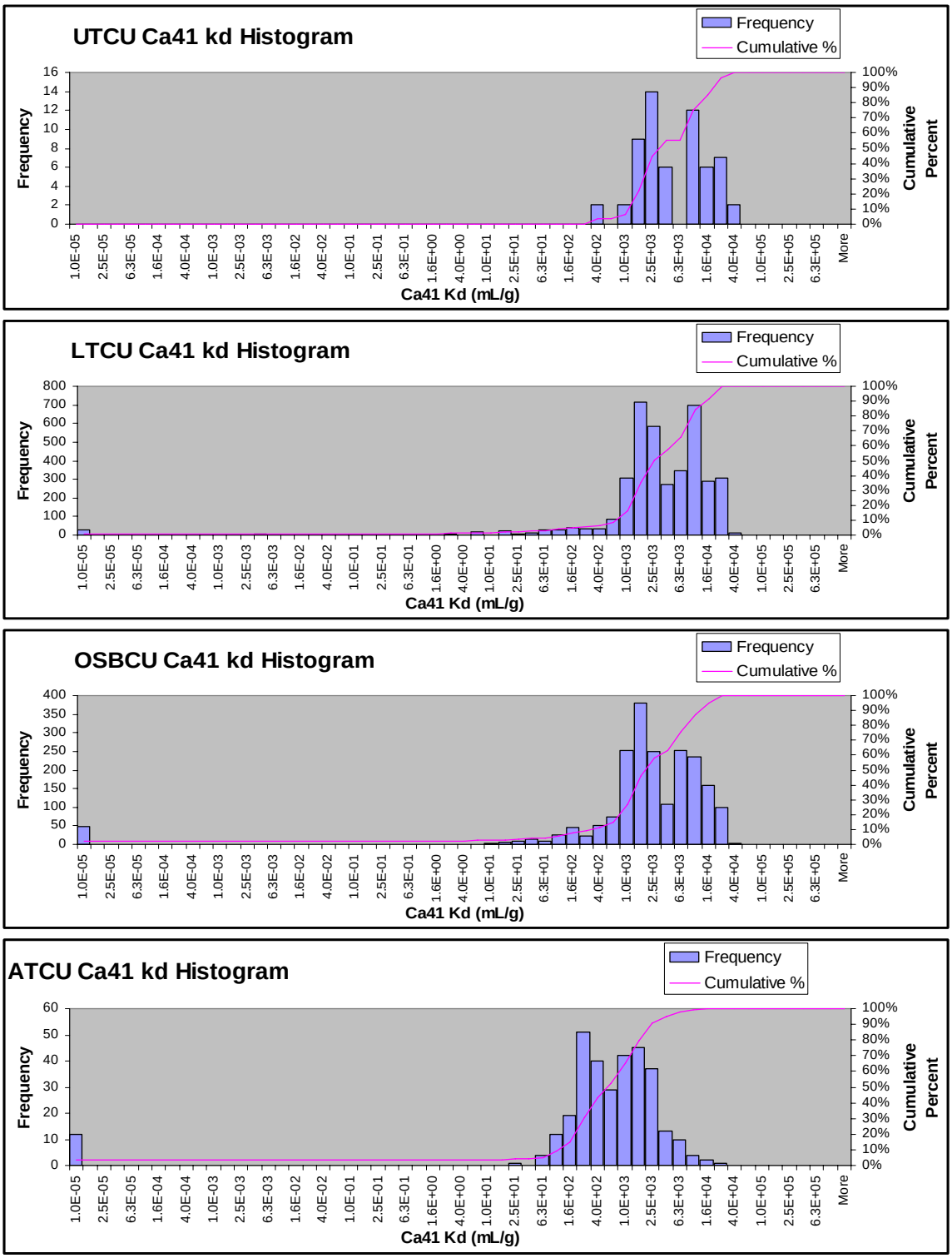

Figure 11-2. Histograms of ^{41}Ca $\log\{K_d\}$ in TCU HSUs estimated by applying component additivity method variability considering composite XRD data set and variability of groundwater chemistry (Stoller-Navarro, 2007).

11.2.3 Mica-Dominated Sorber – Cs

Cs is the only radionuclide class for which mica contributes the largest component additivity exponential coefficient (See Table 8-1). Cs sorbs to zeolite and smectite with similar magnitude to ^{41}Ca and Sr. However, the much larger component additivity exponential coefficient for Cs to mica (5.58 ± 0.18) compared to zeolite (3.75 ± 0.20) and smectite (3.11 ± 0.18) causes mica percentage to dominate estimated Cs $\log\{K_d\}$ distribution in the TCU even though mica is typically present in lower percentages than zeolite and smectite.

Full spectrum "F" XRD data indicate mica is ubiquitous throughout the TCU except in some thin, peralkaline, ash fall tuffs within zeolitic RMUs in the LTCU and UTCU as discussed in Section 5.3. However, because mica percentage is typically low (less than 3%), much of the XRD data does not resolve low mica percentages resulting in many spurious zero mica percentage data. For Cs, zero mica percentage values in the composite XRD data set usually will not produce zero $\log\{K_d\}$ estimates because Cs also sorbs to smectite and zeolite, which are typically have non-zero percentages. However, assumption of zero mica in the TCU is unrealistic except for thin, peralkaline, ash fall tuffs.

Figure 11-3 shows histograms of estimated Cs $\log\{K_d\}$ distributions from Stoller-Navarro (2007) in the UTCU, LTCU, OSBCU, and ATCU HSUs of the TCU. These histograms indicate decreasing Cs $\log\{K_d\}$ and lower magnitudes compared to Cs $\log\{K_d\}$ generated in this study (Figure 8-5). Table 8-4 estimates mean Cs $\log\{K_d\}$ ranging from 3.67 to 4.09 in RMFs, which appears higher in magnitude compared to mean Cs $\log\{K_d\}$ in Figure 11-3. Cs $\log\{K_d\}$ distributions have long tails to the left in the UTCU, LTCU, and OSBCU. Decreasing $\log\{K_d\}$ with depth and left tailing are characteristic of strong K_d dependence on zeolite. Thus, the Stoller-Navarro (2007) mechanistic model estimates of Cs $\log\{K_d\}$ appear to have less (if any) dependence on mica in comparison to this study. Whether or not Cs $\log\{K_d\}$ depends more on mica than zeolite, use of the RMF approach with "F" data will eliminate left tailing and zero K_d values evident in Figure 11-3. Considering that mica is largely ubiquitous and uniformly distributed in the TCU, increased dependence of Cs $\log\{K_d\}$ mica will result in large magnitude and more uniform Cs $\log\{K_d\}$ throughout the TCU compared to Cs $\log\{K_d\}$ distributions in Figure 11-3.

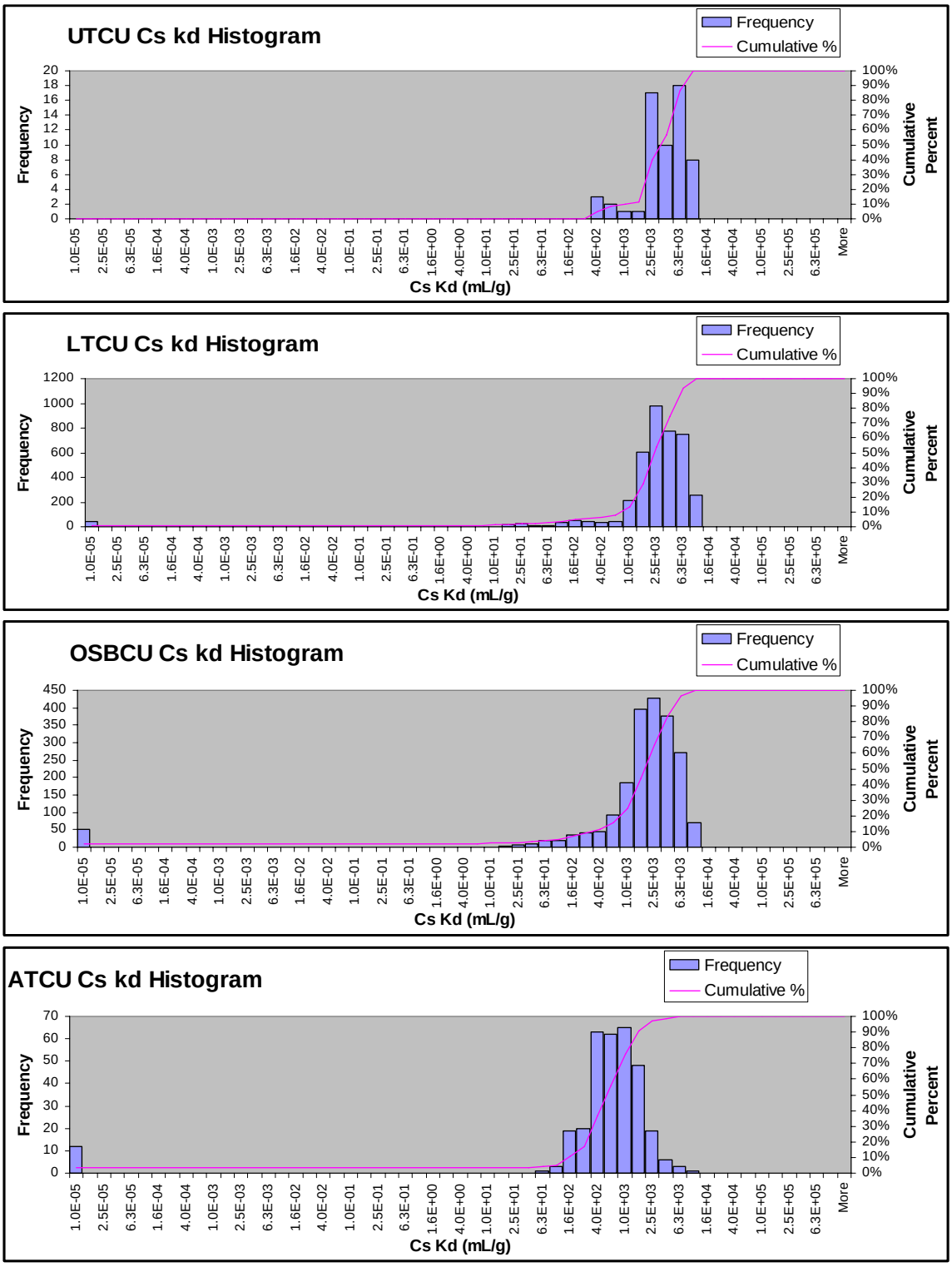

Figure 11-3. Histograms of Cs $\log\{K_d\}$ in TCU HSUs estimated by applying component additivity method variability considering composite XRD data set and variability of groundwater chemistry (Stoller-Navarro, 2007).

11.3 Recommendations

Recommendations derived from this study separate out into subjects related to (1) how to utilize the TCU XRD data, (2) how to assign values of K_d and assess uncertainty in spatial distribution of K_d within the TCU, (3) how to improve characterization of spatial variability of K_d

11.3.1 Utilization of TCU XRD Data

Any study using the southwestern Nevada volcanic field XRD data set (Warren, 2007) should be aware of the differences between the XRD methods used. Without knowledge or consideration of the different XRD methods, erroneous conclusions could be made. For example, the fidelity of the "F" data indicates ubiquity of smectite throughout the TCU and lower proportions of zero-valued data for all reactive minerals. However, if "S" and "E" data are pooled with the "F" data irrespective of data fidelity, different conclusions could easily be made, such as a large proportion of the TCU has zero smectite. Since all ten radionuclide classes sorb to smectite, and smectite is the most important sorbing mineral for 7 of 10 radionuclide classes, an erroneous assumption of a large proportion of zero values of smectite in the TCU would lead to overestimation of uncertainty in $\log\{K_d\}$ and underestimation of mean $\log\{K_d\}$ for most radionuclide classes.

Another important consideration of XRD method is the extent (number) of minerals analyzed for. For the "S" method in particular, hematite and other key minerals such as tridymite and cristobalite were usually not analyzed for. It should be recognized that such null observations should not necessarily be treated as zero values in characterization of frequency distributions. Moreover, limited minerals analyses will underestimate mineral totals. Use of total mineral percentage as a criterion for data quality can lead to bias toward high K_d because samples with unusually high percentages of the minerals analyzed for will be accepted as good quality data, while similar quality data that happen to have low percentages for the minerals analyzed for will be rejected.

11.3.2 Assignment of K_d Distributions Within the TCU

The RMF approach described in this report is designed to merge $\log\{K_d\}$ distributions derived from XRD data (Warren, 2007) and the component additivity methodology (Zavarin et al., 2004) with geometric frameworks from hydrostratigraphic unit and reactive mineral unit models (Bechtel Nevada, 2006; Stoller-Navarro, 2007). $\log\{K_d\}$ distributions derived for RMFs should be assigned to the individual or grouped RMUs used to define RMFs, with consideration for some rare exceptions such as argillic

characteristics within a zeolitic RMU. Estimated standard deviations of $\log\{K_d\}$ derived from XRD data represent small-scale variability within vertical scales of 6 m or less. Therefore, if transport simulation grid block or cell sizes are 6 m or greater in the vertical, upscaled effective $\log\{K_d\}$ values based on RMF $\log\{K_d\}$ distributions are certainly justifiable. However, additional uncertainty in $\log\{K_d\}$ derived from uncertainty in the component additivity parameters should be addressed. This model-based uncertainty in the $\log\{K_d\}$ estimates can be superposed onto data-derived uncertainty.

In the **L-UTCU Zeolitic** and **OSBCU Zeolitic** RMFs, the best quality "F" XRD data are in sufficient quantity and spacing and the major reactive minerals, mica, smectite, and zeolite, are effectively ubiquitous. In these zeolitic RMFs, simulation of ALR distributions with subsequent backtransformation to reactive mineral percentage provides a more accurate representation of the reactive mineral distributions and, subsequently, a more accurate representation of $\log\{K_d\}$ distributions. If feasible, the ALR-based characterization of $\log\{K_d\}$ distributions should take preference over a more empirical Gaussian approach to $\log\{K_d\}$ distribution characterization.

11.3.3 Improving Characterization of Spatial Variability of K_d

Consideration of the different methods indicates that the full spectrum "F" method is very useful in resolving the lower portion of reactive mineral distributions which, in turn, are needed to resolve the lower portion of K_d distributions. Obtaining more XRD data with similar or better fidelity to "F" data can improve characterization of spatial variability of K_d in several ways:

- If high quality XRD data are obtained at close spacing (e.g. 1 m or less vertically, 10-100 m or less laterally), it may be possible to detect spatial correlation of reactive mineral abundances.
- Resolution of the lower portion of the reactive mineral abundance frequency distribution is crucial to characterization of the most mobile radionuclide transport behavior.
- Once spatial variability of mineral abundances is characterized, geostatistical simulation can be used to produce realizations of either ALR or K_d to estimate effective K_d at CAU-scale contaminant transport simulation grid block scales similar to previous work in Frenchman Flat alluvium (Zavarin et al., 2004).

References

Aitchison, J. (1986), *The Statistical Analysis of Compositional Data*, Chapman and Hall, London.

Aitchison, J. (2005), *A Concise Guide to Compositional Data Analysis*, course notes, Department of Statistics, University of Glascow, ima.udg.es/Activitats/CoDaWork05/A_concise_guide_to_**compositional_data**_analysis.pdf

Bechtel Nevada (2006), *A Hydrostratigraphic Model and Alternatives for the Groundwater Flow and Contaminant Transport Model of Correction Action Unit 97: Yucca Flat-Climax Mine, Lincoln and Nye Counties, Nevada*, DOE/NV/11718-1119, 288 p.

Bish, D. L., and S. J. Chipera (1989), Revised mineralogic summary of Yucca Mountain, Nevada," Los Alamos National Laboratory, Los Alamos, NM, LA-11497-MS, 68 p.

Carle, S. F., R. M., Maxwell, G. A. Pawloski, G. A., D. E. Shumaker, A. F. B. Tompson, and M. Zavarin (2007), *Evaluation of the Transient Hydrologic Source Term for the Cambric Underground Nuclear Test at Frenchman Flat, Nevada Test Site*, Lawrence Livermore National Laboratory, Livermore, CA, UCRL-TR-226916.

Chipera, S. J., and D. L. Bish (2002), FULLPAT: *A full-pattern quantitative analysis program for X-ray powder diffraction using measured and calculated patterns*, J. Appl. Cryst., Vol. 35, p. 744-749.

Deutsch, C. V., and A. G. Journel, A. G. (1992), GSLIB, *Geostatistical Software Library and User's Guide*, New York, Oxford University Press, 340 p.

Halford, K. J., R. J. Laczniak, and D. L. Galloway (2005), *Hydraulic characterization of overpressured tuffs in central Yucca Flat, Nevada Test Site, Nye County, Nevada*, U.S. Geological Survey Scientific Investigations Report 2005-5211.

Papelis, C., and W. Um, (2003), *Evaluation of Cesium, Strontium, and Lead Sorption, Desorption, and Diffusion in Volcanic Tuffs from Yucca Flat, Nevada Test Site: Macroscopic and Spectroscopic Investigations* Desert Research Institute, Las Vegas, NV, Publication No. 45189, DOE/NV/13609-18.

Pawloski, G. A. (1983), Quantitative determination of minerals in Nevada Test Site samples by X-ray diffraction, Proceedings of the Second Symposium on Containment of Underground Nuclear Explosions, Lawrence Livermore National Laboratory, Livermore, CA, CONF-830882, Vol. 1, p. 75-96.

Pawloski, G. A., A.F. B. Tompson, S. F. Carle, Eds. (2001), *Evaluation of the hydrologic source term from underground nuclear test on Pahute Mesa at the Nevada Test Site: The Cheshire test*, Lawrence Livermore National Laboratory, Livermore, CA, UCRL-ID-147023.

Pawlosky-Glahn, C., and R. Olea (2004), *Geostatistical Analysis of Compositional Data*, Oxford University Press, New York, 304 p.

Prothro, L. (2005), *Mineralogic Zonation Within the Tuff Confining Unit, Yucca Flat, Nevada Test Site*, Bechtel Nevada, DOE/NV/11718-995, 82p

Schenkel, C. J., T. G. Hildenbrand, and G. L. Dixon (1999), *Magnetotelluric Study of the Pahute Mesa and Oasis Valley Regions, Nye County, Nevada*. U.S. Geological Survey Open-File Report 99-355.

Shaw Environmental, Inc. (2003), *Contaminant Transport Parameters for the Groundwater Flow and Contaminant Transport Model of Corrective Action Units 101 and 102: Central and Western Pahute Mesa, Nye County, Nevada*, Shaw Environmental Inc., 13052-201, 464 p.

Stoller-Navarro (2007), *Phase I Contaminant Transport Parameters for the Groundwater Flow and Contaminant Transport model of Corrective Action Unit 97: Yucca Flat/Climax Mine, Nye County, Nevada*, Stoller-Navarro S-N/99205-096, 704 p.

Tompson, A. F. B., A. L. Schafer, and R. W. Smith (1996), *Impacts of physical and chemical heterogeneity on co contaminant transport in sandy porous medium*, Water Resources Research, v. 26, n. 10, p. 2541-2562.

Tompson, A. F. B., C. J. Bruton, G. A. Pawloski, Eds. (1999), Evaluation of the hydrologic source term from the underground nuclear test in Frenchman Flat and the Nevada Test Site: The Cambric test, Lawrence Livermore National Laboratory, Livermore, CA, UCRL-ID-132300.

Viswanathan, H. S., B. A. Robinson, C. W. Gable, and J. W. Carey (2003), *A geostatistical modeling study of the effect of heterogeneity on radionuclide transport in the unsaturated zone, Yucca Mountain*, Journal of Contaminant Hydrology, v. 62-63, p. 319-336

U.S. Department of Energy, Nevada Operations Office (2000), United States Nuclear Tests, July 1945 through September 1992. DOE/NV-209, Revision 15, Las Vegas, NV.

Ware, S. D., A. Abdel-Fattah, M. Ding, P. W. Reimus, C. Sedlacek, C., M. J. Haga, M. J., and E. Garcia (2005), Radionuclide Sorption and Transport in Fractured Rocks of Yucca Flat, Nevada Test Site, Los Alamos National Laboratory, NM, LA-UR-05-9279, 109 p.

Warren, R. G. (2007), A Compilation of X-ray Diffraction Analyses and Formal Definitions for Alteration within the Southwestern Nevada Volcanic Field, Draft Report.

Wolfsberg, A., L. Glascoe, G. Lu, A. Olson, P. Lichtner, M. McGraw, and T. Cherry, (2001), *TYBO/BENHAM Model Analysis of Groundwater Flow and Radionuclide Migration from an Underground Nuclear Test in Southwestern Pahute Mesa, NTS*, Los Alamos National Laboratory, Los Alamos, NM, LA-UR-012924.

Wolfsberg, A., ???? (2007), Analysis and evaluation of elevated groundwater heads and their impact on flow and solute transport in the Tuff Pile: Areas 3, 4, and of the Nevada Test Site, Nye County, Nevada, Los Alamos National Laboratory, LA-UR-????. Draft.

Zavarin, M., and C. J. Bruton (2004a), *A Non-Electrostatic Surface Complexation Approach to Modelling Radionuclide Migration at the Nevada Test Site: I. Iron Oxides and Calcite*, Lawrence Livermore National Laboratory, UCRL-TR-208673, 220 p.

Zavarin, M., and Bruton, C. J. (2004b), *A Non-Electrostatic Surface Complexation Approach to Modelling Radionuclide Migration at the Nevada Test Site: II. Aluminosilicates*, Lawrence Livermore National Laboratory, UCRL-TR-208672, 220 p.

Zavarin, M., Carle, S. F., and Maxwell, S. F. (2004), *Upscaling Radionuclide Retardation – Linking the Surface Complexation and Ion Exchange Mechanistic Approach to a Linear Kd Approach*, Lawrence Livermore National Laboratory, UCRL-TR-204713, 164 p.